Molecular mechanisms of α-amylase action on retrograded starch
The relationship between digestion kinetics and physicochemical characteristics

Patel, Hamung

Awarding institution:
King's College London

KING'S College LONDON

University of London

Molecular mechanisms of α-amylase action on retrograded starch: the relationship between digestion kinetics and physicochemical characteristics

Hamung Patel

December 2014

A thesis submitted to King's College London for the degree of Doctor of Philosophy

King's College London

Preface

This thesis was submitted to King's College London for the degree of Doctor of Philosophy. The work presented herein was undertaken in the Division of Diabetes and Nutritional Sciences, King's College London, from October 2010 to December 2014.

Hamung Patel

December 2014

Abstract

Depending upon the physicochemical structure and properties of starch, the rate and extent of starch digestion can vary significantly from being very rapid to a much slower process and in some cases being virtually indigestible. The purpose of this mechanistic research project is to produce kinetic and structural data that provides an improved understanding of the interaction between porcine pancreatic α-amylase (PPA) and starch structures.

Native, gelatinised and retrograded starch samples (stored between 0-96h) were digested with PPA to produce digestibility plots from which Michaelis-Menten kinetic parameters were determined. Logarithm of slope (LOS) plots of digestibility curves for prolonged incubations were also constructed to allow the rate constant (k) and the total digestible starch (C_∞) to be calculated.

Following gelatinisation, the k_{cat}/K_m ratio increased drastically compared with native samples. For retrograded starches, the k_{cat}/K_m decreased relative to the non-retrograded samples, with the biggest difference being noticed in wheat, potato and high amylose maize starches. Surprisingly, the binding facility of α-amylase to starch did not change over 96h, indicated by the K_m values. The LOS plots showed no change in k but a decrease in C_∞ when gelatinised starch was stored at room temperature. The LOS plots also revealed a single rate constant for processed starches with only native starches being digested in distinct rapid and slower phases.

Evidence for the structural changes that occur during starch processing was obtained using Fourier transform infrared spectroscopy (FTIR), differential scanning calorimetry (DSC) and X-ray diffraction (XRD). The results showed that the degree of crystalline/ordered structure increased upon storage.

Isolated retrograded starch from high amylose maize was harvested and physically and chemically characterised. The results indicate that retrograded starch material is mainly amorphous with small amounts of crystallinity. Upon digestion with α-amylase however, no starch products were detected indicating that the mainly amorphous retrograded starch material is resistant to digestion. The inhibition studies showed that retrograded starch acts as a non-competitive inhibitor of PPA and can therefore still bind to the enzyme but no amylolysis occurs.

Acknowledgements

I wish to express my gratitude to my supervisors, Prof Peter Ellis and Dr Peter Butterworth for their inspiring supervision and continuing support and encouragement throughout the project. I would like to thank Dr Paul Royall for offering helpful comments on the thermal characterisation section of my work. Special thanks also has to be given to current and past members of the Biopolymers group including Dr Cathrina Edwards, Myriam Grundy, Joanne Cuff, Dr Frederick Warren and Dr Terri Grassby for useful discussions and supportive advice.

A special thanks to my collaborators at UCL; Dr Simon Gaisford for kindly letting me use the differential scanning calorimetry, David McCarthy for providing scanning electron microscopy images and Dr Gareth Williams for his expert assistance with the X-ray diffraction. I am also thankful to Richard Day, a final year Biochemistry undergraduate student, who contributed to the work on the LOS plot analysis.

In addition, I am extremely grateful for the financial support provided by the DRINC BBSRC award. Finally, my warm thanks go to my wonderful friends and family, whose support has pushed me through the long days and nights.

Presentations

(1) Binding of hydrothermally processed starch to α-amylase and its relation to the kinetics of enzyme digestion. *2nd International Conference on Food Digestion, Madrid, Spain, 6-8th March 2013.*

(2) Catalytic action of α-amylase on retrograded starch and its relation to the supramolecular starch structure. *International Conference "From Model Foods to Food Models" in Nantes, 24-26th June 2013.*

(3) Physicochemical properties of retrograded starch and its effects on starch digestibility. *DRINC 10th dissemination event in Nottingham, 27-28th November 2013.*

(4) Effects of retrogradation on the molecular structure and digestion of wheat and potato starch. *3rd International Conference on Food Digestion, Wageningen, Netherlands, 11-13th March 2014.*

(5) Preparation and characterisation of retrograded resistant starch. *The Nutrition Society Summer Meeting, Glasgow, United Kingdom, 14-17th July 2014.*

Publications

(1) **Patel, H.**, Day, R., Butterworth, P. J., & Ellis, P. R. (2014). A mechanistic approach to studies of the possible digestion of retrograded starch by α-amylase revealed using a log of slope (LOS) plot. *Carbohydrate Polymers* **113**, 182-188.

(2) Lovegrove A, Edwards CH, De Noni I, **Patel H,** *et al.* (2014). Role of Polysaccharides in Food, Digestion and Health. *Critical Reviews in Food Science and Nutrition (in press).*

(3) Butterworth, P.J., Warren, F.J., Grassby, T., **Patel, H.** and Ellis, P.R. (2012). Analysis of starch amylolysis using plots for first-order kinetics. *Carbohydrate Polymers* **87**, 2189-2197.

(4) **Patel, H.**, Butterworth, PJ and Ellis, PR. (2012). Binding of hydrothermally processed starch to amylase and its relation to the kinetics of enzyme digestion. *Proceedings of The Nutrition Society*, **71**, E229.

(5) Butterworth PJ, Warren FJ, Edwards CH, Grassby T, **Patel H** and Ellis PR. (2012). How analysis of data from alpha-amylase catalysed starch digestibility performed *in vitro* contributes to an understanding of rates and extent of digestion starchy foods *in vivo*. *The FASEB Journal,* **26**, 638.9.

Table of Contents

Abbreviations and symbols

AMG – Amyloglucosidase

AOAC – Association of Analytical Communities

AUC – Area under the curve

BCA – Bicinchoninic acid

BSA – Bovine serum albumin

CE – Catalytic efficiency

CHD – Coronary heart disease

^{13}C CP/MAS NMR – ^{13}C cross-polarization/magic-angle spinning nuclear magnetic resonance spectroscopy

dH_2O – Distilled water

Da – Dalton

DFP – Diisopropylfluoro-phosphate

DMA – Dynamic mechanical analysis

DMSO – Dimethyl sulphoxide

DSC – Differential scanning calorimetry

FAO – Food and agriculture organisation of the United Nations

FTIR – Fourier transform infrared spectroscopy

FTIR-ATR – Fourier transform infrared-attenuated total resonance

GI – Glycaemic index

GOPOD – Glucose oxidase/peroxidase

HAM – High amylose maize

HMT – Heat moisture treatment

IR – Infra red

LOS – Logarithm of slope

MC DSC – Multi cell differential scanning calorimetry

NMR – Nuclear magnetic resonance

PBS – Phosphate buffered saline

PPA – Porcine pancreatic α-amylase

RDS – Rapidly digested starch

RHAM – Retrograded high amylase maize starch

RS – Resistant starch

RVA – Rapid visco-analyser

± SEM – Standard error of mean

SAXS – Small angle X-ray scattering

SANA – Small angle neutron scattering

SCFAs – Short chain fatty acids

SDS – Slowly digested starch

SDS – Sodium dodecyl sulfate

SDS-PAGE – Sodium dodecyl sulphate polyacrylamide gel electrophoresis

SEM – Scanning electron microscopy

SGAP – Surface granule associated proteins

UCL – University College London

WAXS – Wide angle X-ray scattering

WHO – World health organisation

WM – Waxy maize

XRD – X-ray diffraction

E – Enzyme

ES – Enzyme-substrate complex

$[E]_t$ – Total enzyme concentration

K_d – Dissociation constant

k – Rate constant

C_∞ – C Infinity

[I] – Inhibitor concentration

S – Substrate

[S] – Substrate concentration

P – Product

k_{cat} – Catalytic rate constant

K_m – Michaelis-Menten constant

k_{cat}/K_m – Catalytic efficiency

K_{obs} – Observed binding rate

v – Initial reaction velocity

V_{max} – Maximum enzyme velocity

T_o – Onset gelatinisation temperature

T_p – Peak gelatinisation temperature

T_c – Conclusion gelatinisation temperature

$\Delta_{gel}H$ – Gelatinisation enthalpy

$\Delta_{ret}H$ – Retrogradation enthalpy

K_i – inhibition constant

t – Time

λ – Wavelength

2θ – 2theta

h – Hour

min – Minutes

R^2 - Correlation coefficient

Figures

Tables

Schemes

Equations

Chapter 1 Introduction

1.1 Background and project overview

Starch is one of the most complex macromolecules occurring in nature and is formed photosynthetically by plants in chloroplasts and amyloplasts, as the main energy storage molecule. A large fraction of the daily food intake in humans contains digestible carbohydrates, notably starch, with a smaller but variable amount obtained from simple carbohydrates such as sugars. Therefore as starch is an important dietary component in the human diet, there is considerable scientific interest in understanding its structure and properties and the influence these factors have on starch digestion. Starch is also of particular interest due to its wide industrial applications. As well as being an important animal feedstock, it can be used in the production of biofuels and the manufacture of so-called 'green' bioplastics (biodegradable packaging) as a substitute for traditional plastic products. Starch is also used as a food additive to thicken puddings and added to sauces and processed meat products.

The understanding of starch biosynthesis and structure has increased in recent years especially since the increasing prevalence of metabolic disorders such as Type II diabetes mellitus. However, despite the importance of starch in the human diet and its potential relevance in the management of health and disease, relating changes in starch structure to the interaction between hydrolytic enzymes and starch is still limited. Previous starch digestion studies have mainly been from a nutritional perspective and often lack an enzymological approach in interpreting the results. The purpose of this research project is to provide a more conventional approach to the study of the digestion

of native and hydrothermally processed starch using enzyme kinetics. The aim is to provide an improved understanding of the initial interaction and adsorption between α-amylase and processed starch (gelatinised and retrograded). To achieve this, starches from different botanical sources in their native and processed forms were fully characterised at the granule and molecular level using different characterisation techniques. A series of *in vitro* digestion experiments were conducted on native and processed starches to investigate the binding affinity and the rate of digestion by porcine pancreatic α-amylase acting on starch granules. The most informative enzyme kinetic parameters, K_m and k_{cat}/K_m, which are indices of the availability of starch to α-amylase and the catalytic efficiency, respectively, have been used to obtain a mechanistic understanding of the starch hydrolysis process. The differences in starch structure have then been related to the enzyme kinetic parameters to determine the effect of processing on starch structure and its influence of the susceptibility to amylolysis.

Additional experiments were also conducted to determine the inhibitory effect of pure retrograded starch on α-amylase. The purpose of this related study was to extend the experiments to investigate the catalytic action of α-amylase on processed starch by removing the digestible material leaving only non-digestible starch i.e. retrograded starch. The overall study is the first of its kind to apply a detailed enzyme kinetic approach to the digestion of native and processed (gelatinised and retrograded) starch and relate it to the supramolecular starch structure.

1.2 The physiological and clinical significance of starch

1.2.1 Starch containing food

Starch has become an increasingly prominent component in the human diet with approximately 80% of the calorie intake being attributed to this edible polysaccharide (Keeling and Myers, 2010). However there can be considerable variation in the dietary starch consumption within the human population according to whether high-starch or low-starch diets are consumed. In the latter, the food intake may consist mainly of meat source products (Perry *et al.*, 2007). The main sources of starch are cereals (wheat, maize and rice), tubers (potato) and legumes (pea), although some fruits such as banana also contain significant amounts of starch (Copeland *et al.*, 2009).

Cereal crops refer to the grain that is obtained from the graminaceous family with wheat, maize, and rice being the most common forms of starch in the human diet (World health organisation/Food and agriculture organisation of the United Nations (WHO/FAO) 1997). Cereals generally contain about 65-75% carbohydrate of which starch is the main component. Cereal grains are normally processed to make flour, bread, pasta and breakfast cereals; however, rice is a cereal that is often consumed with minimal processing. Root and tuber crops also make a significant contribution to the starch intake in the human diet. The main types of starch-rich crops are potato, cassava, yams, sweet potato and taro. Tuber crops generally contain about 15-30% carbohydrate (mainly starch) (WHO/FAO 1997). Other sources of starch include pulses, which contain a high starch content (approximately 40-50% in the dried seed) and contribute largely to the dietary intake in some countries (McCance and Widdowson, 2002).

However, the overall consumption of pulses in the United Kingdom is relatively low compared with the intake of foods made from cereal and tuber crops (Kearney, 2010).

1.2.2 Postprandial glycaemia and the glycaemic index (GI)

Understanding the rate, extent and mechanism of the starch digestion process in the gastrointestinal tract is vital to understanding the physiological response triggered from consuming starchy based foods. It was once generally assumed that starch containing foods were digested at a similar rate, although more slowly than simple sugars, resulting in similar postprandial blood glucose concentrations (Bornet *et al.*, 1997). However, studies from the 1970's have shown this is not the case. Work by Crapo and colleagues showed large variations in postprandial blood glucose and insulin responses when starchy foods were digested (Figure 1.1) (Crapo *et al.*, 1977; Crapo *et al.*, 1981). The group demonstrated that dextrose (glucose) and potato produced the highest plasma glucose and insulin concentrations, whereas rice, maize and wheat elicted significantly lower responses. This early research work was the first to highlight differences in the rate of digestion and postprandial glycaemia of different starch foodstuffs. Since then, many researchers have supported the initial findings of Crapo et al. and confirmed that the rate of digestion for different starchy foods varies markedly (Jenkins *et al.*, 1981; Brand *et al.*, 1985; Wolever *et al.*, 1991; Goñi *et al.*, 1997; Englyst *et al.*, 1999).

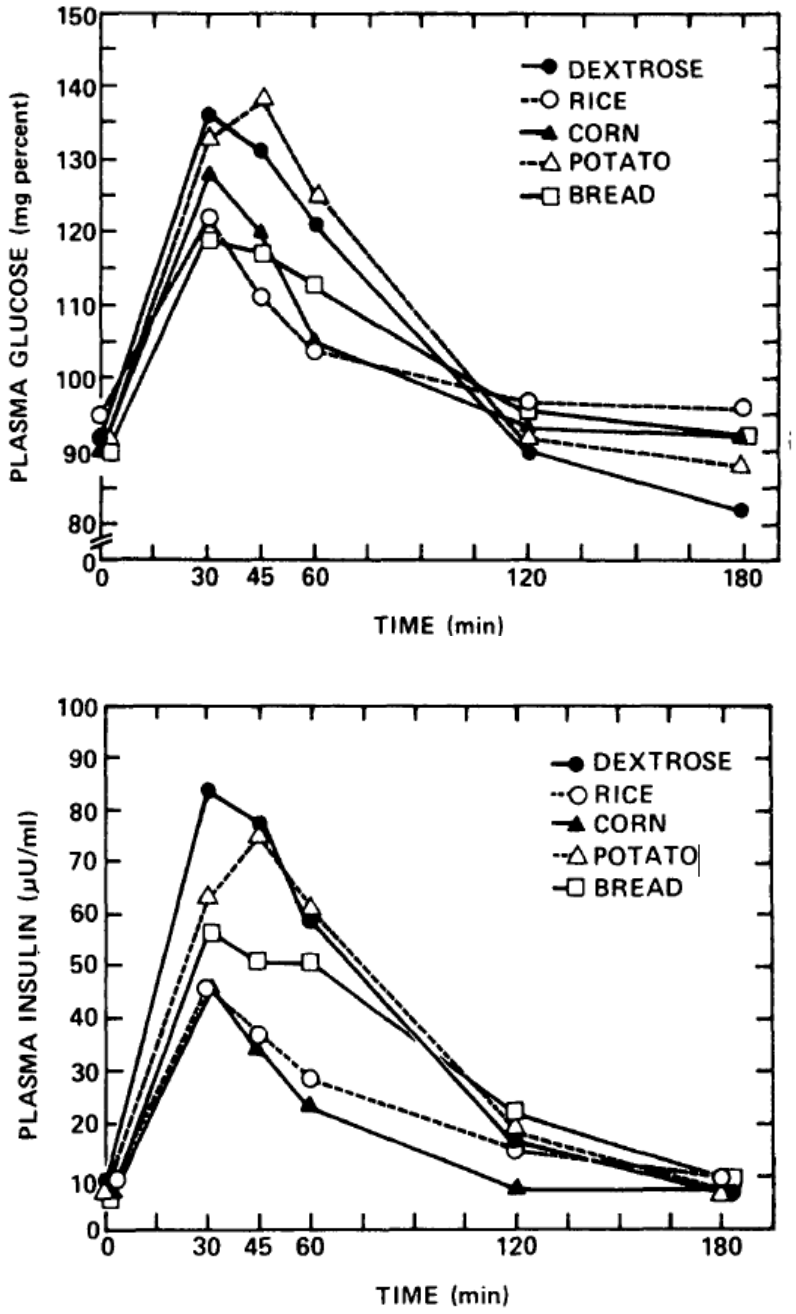

Figure 1.1. Postprandial plasma glucose (top) and insulin concentrations (bottom) after consumption of different starchy foods. Images adapted from (Crapo et al., 1977).

Based upon the postprandial glycaemic response, the term 'glycaemic index (GI)' was introduced and popularised by Jenkins and colleagues (Jenkins *et al.*, 1981). The GI concept was introduced as a method to assess and classify the

postprandial glucose response to foods to provide complementary data on chemical composition given in food tables. The GI is now widely regarded as a useful, physiological mechanism to classify carbohydrate containing foods according to their postprandial glycaemic effect (Foster-Powell *et al.*, 2002).

The glycaemic index is an *in vivo* measure of available carbohydrate in foods, based upon the postprandial glucose response. After an overnight fast, human subjects are provided with a standard weight of available carbohydrate (starch and sugars) in a test food, usually 50 g. The plasma glucose concentration is then measured at certain time points for up to two hours to profile the glucose concentration against time. The area under the blood glucose curve (AUC) over a 2h period following consumption of food is then compared with the AUC from the reference food (normally 50 g of starch in a white bread or pure glucose in water). The AUC after the consumption of the test food is expressed as a percentage of the standard (Figure 1.2). Thus, the GI is calculated using the following equation.

GI = (AUC of postprandial glucose response following ingestion of test food / corresponding AUC of control food) x 100

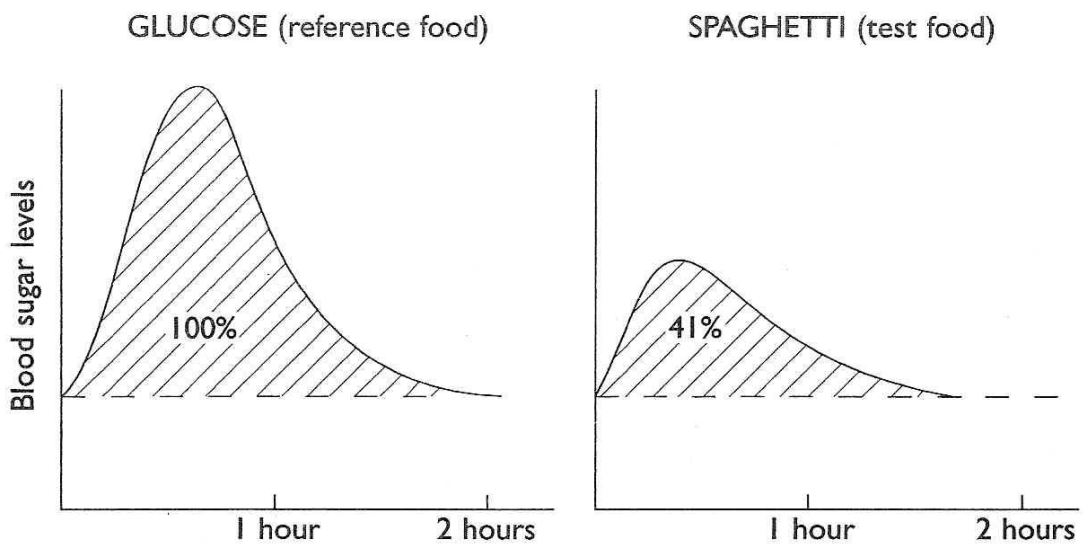

Figure 1.2. The blood glucose concentrations after consumption of reference food (50 g of pure glucose or available carbohydrate in white bread) and test food. The AUC for the test food is compared to the reference food to determine the GI. Figure reproduced from (Leeds et al., 2003).

Foods can be separated into two main categories, i.e., high GI and low GI. High GI foods are digested at a fast rate (rapidly digested starch), resulting in a high postprandial glucose response. Low GI foods result in a lower postprandial glucose response because they are digested at a slower rate (slowly digested starch) (Wolever and Miller, 1995). Table 1.1 shows the standardised GI values for different carbohydrate containing foods. Processed starches (pasta, biscuits) tend to have lower GI values relative to cereal starches (bread and rice). Boiled and mashed potatoes have a much higher GI value and approach that of pure glucose. Legumes however, have the lowest GI values indicating a slow digestion.

Table 1.1. GI values from different carbohydrate containing foods. Table adapted from (Jenkins et al., 1981).

Carbohydrate food	GI
Biscuits	54 ± 4
Spaghetti	50 ± 8
Bread	69 ± 5
Rice	72 ± 9
Boiled potato	70 ± 8
Mashed potato	80 ± 13
Chickpeas	36 ± 5
Kidney beans	29 ± 8

1.2.3 Health benefits of a low glycaemic diet

A low glycaemic diet is comprised of low GI carbohydrate based foods. A number of potential health benefits are believed to arise from a diet rich in foods that are slowly digested and absorbed, resulting in small postprandial glucose and insulin responses (Björck *et al.*, 2000). Reductions in the plasma glucose and insulin concentrations are considered to be beneficial in improving the dietary management and reducing risk factors of a number of non-infective diseases including Type II diabetes, cardiovascular disease and obesity (Wolever, 2000; Foster-Powell *et al.*, 2002; Sluijs *et al.*, 2010). The latter is also commonly considered to be the primary predictor of Type II diabetes. Type II diabetes is a condition in which the insulin receptors do not respond to the action of insulin and therefore become insulin resistant. This causes the beta islet cells in the pancreas to produce more insulin eventually resulting in beta

cell death. A regulated low GI diet and/or hypoglycaemic drugs control the blood glucose levels in patients with Type II diabetes (Brand-Miller *et al.*, 2003; Jenkins *et al.*, 2008).

A diet consisting of low GI starch-containing foods, as opposed to one with high GI foods, will result in a slower digestion rate, consequently resulting in the final product of starch hydrolysis (i.e. glucose) being more slowly absorbed into the blood circulation. Therefore low GI foods are characterised as those that produce a lower postprandial blood glucose response with a concomitant reduction in blood insulin concentrations. This insulin response usually means that the beta islet cells in the pancreas secretes less insulin and thereby reduces the risk of insulin receptors developing resistance (Frayn, 2009). This improves the long-term glycaemic control in individuals with Type II diabetes. Numerous clinical trials have been conducted to show the benefits of low GI diets (Brand *et al.*, 1991; Järvi *et al.*, 1999; Chandalia *et al.*, 2000; Brand-Miller *et al.*, 2003).

Low GI diets are also considered to be an important factor in controlling coronary heart disease (CHD). It has been suggested that a high glycaemic diet, in which the blood glucose concentrations increase, results in an increased risk of CHD. A diet consisting of slowly digested carbohydrates produces favourable blood lipid profiles which may reduce the risk of CHD (Liu *et al.*, 2000; Liu, 2002; Halton *et al.*, 2006). Frost et al. showed that increasing the GI resulted in a decrease in HDL-cholesterol and therefore the glycaemic index

can be a helpful index for predicting the plasma HDL-cholesterol levels (Frost *et al.*, 1999).

1.2.4 Factors that influence the postprandial glycaemic response

Variation in the glycaemic index results from difference in the rate and extent of starch digestion. Several factors have been identified that can influence the rate of starch digestion. These include inherent properties of the native material (particle size, amylase resistant starch and amylose and amylopectin content), protein and lipid interaction, α-amylase inhibitors and the presence of anti-nutrients. Manipulating the processing conditions can severely change starch structure and thus affect the rate of digestion. The external environments of starch (intact cell wall for example) can also play a vital role in determining the digestibility of starch (Arvidsson-Lenner *et al.*, 2004; Brouns *et al.*, 2005; Edwards *et al.*, 2014).

The presence of intact starch granules encapsulated by a cell wall has been known to reduce the hydrolysis rate of starch by acting as a physical barrier and limiting amylase access into the granule and therefore slowing the release of hydrolysed products of starch out of the plant food matrix (Tovar *et al.*, 1992). Cell walls hindering the swelling and solubilisation properties of starch also affect the degree of gelatinisation and digestibility (Würsch *et al.*, 1986; Edwards *et al.*, 2014). Therefore starchy varieties, especially legumes, can have different GI values depending upon their starch bioavailability (Tovar *et al.*, 1990; Osorio-Díaz *et al.*, 2005).

A number of crop plants have also been known to produce high affinity proteinaceous amylase inhibitors, a common anti-nutrient, as a defence mechanism for protection against parasites (Snow and O'Dea, 1981; Le Berre-Anton V, 1997). Such inhibitors reduce pancreatic amylase activity in the small intestine and subsequently reduce the postprandial increase in glucose levels (Layer *et al.*, 1986; Boivin *et al.*, 1987). However most inhibitors denature at high temperatures, and therefore the potential to restrict starch digestion is often limited.

Many reports have shown that processed high amylose starches are associated with a lower metabolic response due to increased levels of resistant starch (Liljeberg *et al.*, 1996; Åkerberg *et al.*, 1998). Amylose can also associate with lipids to form an amylose-lipid complex, which is less susceptible to digestion and significantly lowers the postprandial blood glucose concentration (Goddard *et al.*, 1984; Cui and Oates, 1999). The reported gelatinisation temperature of high amylose starches is also much higher than normal starches and is believed to result in incomplete gelatinisation during cooking (Holm *et al.*, 1988; Hoebler *et al.*, 1999). The effect of starch retrogradation is another factor that plays a role in influencing the rate of digestion. The early stage of retrogradation is primarily attributed to amylose and the resulting material is resistant to amylase attack. Therefore the retrogradation effect is expected to be higher for high amylose varieties with significant effects on the postprandial glycaemic response (Frei *et al.*, 2003).

The starch fraction that escapes digestion in the small intestine and is resistant to amylolysis is termed resistant starch (RS). Englyst and colleagues have categorised resistant starch into three classes, but other authors, however, have classified RS into four classes; Type 1 is starch granules that are entrapped in the food matrix and therefore physically inaccessible to digestible enzymes, Type 2 is native (uncooked) starch granules, Type 3 is retrograded starch formed in cooked and cooled starch and Type 4 is chemically modified starch (Englyst *et al.*, 1992; Haralampu, 2000; Perera *et al.*, 2010). The RS content of food is highly variable (i.e. cereals contain <3% RS, whereas green bananas contain ~75%) and depends heavily on processing conditions (Bravo *et al.*, 1998). The molecular structure of retrograded starch (RS3) has been studied extensively by many groups and is considered to be enzyme resistant (Sievert and Pomeranz, 1989; Eerlingen and Delcour, 1995; Gidley *et al.*, 1995; Htoon *et al.*, 2009). Therefore foods containing a greater proportion of RS are generally associated with a lower GI (Björck *et al.*, 2000; Han *et al.*, 2006).

The majority of the interest in RS however, is focused on the fermentation of resistant starch, by colonic microorganisms, into short-chain fatty acids (SCFAs), particularly butyrate (Cummings and Macfarlane, 1991), which is metabolised by cells of the colonic epithelia and is now considered to provide protection against colo-rectal cancer. SCFAs also provide additional benefits by stimulating colonic blood flow, increasing nutrient circulation, inhibit bacterial growth and prevent the absorption of toxic and carcinogenic compounds (Topping and Clifton, 2001; Brouns *et al.*, 2002; Topping *et al.*, 2003). Propionate, another end product of fermentation, is reported to be an effective

agent in helping to reduce the plasma cholesterol levels by inhibiting cholesterol synthesis (Hara *et al.*, 1999; Wong *et al.*, 2006) RS also has potential to function as a prebiotic, a non-digestible carbohydrate, which stimulates the growth of bacteria in the colon and may therefore improve the properties of the indigenous flora (Nugent, 2005; Fuentes-Zaragoza *et al.*, 2010).

Native starches in the semi-crystalline form are hydrolysed by amylase very slowly (e.g. potato). However upon gelatinisation in excess water, the amorphous starch material is rapidly digested and the amylolysis rate increases drastically (Bornet *et al.*, 1989; Chung *et al.*, 2009). As mentioned before, the storage of gelatinised starch results in the formation of retrograded starch material, which reduces the rate of digestion by having enzyme resistant properties. Studies have reported that the GI values can be estimated from the amount of rapidly digested starch (RDS) and slowly digested starch (SDS) available (Englyst *et al.*, 1999; Zhang *et al.*, 2006; Englyst *et al.*, 2007). A recent study has even shown waxy rice starch with a low RDS and high SDS fraction is associated with a reduced GI (You *et al.*, 2014). Therefore the physical state of starch-rich foods can greatly influence starch digestion and absorption and have a direct impact on the postprandial glucose and insulin responses.

1.3. Starch Structure

Starch is not only a major polysaccharide but it is also one of the most complex macromolecules in nature, despite the fact that it consists of only one monosaccharide repeating unit, i.e. glucose. Previous studies of starch structure using light and scanning electron microscopy (SEM) show starch

granules to have a semi-crystalline granule structure. Microscopy images have revealed starch properties vary in granule size and shape depending upon the botanical starch source. Such differences, along with the proportion of amylose/amylopectin and degree of crystallinity, are known to have significant implications on the digestion kinetics of native and hydrothermally processed (i.e. domestic and industrial cooking) starch.

1.3.1. Starch composition

1.3.1.1. Amylose and amylopectin

Starch granules consist of two main polysaccharides, amylose and amylopectin, with each containing a long chain of anhydroglucose polymers. Amylose consists of essentially straight α-glucan chains and is a smaller molecule with a molecular weight of 10^5 – 10^6, compared with amylopectin which has a molecular weight of 10^7 – 10^9 (Tester *et al.*, 2004). The straight chain glucose residues in amylose and amylopectin are connected by α(1-4) glycosidic bonds; however, amylopectin also contains α(1-6) linked branches resulting in a highly branched macromolecule (Figure 1.3). The incomplete degradation of amylose suggests a small degree of α(1-6) linked glucan branch points may also be present (Wang *et al.*, 1998). Typically most starches consist of 15-30% amylose with the remainder assigned to amylopectin, although genetically modified starches can result in low to high amylose values (Fredriksson *et al.*, 1998; Tahir *et al.*, 2010). These mutant starches can have major effects on the physicochemical properties of starches (Bogracheva *et al.*, 1995).

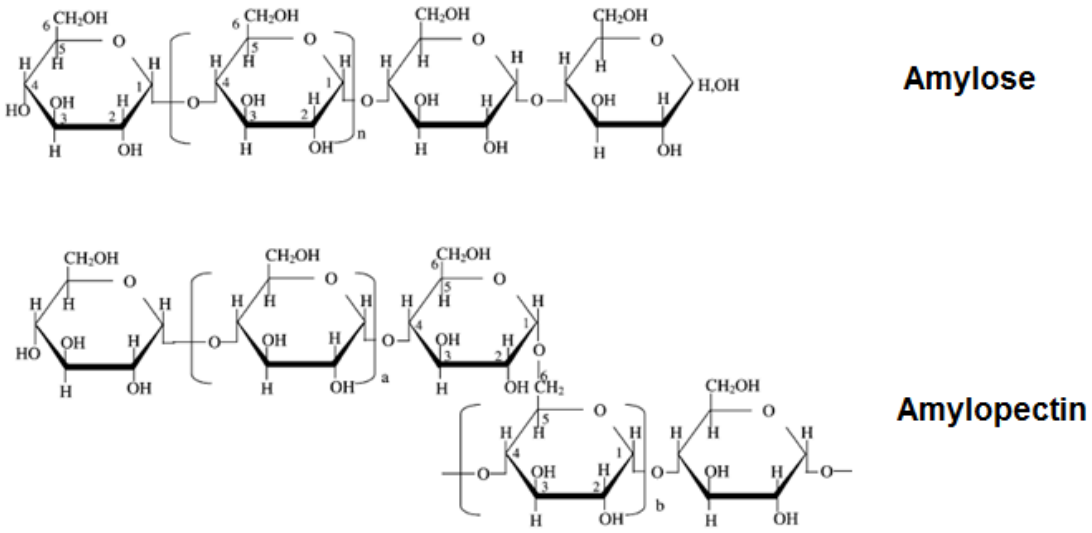

Figure 1.3. Arrangement of α-glucan polymers in amylose and amylopectin. The diagram is adapted from Tester and colleagues (Tester et al., 2004).

In aqueous solution amylose chains have a random coil conformation but can also co-crystallise with a variety of complexing agents such as iodine, dimethyl sulphoxide (DMSO) and fatty acids. Amylose chains form a single left handed helix with six residues per turn with the complexing agent residing in the middle of the hydrophobic cavity (Figure 1.4). This is commonly observed in the amylose-fatty acid complex with the aliphatic part of the lipid located within the hydrophobic core of the helix and the polar group exposed outside (Buléon *et al.*, 1998). This yields the V-type complex which can be observed using DSC and XRD (Zobel *et al.*, 1988). In the absence of complexing agents, amylose can occupy a six fold left handed double helical conformation (Hsein-Chih and Sarko, 1978; Dona *et al.*, 2010). This was investigated using X-ray crystallography and solid state ^{13}C NMR, which showed a type B double helical pattern (discussed in Section 1.3.2) (Gidley, 1989; Pérez and Bertoft, 2010). Another common complex formed is the amylose-iodine inclusion complex

which requires iodine to be dissolved in a basic solvent such as DMSO forming triiodide (I_3^-) ions. The ions then align themselves in the groove of the helical amylose arrangement resulting in a colour change from red to blue. Therefore, this is the most commonly used technique to analyse amylose content in starches (Knutson, 1986; Chrastil, 1987).

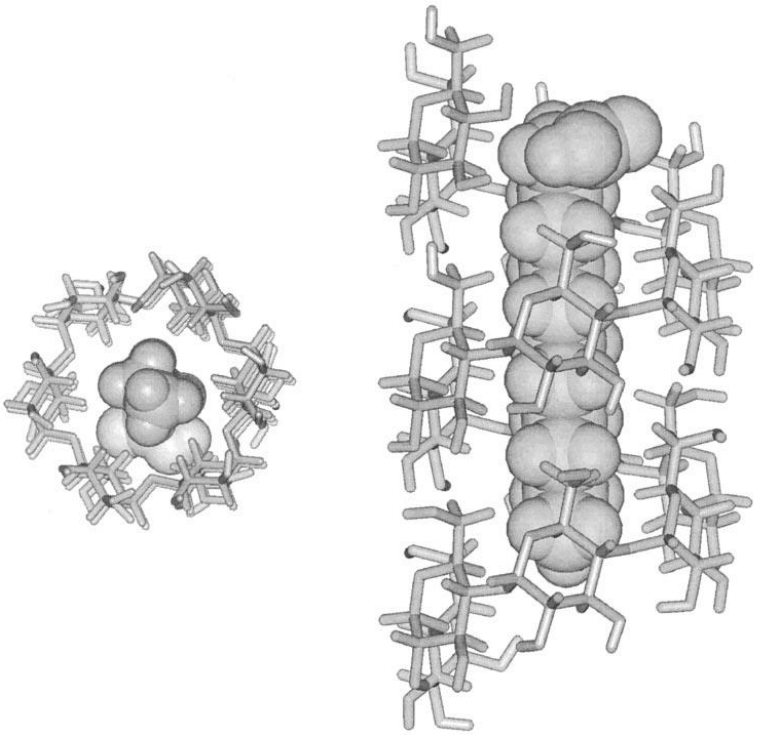

Figure 1.4. Molecular model showing the amylose-fatty acid complex. The fatty acid is located within the hydrophobic cavity of the amylose helix. Adapted from Buléon and co-workers (Buléon et al., 1998).

Amylopectin is a much larger carbohydrate polymer compared with the smaller amylose polymer and consists of a complex branching structure due to 5-6% α(1-6) linkages. Even though the structure of amylopectin is very similar to glycogen, the branch points for glycogen are more frequent with the amylopectin branch point located every 20-25 glucose residue. This results in

the amylopectin structure occupying more space and being larger by weight (Ball *et al.*, 1996).

Early models of amylopectin aim to describe the structure with the Haworth model suggesting multiple side chains branching off one linear chain. The Staudinger model suggests a series of branched chains that are attached to the next chain via 1-6 linkages so that each chain has at least one branch point. The Myer model is a combination of both models suggesting a cluster type structure made up of different poly-glucose residues in length (Beckmann, 1953). The widely accepted amylopectin cluster model is classed into S (small) and L (long) chains. S chains contain 11-16 glucose residues and L chains contain 40-45 sugars (Bogracheva *et al.*, 1995). These chains are further classed into A, B and C glucose chains. The shorter A chains are connected by α(1-6) linkages to the rest of the molecule, longer B chains bind to either one or several chains and the C chain possesses the reducing end. The B chains can be divided into 4 groups, B1-B4, with B1 having the shortest chain length and B4 having the longest chain length (Hizukuri, 1986; Bertoft, 1991). It is also generally accepted that there are slightly more short A chains than longer B chains (Buléon *et al.*, 1998; Yao, 2004).

1.3.1.2. Minor components

Much of the starch granule is composed of amylose and amylopectin polymer chains however very small quantities of non-starch components such as protein and lipids are also present. The moisture content is normally between 10-15% (w/w). The lipid content is generally considered to be very low, with values

between 0.5-1% (w/w), whereas the protein content is usually below 0.5% (w/w). The mineral content is normally very low and therefore can be considered to be negligible (with the exception of potato starch which have negatively charged phosphate ions that increase the swelling properties by associating with amylopectin) (Blennow *et al.*, 2002; Tester *et al.*, 2004; Blennow and Svensson, 2010). Some variations can occur due to the different botanical origins such as cereal starches having relatively high levels of lipids and proteins compared with tuber starches (Swinkels, 1985).

The lipid fraction in a starch-lipid interaction mainly consists of free fatty acids which associate with amylose chains, forming an amylose-lipid complex (see Figure 1.4 above). Significantly higher concentrations of lipids are found at the periphery of the granule than at the core, which is most likely due to the high levels of amylose also located at the periphery (Jane and Shen, 1993; Kuakpetoon and Wang, 2007). The amylose-lipid interactions can have a significant influence on the functional properties such as starch digestibility. The complexes can be inaccessible to digestive enzymes and therefore reduce susceptibility to amylolysis (Svihus *et al.*, 2005). The presence of lipids can also reduce starch swelling and solubility, which in turn influence the extent of starch gelatinisation (Brennan *et al.*, 1996; Vasanthan and Bhatty, 1996).

The proteins found in starch granules are mainly storage proteins and starch granule associated proteins (SGAP). The former are loosely bound to the surface of the granule while the latter are tightly associated with the surface or interior of the granule (Han and Hamaker, 2002). SGAP are mainly starch

synthesis enzymes that are left over after the granule synthesis process (Baldwin, 2001). The presence of proteins may reduce susceptibility to amylolysis by forming a network that acts as a physical barrier between starch and amylase (Brennan *et al.*, 1996; Vasanthan and Bhatty, 1996).

1.3.2. Supramolecular starch structure

Light microscopy shows starch granules have a semi-crystalline structure separated by amorphous regions, commonly referred to as growth rings (100-500 nm wide) (Buléon *et al.*, 1998). SEM was also used to observe the growth rings after acid hydrolysis which removes the amorphous rings leaving the resistant crystalline material to be examined (Planchot *et al.*, 1995). The semi-crystalline growth ring consists of repeating 9 nm layers of crystalline and amorphous lamella observed by small angle neutron (SANS) and X-ray (SAXS) scattering (Blazek *et al.*, 2009; Lopez-Rubio and Gilbert, 2009; Blazek and Gilbert, 2011). The crystalline region (5-6 nm wide) is attributed to the clustered amylopectin while the amorphous region (3-4 nm wide) contains α(1-6) amylopectin branches and linear amylose chains with an increasing concentration of amylose surrounding the hilum (Jenkins *et al.*, 1994; Gallant *et al.*, 1997; Oates, 1997). However amylose-lipid complexes (V-type) have been suggested to be located in the crystalline lamella (Kozlov et al., 2007). The granule starch structure is best described by the schematic diagram in Figure 1.5.

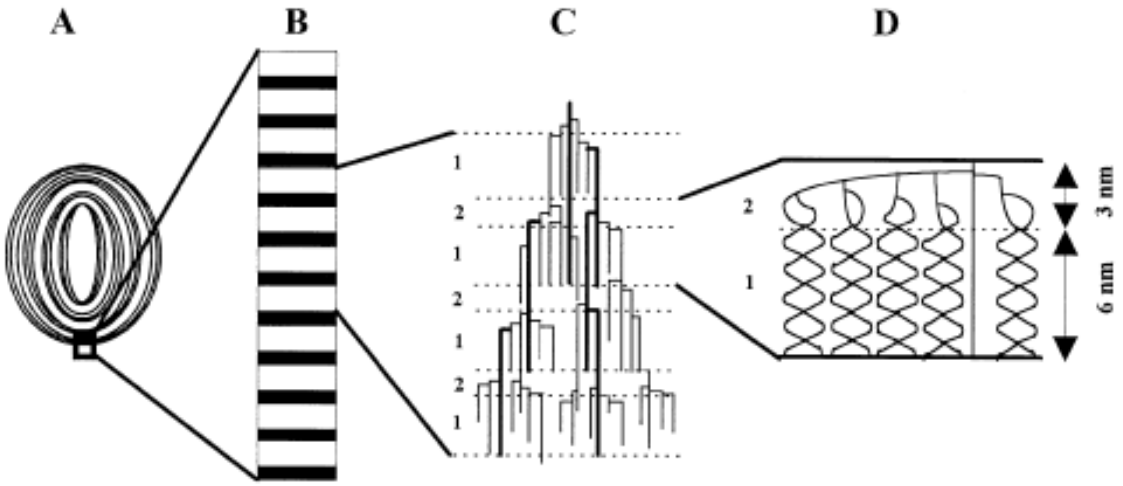

Figure 1.5. Growth rings from a cross section of a starch granule, consisting of alternating layers of semi-crystalline and amorphous material (A). Semi-crystalline growth ring showing the repeating crystalline lamella in white and the amorphous lamella in black (B). Amylopectin clusters located in the semi-crystalline growth ring (C, D). The crystalline lamella (1) shows the clustered amylopectin and the amorphous lamella (2) shows the α(1-6) branch points (Ball et al., 1996).

The amylopectin chains form a double helical structure with 6 residues per turn stabilised by interchain hydrogen bonds and Van deer Waals forces. The specific arrangement of double helical amylopectin chains gives rise to two types of polymorph structures; A-type and B-type starches. Starch types have been investigated using X-ray diffraction (XRD), which also allows the degree of crystallinity to be estimated (Millan-Testa *et al.*, 2005). Different starch types give a specific XRD pattern, allowing starches to be classified as type A, B or C. A-type starches, observed in cereals, have a closely packed arrangement of amylopectin double helices. The tight helix packing only allows eight water molecules per unit cell. B-type starches, observed in tubers, have a looser

double helix packing and therefore allow more water binding (36 water molecules per unit cell) (Figure 1.6). Some starches, such as those from legumes (e.g. pea, chickpea) and banana have a mixture of A and B type crystalline material; these are referred to as type C starches. The specific arrangement of helices in A and B type starches also influences starch digestibility with A starches being more susceptible to hydrolysis compared to B types (Jane *et al.*, 1997; Zhang *et al.*, 2006).

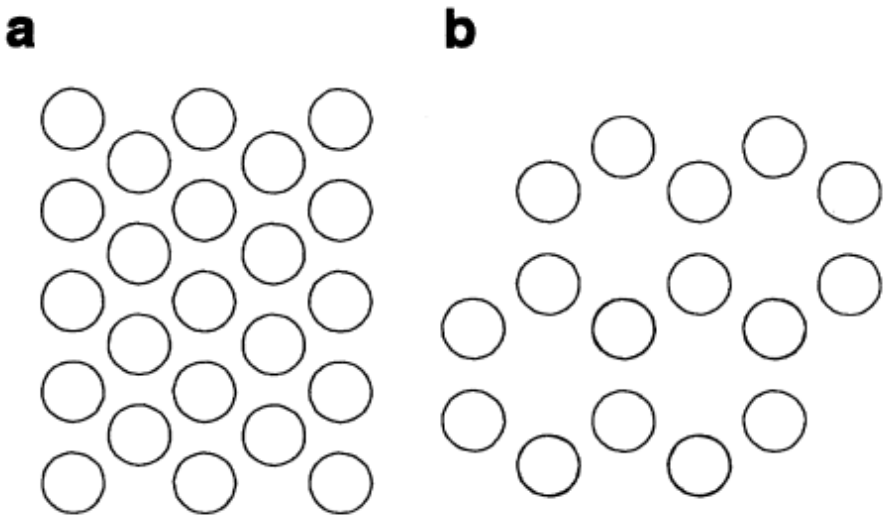

Figure 1.6. Arrangement of amylopectin double helices in A-type (a) and B-type (b) starches. Circles indicate chains as viewed looking down each helix with B-type helical chains arranged in a hexagonal array. Adapted from (Sarko and Wu, 1978).

Even though structural information is known about the amylopectin chains in the individual lamella, very little is known about the overall assembly of the chains within the semi-crystalline region. The specific arrangement of crystallites can be viewed using light microscopy fitted with cross polarising filters. The starch granule exhibits a birefringent pattern showing the characteristic ‘Maltase

cross', indicating a high degree of molecular orientation in the granule (Bogracheva *et al.*, 2002). The centre of the Maltase cross, called the hilum is the original growth point of the starch granule. The amorphous regions however lack such ordered material and therefore polarised filters only allow crystalline regions to be observed. When using specific plates like a *λ* plate, the crystalline and amorphous regions of the starch granules have different colours. The amorphous regions cannot be distinguished from the pink background while the crystalline regions have a blue and yellow colour according to whether crystallites are arranged towards or perpendicular to the plane of polarisation (Wang *et al.*, 1998).

Oostergetel and van Bruggen proposed the first three-dimensional model to explain the semi-crystalline regions of potato starch (Oostergetel and van Bruggen, 1993). Using electron optical tomography and cryo-electron diffraction, the group were able to examine the crystalline sections of potato starch granules. They concluded the double helical amylopectin chains located in the crystalline domains have a continuous network of left-handed helices, forming a super helical structure. Interlocking between adjacent helices also results in a tetragonal organisation. Therefore the complex arrangement of helices acts as a scaffold for the starch granule to build around (Figure 1.7).

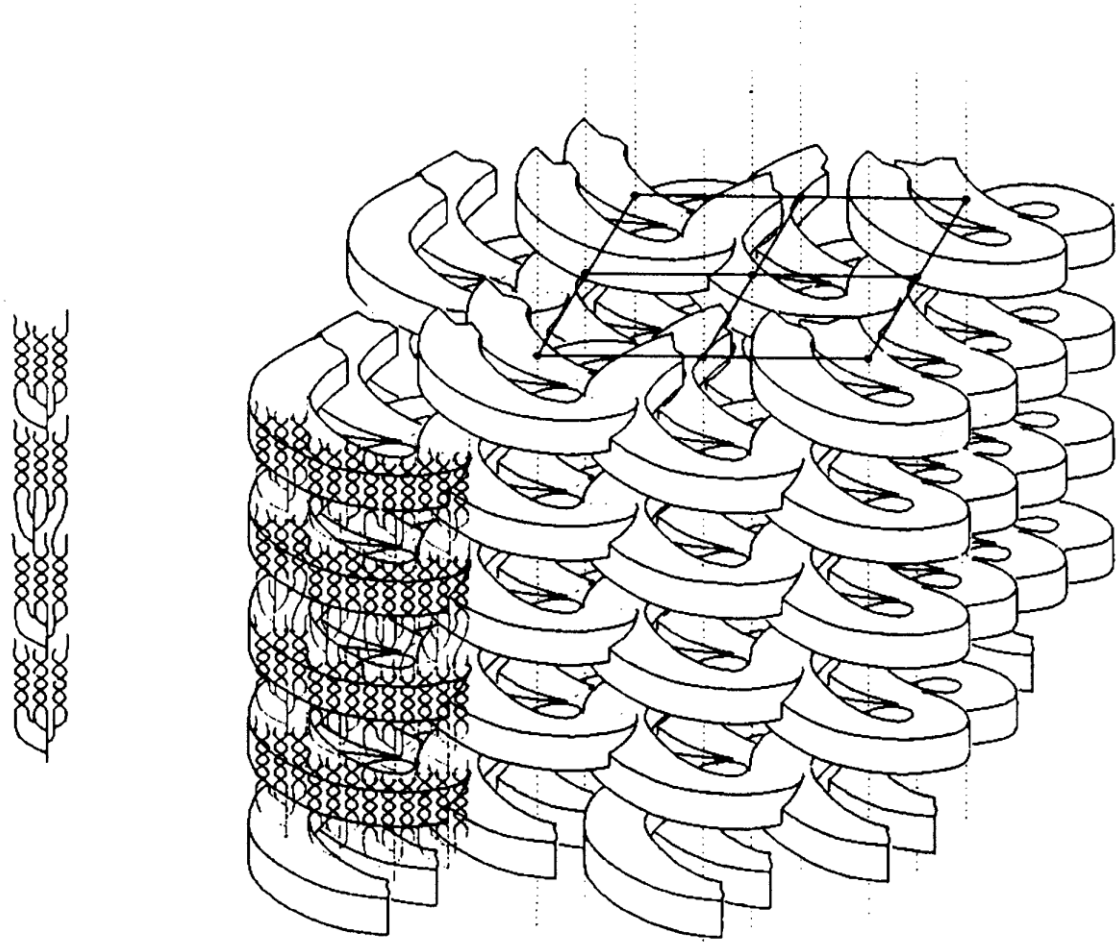

Figure 1.7. Three-dimensional reconstruction model of potato starch crystallites showing the left handed super helical arrangement of amylopectin chains. The amylopectin cluster model is shown on the left. Adapted from Oostergetel and van Bruggen (Oostergetel and van Bruggen, 1993).

A more commonly accepted model is that proposed by Gallant and co-workers. The group studied enzyme-hydrolysed starch granules using atomic force microscopy (AFM) and electron microscopy (Gallant *et al.*, 1997; Baldwin *et al.*, 1998). They observed the double helical amylopectin chains were arranged into spherical-like blocklets found in the crystalline and amorphous regions of the starch granule. These small and large blocklets vary in size depending upon the botanical starch source and location. The sizes of the blocklets play a crucial

role in granule structure. Blocklets are arranged in the amorphous and crystalline regions of the starch granule, with small blocklets (25 nm in diameter) located in the soft amorphous shell and large blocklets (80-120 nm in diameter) in the hard crystalline shell (Figure 1.8). Small blocklets result in a smooth surface while large blocklets result in multiple protrusions at the surface (Gallant *et al.*, 1997; Baldwin *et al.*, 1998). Defects in blocklet structure may also be present in the amorphous shell due to the presence of amylose (Ridout *et al.*, 2003).

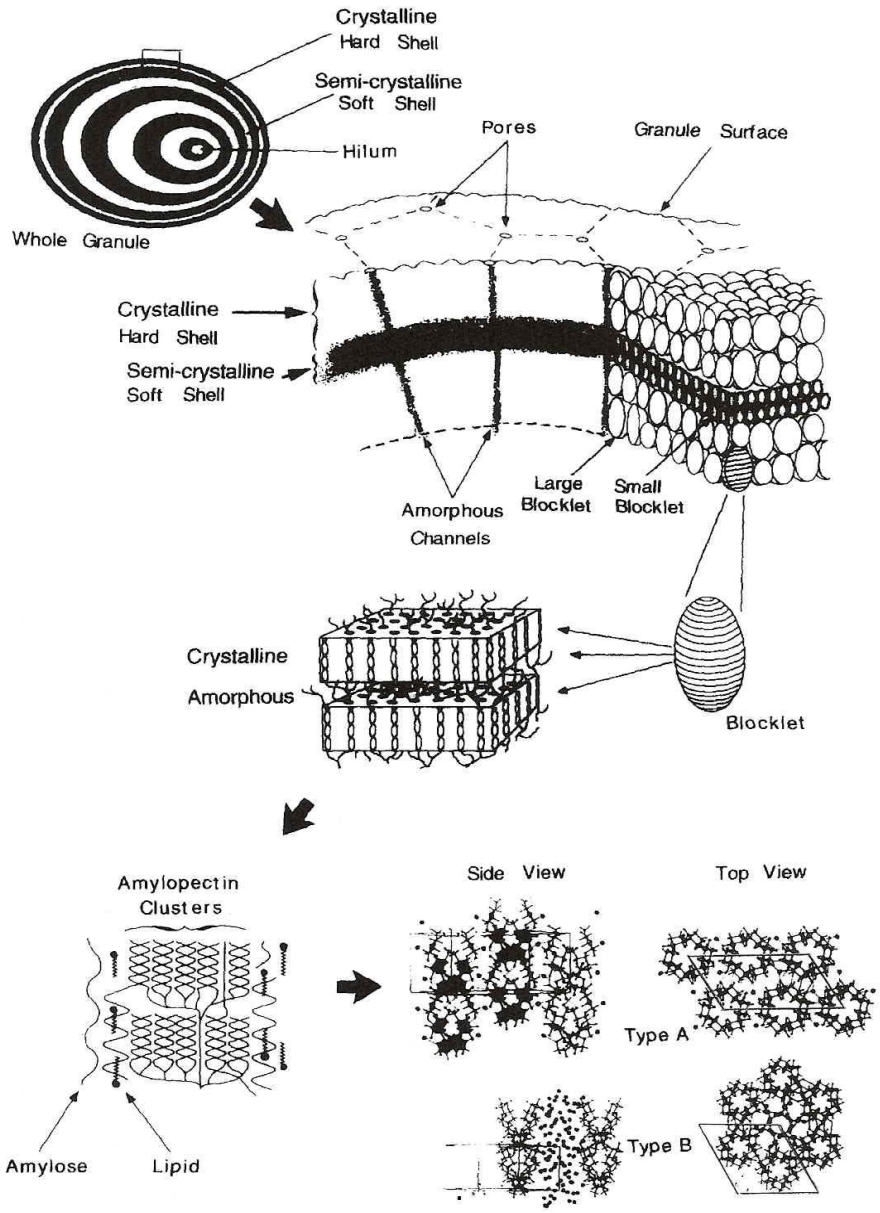

Figure 1.8. Starch structure represented by Gallant's blocklets model. The lowest level of granule organisation, shown at the top, shows the hard crystalline shell with large blocklets and the soft semi-crystalline shell with smaller blocklets. Each blocklet contains separating crystalline and amorphous layers. The highest level of granule organisation, shown at the bottom, shows linear amylose chains and chains associated with lipids to form the amylose-lipid complex. The double helical structure of amylopectin chains in an A-type or B-type starch is also shown (Gallant et al., 1997)

1.3.3. Granule morphology and particle size

Starch in edible plant tissue is always surrounded by a cell wall unless the plant material has been mechanically processed (e.g. milling), which removes some or all of the starch (e.g. wheat flour has a high proportion of ruptured cell walls and therefore contains some free starch). The granular starch structure varies in size with the diameter ranging from 1 to 100 µm depending upon the botanical starch source. Typically, wheat granules are much smaller than potato granules, with size ranges of 2-35 µm and 15-75 µm, respectively (Pérez and Bertoft, 2010). Starch granules also vary in shape depending upon the botanical origin. Maize starch appears to have an edged and polygonal structure with potato having an oval and near-spherical shape. Wheat starch however has bi-modal size distributions with large (22-36 µm) A granules showing a lenticular shape and small (2-3 µm) B granules with a spherical shape (Jane *et al.*, 1994; Tester *et al.*, 2004). A study by Ao and Jane on wheat starch showed large A granules have more B2 amylopectin chains than small B granules (Ao and Jane, 2007). This results in a specific arrangement of amylopectin chains giving A and B granules their unique shape. Genetically modified starches such as high amylose (70%) starches result in elongated and irregular structures showing the importance of amylopectin in maintaining granule structure and morphology (Bogracheva *et al.*, 1995).

Some starches (maize, sorghum, waxy maize and millet) have pores randomly distributed over the granule surface providing a channel into the granule interior. However such porous surfaces are absent in certain starches such as potato and canna and most likely contribute to their resistant nature (Dhital *et al.*,

2010). Large granules in starches with a bi-model distribution such as wheat and barley also have surface pores (MacGregor and Ballance, 1980; Fannon *et al.*, 1992). The presence of these porous channels allows enzymes to enter and hydrolyse the starch granule from the inside out, and therefore affects the rate of starch digestibility (Fannon *et al.*, 1992; Helbert *et al.*, 1996; Dhital *et al.*, 2010; Dhital *et al.*, 2014).

1.3.4. Starch gelatinisation

Profound structural changes occur when starch is heated in excess water (>70% w/v). This endothermic process is termed starch gelatinisation. To achieve such structural changes, starches have to be heated to a specific temperature, known as the gelatinisation point. The gelatinisation point is normally between 50-80^{o}C but can vary for different starch sources and is often determined by differential scanning calorimetry (DSC) (Wang *et al.*, 1998; Bogracheva *et al.*, 2002). For example, mutant starches such as high amylose starches have a gelatinisation point of ~120^{o}C with the width of the transition peak being much wider. As the temperature increases, the original native starch crystalline structure begins to occupy a disordered form. The hydrogen bonds, which provide stability between the polymer chains, begin to break causing the amylopectin double helices to unwind. Water also enters the granule causing rapid swelling and a complete loss of crystalline structure (Jenkins and Donald, 1998). The α-glucan chains become exposed rather than being buried inside the granule, resulting in a greater potential for α-amylase to bind and hydrolyse the chains. Heat input thereby increases susceptibility to starch hydrolysis.

Starches heated in limited water (<30% w/v) results in incomplete or partial gelatinisation. This is commonly observed in the production of biscuits in which the granular native structure is maintained and is apparent under a light microscope (Varriano-Marston *et al.*, 1980; Englyst *et al.*, 2003; Mamat *et al.*, 2010). Therefore crystalline starch granules still remain due to the limited water content and a higher temperature is often required to melt the remaining starch granules. The melting can be followed using DSC in which an endothermic peak appears at a higher temperature. The process of heating starch material in limited water is commonly referred to as 'heat-moisture treatment' (HMT). A few authors have tried to distinguish between HMT and the annealing process. Annealing refers to the heating of starch below the gelatinisation point with an intermediate water content, whereas HMT refers to high temperature heating (100^{o}C) in restricted water (Jacobs and Delcour, 1998; Collado and Corke, 1999).

SEM images from Slaughter and workers show a complete loss of starch structure upon heating in excess water at temperatures above the gelatinisation range (Slaughter *et al.*, 2002). The loss of the natural crystalline state can also be viewed under a light microscope with polarised filters, as the Maltese cross observed with native granules is absent in gelatinised samples (Koch and Jane, 2000). Different characterisation methods have been used to quantitatively study the loss of order and crystallinity during starch gelatinisation at the molecular scale. Such methods include X-ray diffraction (XRD), differential scanning calorimetry (DSC) and ^{13}C cross-polarisation/magic angle spinning nuclear magnetic resonance spectroscopy (^{13}C CP/MAS NMR).

XRD gives an identification of the amount of crystallinity, whereas ^{13}C NMR measures the double helical order content. Cooke and Gidley (1992) showed a relationship between the enthalpy change, determined using DSC, and the degree of crystallinity and molecular order content. The group found that the molecular order values were consistently higher than the degree of crystallinity. Therefore they concluded that the enthalpy loss, observed during starch gelatinisation, was a reflection of the overall loss of molecular order rather than starch crystallinity (Cooke and Gidley, 1992). However as XRD only detects regular repeating ordered helices and not the irregular packed structures (Gidley and Bociek, 1985), Lopez-Rubio and colleagues introduced the Crystal-Defect method. This method takes into account perfect and imperfect crystallites and it was found that the new crystallinity values were very similar to the double helical order content (Lopez-Rubio *et al.*, 2008). XRD reflections are also heavily dependent on hydrated starch material as water causes the disordered helical chains to align into a crystalline arrangement (Perry and Donald, 2000). Therefore the molecular order and crystallinity values complement each other and the enthalpy change is directly proportional to the ordered structure and crystallinity content.

Another method that is used is Fourier transform infrared spectroscopy (FTIR), which examines the degree of order and disorder of polymer chains on the surface of starch granules (i.e. the first 2 μm of the granule surface) using infrared spectroscopy. This allows a ratio of order to disorder to be calculated.

Significant physicochemical changes occur during the endothermic gelatinisation process. Amylose polymer chains begin to leach out of the starch granules (small amylopectin chains may also diffuse out) resulting in changes in rheological properties (Sasaki *et al.*, 2000).The heat-induced gelatinisation process also results in the formation of swollen granule ghosts, which are disordered remains of the starch granule. The insoluble granule ghosts mainly consist of amylopectin with only a small amount of amylose because the majority of amylose leaches out of the granule (Obanni and Bemiller, 1996; Debet and Gidley, 2007; Zhang *et al.*, 2014). Breakdown of granule ghosts can be achieved by starch gelatinisation under high shear conditions, as the high mechanical force applied during cooking disrupts the ghost structure. Zhang and workers have recently studied the effect of granule ghosts on starch digestion and showed a small decrease in amylolysis with starch prepared under low shear. This is because under low shear, granule ghosts are still present while heating under high shear conditions totally disrupts the granule structure leaving no remaining ghosts. Therefore, according to the results by Zhang et al., it is likely the granule ghosts have a small effect on starch hydrolysis and show some enzyme resistant properties (Zhang *et al.*, 2014).

1.3.5. Starch retrogradation

When gelatinised starch is stored for an extended period of time, structural changes occur to the polymer chains of amylose and amylopectin**.** The starch material begins to acquire a more ordered/crystalline structure with an increase in viscosity upon cooling. This phenomenon is termed retrogradation (Htoon *et al.*, 2009), and is commonly observed in the staling of baked foods such as

bread (Hug-Iten *et al.*, 1999). However, the lack of studies of retrogradation kinetics makes it difficult to completely understand the mechanism of starch retrogradation (Hug-Iten *et al.*, 1999; Hug-Iten *et al.*, 2003; Primo-Martín *et al.*, 2007). Starch retrogradation is a multi-step process involving the formation of amylose and amylopectin double helical structures.

The first phase involves the re-association of amylose chains to form a gel-like texture (gelation)**.** At high amylose concentrations (10% w/v) and long chain lengths, linear amylose chains form an ordered gel network in which the chains aggregate together, gradually increasing starch crystallinity (Gidley, 1989; Gidley and Bulpin, 1989). Gidley and Sarko proposed a model for the formation of amylose gels. The groups suggested amylose gels formed at high concentrations due to the presence of 'gel junction zones' connected by mobile amorphous single chains (Sarko and Wu, 1978; Gidley, 1989).

The second phase involves the re-association of branched amylopectin chains to form a double helical structure. Both retrograded amylose and amylopectin provide different levels of resistance of amylolysis. Recrystallisation of amylose chains is considered to be resistant to hydrolysis and is often referred to as ‘resistant starch’ (Tester *et al.*, 2006). However, retrograded amylopectin is only partially resistant to amylolysis as amylopectin crystallites melt at ~60^{o}C (Eerlingen *et al.*, 1994; Cui and Oates, 1997). It is important to note that the resistance to amylolysis by retrograded amylopectin depends upon the temperature at which *in vitro* studies are conducted. At 37^{o}C amylopectin crystallites do not melt and therefore are resistant to digestion. However, if

studies are performed at high temperatures amylopectin crystallites melt and do not contribute to the resistant starch content.

Many factors control the rate of amylose and amylopectin retrogradation. Amylose begins to retrograde almost immediately after gelatinisation (within 30 min) and can continue for up to 48h, while amylopectin retrogradation can take several weeks (Miles *et al.*, 1985; Sajilata *et al.*, 2006)**.** As a result, the behaviour and digestion of retrograded starch depends heavily on the amylose/amylopectin ratio, which varies for different starch sources. The rate of retrogradation is strongly dependent on the storage conditions. Applying lengthy storage periods at low temperatures (4^{o}C) or heat/cool cycles accelerates the retrogradation process and therefore increases the quantity of crystalline starch material (Holl *et al.*, 1959; Sievert and Pomeranz, 1989; Park *et al.*, 2009; Zhang *et al.*, 2011). The extent of retrogradation is also impacted by the amylopectin chain length distribution, which can be studied using high-performance size exclusion chromatography. Cereal starches retrograde to a lesser degree than tuber starches due to the shorter average amylopectin chain lengths (Kalichevsky *et al.*, 1990; Fredriksson *et al.*, 1998).

Previous studies using DSC have shown the degree of retrogradation is greatly affected by starch concentration. Comparisons have been made of DSC thermograms from retrograded starches at low and high concentrations and it was found that larger melting enthalpies were present in concentrated starch samples (Zeleznak and Hoseney, 1986; Zhou *et al.*, 2010). This indicates the effect of starch concentration on retrogradation was greater when concentrated

starch samples were gelatinised and stored compared with diluted concentrations.

Starch retrogradation has been extensively followed using ^{13}C CP/MAS NMR, XRD and DSC. Using these characterisation methods, the degree of crystallinity (measured by XRD), ordered double helical content (determined by ^{13}C CP/MAS NMR) and the melting transitions of ordered molecular chains (sensitive to DSC) can be determined. XRD patterns also reveal retrograded starches to have a B-type crystalline pattern indicative of a loosely packed double helical structure (Gidley *et al.*, 1995) . DSC shows the melting transition of retrograded amylopectin and amylose crystallites. Due to the shorter chain length, retrograded amylopectin crystallites are less stable and melt at lower temperatures (~60^{o}C) compared with retrograded amylose (~120^{o}C) (Eerlingen and Delcour, 1995). Therefore, most studies use a combination of XRD and DSC as the former measures overall starch crystallinity while the latter can be used to differentiate between retrograded amylopectin and amylose crystallites.

1.4. Starch amylolysis

1.4.1 Starch digesting enzymes

The four groups of enzymes that are involved in the degradation of starch glucan polymers into sugars are glucan phosphorylases, glucan transferases, debranching enzymes and amylases. Glucan phosphorylases are associated with the breakdown of glycogen (glycogen phosphorylase) and starch (starch phosphorylase) and are found in different living organisms such as bacteria, yeasts, plants and vertebrates (Hanes, 1940; Graves and Wang, 1972). Glucan

phosphorylase enzymes function by breaking the α(1-4) glycosidic linkages and catalyse the release of alpha-D-glucose-1-phosphate (Schinzel and Nidetzky, 1999). Glucan transferases however break the α(1-4) linkages on the donor molecule and catalyse the transfer of glucosyl chains to an acceptor molecule forming either a new α(1-4) or α(1-6) glycosidic linkage (Van Der Maarel *et al.*, 2002). Starch-debranching enzymes are exclusively involved in the hydrolysis of α(1-6) linkages. Two groups of debranching enzymes exist: isoamylase and pullulanase. Differences in both types lie in the ability to hydrolyse pullulan, which consists of repeating units of α(1-6) linkages. Pullulanase can hydrolyse α(1-6) linkages in both pullulan and amylopectin, but isoamylase can only hydrolyse α(1-6) linkages in amylopectin (Catley and Whelan, 1971; Van Der Maarel *et al.*, 2002). Debranching enzymes are essential in starch biosynthesis and the hydrolysis of starch in conjunction with other hydrolytic enzymes (Kubo *et al.*, 1999).

Amylase enzymes attack the glycosidic linkages holding glucan chains together and can be separated into exo and endo acting enzymes. Exoamylases attack the non-reducing ends of the glucan polymer chain and break one linkage at a time removing singular units. Two types of exo enzymes are beta amylase and amyloglucosidase (glucoamylase). Beta-amylase cleaves α(1-4) linkages leaving individual maltose units (two glucose units) and β-limit dextrin (Hopkins and Jelinek, 1954). Amyloglucosidase, however, releases individual glucose units from the non-reducing ends by cleaving α(1-6) and the last α(1-4) glucan bond of amylose and amylopectin (Van Der Maarel *et al.*, 2002). Active sites of endoamylases accommodate and cleave α(1-4) linkages in the interior parts of

amylose and amylopectin polymer chains. The most common endoamylase is α-amylase, which hydrolyses starch resulting predominantly in the production of maltose, maltotriose and α-limit dextrins (BeMiller and Whistler, 2009).

Most organisms digest starch, using a wide range of hydrolytic enzymes, for a source of energy. The process of starch amylolysis involves a combination of different enzymes that convert the complex starch molecule into shorter and lower molecular weight sugars. The digestion process involves the depolymerisation of starch, catalysed by α-amylase, to shorter polymer chains. Amyloglucosidase then hydrolyses these to glucose units that can be absorbed. Debranching enzymes also cleave α(1-6) branch points in the polymer chain to completely digest the starch (Smith *et al.*, 2005; Dona *et al.*, 2010).

1.4.2 α-Amylase

α-Amylase is widely distributed in humans (salivary and pancreatic secretions), plants and microorganisms and is the main enzyme involved in starch amylolysis. Mammalian α-amylase has three distinct domains; A, B and C (Figure 1.9). Domain A is the largest domain and has a $(\beta/\alpha)_8$ barrel fold, which consists of eight parallel β-strands surrounded by eight α-helices and several highly conserved sequence regions (Janeček, 1992; Svensson, 1994). The active site cleft, containing two aspartate and one glutamate residue, is located towards the carboxyl end of the β strands of the $(\beta/\alpha)_8$ barrel (Buisson *et al.*, 1987). The site contains 5 consecutive subsites for the binding of glucose units. The glycosidic bond between glucose units 3 and 4 are broken, through an acid-base and nucleophilic catalysts mechanism, by the carboxyl groups of

aspartate and glutamate residues (Robyt and French, 1970). Domain A also has a chloride ion, which is required for the activation of the α-amylase enzyme (Butterworth *et al.*, 2011). Domain B is in close contact with domain A and is located between the third β strand and the third α helix of domain A (Janeček *et al.*, 1997). Domain B also contains an essential calcium ion, which connects domain A and B together, stabilising the active site cleft (Buisson *et al.*, 1987). Domain C at the *N*-terminal region is loosely associated with domain A and therefore less likely to play a role in the catalytic starch digestion process (Brayer *et al.*, 1995).

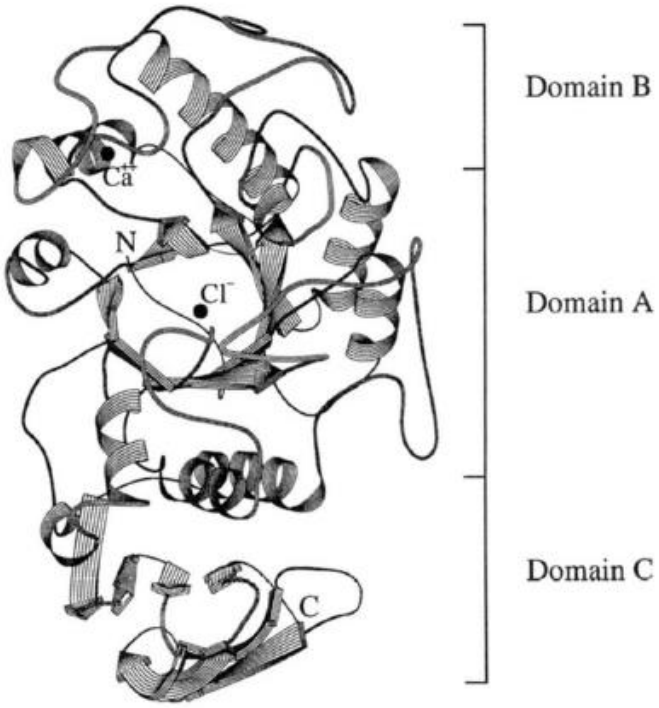

Figure 1.9. Human porcine pancreatic α-amylase structure showing the structural domain A, B and C. The Cl^- and Ca^{2+} ions are located in domain A and B, respectively. Adapted from Brayer and co-workers (Brayer et al., 1995).

In mammals, the two α-amylase encoding genes are termed AMY1 and AMY2, producing salivary and pancreatic α-amylase, respectively. Both genes are located on chromosome 1 and even though AMY1 has an extra exon (Emi *et al.*, 1988), alternative splicing results in both salivary and pancreatic amylase having similar amino acid sequences. The initial stage in starch digestion begins with α-amylase secreted by the salivary gland with full digestion eventually being completed by pancreatic α-amylase. As the structure and function of both human and porcine pancreatic α-amylase is almost identical, most experimental studies use the latter enzyme to study starch digestion because of its availability in pure form at reasonable cost (MacGregor *et al.*, 2001).

1.4.3 *In vitro* digestion models

Different enzyme kinetic models have been introduced to describe *in vitro* starch hydrolysis by α-amylase. Digestibility curves, which plot starch digestion product over time, are often used as the basis of the kinetic models. Such models explain starch digestion over different time periods. Some groups have investigated the initial rate of starch digestion using Michaelis-Menten equation, and therefore only analyse starch digestion up to 16 min (Slaughter *et al.*, 2001; Tahir *et al.*, 2010). However many workers have looked at prolonged starch digestion, lasting from a few hours to multiple days (Frei *et al.*, 2003; Obrien, 2008; Souilah *et al.*, 2014). Surprisingly, some workers have suggested that the Michaelis-Menten equation is not suitable for the study of *in vitro* starch digestion by α-amylase due to high α-amylase activity resulting in product inhibition and substrate exhaustion (Mahasukhonthachat *et al.*, 2010). However,

such workers fail to recognise that during initial starch digestion, the α-amylase and inhibitor concentrations are relatively low compared to the digestion over a long reaction time. Therefore the Michaelis-Menten equation is suitable for studying the early stages of starch digestion, provided that checks are made that product release is linear with time. Such experiments allow reliable kinetic parameters to be obtained.

In vitro starch digestion assays have become extensively used in laboratories and have multiple advantages over *in vivo* studies (animal and/or human subjects). The *in vitro* approach is considerably cheaper to perform and no ethical authorisation is required resulting in the experiments being less time consuming (Mahasukhonthachat *et al.*, 2010; Butterworth *et al.*, 2011; Butterworth *et al.*, 2012). One of the main aims of conducting *in vitro* digestion studies is to mimic *in vivo* amylolysis and, for some researchers, attempt to predict the likely *in vivo* glycaemia resulting from α-amylase acting on starch-rich food materials (Englyst *et al.*, 1996; Englyst *et al.*, 1999).

1.4.3.1 Prolonged starch digestion

In vitro digestion models performed over a long period of time (several hours) aim to stimulate physiological digestion times that are likely to be found in the upper gastrointestinal tract. The most popular and widely used digestion model is that described by Englyst and colleagues (1992). Based upon the digestibility curves, starch digestion was classified into three distinct fractions according to selected time frames of digestion: rapidly digestible starch (RDS), slowly digestible starch (SDS) and resistant starch (RS) (Englyst *et al.*, 1992; Englyst

and Hudson, 1996). Starch digested within the first 20 min and between 20 and 120 min are termed RDS and SDS, respectively. Starch that avoids *in vitro* digestion after 120 min is termed RS and is calculated by difference. *In vivo*, resistant starch escapes digestion in the small intestine but is fermented in the large intestine (Englyst and Cummings, 1987).

However the Englyst system seems to ignore the well-established finding that starch digestion proceeds by a first-order kinetic reaction (Goñi *et al.*, 1997). The initial 20 min time period, assigned to RDS, was obtained by visual inspection of starch hydrolysis curves. After the 20 min time period a slower digestion process was observed, and according to the Englyst system, this slower phase was assigned to SDS. However this slow phase is almost certainly due to substrate exhaustion as the digestion time frame increases. Goñi et al. and more recently Dhital and workers showed that the digestion of cooked starch followed a pseudo-first order kinetic process where the reaction rate decreases with time as the substrate is being converted to product (Goñi *et al.*, 1997; Dhital *et al.*, 2010). The reaction is characterised by a single pseudo first-order rate constant which is an intrinsic property of the enzyme and remains constant throughout the *in vitro* digestion process. Therefore the Englyst classification system, obtained from starch hydrolysis curves, reveals no clear evidence of separate RDS and SDS fractions.

Apart from the rate constant for the digestion process, the C infinity (C_∞) can also be obtained from these enzyme kinetic studies (Goñi *et al.*, 1997). The C_∞ is described as the concentration of the product at the end of the reaction

thereby giving an estimate of the maximum amount of starch digested. The C_∞ also allows the resistant starch fraction to be determined by difference. Estimates from digestibility plots however can be unreliable because of uncertainties about when the reaction has ended. Therefore the first order kinetic model has been recently adapted by Butterworth and co-workers using a 'logarithm of slope' (LOS) plot approach (Butterworth *et al.*, 2012). Scheme 1 shows how the LOS plot equation is derived from the original first-order rate equation.

Scheme 1

$$C_t = C_\infty(1 - e^{-kt})$$

↓ Differentiation

$$\frac{dC}{dt} = C_\infty k e^{-kt}$$

↓ Logarithmic form

$$\ln\left(\frac{dC}{dt}\right) = \ln(C_\infty\, k) - kt$$

Scheme 1. Differentiated and logarithmic form of the first-order rate equation. Where C_t is the concentration of product released at time t, C_∞ is the concentration of product at end time, and k is the pseudo first-order rate constant.

The y axis (ln(d*C*/d*t*)) is obtained by taking the slope between individual data points on the digestibility curve and applying natural logarithms. When ln(d*C*/d*t*) is plotted against *t*, a linear plot is observed with the digestibility rate constant, *k*, given by the negative slope of the plot and the C_∞ value calculated using the y axis intercept (ln($C_\infty k$)). Therefore using the LOS plot approach allows *k* and C_∞ to be estimated directly. The LOS plots also reveal whether changes occur in digestion rate constants by evidence of discontinuities in the plot. Such changes are indicative of starch fractions that differ in digestibility rate. Figure 1.10 clearly shows two separates phases, termed RDS and SDS, during the digestion of native wheat starch as opposed to no discontinuity for the digestion of gelatinised wheat. The length and extent of digestion during each phase can vary depending upon the botanical starch source, as observed with native potato. This method is discussed in more detail in Chapter 5, where we have applied it to the digestion of retrograded starch.

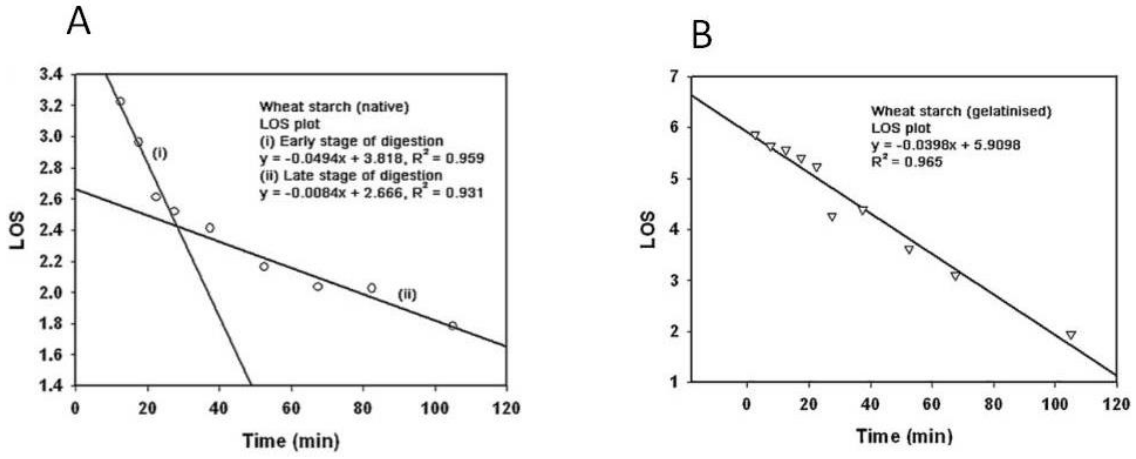

Figure 1.10. LOS plots for the digestion of native (A) and gelatinised (B) wheat starch. Native and gelatinised wheat starch was incubated at 37°C with a porcine pancreatic α-amylase concentration of 4.5 nM and 2.25 nM, respectively. Adapted from the study by Butterworth and co-workers (Butterworth et al., 2012).

1.4.3.2 Initial starch digestion

Enzymologists investigating the very early portion of the digestibility plot (no longer than 16 min) observed a linear relationship between the product formation and time. By taking the slope during the limited time period, the initial reaction velocity (*v*) was determined and plotted as a function of substrate concentration. A hyperbolic curve was observed, showing a constant initial reaction velocity at high substrate concentrations (Figure 1.11).

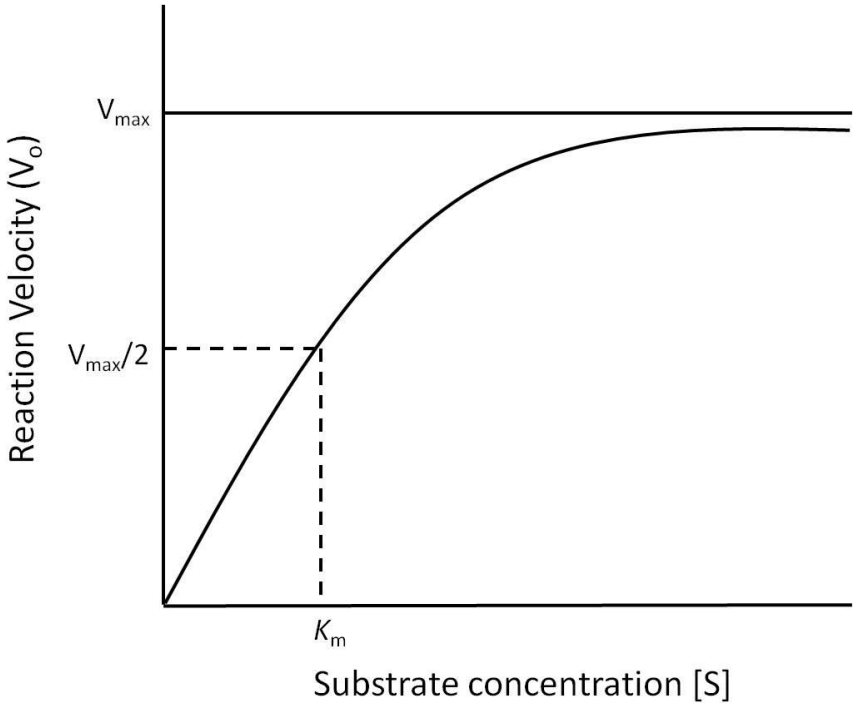

Figure 1.11. Hyperbolic curve showing the effect of substrate concentration on the initial reaction velocity (v). Adapted from Berg and colleagues (Berg et al., 2002).

Brown in 1902 aimed to describe the enzyme-catalysed reaction process by introducing a mechanism which converts the enzyme (E) and substrate (S) to an enzyme-substrate complex (ES), yielding a product (P) and free enzyme

(Scheme 2). The scheme suggests the reaction velocity is proportional to the enzyme-substrate complex, expressed as $v = k$ [ES].

Scheme 2

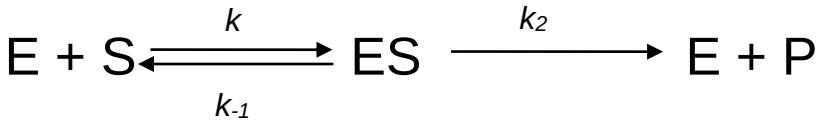

Scheme 2. The enzyme-catalysed reaction mechanism. The rate constant for each individual reaction is represented by k.

At low substrate concentrations [S] the reaction obeys first-order kinetics with the initial velocity being linear to the substrate concentration as [ES] is proportional to [S]. At high substrate concentrations, a saturation point is reached, i.e., all enzyme molecules are in the form of an ES complex and the velocity is thus independent of the substrate concentration (Duggleby, 2001). The latter therefore suggests a zero-order kinetic model. This mechanism was later adapted by Henri (1903) and Michaelis and Menten (1913) and led to the widely used Michaelis-Menten equation (Equation 1).

Equation 1

$$v = \frac{V_{max}[S]}{K_m + [S]}$$

Equation 1. The Michaelis-Menten equation with the initial rate of hydrolysis (v), substrate concentration (S), maximum enzyme velocity (V_{max}) and Michaelis-Menten constant (K_m).

V_{max} (maximum enzyme velocity reached) can be used to calculate k_{cat} (catalytic rate constant) by dividing V_{max} by the total enzyme concentration (V_{max} / $[E]_t$). The K_m (Michaelis-Menten constant) is defined as the substrate concentration at ½V_{max}, thus if K_m is high, the enzyme affinity is low as most of the substrate remains unbound to the enzyme. By using k_{cat} and K_m, a k_{cat}/K_m ratio can be defined as the rate constant determining the rate at which the enzyme-substrate complex is formed and therefore can be used as a measure of the catalytic efficiency (CE). It is also often used to compare hydrolysis rates between different starches (Eisenthal *et al.*, 2007). Figure 1.12 shows how the K_m and V_{max} kinetic parameters can be derived from a Michaelis-Menten graph. However, it is now customary for experimental data points to be fitted to the Michaelis-Menten equation, using specialised computer software (e.g., EnzFitter, SigmaPlot etc.). This allows the kinetic parameters (V_{max} and K_m) to be calculated with greater precision and reliability.

Michaelis-Menten kinetic parameters have been widely used to study the adsorption of α-amylase to starch granules and the rate of digestion as a result of using different processing methods (Slaughter *et al.*, 2001; Roder *et al.*, 2009; Tahir *et al.*, 2010; Tahir *et al.*, 2011). Kinetic parameters can also act as a probe to study structural changes occurring to the starch granule during hydrothermal treatment. However the kinetic parameters may not be completely reliable in reference to heterogeneous material where the substrate availability is unknown. For this reason the kinetic model is commonly used for pure starch systems where the substrate concentration is known with certainty.

An alternative graphical method to obtain enzyme kinetic parameters from initial rate measurements is the Lineweaver-Burk plot. Other graphical methods include the Eadie-Hofstee and Hanes-Woolf plot but the Lineweaver-Burk plot remains the most popular method used particularly for investigations of enzyme inhibition (see below). The Michaelis-Menten equation can be rearranged into a straight line equation with the form y = mx + C, known as the Lineweaver-Burk equation (Equation 2) (Owusu-Apenten, 2004).

Equation 2

$$\frac{1}{v} = \frac{K_m}{V_{max}\,[S]} + \; 1/V_{max}$$

Equation 2. The Lineweaver-Burk equation.

Therefore plotting a double reciprocal (1/*v* against 1/[S]) will produce a linear graph (Figure 1.13), with the gradient being K_m/V_{max} and the intercept on the y and x axis being $1/V_{max}$ and $1/K_m$, respectively.

1.4.4 Inhibition modes

The Lineweaver-Burk plot can also used to study and identify competitive and/or non-competitive inhibition at a variety of different substrate concentrations. A non-competitive inhibitory effect is represented by constant K_m with a changing V_{max}, suggesting the inhibitor is able to bind to the free enzyme and/or the enzyme-substrate complex with identical affinity. The binding action to this remote site renders the enzyme inactive, substantially reducing the enzyme activity and V_{max}. However in competitive inhibition, the

inhibitor competes with the substrate for the enzyme active site and therefore the K_m changes but with no change in V_{max}. This is because if the substrate concentration is raised sufficiently the inhibitor will be displaced from the active site. The effects non-competitive and competitive inhibitors have on V_{max} and K_m are graphically illustrated in Figure 1.12. It is important to note many data points are obtained at high substrate concentrations and therefore V_{max} is liable to be low in precision. Also the Lineweaver-Burk plot has majority of the experimental error in the initial velocity (*v*) variable. At low S concentrations, *v* values are also low and so even though these errors are small, taking the reciprocals enlarges such errors. Therefore the errors present in low *v* values greatly affect the slope of the plot (Ranaldi *et al.*, 1999). For these reasons many enzymologists have been critical of using such a plot to quantitatively estimate V_{max} and K_m (Copeland, 2004). A Lineweaver-Burk plot is also not suitable for study of the interaction between inhibitor and enzyme in a more complex system beyond the classical competitive and non-competitive inhibition (Butterworth, 1972). Combinations of Dixon plots and S/v vs. [I] plots (introduced by Cornish-Bowden in 1974) are commonly used for the detection of multiples modes of inhibition (Cornish-Bowden, 1974).

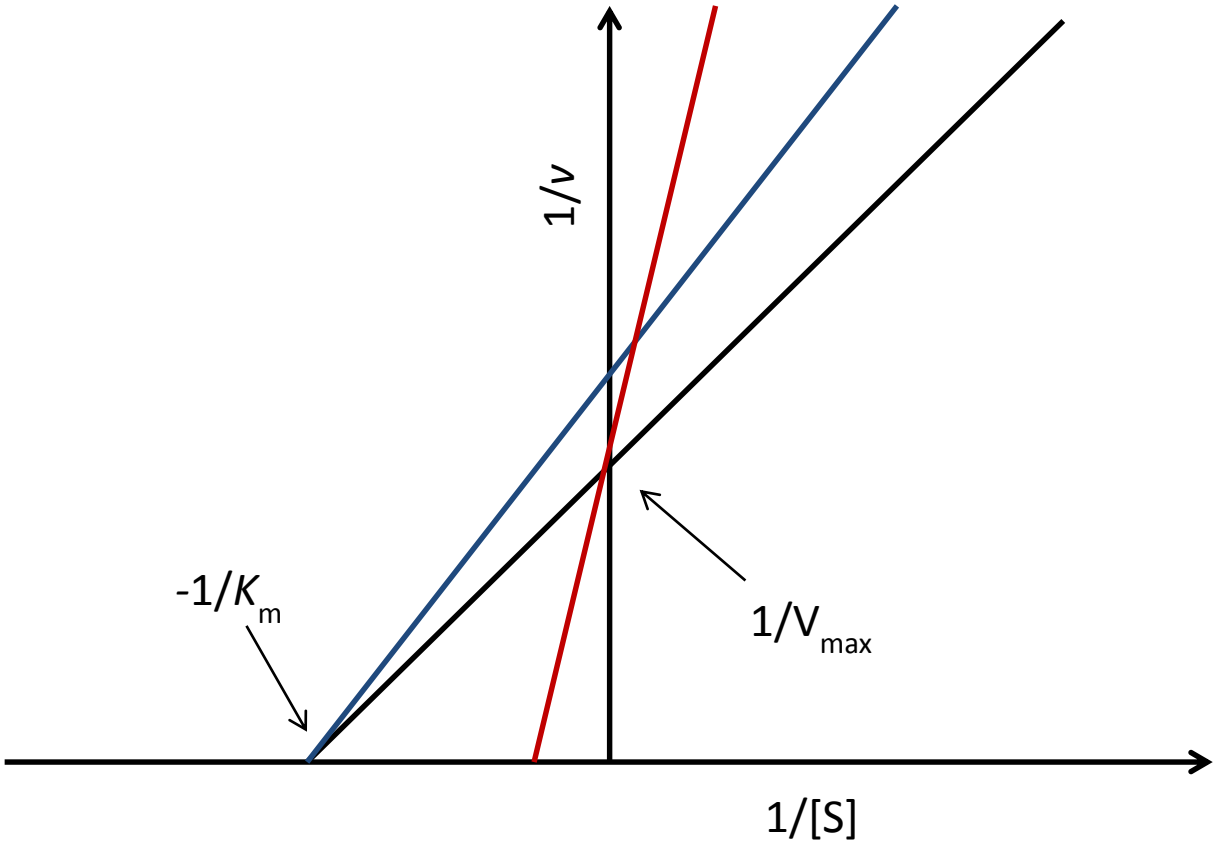

Figure 1.12. Double reciprocal plot (Lineweaver-Burk) used to estimate V_{max} and K_m values from the intercepts. The absence of an inhibitor is shown in black, with a competitive inhibitor in red and non-competitive inhibitor in blue. Adapted from Motulsky and Christopoulos (Motulsky and Christopoulos, 2004).

In the Dixon method the reciprocal of the enzyme rate is plotted over a range of inhibitor concentrations for two or more substrate concentrations (Dixon plot). The interception point for each extrapolated straight line indicates the inhibitor constant ($-K_i$). For non-competitive inhibition the straight lines intercept on the negative inhibitor axis allowing the inhibitor constant to be read off directly. However for a competitive inhibitor the interception is above the x axis (Figure 1.13) (Cornish-Bowden, 1974). Additional useful information from the Dixon plot also shows when multiple inhibition occurs as deviation from linearity is

observed (Yon-Kahn and Hervé, 2009). However the Dixon plot cannot distinguish between competitive and mixed inhibitors while the Cornish-Bowden modification (S/*v* vs. I) plot produces distinctive graphs for competitive and mixed inhibitors (Figure 1.14).

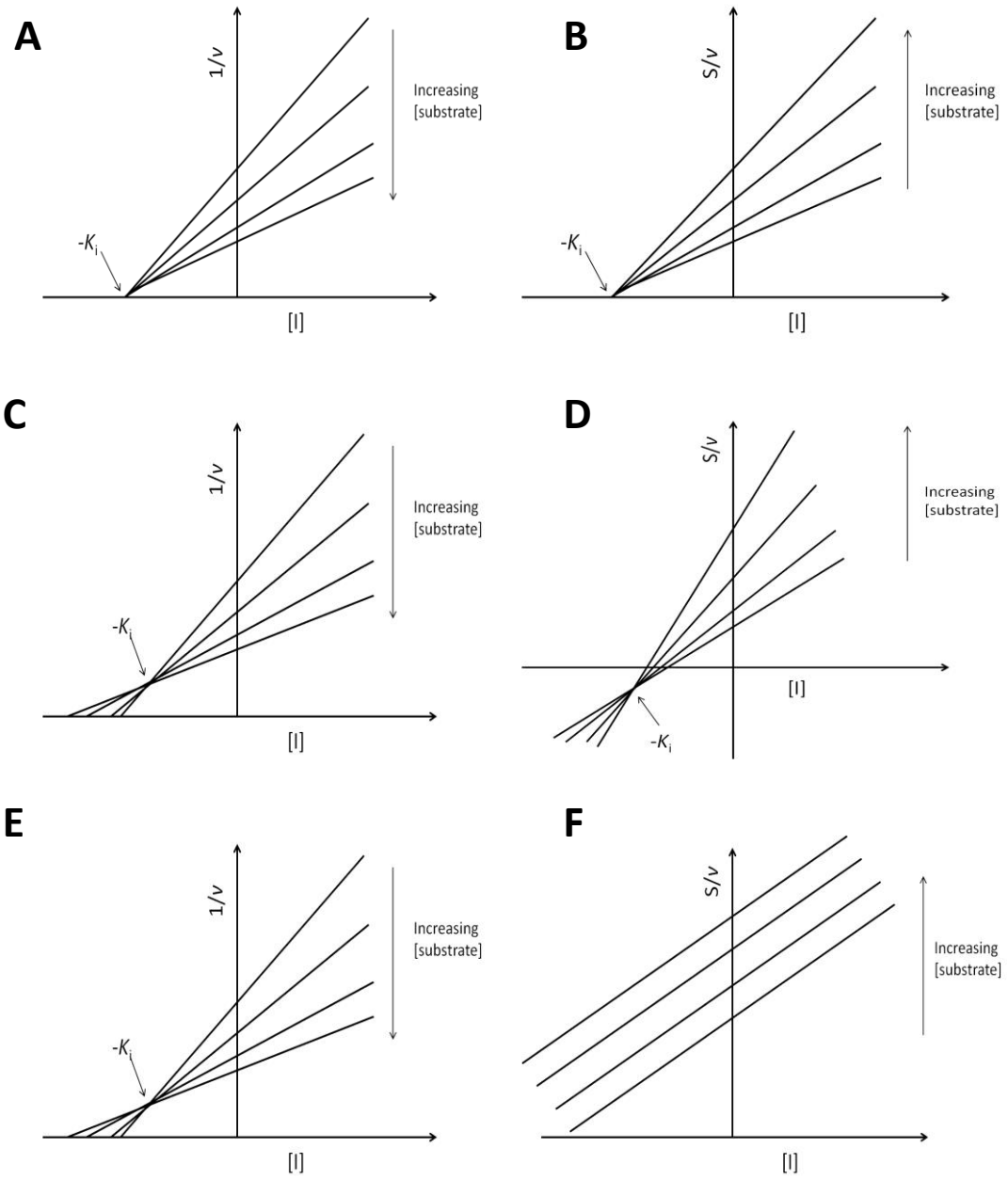

Figure 1.13. Graphical representation of the Dixon plot (left) and the Cornish-Bowden plot (right) showing a non-competitive (A, B), mixed (C, D) and competitive inhibitory action (E, F). The point at which the lines converge is the inhibitor constant (K_i). Image adapted from (Cornish-Bowden, 1974).

1.4.5 Factors influencing starch digestion kinetics

There are number of factors which can affect the kinetics of starch digestion by α-amylase. Certain starch characteristics such as amylose/amylopectin content, granular size and surface pores all play an important factor in the rate of enzyme hydrolysis. Small native starch granules (wheat, rice) show a greater rate of hydrolysis due to their higher surface area compared to larger granules such as native potato starch (Knutson *et al.*, 1982). Warren and co workers aimed to show a relationship between the dissociation constant (K_d) for α-amylase binding to different starches and the specific surface area for different particle sizes. The results showed a decrease in K_d when the specific surface area increased indicating substrate affinity was greater for smaller granules with a large surface area (Warren *et al.*, 2011). The group also showed a direct relationship between K_m (determined from initial rate studies) and K_d determined from binding studies (Warren *et al.*, 2013). This provides evidence that the K_m value is a reliable estimate of the binding affinity between PPA and starch.

Some cereal starches also have a porous surface, which facilitate α-amylase binding to the glucan chains by providing a unique channel into the granule. This increases the accessibility of amorphous glucan chains and thereby α-amylase adsorption and starch hydrolysis is initiated from the inside (Benmoussa *et al.*, 2006; Lehmann and Robin, 2007). Such structural features are absent in certain starches like potato and may contribute to the reduced rate of hydrolysis (Fannon *et al.*, 1992; Dhital *et al.*, 2010).

The effect of amylose on starch hydrolysis is not fully understood and results seem to be conflicting. Some studies show native high amylose starches to be less susceptible to α-amylase attack and even suggest the resistance is similar to that of native potato starch (Planchot *et al.*, 1995; Vasanthan and Bhatty, 1996; Rendleman Jr, 2000; Tester *et al.*, 2006). Contrary to this, a few studies have reported that native high amylose starches are digested at a higher rate than some non-mutant starches (Lee *et al.*, 1985; Tahir *et al.*, 2010; Tahir *et al.*, 2011). The conflicting results not only indicate more work has to be conducted but also suggests other factors must contribute to provide resistance to starch digestion, besides any dependence on the amylose content (Sandstedt *et al.*, 1962).

The packing of double helical chains into an A-type or B-type affects native starch digestibility. Planchot et al. showed A-type starches (cereals) are more susceptible to amylolysis than B-type starches (tubers) (Planchot *et al.*, 1997). The amylopectin blocklet size also affects susceptibility towards α-amylase with an large blocklet (potato) offering more resistance than smaller blocklets (wheat) (Gallant *et al.*, 1997). Amylose may also interact with lipids, forming an amylose-lipid complex which is known to provide resistance to digestion by α-amylase (Holm *et al.*, 1983).

The proportion of amorphous to crystalline material is another factor that can influence starch digestion. Leloup and workers showed that removing the amorphous chains on the surface of the granule by acid hydrolysis, leaves a smooth surface with highly resistant B-type crystalline chains that prevent

α-amylase adsorption (Leloup *et al.*, 1991; Leloup *et al.*, 1992). The removal of amorphous chains is often referred to as removing the hairs of the 'hairy billiard ball' structure model, introduced by Lineback nearly 30 years ago (Lineback, 1986). The group concluded that amylase adsorption was a prerequisite to subsequent hydrolysis and for this to occur, amorphous chains would have to be present. Tahir and colleagues also showed native starches with a greater proportion of amorphous material have a higher catalytic efficiency than starches with less amorphous material (Tahir *et al.*, 2010; Tahir *et al.*, 2011). Therefore differences in the amorphous to crystalline ratio for different starches may give rise to different starch kinetic parameters.

Processing methods can have a major influence on the enzyme kinetic parameters (K_m, k_{cat}/K_m, and C_∞) due to structural changes. Starch gelatinisation is regulated by two variables: heating temperature and moisture content. When starches are heated at high temperatures but in limited water availability (heat-moisture treatment), complete gelatinisation does not occur. Even though structural changes are observed during this process, the lack of water means starch swelling is limited resulting in some granules maintaining their original crystalline structure (Roder *et al.*, 2009). As mentioned before, this is commonly observed for starch in the production of biscuits. A similar effect is observed when starches are heated in intermediate/excess water below the gelatinisation temperature but above the glass transition point (i.e. the annealing process). The effect of heating below the gelatinisation temperature with intermediate levels of water availability results in reorganisation of the crystalline domains in the starch granule, improving crystalline perfection and

granule stability (Hoove and Vasanthan, 1993; Jacobs *et al.*, 1995). Annealing can also cause interactions between amylose and amylopectin chains resulting in a double helical formation (Jacobs and Delcour, 1998; Jayakody and Hoover, 2008). Many reporters have studied the effects of annealing on starch digestion although the results seem to be conflicting. Some studies suggest susceptibility increases while others have shown hydrolysis of annealed starch to be lower (Hoove and Vasanthan, 1993; Jacobs *et al.*, 1998; Jayakody and Hoover, 2008; Obrien, 2008). Nevertheless, both heat-moisture treatment and annealing result in physiochemical changes to the starch granule without total granule disruption (Zavareze and Dias, 2011).

As mentioned previously, when starches are heated at high temperatures and in excess water, complete granule disruption occurs along with granule swelling and amylose leaching. Molecular order is completely lost with the gelatinised material being primarily all amorphous. This results in more available α-glucan chains, which increases α-amylase adsorption and starch hydrolysis, subsequently affecting C_∞ and k_{cat}/K_m. Tahir and Slaughter have both previously demonstrated dramatic changes in enzyme kinetic parameters for different starches upon gelatinisation (Slaughter *et al.*, 2001; Tahir *et al.*, 2011).

Starch retrogradation also has a major effect on structural properties. Upon cooling and storage, the disordered glucan chains from the gelatinisation process begin to occupy a more ordered and, to some extent, crystalline structure. This in turn reduces the percent of starch that can be degraded by α-amylase (Cui and Oates, 1997; Fredriksson *et al.*, 2000; Frei *et al.*, 2003;

Chung *et al.*, 2006). Many studies have examined the digestion and structure of retrograded starch (both amylose and amylopectin); however, the lack of enzymological studies on the digestion of retrograded starch means that the topic is ripe for a full investigation.

1.5 Hypothesis and aim

Previous studies have shown that starch digestibility is greatly affected by the physicochemical structural changes observed during processing. On this basis it was hypothesised that the rate and extent of digestion would be reduced in the presence of retrograded starch due to the increase in structural order during the hydrothermal processing and storage of starch.

The overall aim of this research project is to study the molecular mechanisms of native and processed starch digestion from different botanical sources using PPA. The quantitative digestion kinetic data will then be related to the physicochemical properties of starch substrates, obtained using a range of different chemical and physical techniques, to determine the relationship between structure and function. The experimental approach carried out in this project will help to improve our understanding of the role of starch structure in the interaction with PPA and the subsequent hydrolysis step.

Chapter 2 Materials and methods

2.1 Materials

2.1.1 Sources of starch

Wheat starch (Cerestar, CV. GL04) was a gift from Prof. Cliff Hedley (formerly of the John Innes Centre (JIC), Norwich, UK). Purified potato starch and wild type pea starch were gifts from the National Starch and Chemical Company (member of the ICI group, London, UK) and from Prof. T. Bogracheva (JIC), respectively. Maize, waxy maize and high amylose maize starches were gifts from C. Pelkman at Ingredion. Rice starch was obtained from Sigma-Aldrich Ltd (Poole, Dorset, UK). Starch obtained from durum wheat was extracted using the method described below. The Durum wheat grains (*Triticum durum L.*; Svevo cv.), for starch extraction were provided by Millbo S.p.A., Trecate, Italy.

2.1.2 Chemicals for starch characterisation

Total starch and resistant starch assay kits were obtained from Megazyme International Ireland ltd, Ireland. All other reagents used for starch characterisation were purchased from Sigma-Aldrich Ltd unless stated otherwise.

2.1.3 Chemicals for biochemical assays

Porcine pancreatic α-amylase (Type 1-A), which was diisopropyl fluorophosphate (DFP) treated to inhibit protease activity was bought from Sigma-Aldrich Ltd suspended in 2.9 M NaCl solution containing 3 mM $CaCl_2$. The total protein content was 30 mg/mL, which was determined by the

Bicinchoninic acid (BCA) assay. The activity of amylase was 1017 U/mg, tested using gelatinised wheat starch and the standard Prussian blue assay. This falls within the specific activity range of 700-1400 U/mg quoted by the manufacture. The purity of α-amylase was checked by SDS-PAGE and the molecular weight of 56 kDa was confirmed. Phosphate Buffered Saline (PBS) tablets were bought from Oxoid, Basingstoke, UK (pH 7.3 ± 0.2 at 25 ^{o}C).

2.2 Starch characterisation

2.2.1 Durum wheat starch extraction

Durum wheat starch was extracted from the grains using a modified method described by (Vansteelandt and Delcour, 1999). Five hundred grams of durum wheat grains were steeped overnight in 0.24% (w/v) aqueous sodium bisulphite (1.68 g dissolved in 700 mL distilled water (dH_2O)). The suspension was incubated at 30^{o}C on a mixing plate for 48h. The sample was then blended using an Ultra-Turrax® (IKA T25 digital) until a souplike consistency was obtained. The contents were then passed through a 250 µm sieve. Deionised water and a spatula were used to help with this process. The contents were then passed through a second 125 µm sieve and the final mixture was collected in the bottom base. Once mixed with a spatula, the collected filtrate was transferred into separate 50 mL Falcon tubes. These were then vortex mixed before centrifuging at 1,800 g (Mistral 3000 MSE centrifuge) for 10 min at room temperature (22^{o}C). The supernatant was removed and the off-white layer of impurities at the surface was scrapped off from each 50 mL Falcon tube leaving just the precipitate (starch). The precipitates were re-suspended in dH_2O water and centrifuged again until no impurities appeared. The Falcon tubes containing

the starch were filled with dH_2O and stored at 4°C overnight. All Falcon tubes were then centrifuged again and the supernatant was discarded before each tube was filled with ethanol. Tubes were shaken vigorously to re-suspend the contents in ethanol then centrifuged at 1,800 g for 10 min at room temperature before the ethanol was discarded. The starch was scraped into a container and ethanol allowed to evaporate overnight at room temperature, leaving dried starch. This was then stored in an airtight container at room temperature. The total starch content was later determined (see next section).

2.2.2 Total starch content

All starches used in the investigation were tested for the total starch content using the Megazyme Total Starch Test (AOAC 996.11 Official Method), with slight modifications. Briefly, starch was hydrolysed to maltodextrins by α-amylase and then to glucose by amyloglucosidase (AMG). The glucose was then determined using the glucose oxidase/peroxidase reagent (GOPOD). To ensure complete gelatinisation of high amylose maize starch, the DMSO method was used (McCleary *et al.*, 1994). The assay was scaled down to 1/20th of the original assay to allow analysis of all starch samples using one assay kit. The Megazyme kit contents and the preparation of reagents can be found in Appendix A.

A known weight of starch was accurately weighed into Eppendorfs suitable for boiling and solubilised in 200 µL of dimethyl sulphoxide (DMSO). Ethanol was not used in this method because the distinction between undigested starch and sugars was not needed. Each tube was then vortex mixed and placed in a

boiling water bath for 16 min to solubilise the starch samples (tubes were vigorously mixed every 3 min to ensure complete homogeneity). This step was longer than that mentioned in the Megazyme manual so as to ensure that complete starch gelatinisation was achieved. The tubes were taken out of the water bath and 300 µL of diluted thermostable α-amylase (solution 1) was added. Tubes were vortex mixed and incubated in an 80-90^{o}C water bath for 6 min to allow starch hydrolysis (Megazyme specify thermostable α-amylase to have the highest activity at >80^{o}C). Samples were then removed from the water bath and 5 µL AMG (solution 2) were added and each tube was mixed before being placed in 50^{o}C water bath for 30 min to allow glucose production. All samples were then centrifuged at 12,000 g for 1 min before the supernatant was diluted in water (1 in 4) to allow the glucose concentration to be within the working range (0.1-1 mg/mL). A 33 µL aliquot of the diluted supernatant was then transferred into new Eppendorfs with 1 mL of GOPOD reagent (solution 4). All tubes were then placed in a 50^{o}C water bath to allow colour development. This procedure was performed in conjunction with reagent blanks (water), glucose standards and maize starch controls. The absorbance of each sample was read at 510 nm against the reagent blank (CE 2041 spectrophotometer, Cecil Instruments, Cambridge, UK). The total starch content was then calculated using the equation provided by Megazyme (Equation 3). The starch content is expressed on a wet weight basis.

Equation 3

$$\text{Starch } \% = \Delta\text{Abs x F x D x} \frac{162}{180}$$

Equation 3. Total starch content calculation. ΔAbs is the absorbance read against the reagent blank. F is the conversion of absorbance to mg. D is the dilution factor for the multi step dilution process and 162/180 represents the adjustment from free D-glucose to anhydro D-glucose.

2.2.3 Moisture determination

Aluminium pans were heated overnight at approximately 103ºC. Upon removal the pans were allowed to cool in a desiccator and then weighed with the lids on. A known weight of starch was added to the pan and the total weight of starch and pan was recorded. The samples were then heated at approximately 103ºC overnight. Upon removal from the oven, samples were placed in a desiccator to cool before the weight was recorded. The moisture content was calculated by the difference between the fresh and dry weights.

2.2.4 Amylose-amylopectin ratio

The percentage amylose content in starches was determined using the iodine binding method (Knutson, 1986, 2000). The percentage of amylopectin was then calculated by difference. This method was preferred over the concanavalin A precipitation with amylopectin because in this method, co-precipitation with amylose results in underestimation of the actual amylose content (Vilaplana *et al.*, 2012).

For the iodine binding method, between 1 to 5 mg of each starch sample was weighed into 15 mL Falcon tubes. Standards ranging from 0 to 5 mg, using potato amylose type III, were also prepared. A 0.229 g sample of re-sublimed iodine was dissolved in 90% DMSO and 10% dH_20. Starch samples and standards were dissolved at room temperature in 10 mL of this iodine solution and placed on a blood rotator mixer to provide end-over-end mixing overnight. A 100 µL aliquot from each tube was diluted in 800 µL dH_20. This was left for 30 min to allow colour development and maximum iodine-amylose complex formation. The absorbances of all the samples were recorded at 600 nm using a Cecil CE 2041 spectrophotometer. The amylose percentage was then calculated using the amylose standard curve and Equation 4. This equation takes into account the interference by the colour developed from the small amount of iodine binding to amylopectin (Vilaplana *et al.*, 2012).

Equation 4

$$\%\ \text{amylose} = \%\ \text{apparent amylose} - 6.2/93.8$$

Equation 4. Amylose content calculation. The small amount of iodine binding to amylopectin is represented by 6.2/93.8.

2.2.5 Protein content

Previous workers in our group determined the protein content for most of the starches used by the Kjeldahl method (Tahir *et al.*, 2010). Briefly, starch samples are boiled in sulphuric acid producing nitrogenous compounds which then produce ammonia by addition of excess NaOH. Following titration, the nitrogen content can be determined and multiplying this by a pre-determined

factor (nitrogen x 6.25) allows the protein content to be estimated. However this method is time consuming and relies on the conversion factor to convert the nitrogen to protein content, which varies for different starches. Therefore, the novel BCA assay, which measures protein directly, was used instead.

A 50-100 mg starch sample was accurately weighed into Eppendorf microcentrifuge tubes and 1 mL of 2% (w/v) SDS was added. The tubes were then vortex mixed and boiled for 90 min to solubilise and extract the proteins from the starch. The mixture was then left to cool at room temperature for 5 min before being centrifuged at 13,000 g for 10 min. A 50 µL aliquot of the supernatant was then removed.

The protein content was determined by the BCA assay, which involves preparing a working reagent containing 50 parts of reagent A (bicinchoninic acid, sodium carbonate, sodium tartrate, and sodium bicarbonate in 0.1 M NaOH) and 1 part of reagent B (4%, w/v, copper (II) sulphate pentahydrate in water). One mL of the working reagent was added to 0 to 1 mg/mL bovine serum albumin (BSA) standards and all the starch protein samples and then vortex mixed. The standards and starch protein samples were incubated in a water bath at 37^{o}C for 30 min. The absorbance was then recorded at 562 nm using a Cecil CE 2041 spectrophotometer. The total starch protein content was determined by using the BSA standard curve.

2.2.6 Starch damage

Starch damage was determined using the method described by Slaughter et al. (2001). A 0.2% (w/v) solution of Congo red was prepared in dH_20 and 1 mL was pipetted into Eppendorf tubes containing 2 mg starch. The tubes were then vortexed and left for 15 min at room temperature before being centrifuged at 13,000 g for 5 min. The supernatant was then removed and the pellet was washed in 1 mL water and centrifuged again at 13,000 g for 5 min. This was repeated until the supernatant was clear (roughly three times). The final pellet was resuspended in 1 mL dH_20 and vortex mixed. A 20 µL aliquot was pipetted onto a microscope slide with a cover slip placed on top. All starches were examined with a Zeiss Axioskop 2 mot *plus* light microscope at 10x magnification (rice starch was examined under a 20x magnification due to the small particle size). One thousand granules were counted and the numbers of stained granules were expressed as a percentage.

2.2.7 Birefringence of native starch

All native starches were examined for birefringence using a Nikon Microphot-FXA light microscope equipped with crossed polarisers. Images were captured using an Infinity 2 camera connected to a PC equipped with Infinity capture software. Native starch samples were suspended in water before a droplet was placed onto a microscope slide and covered with a glass cover slip. Images were photographed using a Nikon objective 10x magnification.

2.2.8 Scanning electron microscopy (SEM)

The microstructure characteristics of native maize, waxy maize and high amylose maize starches were also studied using a FEI Quanta 200F scanning electron microscope. All starch samples were adhered onto an aluminium SEM stub using double sided carbon impregnated discs and given a 10 nm gold coating in a Quorum Q150T sputter coater prior to viewing. SEM images were provided by Dr David McCarthy of University College London.

2.3 Physicochemical starch analysis

2.3.1 Fourier transform infrared spectroscopy (FTIR) with attenuated total reflectance (ATR)

FTIR-ATR is a relatively quick analytical technique used to quantitatively study short range molecular order on the surface of starch granules. The IR beam penetrates the samples resulting in absorption of radiation, with the depth of penetration being ~2 µm and therefore limited to the surface of the granule (Sevenou *et al.*, 2002). However for very small granules (wheat and rice) the IR beam penetrates a relatively higher proportion of the starch granule. The IR spectrum of starch is sensitive to conformational changes in structure within the region 1300-800 cm^{-1}. The absorbance bands in this region are related to the C-C, C-O and C-H stretching and C-O-H bending. The absorbance band noticed at 1022 cm^{-1} is a result of the vibration of C-O-H deformation and is described as a characteristic of amorphous structure (Liu *et al.*, 2002; Capron *et al.*, 2007). The absorbance band at 1000 cm^{-1} is very sensitive to water and is therefore assigned to ordered starch material (van Soest *et al.*, 1995). The peak

ratio of 1000/1022 cm^{-1} can therefore be used to represent the proportion of ordered to disordered carbohydrate starch material on the surface. The development of an additional band at 1047 cm^{-1} can be used to represent the crystalline state, hence the ratio intensity of 1047/1022 cm^{-1} can also be used to express the degree of molecular order (Liu *et al.*, 2014). FTIR-ATR can therefore be used to effectively monitor the degree of order on the surface of starch granules for native, gelatinised and retrograded starches.

2.3.1.1 Native starch

All FTIR spectra were obtained using a Perkin Elmer Spectrum One® FTIR spectroscope equipped with a SensIR technologies IR II Durascope® diamond cell ATR device. This was accompanied with a diamond crystal with an angle of incidence of 45º. A 10 µL aliquot of 10 mg/mL starch in water was placed on the surface crystal and scanned over the wavelength range of 4000-550 cm^{-1}, with a total of 24 scans. A background spectrum was also measured and subtracted from the final sample spectra before analysis.

2.3.1.2 Gelatinised and retrograded starch

For gelatinised starch, a 10 mg/mL mixture was heated in water at 90ºC for 20 min and then left to cool at room temperature for another 20 min before an FTIR-ATR spectrum was taken. The preparation for retrograded starch was identical to that of gelatinised starch but stored at room temperature for up to 96h with measurements being taken every 24h.

2.3.2 Differential Scanning Calorimetry (DSC)

DSC has been used by many workers to study the endothermic starch gelatinisation process. The heat input breaks non-covalent interactions between polymer chains which hold the starch granule together. DSC measures the amount of heat required to do this and is therefore used to determine the amount of ordered starch material. The adiabatic DSC chamber contains metal reference pans (containing water) and sample pans which are both heated at a constant heating rate. In a heat flux mechanism, the reference and sample pans are linked by a heating metal plate with thermocouples recording the amount of energy required to maintain the same heating rate for both pans. This allows changes in the heat flow (considered to be proportional to the heat capacity) between the reference and sample pan to be recorded as a function of temperature (Gill *et al.*, 2010). The melting of ordered chains gives rise to an endothermic transition peak that can be observed along the thermogram. Integrating the endothermic peak then allows the gelatinisation/retrogradation enthalpy change ($\Delta_{gel}H/\Delta_{ret}H$) to be determined (Figure 2.1). Therefore the enthalpy change can be used to represent the relative amounts of ordered material present in the starch granule. The peak, onset and conclusion temperatures (T_o, T_p, T_c) can also be determined from the thermograms (Bogracheva *et al.*, 2002).

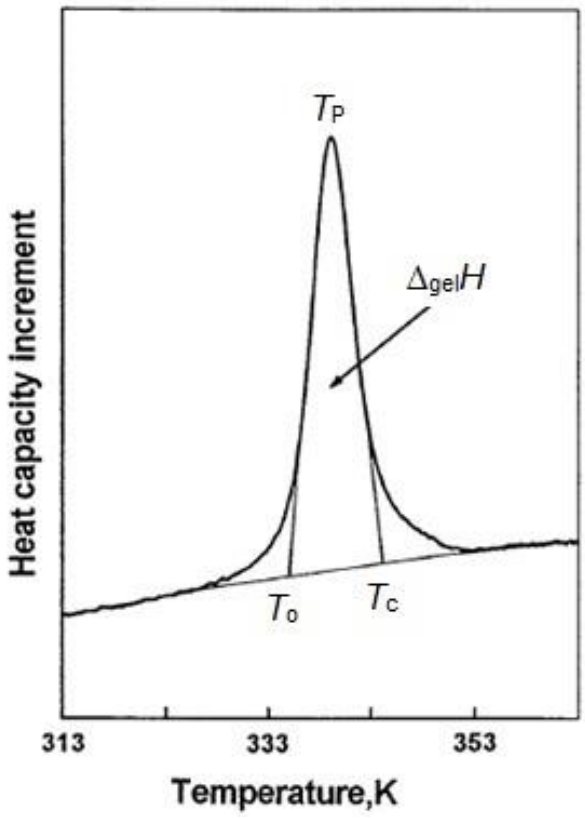

Figure 2.1. Example of a DSC thermogram showing the gelatinisation enthalpy ($\Delta_{gel}H$), onset (T_o), peak (T_p) and conclusion (T_c) temperatures. Adapted from (Bogracheva et al., 2002).

2.3.2.1 Native starch

All DSC thermograms were obtained using a TA instruments Multi-Cell Differential Scanning Calorimeter (MC DSC). Each starch sample was analysed for the gelatinisation temperature and the gelatinisation enthalpy, represented by the maximum peak temperature and the area under the heat absorption peak, respectively. In addition, the onset and conclusion temperatures were also determined. Native starch samples (50 mg) were accurately weighed into Hallestoy steel ampoules with 1 g of dH_2O. A blank ampoule containing 1 g of dH_2O only was also used in each run as a reference. All ampoules were then

placed inside the MC DSC and left to equilibrate for 2h at 20^{o}C to attain an even distribution of water. Samples were then scanned from 20^{o}C to 100^{o}C at a rate of 0.5^{o}C min^{-1}. High amylose maize starch was scanned from 20^{o}C to 150^{o}C at a rate of 0.5^{o}C min^{-1}, to ensure complete gelatinisation of the amylose polymer chains. The chamber was cooled with liquid nitrogen at a constant flow rate of 50 mL min^{-1}. The slow heating rate of 0.5^{o}C min^{-1} ensures the gelatinisation process is 'quasi-equilibrium'. The samples were then cooled from 100^{o}C to 20^{o}C (150^{o}C to 20^{o}C for high amylose maize) at a rate of 1^{o}C min^{-1}.

2.3.2.2 Gelatinised starch

For gelatinised starches, MC DSC was used to examine each sample after the cooling period from the initial heating process of native starch (mentioned above). An identical heating rate and temperature range was used. However to avoid retrogradation, the gelatinised starch samples were left to equilibrate for 30 min only (instead of 2h) at 20^{o}C before being scanned.

2.3.2.3 Retrograded starch

To obtain DSC thermograms for retrograded starch material, two starch concentrations were prepared: 50 mg/mL and 200 mg/mL. A 50 mg sample of native starch was placed into Hallestoy steel ampoules with 1 g of dH_2O. Starch samples were then gelatinised as mentioned before, with a reference ampoule containing 1 g of dH_2O. The steel ampoules were then stored at room temperature for 48h to produce retrograded starch material. Retrograded starch samples were then scanned at a heating rate of 0.5^{o}C min^{-1} from 20^{o}C to

150^{o}C. The slow heating rate and high temperature ensures the retrograded amylose chains were completely gelatinised.

To prepare a starch concentration of 200 mg/mL, a 200 mg sample was accurately weighted into Hallestoy steel ampoules with 1 mg of dH_2O. A reference ampoule containing 1 mg of dH_2O was also used. The heating parameters for 200 mg/mL starch concentrations were identical to the 50 mg/mL samples. Starch samples were then gelatinised as mentioned previously. Immediately after the first heating scan another heating scan was performed to ensure complete gelatinisation occurred at a 200 mg/mL concentration. Ampoules were then stored at 4^{o}C for 1 week before being scanned again.

Thermograms for native, gelatinised and retrograded starches were analysed using NanoAnalyze and TA instruments Universal Analysis© software to determine onset, conclusion and peak temperatures and gelatinisation enthalpies. All DSC measurements were performed in triplicate and results are presented as mean values. However the 50 mg/mL and 200 mg/mL retrograded starch experiments were conducted in duplicate only.

2.3.3 Powder X-ray diffraction (XRD)

Powder X-ray diffraction (XRD) is an analytical technique commonly used to determine the degree of crystallinity. A static X-ray tube projects X-rays, from high energy electrons, towards the crystalline material causing X-ray scatter at various different angles. A detector is rotated through an arc to count the X-ray

scatters at different angles to produce a diffraction pattern. Amorphous material has no regular arrangement of atoms and therefore no diffraction pattern is produced (Suryanarayana and Norton, 1998). Figure 2.2 shows a schematic diagram of diffracted X-rays.

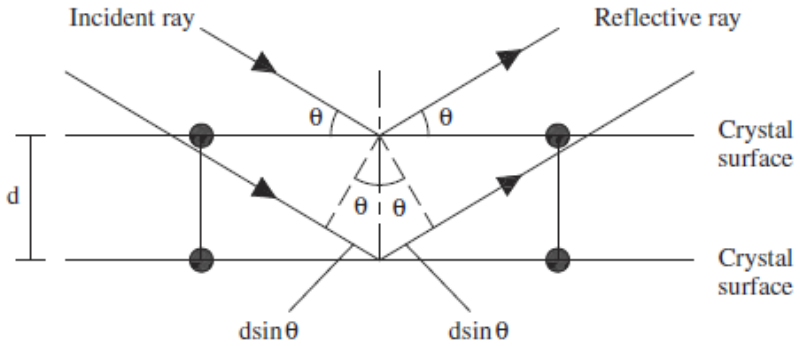

Figure 2.2. Schematic diagram of X-rays being diffracted from the crystal surface. Adapted from (Tong et al., 2012).

Two different X-ray scattering methods are often used; small angle X-ray scattering (SAXS) and wide angle X-ray scattering (WAXS). Wide angle detects X-ray scattering over larger scattering angles compared with SAXS and therefore yields information about starch crystallinity, while identification of starch structure (pores, growth rings, and diameter) is revealed by SAXS (Jenkins and Donald, 1998). X-ray diffraction is often employed to study precise changes in starch structure and crystallinity upon processing treatment (gelatinisation and retrogradation).

2.3.3.1 Native starch

The starch granule structure contains repeating units of amorphous and semi-crystalline regions, in which the crystalline regions have been previously

examined using Powder XRD by many groups (Buléon *et al.*, 1998). Crystalline starch material consists of mainly double helical amylopectin chains which causes diffraction to occur when high energy waves encounter such ordered starch material. The amorphous regions contain loose amylose chains, which have no regular arrangements of atoms and therefore do not diffract X-rays and remain undetectable.

Wide-angle X-ray scattering was recorded using a Rigaku MiniFlex 600 instrument with CuKα radiation (λ= 1.548Å) at 40 kV, 15 mA. A small quantity of native starch powder was mounted on an aluminium sample holder, with a piece of glass being used to level the sample to reduce errors during the scanning process. The samples were scanned over an angular range (2θ) of 3-40^{o} and analysed using OriginPro 9.1© software. The degree of crystallinity was calculated by separating the crystalline peaks from the amorphous region. Firstly, an amorphous background was fitted by applying a linear baseline from the beginning of the XRD pattern to the end (tail to tail). A smooth curve was then computer plotted under the crystalline peaks, with the area above the curve representing crystalline material and the area below representing amorphous material. Both crystalline and amorphous patterns were then integrated using OriginPro 9.1©. Figure 2.3, adapted from Xia et al. (2012), shows how the degree of amorphous and crystalline starch material can be determined from a typical XRD pattern.

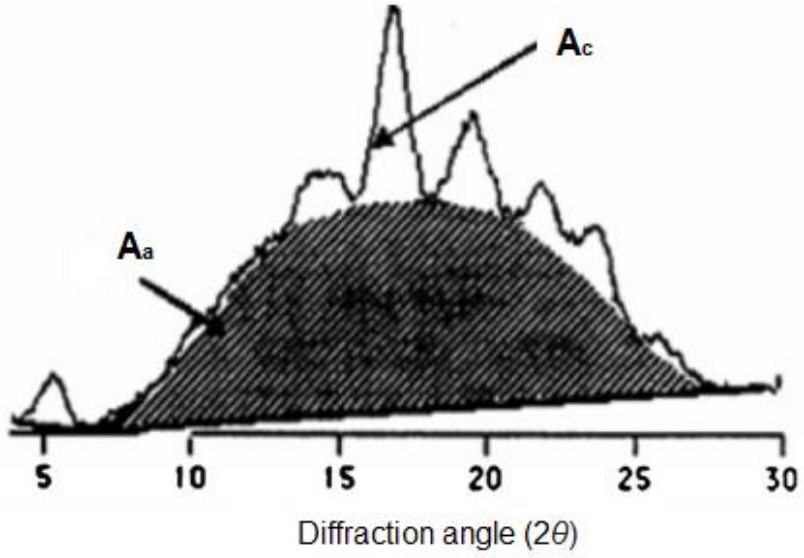

Figure 2.3. Schematic diagram showing how the degree of crystallinity can be estimated from an XRD pattern. A_a and A_c refer to the amorphous and crystalline area, respectively. Adapted from (Xia et al., 2012).

The area under the amorphous background corresponds to the amount of amorphous material (A_a) and the sum of the area under all reflection peaks represents the total starch crystallinity (A_c). The degree of crystallinity was therefore estimated using Equation 5 (Lopez-Rubio *et al.*, 2008). The curve fitting procedure was repeated three times to ensure accurate fittings were applied.

Equation 5

$$\text{Crystallinity } (\%) = \frac{A_c}{A_c + A_a}$$

Equation 5. Starch crystallinity calculation.

2.3.3.2 Gelatinised and retrograded starch

A 10 mg/mL wheat and high amylose maize starch was prepared in dH_2O and gelatinised at 121^oC for 20 min before the mixture was transferred to individual 50 mL Falcon tubes. Excess ethanol was then added and centrifuged at 2,500 g for 10 min, allowing the gelatinised starch material to sediment to the bottom of the tube. However at this point no sedimentation for high amylose maize starch occurred and therefore only wheat starch was used. The supernatant from each Falcon tube was discarded and the pellet transferred to large aluminium pans. Samples were frozen at -20^oC before being freeze dried to a powder form for XRD analysis. Retrograded starch material was prepared in an almost identical way except high amylose maize starch was used and autoclaved at 121^oC. All tubes were then stored at room temperature for 48h to produce retrograded starch material. The samples were scanned over 3-40^o 2θ and analysed using OriginPro 9.1©. The degree of crystallinity was then calculated using Equation 5.

2.4 Log of slope (LOS) plot

2.4.1 Preparation and processing treatment of starch

For native (non-heat treated) starch, a 100 mg sample was prepared in 20 mL PBS to give a starch concentration of 5 mg/mL. This was agitated in a glass beaker on a magnetic hotplate for 20 min at room temperature (22^oC), to ensure no large starch lumps were present. Four mL aliquots of the stock solution were then pipetted into separate 15 mL Falcon tubes using an Eppendorf Multipette Plus Pipettor. The final volume inside the reaction mixture was 4 mL.

For gelatinised (heat treated) starch, a 5 mg/mL stock solution was prepared in a conical flask and covered with aluminium foil to minimise evaporation. The flask was then agitated in a water bath on a magnetic hotplate (IKA® RET basic), with a target temperature set at 90ºC. A thermocouple probe (IKA® Ikatron, supplied by Fisher Scientific, Loughborough UK) was placed inside the water bath to regulate the temperature of the heating process. Once the target temperature was reached, the stock solution was cooked at 90ºC for 20 min. This allows the starch to be completely gelatinised. The solution was then allowed to cool for 20 min at room temperature. The cooling time allows the solution to reach ~40ºC (monitored by digital thermocouple thermometer) and thus allows accurate pipetting of the viscous solution. Four mL aliquots were collected from the stock solution using an Eppendorf Multipette Plus pipettor and pipetted into separate 15 mL Falcon tubes before use in the enzyme assay.

For retrograded starch (heat-cooled), a 5 mg/mL stock solution was heated and prepared similar to gelatinised starch. However the 4 mL aliquots in the Falcon tubes were stored at room temperature for 24h to produce retrograded starch material. In addition to storage at room temperature, genetically modified maize starches were also stored at a constant temperature of 4ºC for 24h. This was to determine the effects of retrogradation at low temperatures. Both gelatinised and retrograded starch suspensions were weighed before and after gelatinisation and any water loss was adjusted for with dH_2O.

2.4.2 Enzyme assay: Prolonged starch digestion

To calculate C_∞ from the digestion of native and processed starches by PPA the assay explained by Goñi et al. (1997) was performed with a few changes. Native, gelatinised and 24h retrograded starch samples were placed in a mixing rotator inside an incubator at 37^{o}C for 20 min (native and retrograded starch) or 5 min (gelatinised starch). This ensured the temperature inside the reaction tube was 37^{o}C, which was also checked with a digital thermocouple thermometer. The difference in the incubation time is because gelatinised starch was pre-cooled to ~40^{o}C, but native and retrograded starch was stored at 22^{o}C, therefore taking a longer time to reach the desired reaction temperature of 37^{o}C.

After the incubation time, the tubes were removed and placed into a 37^{o}C water bath to maintain the correct temperature. At time zero, 300 µL was removed from each tube and transferred into an Eppendorf tube on ice containing 300 µL of 0.3 M sodium carbonate solution. Sodium carbonate is also referred to as 'stop solution' as the high pH renders PPA inactive. Different PPA concentrations were used for native and processed starches. Native starch digestion was started when 200 µL of 89.29 nM α-amylase solution (diluted in PBS) was added to each tube, giving a final concentration of 4.5 nM. Gelatinised and 24h retrograded starch digestion began when 100 µL of 89.29 nM α-amylase solution was added to each tube, giving a final concentration of 2.25 nM. Therefore the final α-amylase concentration was 4.5 nM for native starch and 2.25 nM for gelatinised starch. The reason for the doubled PPA concentration in native starch was because the rate is very slow and therefore

more enzyme is needed in order to obtain a reliable measurement of product within the time of the experiment.

The tubes were then placed back into the mixer and 300 µL aliquots were collected every 5 min up to 30 min, then every 15 min up to 1.5h with the last aliquot being collected at 2h. Each aliquot was transferred into an Eppendorf tube on ice containing 300 µL of stop solution. Eppendorfs were then centrifuged at 13,000 g for 5 min and 400 µL of the supernatant was pipetted into empty Eppendorfs. All tubes were then frozen (-20^{o}C) for later use in the Prussian blue assay.

2.4.3 Prussian blue assay

2.4.3.1 Background

Reducing sugars released from the digestion of starch by PPA are mainly maltose and maltotriose. The sugars can be detected using a sensitive colorimetric Prussian blue assay, which was introduced by Park and Johnson (1949) and involves the reduction of ferricyanide ions to ferric ferrocyanide (Prussian blue). Moretti and Thorson (2008) ranked the Prussian blue assay as the most sensitive sugar indicator, with the 3, 5-dinitrosalycylic acid (DNS) method being the least sensitive. Therefore, the Prussian blue assay was selected instead of the DNS assay due to its higher sensitivity and reliability. The former method was further modified by Schinner and Von Mersi (1990) by increasing the quantity of cyanide. This ensures that the ferricyanide ions are completely reduced. However, as colour development still continued after 1h, Slaughter and workers suggested leaving the samples for 2h (Slaughter *et al.*,

2001). This was later extended to 2.5h by Tahir and colleagues (Tahir *et al.*, 2010).

2.4.3.2 Methodology

The frozen samples from the enzyme assay (Section 2.4.2) were allowed to thaw at room temperature. Each sample was diluted with dH_2O into 1.5 mL Eppendorfs, which are suitable for use at boiling temperature, to ensure the maltose concentration fell within the working range (0-100 µM maltose).

To each Eppendorf, 150 µL of solution A (16 mM KCN, 0.19 M Na_2CO_3 in dH_20) and solution B (1.18 mM $K_3Fe(CN)_6$ in dH_20) were added and each tube was vortex mixed before being placed in a boiling water bath for 15 min. The samples were then removed and allowed to cool at room temperature for 10 min before 750 µL of solution C (3.11 mM $NH_4Fe(SO_4)_2$, 0.1% (w/w) SDS, 0.2% (v/v) H_2SO_4 in dH_20) was added. The tubes were allowed to stand at room temperature for 2.5h before the absorbance was read at 695 nm. Maltose standards ranging from 0-100 µM were prepared from a 3.4 mg/mL (10 mM) pre-frozen maltose stock solution and assayed at the same time. To obtain a maltose standard range between 0-100 µM, a 100 µL aliquot of 10 mM maltose stock solution was diluted in 10 mL water.

2.4.4 Data analysis

The maltose concentrations were obtained from the standard curve and plotted against time to obtain a digestibility plot. A slope was taken between each data point on the digestibility plot and natural logarithms were applied. Values were

then plotted against the mean time to give a linear plot, allowing the rate constant (k) and C_∞ to be calculated from the slope and y intercept, respectively.

2.5 Enzyme kinetic studies

2.5.1 Preparation and processing treatment of starch

2.5.1.1 Native starch

A 10 mg/mL stock solution of native starch was prepared and agitated in a glass beaker on a magnetic hotplate for 20 min at room temperature. Aliquots from the stock solution were then diluted into separate 15 mL Falcon tubes with PBS using an Eppendorf Multipette Plus pipettor. The final volume inside the reaction mixture was 4 mL.

2.5.1.2 Gelatinised starch

A 10 mg/mL stock solution of gelatinised starch was prepared in a conical flask and covered with aluminium foil to minimise evaporation. The flask was then agitated in a water bath on a magnetic hotplate with a target temperature set at 90^{o}C. A thermocouple probe was placed inside the water bath to monitor the temperature of the heating process. Once the target temperature was reached, the stock solution was cooked for 20 min at 90^{o}C to allow the starch to be completely gelatinised. All starches were prepared in this way except high amylose maize starch. A 10 mg/mL stock solution of high amylose maize starch was pre-gelatinised at 100^{o}C for 10 min before being autoclaved at 121^{o}C for 20 min. The pre-gelatinisation step ensures no starch sedimentation occurs during

the autoclaving process. The 121^{o}C autoclaving process ensures complete gelatinisation of the amylose chains. All gelatinised starch suspensions were weighed before and after heating to ensure water evaporation was minimal.

All starch stock solutions were then allowed to cool for 20 min at room temperature. The cooling time allows the solution to reach ~40^{o}C and thus allows accurate pipetting of the viscous solution. Aliquots were collected from the stock solutions using an Eppendorf Multipette Plus pipettor and diluted to 4 mL with PBS into separate 15 mL Falcon tubes before use in the enzyme assay. The dilution process results in different starch concentrations for the enzyme assay.

2.5.1.3 Retrograded starch

For retrograded starch, a 10 mg/mL stock solution was heated and prepared similar to gelatinised starch. However aliquots from the stock sample were first transferred into 15 mL Falcon tubes and then stored at room temperature for 6, 18, 24, 48, 72 and 96 hours. Samples were then diluted to 4 mL with PBS to achieve a range of different starch concentrations. The dilution process only occurred after the specified storage time to ensure starch retrogradation was achieved at the same concentration. This step is very important, as previous studies have shown starch concentration plays a role in the rate of retrogradation (Longton and Legrys, 1981; Zeleznak and Hoseney, 1986).

To study the effects of retrogradation at 4^{o}C, a 10 mg/mL stock solution of gelatinised wheat and potato starch was stored in a cold room at a constant

temperature of 4^{o}C for 7 days. After 7 days, the starch samples were taken out of the cold room and diluted with PBS to achieve the desired starch concentrations.

To ensure no bacterial growth was occurring in the 15 mL Falcon tubes, additional studies were conducted with sodium azide. Sodium azide has been known to be an inhibiting substance that prevents the growth of bacterial microorganisms. Therefore, 48h and 96h retrograded wheat starch was prepared as mentioned before. However to each 15 mL Falcon tube, 0.02% (w/v) sodium azide was added to prevent bacterial contamination (Snyder and Lichstein, 1940; Slack *et al.*, 1979).

2.5.2 Enzyme assay: Initial starch digestion

In order to study the initial rate of digestion of native and processed starches by PPA, the enzyme assay originally described by Holm et al. (1988) was used. This assay was later modified by Slaughter et al. (2001) and Tahir et al. (2010); however, changes were further introduced to make the assay suitable for the digestion of retrograded starch. In short, the assay involved taking aliquots at regular time intervals (up to 12 min) from the reaction mixture to study the extent of initial starch hydrolysis.

Aliquots were collected from the pre-treated 10 mg/mL stock solution of native, gelatinised and retrograded starches. These were then diluted with PBS into separate 15 mL Falcon tubes. However for retrograded starch, the sample was first transferred to the Falcon tubes and then stored (dilution with PBS only

occurred after the specific storage time). The dilution process gives a range of starch concentrations (10, 7.5, 5, 2.5, 1 and 0.5 mg/mL[1]) to be used for the enzyme assay. [1]0.5 mg/mL was not used for native starch.

The Falcon tubes were then placed in a mixing rotator inside an incubator at 37 ^{o}C for 5 min (gelatinised starch) or 20 min (native and retrograded starch). This ensured the temperature inside the reaction tube was 37^{o}C, which was also checked with a digital thermocouple thermometer. The difference in the pre-incubation time required for reaching 37^{0}C was attributed to gelatinised starch being pre-cooled to ~40^{o}C, while native and retrograded starch was stored at room temperature.

After the incubation time, the tubes were removed and placed into a 37^{o}C water bath. At time zero, 300 µL was removed from each tube and transferred into an Eppendorf tube placed on ice containing 300 µL of 0.3 M sodium carbonate solution (stop solution). Starch digestion was started when 50 µL of 89.29 nM α-amylase solution (diluted in PBS) was added to each tube. The final α-amylase concentration in each tube was 1.2 nM. The tubes were then placed back into the mixer and 300 µL aliquots were removed at 4, 8, and 12 min and quenched as before. The sample tubes were placed in a 37^{o}C water bath when removed from the incubating mixer; this ensures the correct temperature of 37^{o}C is maintained inside the reaction mixture.

Eppendorfs were then centrifuged at 13,000 g for 5 min and 400 µL of the supernatant was pipetted into empty Eppendorfs. All samples were then frozen

at -20°C for later use in the Prussian blue assay. A flow diagram of the initial starch digestion assay is shown in Figure 2.4.

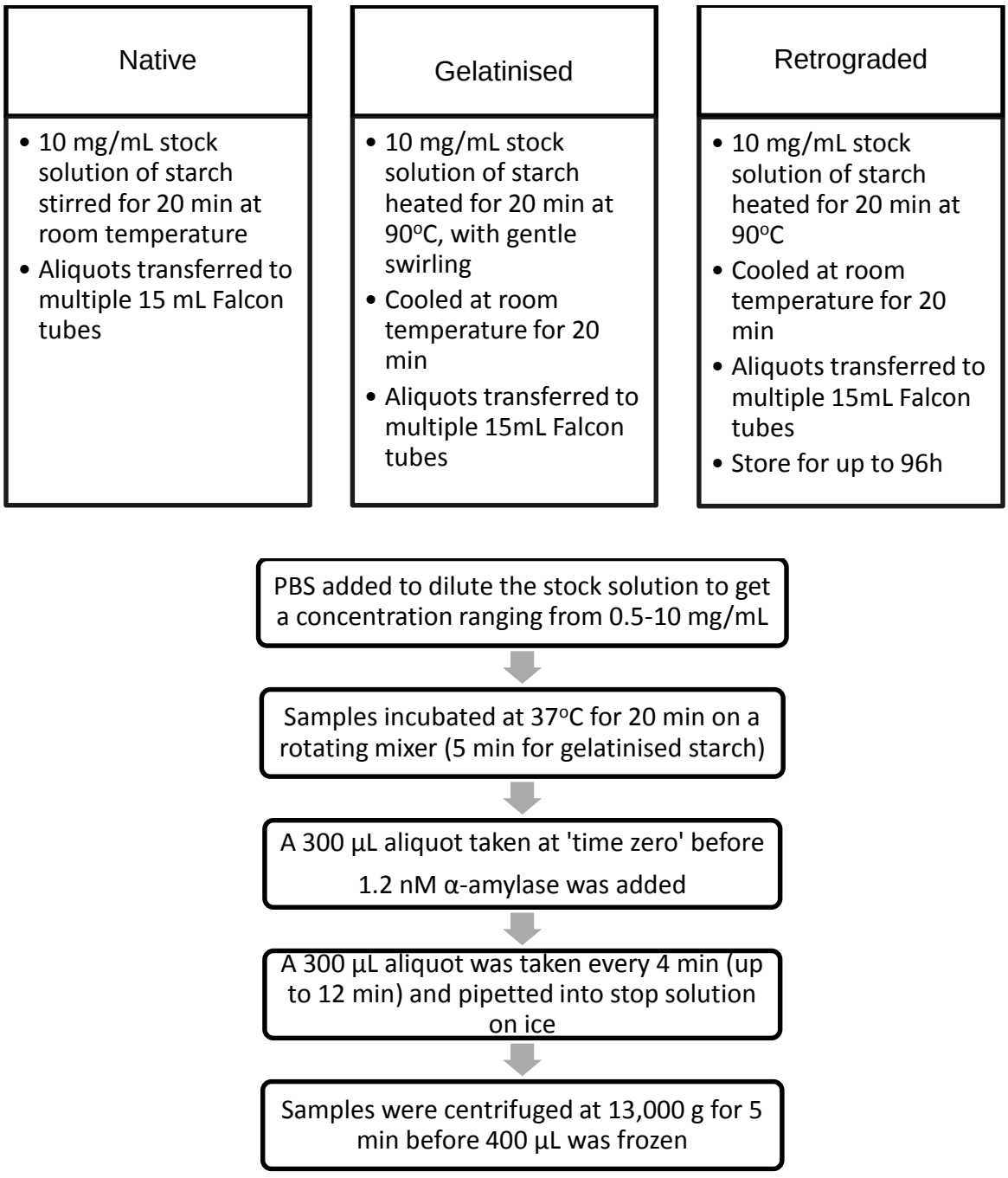

Figure 2.4. Flow chart showing the starch preparation and digestion process by PPA.

2.5.3 Prussian blue assay

The Prussian blue assay method used was identical to that mentioned in Section 2.4.3.

2.5.4 Data analysis

The initial rate of digestion was then calculated by plotting the maltose produced from starch digestion against time in Microsoft Excel, with the slope being the initial rate. The maltose production was calculated from the absorbance values obtained from the reducing sugar assay. The calculated initial rate for each starch concentration was then entered into Sigmaplot 12.0, which fits the data to the Michaelis-Menten equation using non-linear regression. This allows K_m and V_{max} to be calculated, which can then be used to calculate k_{cat} (V_{max}/[PPA]) and k_{cat}/K_m.

2.6 Purified retrograded high amylose maize starch (purified RHAM)

2.6.1 Producing purified RHAM

The Megazyme kit contents and the preparation of reagents can be found in Appendix B. A 10 mg/mL high amylose maize starch suspension was prepared in dH_2O and gelatinised at 100^oC for 10 min prior to being autoclaved at 121^oC for 20 min. The pre-heat treatment effect before autoclaving ensures there is minimal starch sedimentation during the autoclaving process. The starch samples were then transferred into multiple 50 mL Falcon tubes and stored at 4^oC for 24h. The cooled starch paste was then stored at 37^oC for another 24h

(cycle of 4/37^{o}C). This heat-cool cycle was repeated three times, a method that has previously been shown to significantly increase the production of retrograded starch material under heat-cool conditions (Sievert and Pomeranz, 1989; Park *et al.*, 2009). To each Falcon tube, 3 mL of PPA (10 mg/mL) containing AMG (3 U/mL) (solution 2) was added and vortex mixed. All tubes were then placed on a rotatory mixer to allow end-over-end mixing inside an incubator at 37 ^{o}C for 18h; this process ensures all non-resistant starch material was digested. The reaction was then stopped by the addition of 3 mL ethanol. The samples were then centrifuged at 1,500 g for 10 min and the supernatant was discarded leaving only the starch pellet. This removes all reducing sugars produced from the digestion process, leaving only purified RHAM at the bottom of the Falcon tube. The starch pellet from each tube was then transferred into aluminium pans and frozen at -80^{o}C for 3h to solidify the sample. The aluminium pans containing purified RHAM were freeze dried to a powder form and stored in 50 mL Falcon tubes inside a desiccator.

2.6.2 Measuring resistant starch content

The amount of resistant starch present in purified RHAM was determined by using the Megazyme Resistant Starch Test (AOAC 2002.02 Official Method), with slight modifications. An accurately weighted quantity of starch material (20 mg) was placed into three 50 mL Falcon tubes (triplicates). To each tube, 3 mL of pancreatic amylase (10 mg/mL) containing AMG (3 U/mL) (solution 2) was added. The tubes were then vortex mixed and incubated at 37^{o}C on a rotatory mixer for end-over-end mixing for 16h. To each tube, 8 mL of 50% ethanol was added to stop the reaction and the samples were centrifuged at 1,500 g for

10 min. The supernatant was then removed and a magnetic stir bar was added along with 2 mL of 2 M potassium hydroxide. The samples were placed in an ice bath over a magnetic stirrer for 20 min. An 8 mL solution of 1.2 M sodium acetate buffer (pH 3.8) was added along with 0.1 mL AMG (bottle 1; 3300 U/mL). Tubes were then mixed and placed in a 50^{o}C water bath for 30 min with intermittent mixing.

The solution was transferred to a 100 mL volumetric flask and brought up to the mark by adding dH_2O and mixed well. An aliquot of the solution was centrifuged at 1,500 g for 10 min. A 33 µL aliquot of the centrifuged sample was pipetted into a blank Eppendorf tube, to which 1 mL of GOPOD reagent (solution 4) was added. The samples were then incubated in a water bath at 50^{o}C for 20 min to allow colour development. This method was run in parallel with the maize starch control (bottle 6) which has a quoted resistant starch content of 52.5%.

Reagent blank and D-glucose standards were also prepared. The reagent blank was prepared by mixing 33 µL of 100 mM sodium acetate buffer (pH 4.5) and 1 mL of GOPOD reagent. D-glucose standards were prepared in quadruplicates and consisted of 33 µL of D-glucose (bottle 5) with 1 mL of GOPOD reagent. The absorbance of each sample, maize starch control and D-glucose control was read at 510 nm against the reagent blank. The resistant starch content was then calculated using the Megazyme online spreadsheet and Equation 6.

Equation 6

$$\text{Resistant starch } \% = \Delta E \text{ x } \frac{F}{W} \text{ x } \frac{162}{180}$$

Equation 6. Resistant starch content. ΔE is the absorbance read against the reagent blank. F is the conversion from the absorbance to micrograms (100 µg) divided by the GOPOD absorbance for 100 µg of D-glucose. W is the dry weight of the sample analysed (not accounting for the moisture content) and 162/180 represents the adjustment from free D-glucose to anhydro D-glucose.

2.6.3 Starch characterisation

2.6.3.1 Moisture, amylose/amylopectin ratio and protein content

The moisture, amylose/amylopectin ratio and protein content were determined as described previously in Section 2.2 of this chapter.

2.6.3.2 Differential scanning calorimetry (DSC)

A 50 mg sample of purified RHAM was weighed into Hallestoy steel ampoules with 1 g of dH_2O (50 mg/mL). A reference ampoule containing only 1 g of dH_2O was also prepared. All ampoules were then left to equilibrate for 2h at 20^oC inside the MC DSC before being scanned from 20^oC to 150^oC at a rate of 0.5^oC min^{-1}. The high temperature ensures complete gelatinisation of retrograded amylose. The chamber was cooled with liquid nitrogen at a constant flow rate of 50 mL min^{-1}. After the gelatinisation process, samples were cooled from 150^oC to 20^oC at a rate of 1^oC min^{-1}. NanoAnalyze and TA instruments Universal Analysis© software were then used to analyse retrograded crystallites along the thermograms.

2.6.3.3 X-ray diffraction (XRD)

Wide-angle X-ray diffraction was performed on purified RHAM at University College London (UCL), with the assistance of Dr Gareth Williams. The sample was scanned over an angular range of 3º to 40º 2θ and the XRD pattern was analysed to calculate crystallinity using OriginPro 9.1©. Specific details of the parameters used can be found in Section 2.3.3.

2.6.3.4 Scanning electron microscope (SEM)

The microstructure and morphology of purified RHAM was characterised using a FEI Quanta 200F scanning electron microscope. The sample was adhered onto an aluminium SEM stub using double sided carbon impregnated discs and given a 10 nm gold coating in a Quorum Q150T sputter coater prior to viewing. Dr David McCarthy at University College London (UCL) kindly provided the SEM images.

2.6.3.5 FTIR-ATR

The degree of ordered starch material on the surface of the retrograded granule was determined by FTIR-ATR. A 10 mg/mL solution of was prepared in dH_2O and scanned over the wavelength range of 4000 cm^{-1} to 550 cm^{-1}, with a total of 24 scans. All measurements were carried out at room temperature.

2.6.4 *In vitro* digestion

Purified RHAM concentrations ranging from 1-10 mg/mL were prepared in PBS and placed on a rotatory mixer incubated at 37ºC for 20 min. The starch

samples were then digested with 1.2 nM PPA. Aliquots of 300 µL were collected every 4 min up to 12 min and pipetted into new Eppendorfs on ice containing 300 µL of stop solution. Samples were then centrifuged at 13,000 g for 5 min and 400 µL of the supernatant for each sample was collected. All samples were frozen at -20^{o}C until the Prussian blue assay was performed to determine the enzyme kinetic parameters (K_m, V_{max}, k_{cat} and k_{cat}/K_m).

2.6.5 Mode of Inhibition

2.6.5.1 Substrate preparation

A 10 mg/mL wheat starch sample was prepared in PBS and gelatinised at 90^{o}C for 20 min. Samples were then pipetted into 15 mL Falcon tubes and diluted in PBS to give a working substrate concentration ranging from 0.5-2 mg/mL.

2.6.5.2 Inhibitor preparation

A 10 mg/mL purified RHAM sample was prepared in PBS and agitated gently for 10 min by swirling. This was diluted to give a working inhibitor concentration of 0.25 mg/mL. Aliquots were then added to each 15 mL Falcon tube containing gelatinised wheat substrate (the substrate concentration ranged from 0.5-2 mg/mL). The final volume inside the reaction mixture was 4 mL. Table 2.1 shows the volume of substrate, inhibitor and PBS used to obtain an inhibitor concentration of 0.25 mg/mL. This process was then repeated for varying inhibitor concentrations (0.5, 0.75 and 1 mg/mL).

Table 2.1. Volume of wheat substrate and purified RHAM inhibitor used from a 10 mg/mL stock solution to obtain a final inhibitor concentration of 0.25 mg/mL. The gelatinised wheat substrate concentration ranged from 0.5-2 mg/mL.

Substrate (mL)	0.2	0.4	0.6	0.8
Inhibitor (mL)	0.1	0.1	0.1	0.1
PBS (mL)	3.7	3.5	3.3	3.1
Substrate (mg/mL)	0.5	1	1.5	2
Inhibitor (mg/mL)	0.25	0.25	0.25	0.25

2.6.5.3 In vitro digestion

Samples were mixed and placed into the incubator for end-over-end mixing for 5 min before 300 µL was withdrawn at 0 min. A 50 µL aliquot of 89.29 nM α-amylase (diluted in PBS) was then added to each Falcon tube. The final α-amylase concentration in each tube was 1.2 nM. The reaction mixture comprising of α-amylase, gelatinised wheat substrate and purified RHAM inhibitor was incubated for 12 min with 300 µL aliquots collected every 4 min. Transferring the aliquots into new Eppendorf tubes on ice containing 300 µL of 0.3 M sodium carbonate solution stopped the reaction. A starch control containing no inhibitor was also prepared to ensure the inhibition effect was a direct result of retrograded high amylose maize starch. Eppendorfs were then centrifuged at 13,000 g for 5 min and 400 µL of the supernatant was pipetted into empty Eppendorfs. Reducing sugars were then determined using the

standard Prussian blue assay before being recorded spectrophotometrically at 695 nm.

The reducing sugar concentration was expressed as maltose equivalents by reference to a maltose standard curve. Initial reaction rates were then calculated at various substrate concentrations and entered into Sigmaplot 12.0. The mode of inhibition was determined using Lineweaver-Burk and Dixon plots. The former provides values for $1/K_m$ and $1/V_{max}$ while the latter provides values for K_i.

2.7 Amylose leaching

2.7.1 Light Microscopy

Amylose leaching was examined using a Nikon Microphot-FXA light microscope. Images were captured using an Infinity 2 colour camera connected to a computer equipped with Infinity capture software. A 5 mg/mL stock solution of wheat and potato starch was gelatinised at 90^{o}C for 20 min. A small aliquot of the gelatinised sample was then placed onto a microscope slide with a small drop of Lugol's iodine (5% (w/v) I_2 with 10% (w/v) KI). A glass coverslip was placed on top and the slides were then visualised under the microscope at magnification x10. Granule ghost and supernatant starch material was also isolated from the original stock solution by centrifugation at 2,000 g for 10 min. The supernatant was then carefully transferred into a separate 15 mL Falcon tube and the remaining ghost material was resuspended in water. A small aliquot (10 µL) of the supernatant and granule ghost material was stained with Lugol's iodine before analysis under a light microscope.

The original wheat and potato stock solution was then stored at room temperature for 24h to retrograde. The granule ghost and supernatant were separated by the centrifugation process mentioned before. The staining and imaging process was repeated again for the stock solution, granule ghost and supernatant of retrograded starch.

2.7.2 FTIR-ATR

To determine the amount of ordered material in the leached solution, a 10 mg/mL stock solution of wheat and potato starch was gelatinised in dH_2O at 90^oC for 20 min. Both starches were then centrifuged at 2,000 g for 10 min before a 10 µL aliquot of the supernatant was scanned as mentioned previously in Section 2.3.1. This experiment was conducted to confirm no ordered material was present in the supernatant immediately after gelatinisation. This process was repeated for retrograded wheat and potato starch with the inclusion of a 24h storage time at room temperature before analysis. By noting the total ordered material in the stock solution of gelatinised and retrograded starch, the percentage of ordered leached material could be calculated.

Chapter 3 Starch characterisation

3.1 Introduction

The starches used in all the experiments described in this thesis were obtained from different commercial suppliers having been extracted from different botanical sources. Therefore it is essential to characterise these starches using a range a physical and chemical methods to provide explanations about likely variations in their digestibility behaviour. Native starch has a semi-crystalline granule structure which varies in granule size (1-100 µm) and shape (e.g. round, lenticular, polygonal) depending upon the botanical starch source (Tester *et al.*, 2004; Kaur *et al.*, 2010). The size and shape of starch granules are important morphological features which allow some distinction to be made between different botanical sources. Information on the size and shape of granules can be achieved by using conventional light microscopy. Viewing starch granules under polarised filters however can also reveal information on the birefringence pattern. Such light microscopy methods are often used to observe granule transformation during hydrothermal processing.

Starch granules contain small amounts of non-carbohydrate components such as lipids and proteins. Different starch sources vary in protein content, amylose-amylopectin ratio and proportion of crystalline and amorphous regions due to different environmental conditions during growth and harvesting (Chatakanonda *et al.*, 2003). These differences influence the properties of raw and hydrothermally processed starch (i.e. domestic and industrial cooking), which are known to have a significant impact on the rate and extent of starch digestion. Therefore to be able to provide a better explanation of the enzyme

kinetic data, described in subsequent chapters, accurate analysis of the composition, structure and properties of starch is required. The following section introduces methods to determine the structure and physicochemical properties of cereal, tuber and legume starches. This will allow a comparison to be made of the main structural features and properties of the different starch samples.

3.2 Materials and methods

For this study various starches were characterised and used in the experiments described in subsequent Chapters: 4, 5 and 6. Full details of the sources of all the starches used are given in Chapter 2, Section 2.1 and any additional chemical purity was provided by Tahir and workers (Tahir *et al.*, 2010). The total starch content was determined using the Megazyme Total Starch Assay kit. BCA protein assay kit and all other reagents were purchased from Sigma chemical company (Poole, Dorset, UK).

The iodine binding method was used to determine the amylose/amylopectin ratio, the details of which are given in Section 2.2.4 of Chapter 2. Briefly, a known weight of starch was dissolved in DMSO with iodine at room temperature overnight. Aliquots were then diluted in water and the absorbance recorded at 600 nm. Potato amylose type III standards were also prepared alongside to generate a calibration graph.

All starches were boiled in 2% (w/v) SDS to extract the proteins from the starch granule and the protein content was determined using the BCA protein assay kit. The moisture contents of the starch samples were determined by drying

overnight at 103^{o}C, in a forced-air oven, a known weight of starch placed in aluminium pans and recording the difference in weight between the original and the dried samples.

The Congo red dye binding method was used to determine the amount of damaged starch granules. The granular structure of native starch was examined using light microscopy fitted with cross polarisers and scanning electron microscopy. Gelatinised and retrograded starch, granule ghosts and leached amylose was also stained with Lugol's iodine and viewed under a light microscope.

Further details of the characterisation methods are given in Chapter 2, Section 2.2 but the physical characterisation of starches using FTIR, DSC and XRD are described in Chapter 4.

3.3 Results and Discussion

3.3.1 Total starch and moisture content

The total starch content was determined for all starches using the Megazyme Total Starch Assay kit. The moisture content of starch samples was measured as described in Chapter 2. The total starch and moisture content values are presented in Table 3.1. The starch content was relatively high for all starches on a dry weight basis indicating an efficient extraction process with little impurities. The moisture contents of the starches were also consistent with previous data provided by Tahir and colleagues (Tahir *et al.*, 2010).

Table 3.1. Total starch (wet weight) and moisture contents of native starches. All values are means of three replicates ± SEM.

Starch	Total starch (%)	Moisture (%)
Wheat	86.3 ± 1.12	11.1 ± 0.6
Potato	86.7 ± 2.92	16.3 ± 0.5
Wild type pea	85.4 ± 1.46	12.8 ± 1.9
Durum wheat	87.0 ± 0.10	15.1 ± 0.4
Maize	85.9 ± 1.58	11.3 ± 0.6
Waxy maize	84.5 ± 2.67	13.7 ± 0.4
High amylose maize	82.6 ± 2.72	12.0 ± 1.2
Rice	81.6 ± 3.07	15.0 ± 0.6

3.3.2 Protein content

All starch granules contain a relatively small fraction of proteins (less than 0.6%) which are surface bound and/or located inside the starch granule (Tester *et al.*, 2004). Surface bound proteins have a lower molecular weight than internal proteins and collectively these proteins are referred to as starch granule associated proteins (SGAP) and contribute to starch biosynthesis (Martin and Smith, 1995; Baldwin, 2001). The fraction of proteins present depends upon the botanical starch source and purification process.

The most common method used to determine the starch protein content is the Kjeldahl method. Briefly, this method measures the total amount of nitrogen produced during starch digestion and uses an empirical factor (6.25) to convert the nitrogen value to total protein content. However as mentioned in Chapter 2,

the Kjeldahl method is extremely time consuming and is not a direct measure of protein. Therefore the protein contents for all the starch samples were determined using the BCA assay. The method of protein extraction was adapted from previous work (Debet and Gidley, 2007; Zhang *et al.*, 2014); these groups used SDS to extract surface proteins from maize and wheat starch before SDS-PAGE analysis. The results presented in Table 3.2 are within the reported range of the literature (Baldwin, 2001; Pérez and Bertoft, 2010). The BCA method does seem to be a simpler and more direct method of determining the protein content, compared with the more time consuming standard Kjeldahl method which has multiple steps providing many opportunities for error.

Table 3.2. Protein content determined by the BCA assay. Values expressed as a percentage are mean values ± SEM from three-four replicates.

Starch	Protein (%)
	BCA assay
Wheat	0.14 ± 0.01
Potato	0.05 ± 0.00
Wild type pea	0.25 ± 0.01
Durum wheat	0.10 ± 0.00
Maize	0.16 ± 0.03
Waxy maize	0.32 ± 0.04
High amylose maize	0.46 ± 0.02
Rice	0.20 ± 0.03

3.3.3 Amylose-amylopectin ratio

The amylose-amylopectin ratio varies depending upon the starch source and variations can also occur within the same botanical source (Davydova *et al.*, 1995). Typically most starches consist of 15-30% amylose, with the exception of mutant genotype starches. These include waxy starches (virtually no amylose) and high amylose starches (70-80% amylose). The iodine binding method was used to determine the amylose content, from which the amylopectin content can be calculated by difference (Table 3.3). The amylose contents determined by Tahir et al. (2010) using the Megazyme kit method were higher than the respective values produced by the iodine binding method (20.3% vs. 28.3% and 15.5% vs. 21.0% for wheat and potato starch, respectively). The reasons for the discrepancies are unknown exactly, but the iodine binding is a physical property whereas the Megazyme kit is based upon digestion with enzymes. Therefore some differences in the estimations are expected. Nevertheless, the iodine results were regarded as reliable for comparisons between the starches studied given that the estimates fell within the widely reported range of 15-30% amylose in starches (Pérez and Bertoft, 2010).

Table 3.3. Amylose content determined by the iodine binding method presented as mean values ± SEM from three-four replicates.

Starch	Amylose (%)
	Iodine binding method
Wheat	20.3 ± 0.9
Potato	15.5 ± 1.9
Wild type pea	26.8 ± 1.6
Durum wheat	29.2 ± 1.5
Maize	22.8 ± 0.8
Waxy maize	1.2 ± 0.1
High amylose maize	79.1 ± 4.3
Rice	17.8 ± 1.1

Previous workers have commonly used the concanavalin A method to quantify the amylose content. This method involves the interaction of concanavalin A with the non-reducing ends of the amylopectin glucan polymers chains. Precipitate formation occurs at the bottom of the sample tube, with the non-associated amylose chains remaining in the supernatant being determined by enzymic hydrolysis. However amylose chains can co-precipitate with amylopectin resulting in an underestimation of the total amylose content. This procedure is also more complex and time consuming than the iodine binding method. Many reports have suggested the iodine binding method can result in overestimation of the amylose content due to amylopectin-iodine complex formations. However, the use of the correction factor in the equation accounts

for the small amount of amylopectin bound iodine, and therefore previous workers have indicated that it provides an accurate estimate of the total amylose content (Gibson *et al.*, 1997; Vilaplana *et al.*, 2012).

3.3.4 Starch damage

Starch damage was determined using Congo red dye, which enters and stains damaged starch granules and can be observed under a light microscope. Table 3.4 shows a very small amount of damaged starch granules for the non-vigorous processing method used during starch extraction.

Table 3.4. Starch damage (%) determined using the Congo red method. Stained starch granules were counted from a total of 1000 granules.

Starch	Starch damage (%)
Wheat	0.3
Potato	n.d.*
Wild type pea	0.2
Durum wheat	n.d.*
Maize	n.d.*
Waxy maize	n.d.*
High amylose maize	n.d.*
Rice	0.2

*not detectable

3.3.5 Birefringence

Granular birefringence was determined for native starch granules, as shown in Figure 3.1 and 3.2. Examination of the starch granules under polarised light reveals a birefringence pattern with a characteristic “Maltese cross”, which for most starches appears in the centre but for potato it appears towards the edge of the granule. Birefringence is indicative of a high degree of molecular orientation within the starch granule, with the dark Maltese cross pattern indicating an aligned crystalline structure. Different starch granule sizes were also observed with rice being the smallest and potato being the largest. This explains why the small rice starch granules are very difficult to observe at 10x magnification (Figure 3.1C).

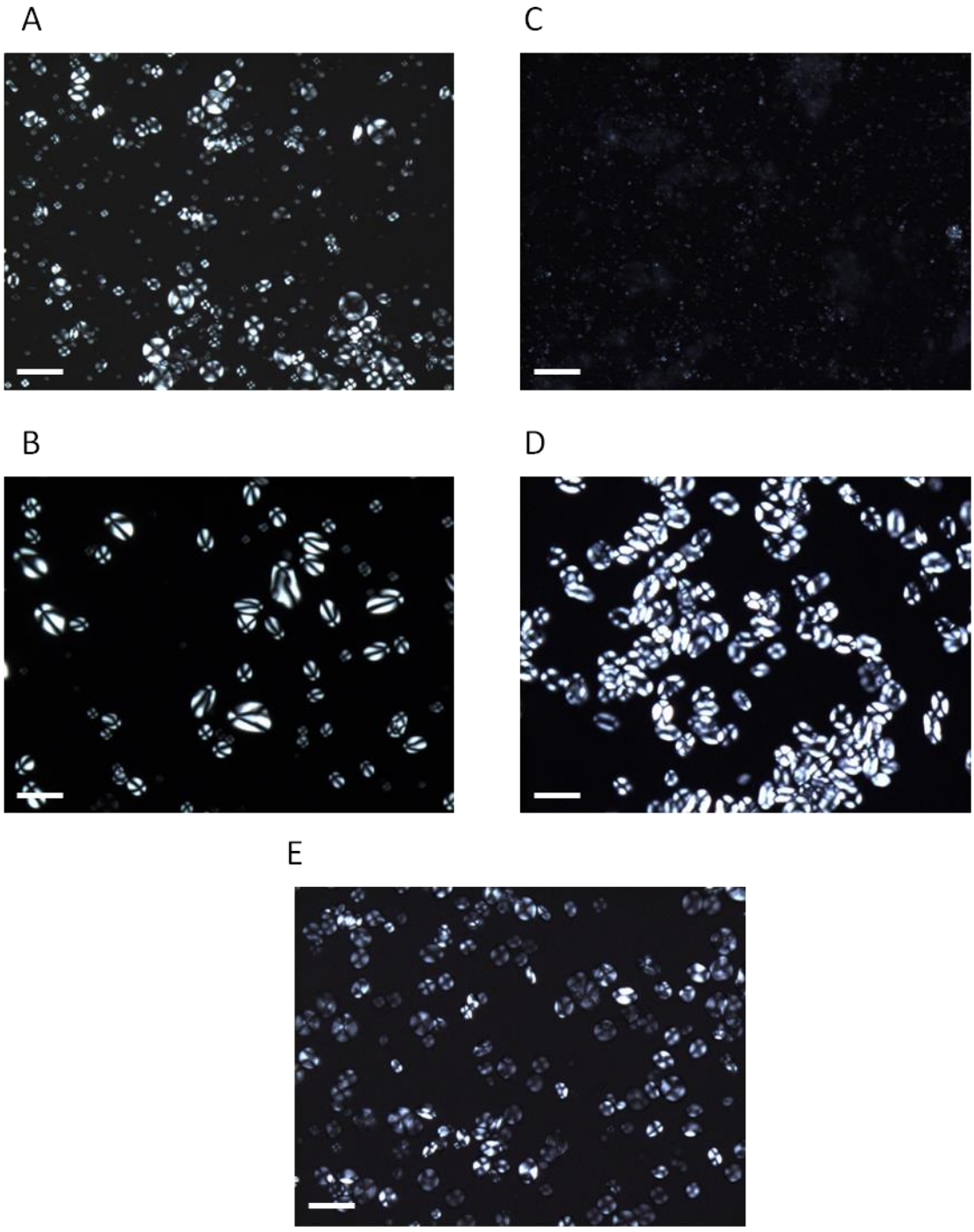

Figure 3.1. Polarised light micrographs of native wheat (A), potato (B), rice (C), wild type pea (D) and durum wheat (E) starch. Images were photographed at 10x magnification. Scale bar = 50 µm.

A similar birefringence pattern for maize and waxy maize starch was also observed (Figure 3.2). However, high amylose maize starch showed less birefringence compared with normal and waxy maize. This is most likely due to the high amylose content, which is localised in the amorphous regions of the starch granule. As a result, the amount of amorphous material in high amylose maize starch is higher than other starches. Therefore the quantity of ordered α-glucan chains is reduced resulting in less birefringence. Similar studies have also observed a reduced birefringence for different high amylose starches under crossed polarised light (Schwall *et al.*, 2000; Xie *et al.*, 2006; Tahir *et al.*, 2011).

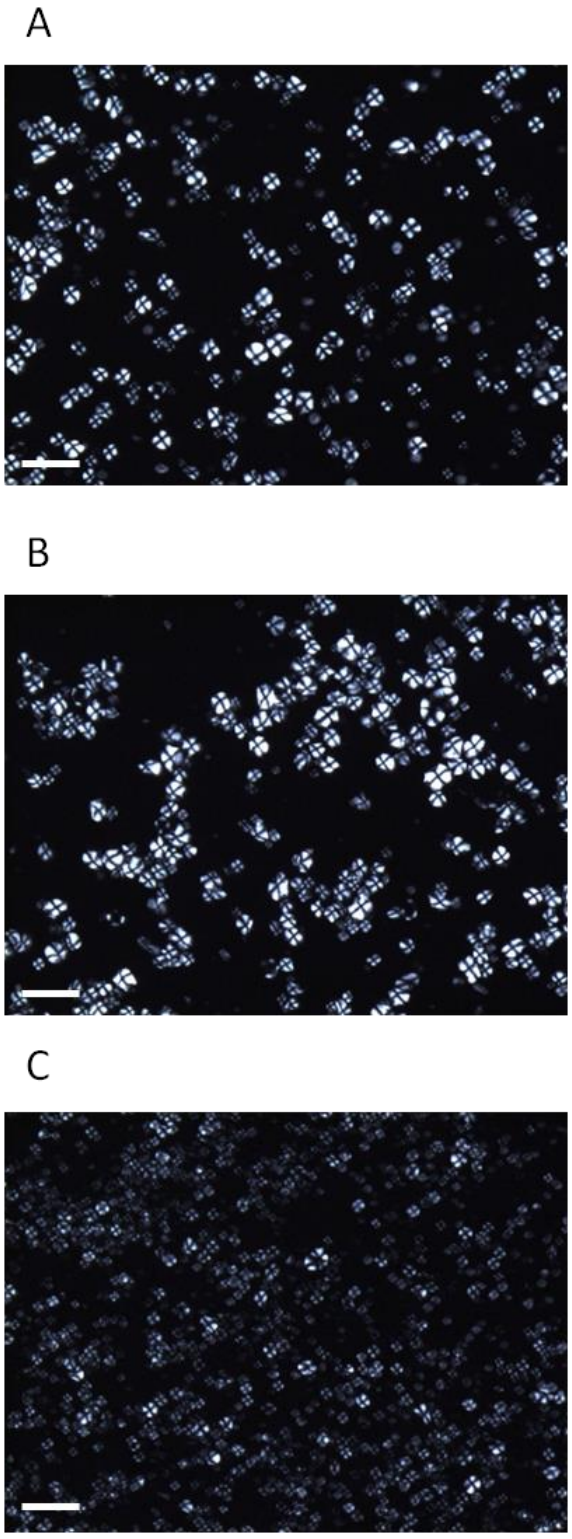

Figure 3.2. Polarised light micrographs of native maize (A), waxy maize (B) and high amylose maize (C) starch. Images were photographed at 10x magnification. Scale bar = 50 µm.

3.3.6 Scanning electron microscope (SEM)

Native maize (Figure 3.3), waxy maize (Figure 3.4) and high amylose maize (Figure 3.5) starches were examined using SEM. The granular structure for native maize starch showed significant variations in size and shape with a mixture of small and large granules containing some spherical and some polygonal shapes. The morphology and granular size of waxy maize starch was identical to that observed in normal maize starch.

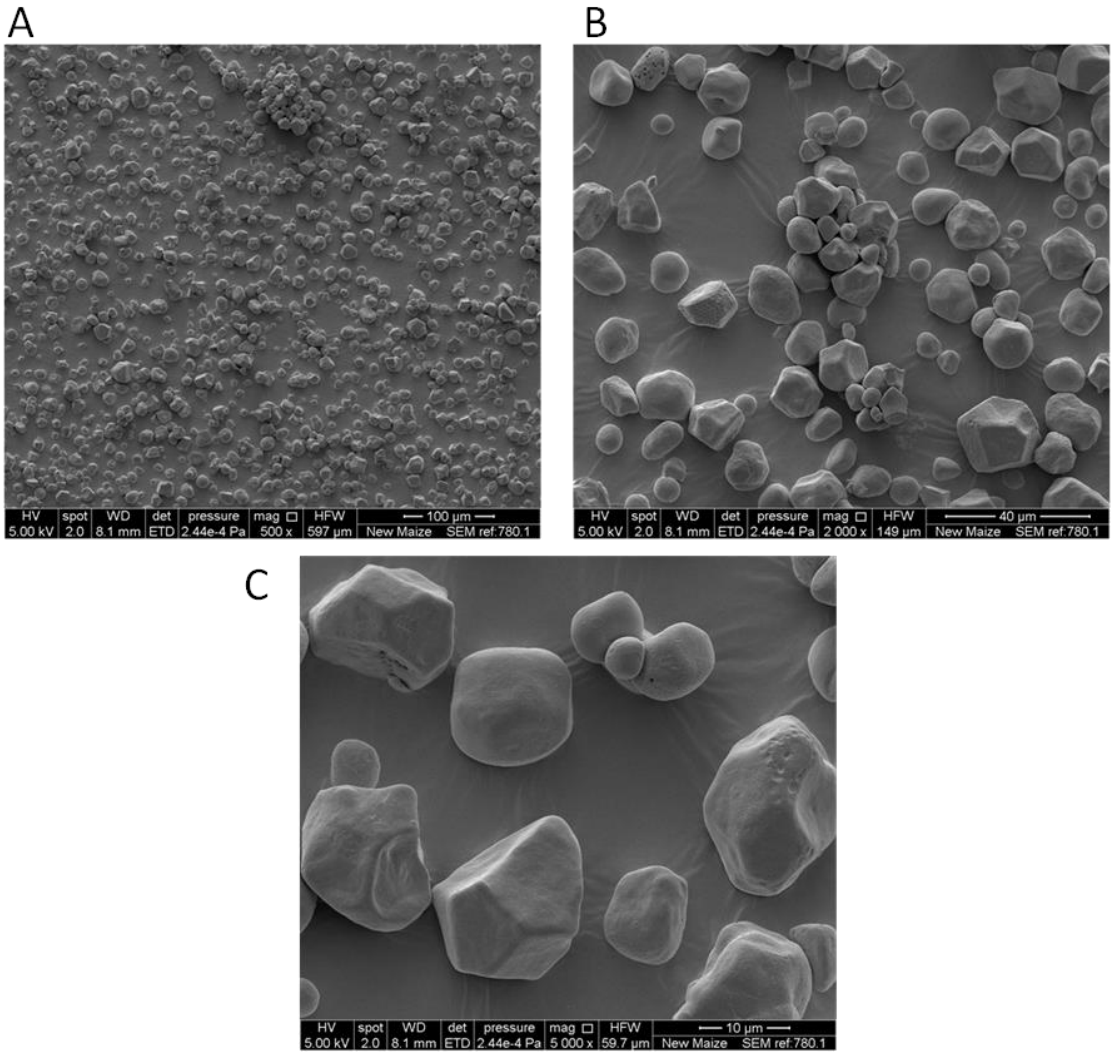

Figure 3.3. SEM micrographs of native maize starch granules at magnification 500x (A), 2,000x (B) and 5,000x (C), with scale bars of 100, 40 and 10 µm, respectively.

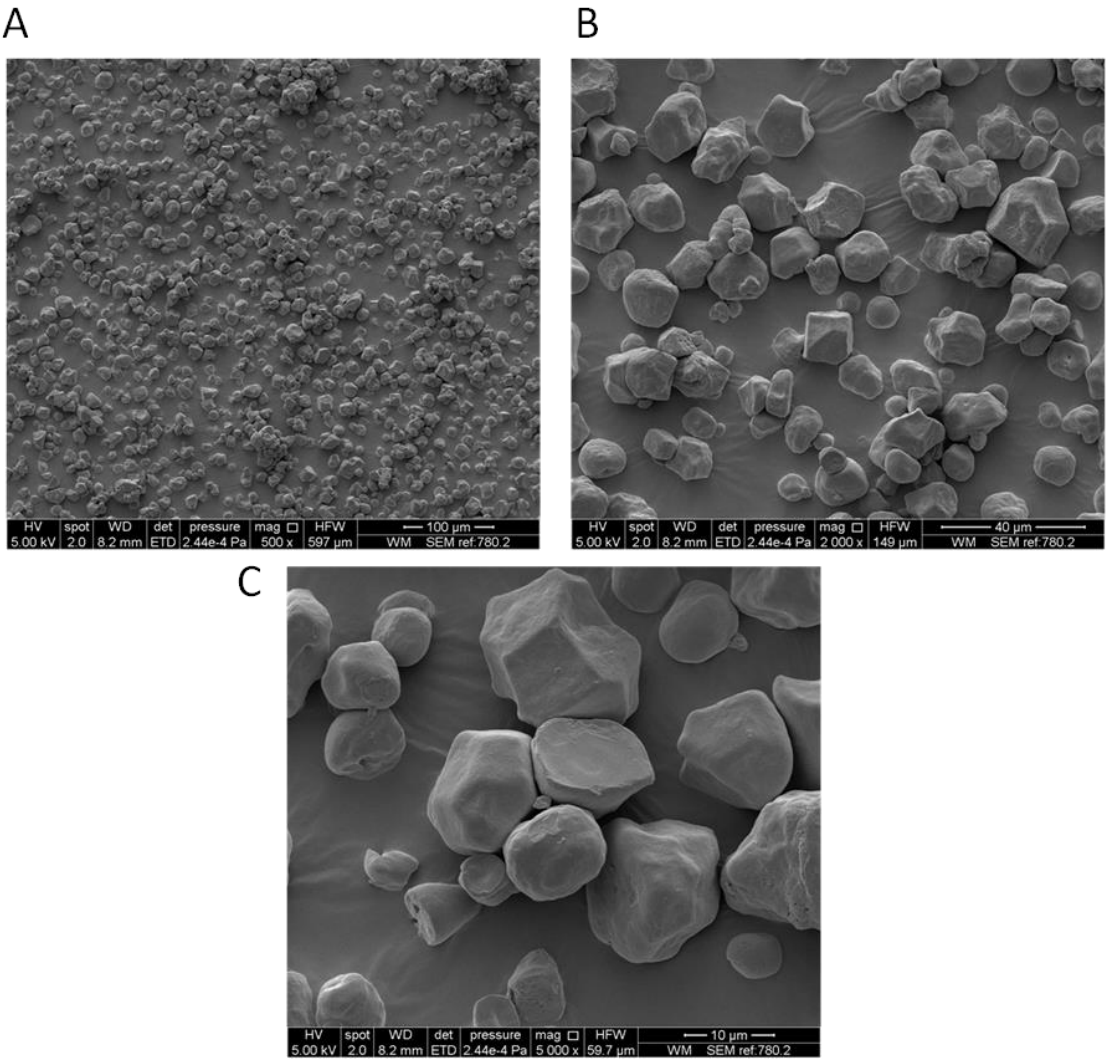

Figure 3.4. SEM micrographs of native waxy maize starch at magnification 500x (A), 2,000x (B) and 5,000x (C), with scale bars of 100, 40 and 10 µm, respectively.

SEM images of native high amylose maize starch showed significant differences in size and granular shape. Micrographs of the individual granules were much smaller with the surfaces appearing to be smoother and more spherical compared with the angular shapes observed in normal and waxy maize. Buléon and workers have reported a granule size ranging from 5-25 µm for high amylose maize starch (Buléon *et al.*, 1998). High amylose maize starch

granules also showed greater heterogeneity in shape in the granule population observed, including the presence of elongated granules in agreement with previous observations (Cai *et al.*, 2014).

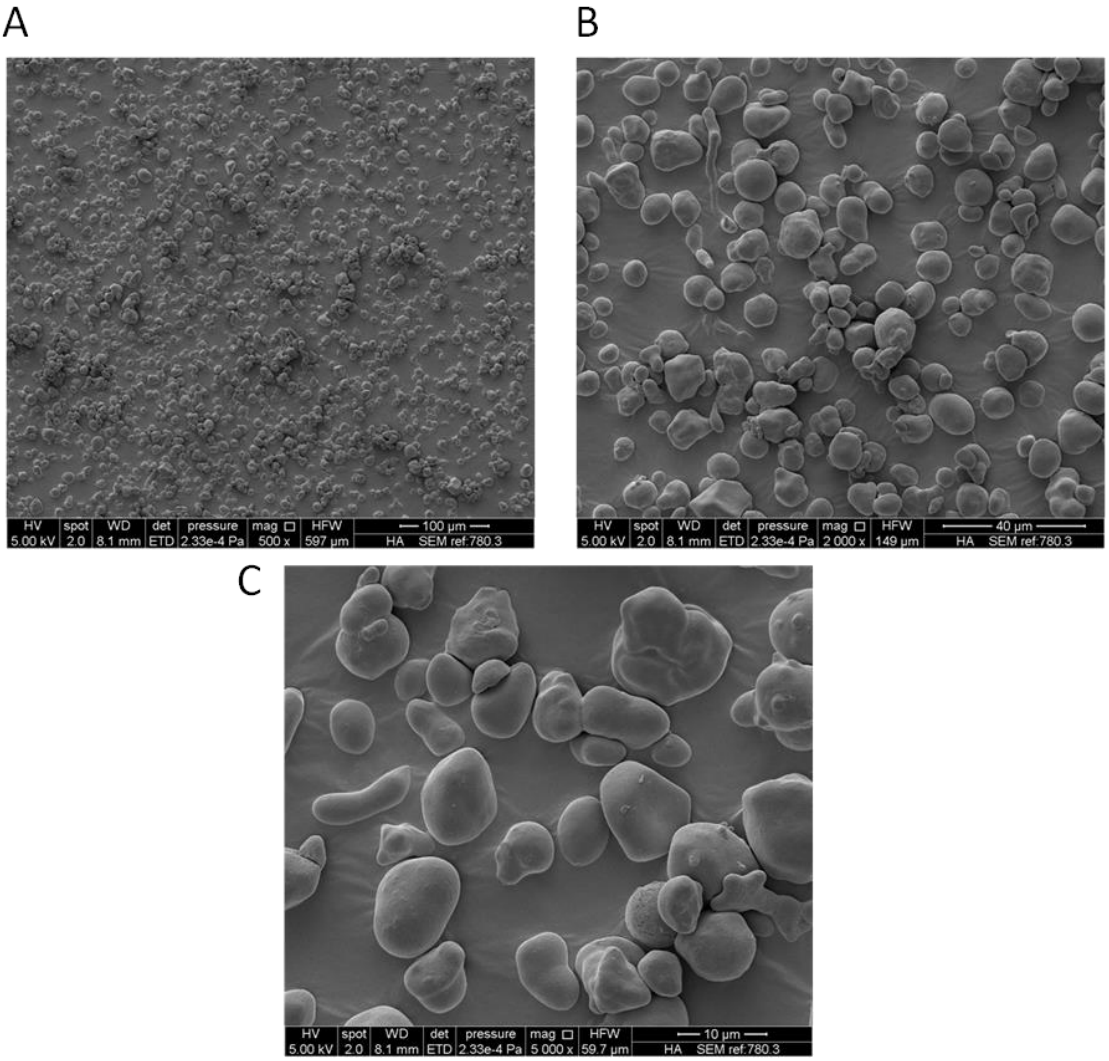

Figure 3.5. SEM micrographs of native high amylose maize starch at magnification 500x (A), 2,000x (B) and 5,000x (C), with scale bars of 100, 40 and 10 µm, respectively.

SEM can also be used to examine the granule surface to identify surface pits and pores, which are believed to facilitate amylase entry into the granule (Dhital

et al., 2010). However, in this study SEM was only used to reveal information about granule size and shape for native starches.

3.3.7 Microscopy of leached amylose

3.3.7.1 Gelatinised starch

Gelatinised samples of wheat and potato starch were stained with Lugol's iodine and assessed using light microscopy (Figure 3.6A and 3.6B). The dark red/brown stains indicate amylopectin granule ghosts, with the blue background being the leached amylose that diffuses out of the granule during gelatinisation.

Figure 3.6C and 3.6D represents isolated suspensions of wheat and potato granular ghosts separated by centrifugation. The red/brown stain suggests that the majority of the granule ghost material contains amylopectin with small amounts of amylose. Wheat granule ghosts also maintain more structural integrity relative to the collapsed granule ghosts of potato starch. This is similar to the SEM images by Zhang and workers which showed deterioration of the granule ghosts for potato starch (Zhang *et al.*, 2014). A possible explanation for this may be the thinner walls of the ghost material resulting in greater expansion and remnant fracture. Debet and Gidley also used microscopy to determine the integrity of maize and wheat starch and concluded that granule ghost integrity was intermediate for wheat starch (Debet and Gidley, 2007). This is most likely due to the higher surface protein content in wheat starch which is linked to ghost stability whereas the low protein content in potato starch possible results in more fragile ghosts. In addition to this, the relatively high levels of phosphate

ions in potato starch favour rapid swelling in aqueous solution and contribute to the loss of structural integrity (Debet and Gidley, 2007).

Light microscope images were also taken of the isolated supernatant containing amylose leached from the gelatinisation of wheat and potato starch (Figure 3.6E and 3.6F). Micrographs for both starches only show leached amylose represented by the blue stain. The absence of a red/brown stain suggests the isolated supernatant only contains amylose and no visible amylopectin.

Using light microscopy, Obanni and Bemiller studied granule ghosts from different botanical starch sources and identified ghosts in the supernatant of potato starch (Obanni and Bemiller, 1996). This result is not compatible with our observations of the micrograph images and one explanation of this could be the difference in centrifugation speed used for preparation of the ghosts and supernatant (i.e. 2,000 g compared with 1,000 g) and indeed this probably plays a crucial role. A centrifugation speed of 2,000 g was decided upon as more recent work by others used this speed to isolate and examine granule ghosts (Debet and Gidley, 2007; Zhang *et al.*, 2014). Previous workers have also used this centrifugation speed to isolate and quantitatively estimate the extent of leached amylose post gelatinisation by the iodine binding method (Hoover and Manuel, 1996; Chung *et al.*, 2009).

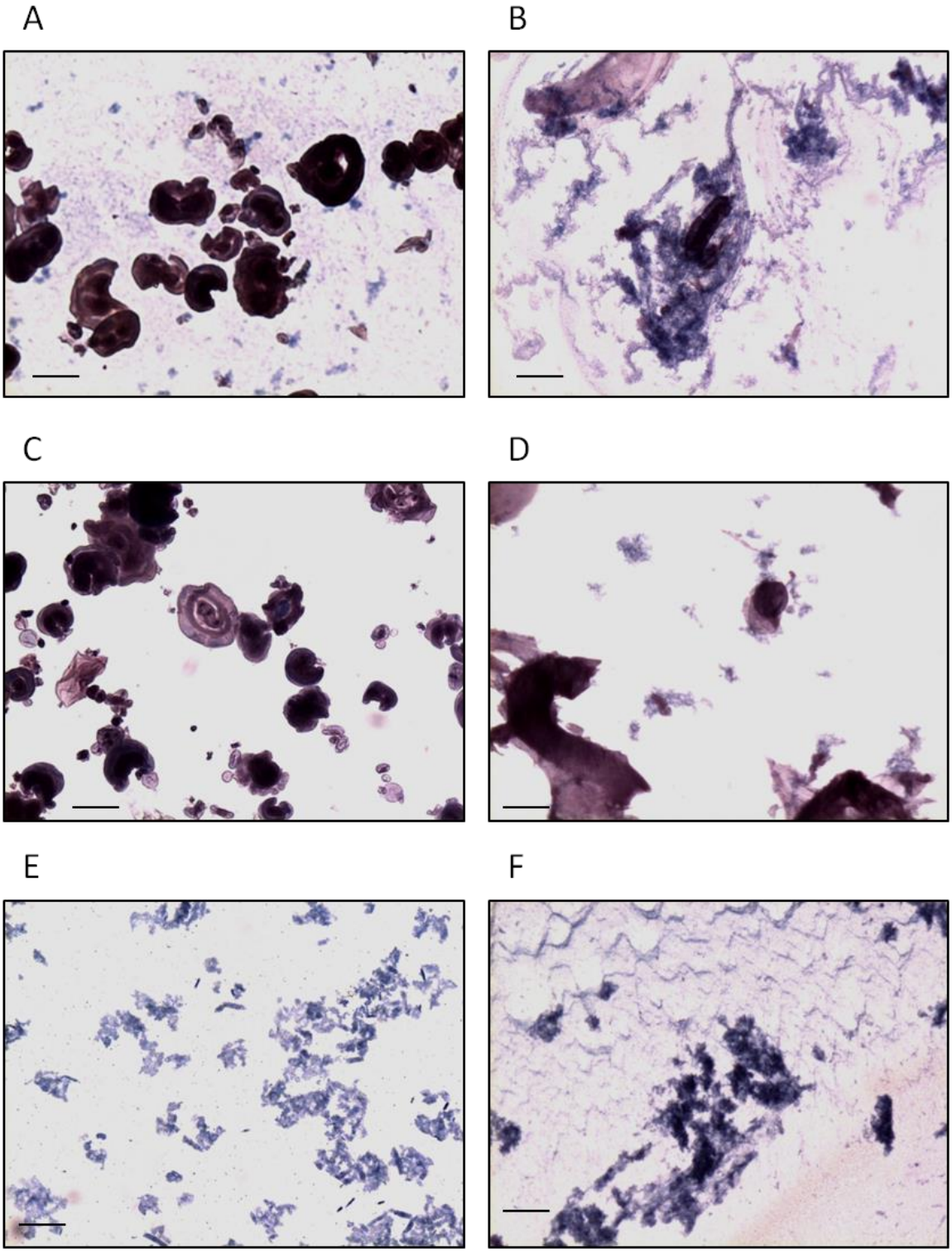

Figure 3.6. Light microscope images of gelatinised starch; wheat (A) and potato (B), granule ghosts; wheat (C) and potato (D), and leached amylose; wheat (E) and potato (F). All samples were stained with Lugol's iodine and viewed at magnification x10. Scale bar = 50 µm.

3.3.7.2 Retrograded starch

Wheat and potato starches were stored for 24h at room temperature to produce retrograded starch material before being stained with Lugol's iodine and examined under a light microscope (Figure 3.7A and 3.7B). Similar to the images obtained for gelatinised starch, ghost remnants and leached amylose can still be identified after storage for 24h. Micrographs of isolated granule ghosts in retrograded starch are similar to that of the granule ghosts observed in gelatinised starch (Figure 3.7C and 3.7D). The dark red/brown stain suggests the granule ghosts consist mainly of amylopectin with minimal amylose. Leached amylose from retrograded wheat and potato starch was also examined, showing no granule ghosts remained in the supernatant. Therefore the extracted supernatant only contains leached amylose as shown in Figure 3.7E and 3.7F.

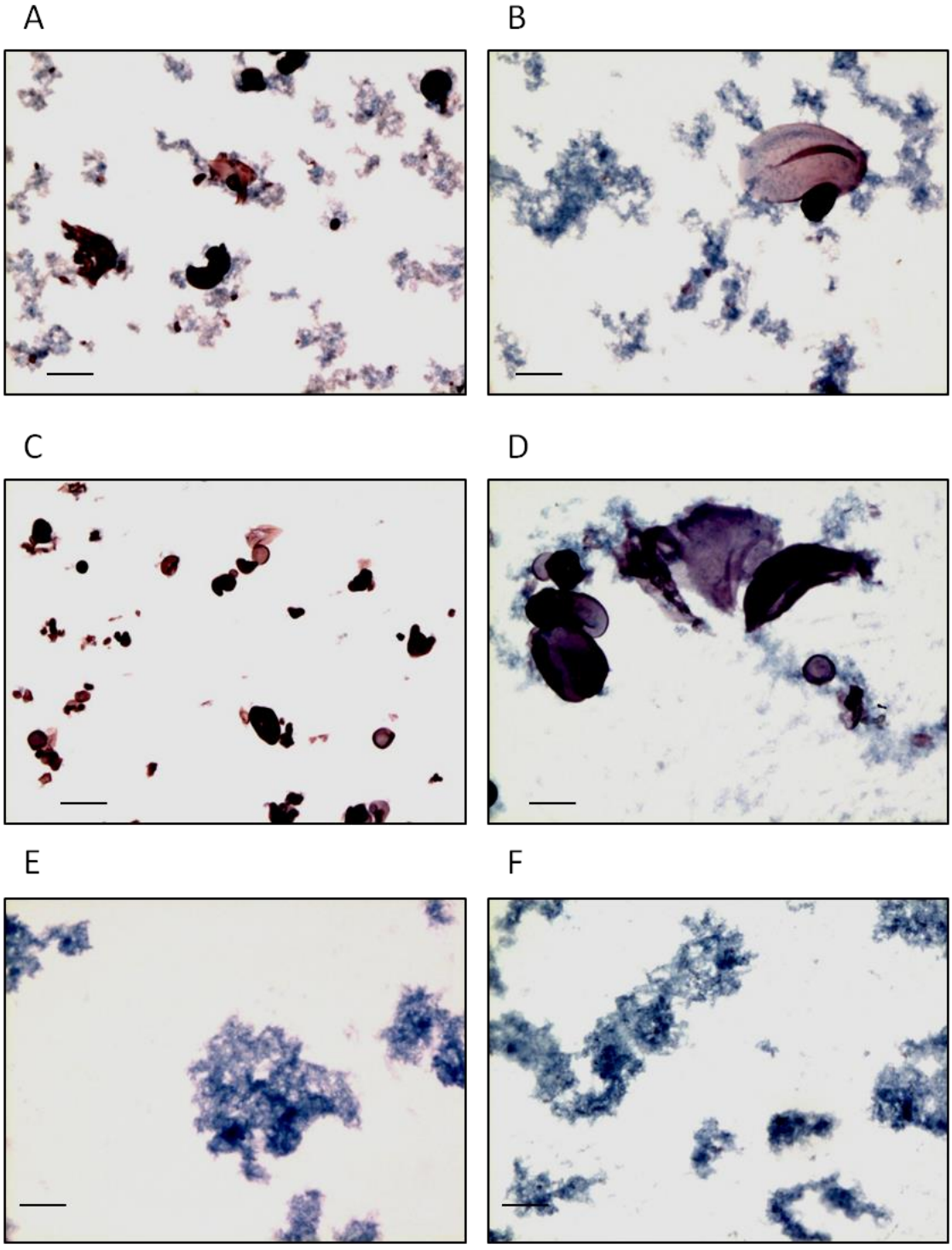

Figure 3.7. Light micrographs of 24h retrograded starch; wheat (A) and potato (B), granule ghosts; wheat (C) and potato (D), and leached amylose; wheat (E) and potato (F). All samples were stained with Lugol's iodine and viewed at magnification x10. Scale bar = 50 µm.

3.3.8 Overall starch composition

A summary of the physicochemical properties of all starches used in this study is presented in Table 3.5.

Table 3.5. Summary of the physicochemical properties (protein, amylose, moisture and total starch content) for all starches used in this study.

Starch	Protein (%)	Amylose (%)	Moisture (%)	Total starch (%)
Wheat	0.14	20.3	11.1	86.3
Potato	0.05	15.5	16.3	86.7
Wild type pea	0.25	26.8	12.8	85.4
Durum wheat	0.10	29.2	15.1	87.0
Maize	0.16	22.8	11.3	85.9
Waxy maize	0.32	1.2	13.7	84.5
High amylose maize	0.46	79.1	12.0	82.6
Rice	0.20	17.8	15.0	81.6

3.4 Conclusion

The physicochemical properties of raw starches determined in this chapter may allow for a better understanding of how starch properties can influence the changes observed during processing and digestion. With the moisture content being between 11-16%, the total starch content was calculated to be >80%, indicating only a small quantity of non-starch components were present. The protein content, determined by the BCA method, compared well with previously

published literature. The amylose content for all starches was tested using the iodine binding method. There was a diverse range of amylose in the starches tested, with some mutant genotypes of maize starch having virtually no amylose whereas high amylose maize sample contained as much as 79% amylose. These starches are termed mutant starches, as the biosynthetic enzymes that synthesise the glucan polymers have various genetic mutations which can alter the relative proportion of amylose-amylopectin present (Bogracheva *et al.*, 1995). Nevertheless, common starch types used in this investigation contained between 15-30% amylose, which is in agreement with the values quoted in the literature. Differences in amylose content often influence granule morphology and crystallinity. Therefore native starches were also studied using light microscopy fitted with crossed polarisers to reveal the extent of birefringence. This was coupled with SEM to reveal the granular size and shape of native starches. Additional studies were also conducted to study the extent of amylose leaching in wheat and potato starch using light microscopy.

Chapter 4 Starch structural analysis

4.1 Introduction

Starch granules have a semi-crystalline granular structure, consisting of alternating layers of crystalline and amorphous regions separated by larger amorphous growth rings (Vandeputte *et al.*, 2003; Pérez and Bertoft, 2010). Crystalline regions contain mainly double helical branched amylopectin chains while the amorphous regions consist of essentially linear amylose chains. Using different analytical techniques, many researchers have studied the structure of amorphous and crystalline proportions to determine the effects on starch behaviour and digestibility (Bogracheva *et al.*, 2006; Tahir *et al.*, 2010).

The structure and organisation of starch granules have previously been studied at a molecular and granular level, using a combination of analytical and microscopic techniques (Gallant *et al.*, 1997). Investigations at the granular scale allow whole starch granules to be analysed while the molecular scale allows analysis of glucose residues in individual chains. Scanning electron microscopy (SEM) is typically used to study starch structure at the granular scale (micrometre). This reveals information about the granule size and morphology; however, SEM is often limited in revealing information about starch crystallinity and molecular order. Powdered X-ray diffraction (XRD) is a common method used to obtain information about the starch crystalline structure at the nanometre scale. Quantitative analysis of X-ray diffractograms allows the relative amounts of crystalline and amorphous material to be estimated, and also provides information on the packing of double helices into ordered crystalline arrays (Imberty *et al.*, 1988). Starch granules possess both short

range (crystalline double helices) and long range (alternating crystalline and amorphous lamellae) order and therefore wide angle and small angle X-ray scattering can be used to probe the ordering of helices throughout the granule (Jenkins *et al.*, 1994; Liu *et al.*, 2009). However, XRD is most sensitive to long range order while ^{13}C cross polarisation/magic angle spinning NMR (^{13}C CP/MAS NMR) is sensitive to short range molecular order (Tan *et al.*, 2007). Solid-state ^{13}C CP/MAS NMR has been extensively used to directly study the relative proportion of ordered double helices and therefore is used to obtain an estimate of the double helix content (Gidley and Bociek, 1985). Unlike X-ray scattering, NMR is independent of the water content and as a result the molecular order content is normally higher than the crystallinity value (Gidley *et al.*, 1995). This is because the absence of water produces imperfect crystallites that do not reflect X-rays and therefore are not detected using X-ray diffraction. However, hydration of starch granules results in an increase in the formation of crystalline regions with values correlating well with the molecular order content (Cheetham and Tao, 1998; Lopez-Rubio *et al.*, 2008).

The short range molecular order at the surface of the starch granule can be indirectly analysed using FTIR-ATR spectroscopy. As the IR beam can only penetrate to a depth of ~2 μm, FTIR-ATR is limited to examining starch structures on the surface of the granule (Sevenou *et al.*, 2002). Absorbance bands within the region of 1300-800 cm^{-1} of the IR spectra correspond to C-C, C-O and C-H stretching and C-O-H bending. The absorbance band at 1022 cm^{-1} relates to amorphous carbohydrate material while the band noticed at 1000 cm^{-1} relates to ordered starch helices (Liu *et al.*, 2002; Capron *et al.*, 2007).

Therefore a peak ratio of 1000/1022 cm^{-1} can be used to quantitatively measure the proportion of ordered to disordered starch material on the surface of granules (van Soest *et al.*, 1994; Ottenhof *et al.*, 2005). Additional peak ratios such as 1047/1022 cm^{-1} can also be used to study the degree of molecular order (Liu *et al.*, 2014). Capron and workers showed that the starch crystallinity values, estimated using X-ray diffraction, were closely related to the molecular order values represented by the FTIR-ATR peak ratio 1000/1022 cm^{-1} (Capron *et al.*, 2007).

Heat treatment of starch material in excess water is an endothermic process that requires heat energy to be absorbed by the sample to allow disruption of non-covalent interactions holding the ordered structures together (Gill *et al.*, 2010). This process is referred to as starch gelatinisation and the temperature at which melting of crystalline regions occurs, termed gelatinisation temperature, varies between different botanical starch sources (Wang *et al.*, 1998). The application of DSC has been widely used to follow and characterise the thermal properties of starch during the endothermic gelatinisation process. Starch gelatinisation results in a clear endothermic peak, within the given transition temperature range, enabling gelatinisation parameters to be obtained (Bogracheva *et al.*, 2002). Integration of the endothermic peak allows the gelatinisation enthalpy to be calculated, which represents the heat energy required to melt starch crystallites and reflects the total loss of molecular order (Cooke and Gidley, 1992; Jenkins and Donald, 1998). Therefore the gelatinisation enthalpy is an index which is often used to indirectly measure the

degree of molecular order and amount of crystallinity present in starches (Ottenhof *et al.*, 2005; Warren *et al.*, 2011).

Rapid visco-analyser (RVA), Dynamic mechanical analysis (DMA) and solution calorimetry are additional characterisation methods used by researchers to study starch gelatinisation. RVA is used to determine the viscous properties of starch during heating (Deffenbaugh and Walker, 1989; Zaidul *et al.*, 2007) while the novel DMA method investigates thermal transitions during starch gelatinisation under shear stress (Jones, 1999; Xie *et al.*, 2008; Warren *et al.*, 2012). Solution calorimetry can be used to quantify the amorphous and crystalline contents based upon the exothermic energy generated during granule hydration (Royall and Gaisford, 2005; Bogracheva *et al.*, 2006). However in this chapter XRD, FTIR-ATR and DSC have been used to study starch properties in their native, gelatinised and retrograded forms, as these are the most conventional methods used by most researches.

The structure and behaviour of starch material can be accurately determined using a range of well-established analytical techniques. In this chapter, the main objective was to obtain experimental data that characterises the physical and chemical properties of native and thermally processed starches. This helps in producing a sensible interpretation of the enzyme kinetic parameters.

4.2 Methods

Full details of the methods are given in Chapter 2, Section 2.3. In brief, all FTIR spectra were obtained using a Perkin Elmer Spectrum Two® FTIR

spectroscope. This was equipped with a SensIR technologies IR II Durascope® diamond cell ATR device, accompanied with a diamond crystal with an angle of incidence of 45°. Spectra for 10 mg/mL native, gelatinised and retrograded starches were collected from a wavelength range of 4000 cm^{-1} to 550 cm^{-1}. A spectrum was also taken for leached amylose chains, present in the supernatant of gelatinised and retrograded wheat and potato starch.

All DSC thermograms were obtained using a TA instruments Multi-Cell Differential Scanning Calorimeter (MC DSC). Native starch samples (50 mg) were scanned from 20°C to 100 or 150°C at a heating rate of 0.5°C min^{-1}. To obtain DSC thermograms for gelatinised starch, two consecutive heating cycles were applied from 20°C to 100 or 150°C at a heating rate of 0.5°C min^{-1} (with a cooling rate of 1°C min^{-1}). DSC thermograms for retrograded starches were obtained by applying a heating cycle from 20°C to 100/150°C at a heating rate of 0.5°C min^{-1} to native starch. Samples were then stored at room temperature for 48h before another heating cycle was performed from 20°C to 150°C at a heating rate of 0.5°C min^{-1}. Additional studies were also conducted, applying different storage conditions to a higher starch concentration; specific details of this study can be found in Chapter 2, Section 2.3.2 (page 94).

Wide-angle X-ray scattering patterns were obtained for native, gelatinised and retrograded starches using a MiniFlex Rigaku X-ray Diffractometer with CuKα (λ= *1.548*Å) radiation (40 kV, 15 mA). All other parameters are described in Chapter 2, Section 2.3.3. Gelatinised starch was prepared by heating the starch sample at 90°C for 20 min followed by centrifugation to sediment the starch

material to the bottom of the tube. The sample was then immediately freeze dried. Retrograded starch was prepared in an almost identical fashion except that the starch sample was stored for 48h at room temperature after gelatinisation (more detail of the preparation process can be found in Section 2.3.3, page 99). All starches were scanned at room temperature (22^{o}C) over an angular range (2θ) of 3-40^{o}.

4.3 Results and Discussion

4.3.1 FTIR-ATR spectra

4.3.1.1 Native and processed starch

Spectra were recorded for 10 mg/mL native, gelatinised and retrograded starches. Gelatinised starches were cooked at 90^{o}C for 20 min and left to cool for 10 min before a spectrum was taken. Retrograded starches were produced by gelatinisation followed by storage at room temperature for 96h with a spectrum taken at 24h intervals. The absorbance band at 1000 cm^{-1} is very sensitive to water content and represents the hydrogen bonding occuring between crystalline regions of α-glucan chains and water. Band 1000 cm^{-1} is therefore characteristic of the ordered regions at the granule surface. The peak observed at 1022 cm^{-1} arises due to C-O-H bending modes, and therefore can be associated with the amorphous regions at the starch surface (Capron *et al.*, 2007; Warren *et al.*, 2011). Sevenou and workers also showed the band disappearing after acid hydrolysis and thus attributed the band to the amorphous fraction of the granule (Sevenou *et al.*, 2002).

The band observed at 1000 cm^{-1} decreases upon starch gelatinisation, indicating a loss of ordered structure as the heat treatment disrupts the starch granule. However upon retrogradation, the 1000 cm^{-1} peak rises indicating the α-helical polymer chains transform from an unstructured state to a ordered state (Dona *et al.*, 2010). Surprisingly, the band intensity at 1022 cm^{-1} does not significantly change upon hydrothermal treatment and subsequent storage (Figure 4.1). Absolute values obtained using FTIR-ATR can often vary depending upon the level of contact between the starch sample and the surface of the ATR device as this dictates the intensity of absorption (Sevenou *et al.*, 2002). For this reason the peak ratio 1000/1022 cm^{-1} is best used to quantify the degree of ordered starch structure.

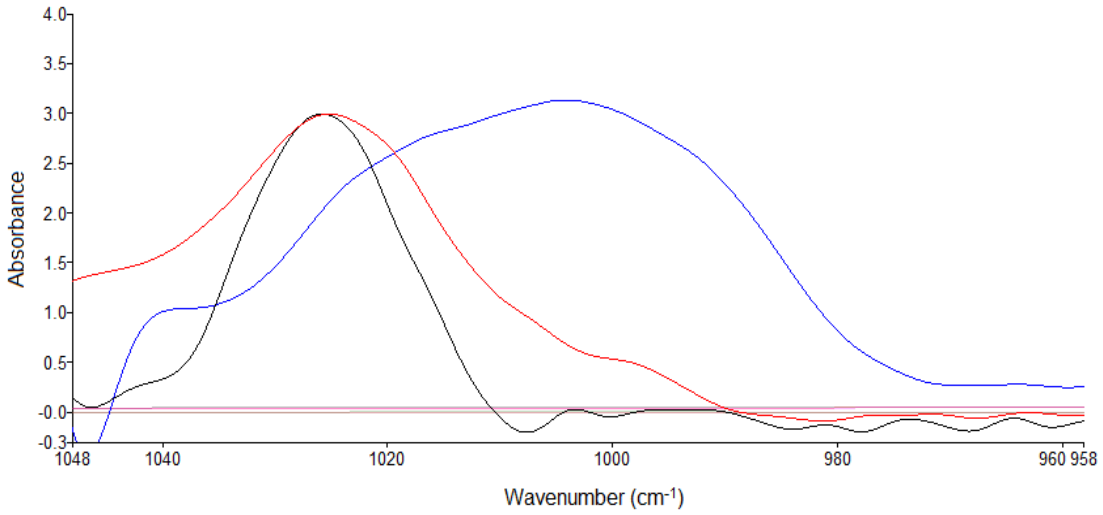

Figure 4.1. FTIR-ATR spectrum of absorbance versus wavelength for native (blue), gelatinised (black) and 96h retrograded (red) potato starch.

Table 4.1 shows the peak ratio between 1000 cm^{-1} and 1022 cm^{-1} for native, gelatinised and retrograded starches. Note that the FTIR data were not obtained for retrograded durum wheat and rice starch stored beyond 24h as these storage times were not used in the initial digestion studies described in Chapter 6.

Table 4.1. FTIR-ATR peak ratio 1000/1022 cm^{-1} for native, gelatinised and retrograded starches. All values are presented as mean values ± SEM from three to four replicates.

	FTIR-ATR peak ratio 1000/1022 cm^{-1}					
Starch	Native	Gelatinised	Retrograded			
			24h	48h	72h	96h
Wheat	1.04 ± 0.02	n.d.*	0.24 ± 0.02	0.27 ± 0.01	0.24 ± 0.01	0.32 ± 0.02
Potato	1.31 ± 0.08	0.02 ± 0.02	0.19 ± 0.00	0.19 ± 0.04	0.16 ± 0.01	0.23 ± 0.04
Wild type pea	1.22 ± 0.00	0.01 ± 0.00	0.09 ± 0.04	0.06 ± 0.00	0.06 ± 0.01	0.30 ± 0.03
Durum wheat	1.14 ± 0.01	n.d.*	0.28 ± 0.01	-	-	-
Maize	1.02 ± 0.00	0.15 ± 0.01	0.26 ± 0.03	0.29 ± 0.01	0.30 ± 0.02	0.28 ± 0.03
Waxy maize	1.03 ± 0.00	0.13 ± 0.00	0.14 ± 0.00	0.15 ± 0.03	0.15 ± 0.01	0.19 ± 0.01
High amylose maize	1.34 ± 0.01	0.35 ± 0.04	1.06 ± 0.02	1.24 ± 0.01	1.08 ± 0.00	1.09 ± 0.01
Rice	0.79 ± 0.00	0.09 ± 0.01	0.33 ± 0.00	-	-	-

*n.d. = not detectable

Native starch samples were found to have a relatively high peak ratio suggesting that the α-glucan chains at the surface of the granule are mainly ordered. High amylose maize starch however was also observed to have a high peak ratio, which is surprising as the granule contains mainly amorphous amylose chains located at the periphery. The reason for this anomaly is not fully understood and becomes very difficult to explain as past literature produces conflicting results. Sevenou and workers have reported a high peak ratio while Warren and workers have reported a low peak ratio for high amylose starches (Sevenou *et al.*, 2002; Capron *et al.*, 2007; Warren *et al.*, 2011). Since many reports have shown high amylose starches to contain a low double helix and crystalline content (a more accurate representation of starch structure) (Cheetham and Tao, 1998; Matveeva *et al.*, 2001; Tan *et al.*, 2007; Lopez-Rubio *et al.*, 2008; Htoon *et al.*, 2009), it is likely FTIR produces unreliable results when studying the surface of high amylose starches.

Upon gelatinisation at 90^{o}C, complete disorder of the starch granule occurs with a decrease in ordered starch material. This is reflected in the extremely low, and in some cases, non detectable peak ratio. When stored at room temperature, the peak ratio begins to increase suggesting the recrystallisation of polymer chains. The biggest increase in the peak ratio was observed within 24h and is believed to be a result of recrystallised amylose chains. This is because amylopectin recrystallisation is a slow process lasting several days (Orford *et al.*, 1987; Roder *et al.*, 2009). Waxy maize starch has a high proportion of amylopectin, with only very small amounts of amylose (~1%). This explains why the peak ratio for waxy maize does not change significantly when

stored up to 96h. Table 4.1 shows the peak ratio for gelatinised high amylose maize starch to be slightly higher than other tested starches. This is almost certainly due to the high amylose content, resulting in some of the starch material forming ordered crystalline structures immediately after cooling (post-gelatinisation) (Miles *et al.*, 1985).

Figure 4.2 shows a histogram of the 1000/1022 cm^{-1} peak ratio for native, gelatinised and 24h retrograded starches. This allows for an easier interpretation of the FITR-ATR data. Only the peak ratio for 24h retrograded starches was used in this histogram as the most significant change occurred within 24h storage.

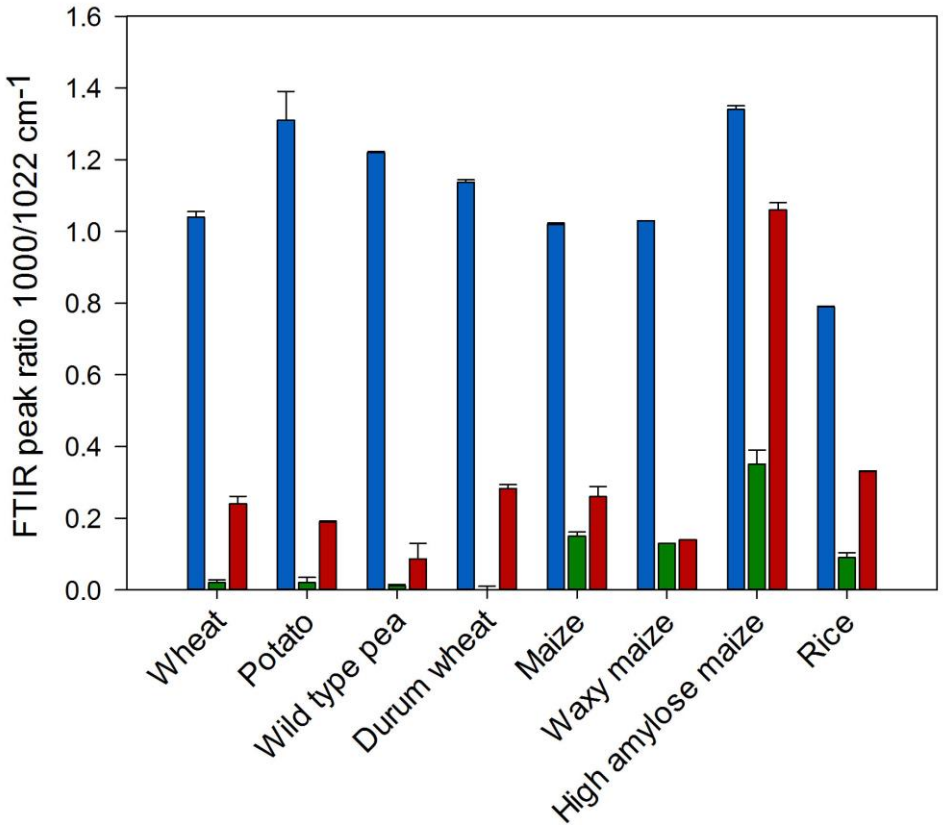

Figure 4.2. Histogram of the 1000/1022 cm^{-1} peak ratio for native (blue), gelatinised (green) and 24h retrograded (red) starches.

Researchers have previously used alternative peak ratios (995/1022 cm^{-1} and 1047/1022 cm^{-1}) to study the degree of order/disorder (van Soest *et al.*, 1995; Sevenou *et al.*, 2002; Noosuk *et al.*, 2003; Man *et al.*, 2013). Therefore absorbance values were also obtained at different wavelengths to give a peak ratio of 995/1022 cm^{-1} and 1047/1022 cm^{-1}. Both peak ratios were then compared with the original ratio of 1000/1022 cm^{-1}. As Table 4.2 shows, the peak ratio of 1000/1022 cm^{-1} and 995/1022 cm^{-1} produces very similar results; however, the ratio of 1047/1022 cm^{-1} was small, relative to 1000/1022 cm^{-1}. This was because the absorbance intensity at 1047 cm^{-1} was much lower compared to 1022 cm^{-1}. As the maximum absorbance was obtained at 1000 cm^{-1} rather than 1047 cm^{-1}, we used the absorbance value at the former wavelength to probe the degree of order.

Table 4.2. FTIR-ATR peak ratio 1000/1022 cm^{-1}, 995/1022 cm^{-1} and 1047/1022 cm^{-1} for native starches.

Starch	FTIR-ATR peak		
	1000/1022 cm^{-1}	995/1022 cm^{-1}	1047/1022 cm^{-1}
Wheat	1.04	0.96	0.45
Potato	1.31	1.20	n.d*
Wild type pea	1.22	1.14	0.46
Durum wheat	1.14	1.07	0.45
Maize	1.02	1.10	0.44
Waxy maize	1.03	0.88	0.48
High amylose maize	1.34	1.05	0.49
Rice	0.79	0.64	0.48

*n.d. = not detectable

4.3.1.2 FTIR-ATR of leached amylose

It has widely been reported that amylose polymer chains diffuse out of swollen granules during starch gelatinisation (amylose leaching). During the storage process, the leached amylose chains retrograde forming an ordered structure. Therefore FTIR was used to determine the degree of ordered leached material in the supernatant of gelatinised and 24h retrograded wheat and potato starch (Table 4.3). Gelatinised and retrograded starch forms were centrifuged to ensure the supernatant only contained leached amylose chains and no granular ghosts. Gidley and workers have used a similar method to separate the supernatant from the granular ghosts to allow appropriate characterisation (Debet and Gidley, 2007; Zhang *et al.*, 2013).

Table 4.3. Peak ratio 1000/1022 cm^{-1} of the supernatant from gelatinised and 24h retrograded wheat and potato starch. The peak ratio from the stock solution of gelatinised and 24h retrograded wheat and potato starch, taken from Table 4.1, is also shown. Using both peak ratios, the % of ordered leached material can be calculated. All values are presented as mean values ± SEM from three replicates.

Starch	Peak ratio for stock solution	Peak ratio for supernatant	% of ordered leached material
Wheat (gelatinised)	n.d.*	n.d.*	-
Wheat (24h retrograded)	0.24 ± 0.02	0.18 ± 0.00	75.0
Potato (gelatinised)	0.02 ± 0.02	n.d.*	-
Potato (24h retrograded)	0.19 ± 0.00	0.09 ± 0.00	47.3

*n.d. = not detectable

No absorbance peaks were observed for the supernatant of gelatinised starch and therefore a peak ratio was not determined. The results show no evidence of retrograded polymer chains in the supernatant of gelatinised samples as no ordered material was detected. The data in Table 4.3 suggests that the material leached from the granule accounts for approximately 75% and 47% of the total ordered material detected in the stock solution of wheat and potato starch, respectively. Previous studies have demonstrated amylose leaching occurs as a result of starch gelatinisation and that amylose retrogrades much faster than amylopectin (Miles *et al.*, 1985; Obanni and Bemiller, 1996; Debet and Gidley, 2007; Zhang *et al.*, 2014). Therefore the ordered leached material detected in the supernatant of retrograded starch most likely consists of retrograded amylose chains.

4.3.2 DSC thermograms

All native, gelatinised and retrograded DSC thermograms were obtained using the TA instruments Multi-Cell Differential Scanning Calorimeter (MC DSC). Analysis of thermograms allows T_o, T_p, T_c and $\Delta_{gel}H$ to be calculated. T_o, T_p, and T_c represent the temperature onset of gelatinisation, the temperature peak and the temperature conclusion, respectively. The area under the curve of the gelatinisation peak, obtained through peak integration, represents the gelatinisation enthalpy ($\Delta_{gel}H$ expressed as J/g)**.**

4.3.2.1 Native and gelatinised starch

Figure 4.3 shows the DSC thermogram (endothermic down) obtained for native potato starch, with the positions of T_o, T_p, T_c and $\Delta_{gel}H$ shown on the

thermogram. Table 4.4 shows the onset, peak and conclusion temperatures along with the gelatinisation range for all native starches. The peak temperature is also referred to as the gelatinisation temperature whereas the gelatinisation range (conclusion temperature minus onset temperature) is the temperature range over which all granules completely gelatinise. The peak position and height vary for native starches depending upon the botanical source, resulting in different gelatinisation parameters (Bogracheva *et al.*, 2002).

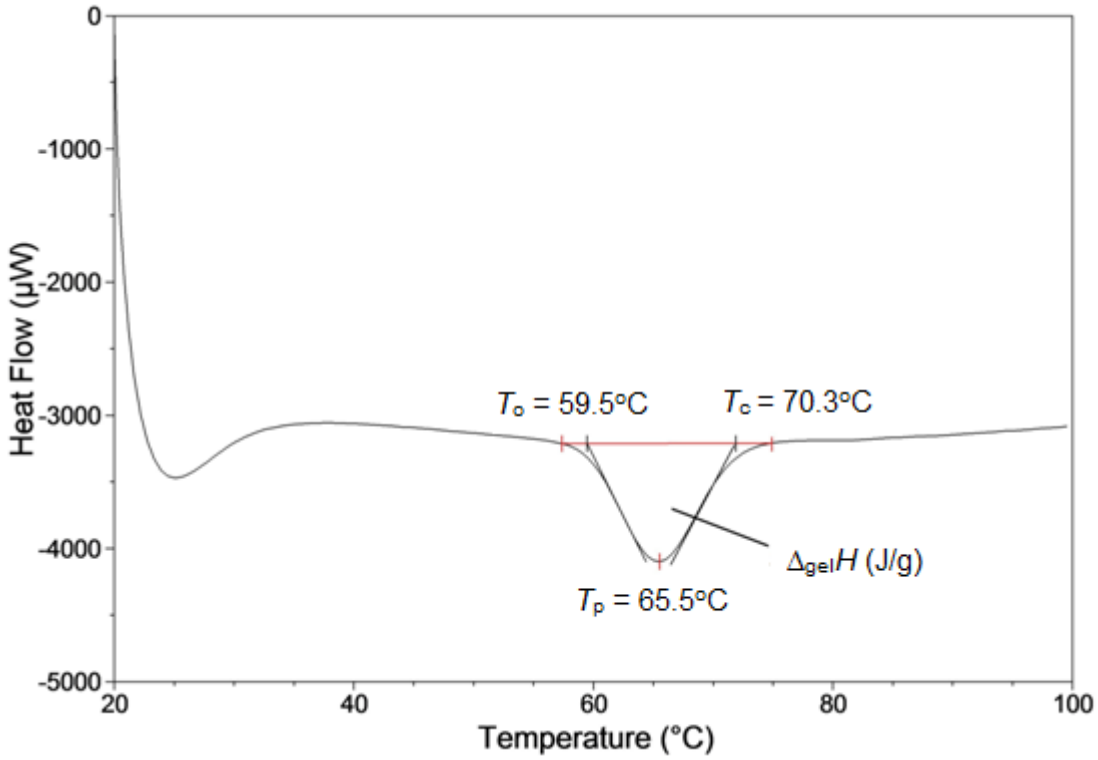

Figure 4.3. DSC thermogram obtained for native potato starch. The thermogram shows the gelatinisation enthalpy ($\Delta_{gel}H$), temperature onset (T_o), temperature peak (T_p) and temperature conclusion (T_c). The area of the endothermic peak provides a calculation of $\Delta_{gel}H$.

Table 4.4. The endothermic transition temperatures for native starches. Data represents mean from three replicates ± SEM.

Starch	Temp. Onset (°C)	Temp. Peak (°C)	Temp. Conclusion (°C)	Gelatinisation range (°C)
Wheat	47.8 ± 1.1	59.2 ± 0.2	74.1 ± 0.7	26.3
Potato	59.5 ± 0.3	65.5 ± 0.0	70.3 ± 0.2	10.8
Wild type pea	48.0 ± 0.8	59.5 ± 0.0	77.3 ± 0.2	29.3
Durum wheat	48.0 ± 0.5	59.0 ± 0.0	71.3 ± 1.4	23.3
Maize	59.9 ± 0.4	70.7 ± 0.2	79.2 ± 0.3	19.3
Waxy maize	59.5 ± 1.4	73.0 ± 0.0	80.0 ± 0.3	20.5
High amylose maize	67.5 ± 1.7	87.5 ± 0.3	103.5 ± 0.9	36.0
Rice	56.5 ± 0.5	68.5 ± 0.5	82.0 ± 0.0	25.5

High amylose maize starch shows the largest gelatinisation range of 36°C, this is due to the high amylose content resulting in a highly disordered starch structure. This gives the DSC thermogram for high amylose maize starch a broad and flat peak as seen in Figure 4.4. Similar traces have been previously reported by many groups using DSC analysis on native high amylose starches (Shi *et al.*, 1998; Matveeva *et al.*, 2001; Tahir *et al.*, 2010; Ma *et al.*, 2011).

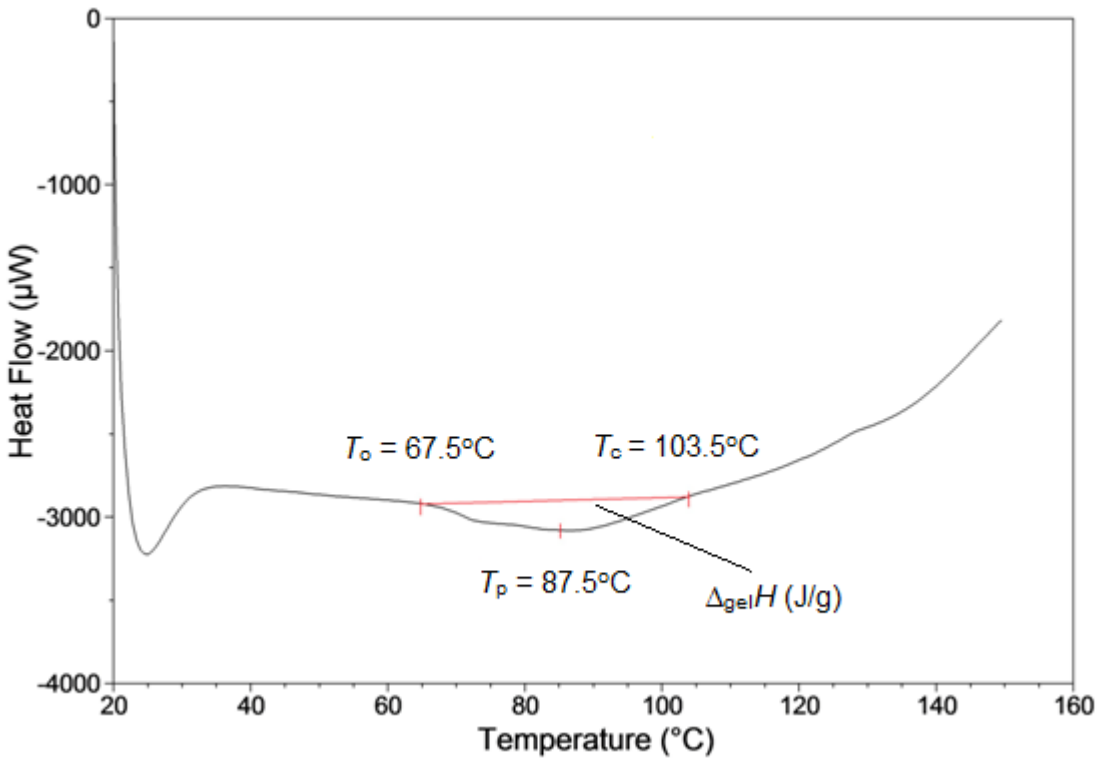

Figure 4.4. DSC thermogram for native high amylose maize starch with the gelatinisation enthalpy ($\Delta_{gel}H$), temperature onset (T_o), temperature peak (T_p) and temperature conclusion (T_c).

The amount of heat required to melt starch crystals per mass of substance is represented by the gelatinisation enthalpy ($\Delta_{gel}H$) (Table 4.5). Native potato starch has the highest gelatinisation enthalpy compared with other starches, revealing a highly ordered crystalline structure which requires more heat for melting. This accords with previous data that indicates native potato starch is almost resistant to digestion due to its highly ordered structure (Jacobs *et al.*, 1998; Jacobs *et al.*, 1998; Schirmer *et al.*, 2012). High amylose maize starch has the lowest gelatinisation enthalpy with a value of 5.5 J/g, indicating minimal heat input was required to melt the crystals present. This is presumably because the majority of the starch material consists of amylose, which is mainly

located in the amorphous regions of the semi-crystalline starch granule (Matveeva *et al.*, 2001; Liu *et al.*, 2013).

Table 4.5. Starch gelatinisation enthalpies ($\Delta_{gel}H$). DSC experiments were repeated three times from the same batch of starch.

Starch	$\Delta_{gel}H$ (J/g)
Wheat	9.7 ± 0.9
Potato	17.5 ± 0.8
Wild type pea	10.9 ± 0.5
Durum wheat	8.9 ± 0.5
Maize	11.7 ± 0.6
Waxy maize	10.2 ± 0.9
High amylose maize	5.5 ± 1.1
Rice	9.6 ± 0.4

Starch samples were immediately rescanned after the initial gelatinisation process to ensure no peaks appeared. It is well known that hydrothermal treatment of starch results in a physical modification of starch structure with a disruption of granule crystallinity (Wang *et al.*, 1998). As expected, all thermograms produced baselines with no peaks, and thus no gelatinisation parameters were determined. No ordered starch material was present as the initial gelatinisation process resulted in an order to disorder transformation of starch structure. An example of the DSC thermogram for pre-gelatinised potato starch is shown in Figure 4.5.

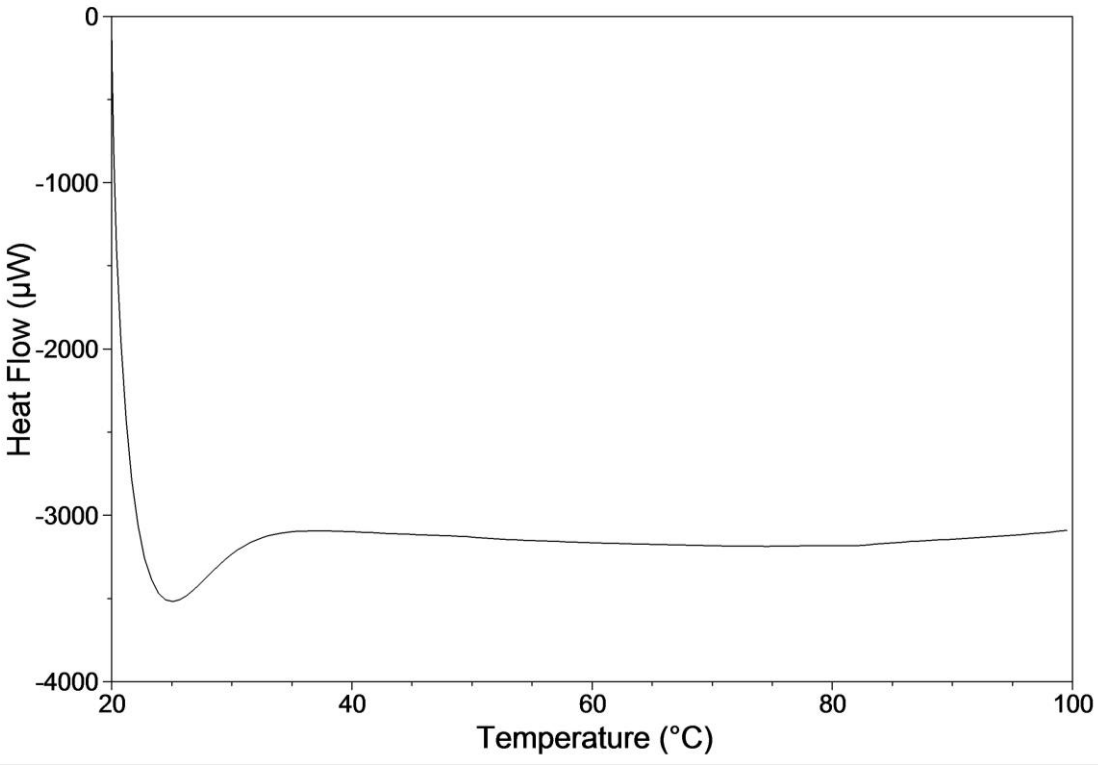

Figure 4.5. DSC thermogram of pre-gelatinised potato starch.

4.3.2.2 Retrograded starch

DSC analysis of retrograded starch was performed with a diluted and a concentrated starch sample of 50 and 200 mg/mL, respectively. Different storage conditions were also applied to both starch concentrations. Therefore the effect of starch concentration and storage conditions on the rate of retrogradation was studied. As retrogradation is a well-established process that occurs when starch is cooled and stored we expected to observe crystalline peaks to calculate the enthalpy change associated with retrogradation ($\Delta_{ret}H$).

4.3.2.2.1 Low starch concentration

Native potato, wild type pea and high amylose maize starch samples were gelatinised and stored at room temperature for 48h before another heating cycle was performed. Similar to the thermograms obtained for pre-gelatinised starch, no prominent endothermic peaks were detected and therefore only the thermogram for retrograded potato starch is shown in Figure 4.6.

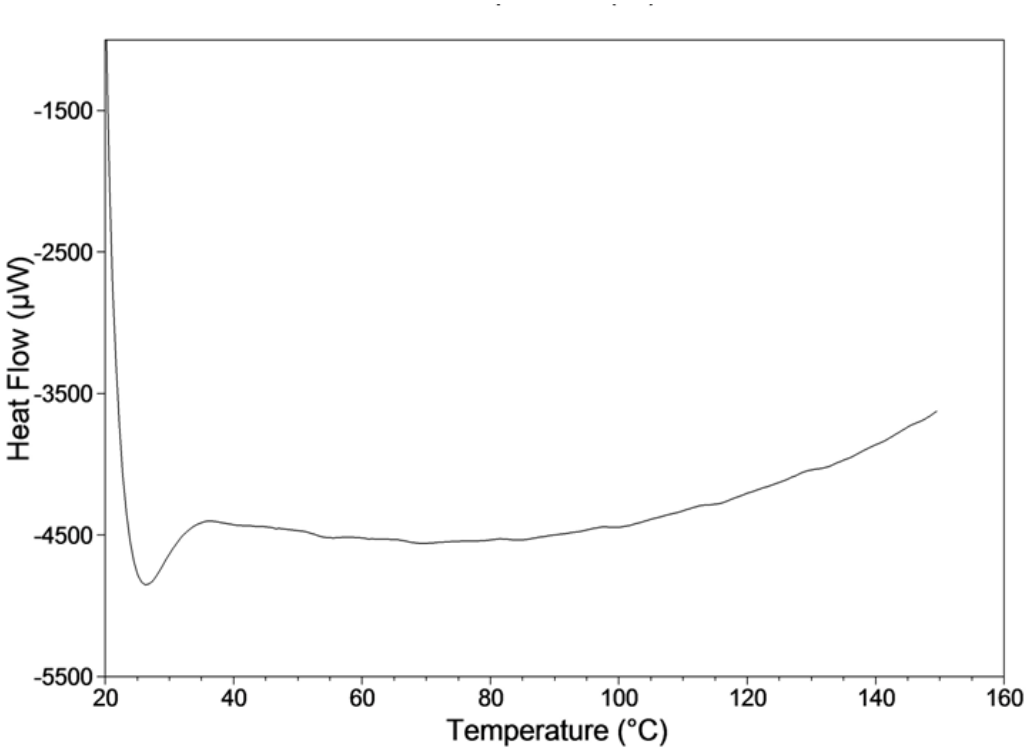

Figure 4.6. DSC thermogram of retrograded potato starch, which was prepared by storing at room temperature for 48h. Starch concentration was 50 mg/mL.

The absence of a retrograded amylose peak at 130-150^{o}C suggests that either no amylose crystallites were present, or they were present at very low concentrations, when a 50 mg/mL starch solution was used. A peak for retrograded amylopectin was also not detected since amylopectin chains take several days to retrograde.

Previous researchers have used DSC for retrograded starch analysis and observed a peak between 130-150^{o}C corresponding to the melting of retrograded amylose crystallites (Sievert and Pomeranz, 1989; Gidley *et al.*, 1995; Cui and Oates, 1997; Han *et al.*, 2006). In such studies, the rate of retrogradation was accelerated by storing starches for lengthy periods at reduced temperatures (4^{o}C), and thereby increasing the amount of retrograded starch material. However in our initial studies, starches were stored for 48h at room temperature before DSC analysis, and therefore it is likely the concentration of retrograded starch material present was below the sensitivity limit for detection by the DSC.

4.3.2.2.2 High starch concentration

The role of starch concentration (moisture) on the extent of retrogradation was studied by Zeleznak and Hoseney, (1986). The group observed a bell shaped curve for the energy required to melt retrograded starch crystallites ($\Delta_{ret}H$) as a function of starch concentration. The highest $\Delta_{ret}H$ was observed at 50% (w/w) with the lowest observed at 10-20% (w/w) (Zeleznak and Hoseney, 1986). Another study by Sievert and Pomeranz, (1990) showed no clear retrograded amylose peak. However when the retrograded crystallites were isolated by enzyme treatments, a prominent transition peak at ~155^{o}C was observed (Sievert and Pomeranz, 1989, 1990). Therefore the results indicate that a high concentration of retrograded amylose crystallites have to be present for detection by DSC.

Various other groups reporting gelatinisation parameters have used starch concentrations in excess of 50 mg/mL, as shown in Table 4.6. Therefore in our DSC studies, analysis was performed on 200 mg/mL high amylose maize and potato starch to determine if peaks corresponding to retrograded amylose/amylopectin could be detected at higher starch concentrations.

Table 4.6. Starch concentrations used in DSC studies by various other groups.

Authors	Weight (mg)	Water (µL)	Starch (mg/mL)
(Gidley *et al.*, 1995)	10	50	200
(Liu *et al.*, 2009)	5	40	125
(Zhang *et al.*, 2011)	2	4	500
(Sievert and Pomeranz, 1989)	20	40	500

A 200 mg/mL concentration of high amylose maize and potato starch was stored for 1 week at 4^{o}C (Figure 4.7) to reproduce storage conditions and starch concentrations used by the groups mentioned in Table 4.6. A transition peak at 93^{o}C, corresponding to the amylose-lipid complex, was observed for retrograded high amylose maize, while a retrograded amylopectin peak at 57^{o}C was observed for retrograded potato starch. However, in both thermograms no retrograded amylose peak was detected. Additional peaks along both DSC thermograms were also observed, however the small size of the peaks makes data interpretation difficult and highly unreliable. It is likely these peaks are due to instrumental noise detected by the sensitive DSC machine and not due to the

melting of crystalline material. The absence of a flat baseline also means any quantitative data extracted from peak integration would be unreliable, hence this is why $\Delta_{ret}H$ was not calculated.

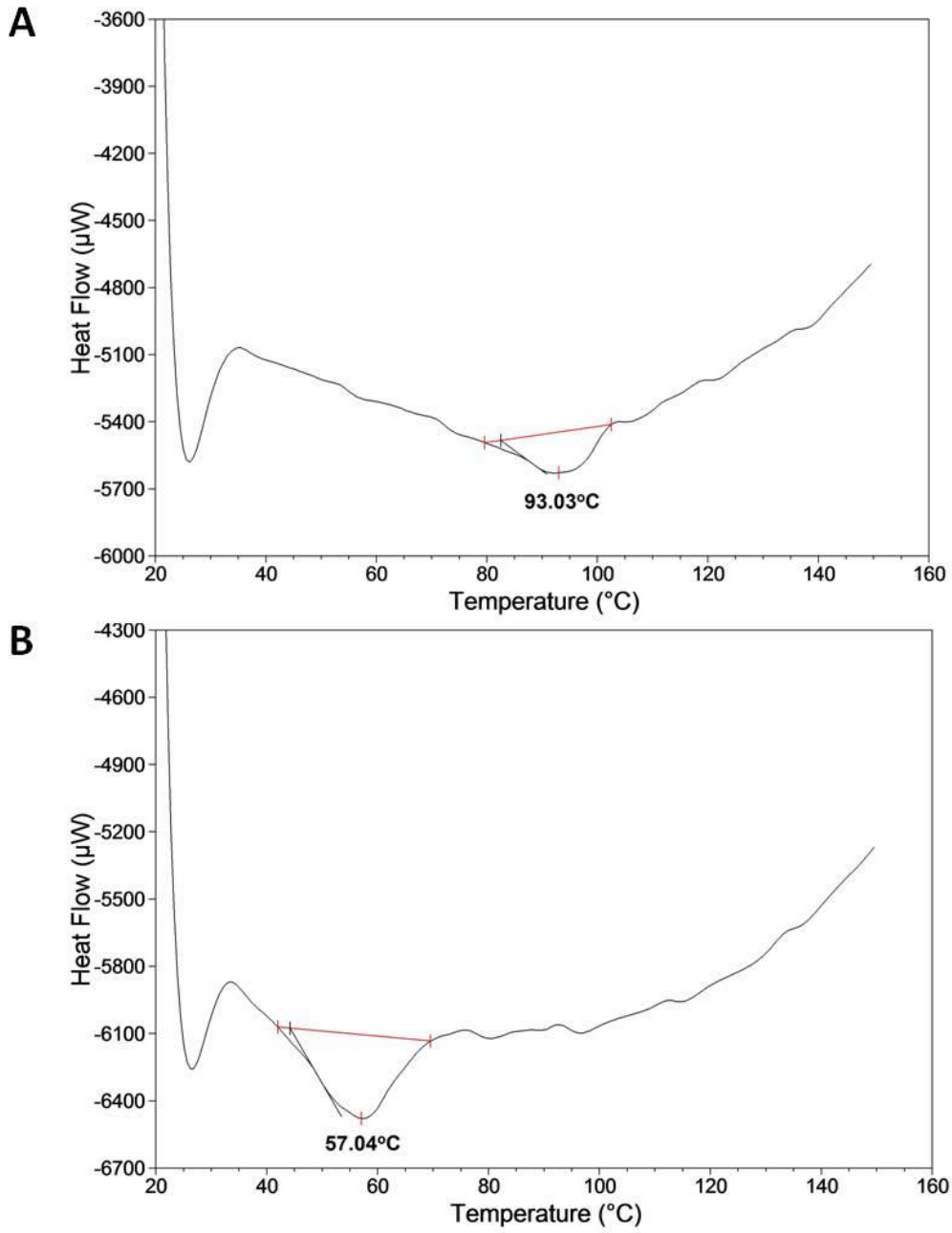

Figure 4.7. DSC thermogram of high amylose maize (A) and potato (B) starch stored at 4°C for 1 week. The melting temperatures for the amylose-lipid complex (A) and retrograded amylopectin (B) are shown below the thermogram. The starch concentration was 200 mg/mL.

A DSC scan of pure water (reference sample) was also performed to confirm the small additional peaks observed did not arise from the melting of retrograded starch material (Figure 4.8). The small peaks observed in retrograded starch samples (excluding the amylose-lipid complex and retrograded amylopectin) were also observed in the water sample. Therefore these peaks are most certainly due to instrumental noise and do not represent the melting of any crystalline material.

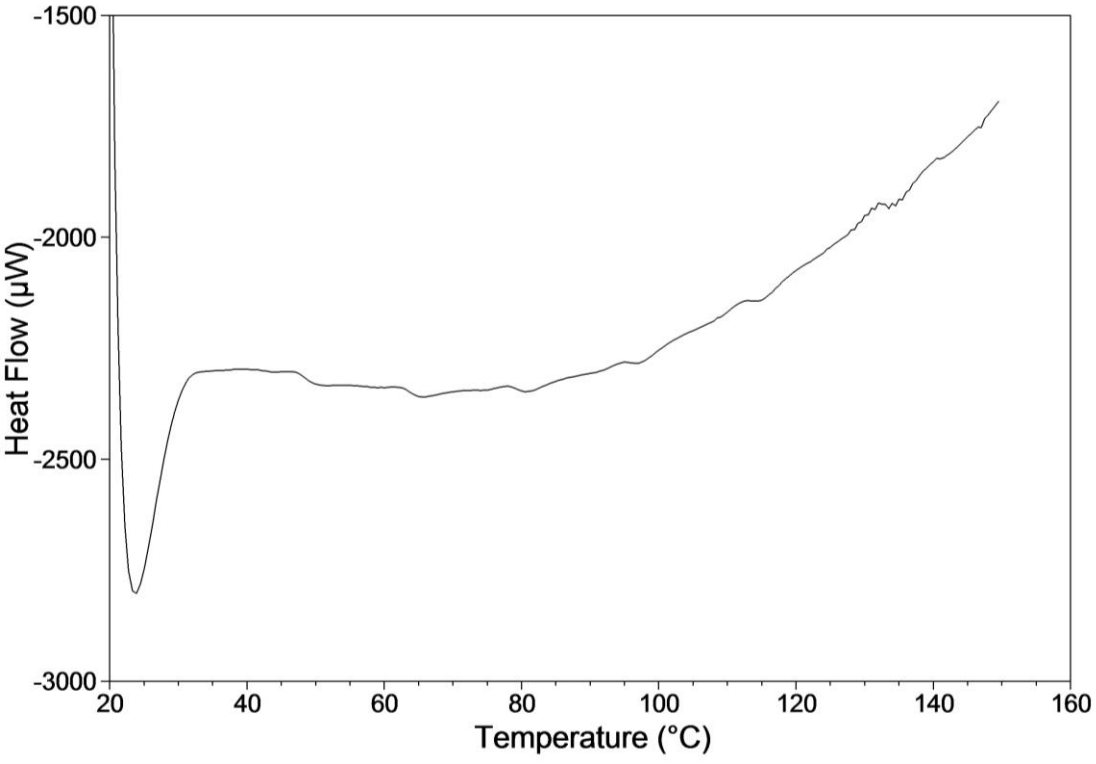

Figure 4.8. DSC thermogram of water. Temperature scan rate was 0.5°C/min.

It is important to note that thermal treatment and storing of highly concentrated starch samples (low moisture) in the ampoules resulted in a thick paste-like material being formed. This may have resulted in incomplete gelatinisation of starch granules. A previous study by Roder and colleagues showed crystallinity values remained relatively unchanged when starches were gelatinised in limited

water (Roder *et al.*, 2009). Therefore the thick paste-like material formed during storage could result in poor gelatinisation conditions resulting in limited crystal melting. Therefore the intensity of the transition peaks observed in high amylose maize and potato starch are likely to underestimate the order-disorder transition.

Using a high starch concentration may also result in incomplete gelatinisation of native starch during the initial scan, i.e. native starch material may still be present inside the DSC pan. Also the amylose-lipid complex and retrograded amylopectin peaks appear in the same region as the peak for the melting of native starch. It is vital therefore to evaluate whether the observed peak is from the melting of the crystalline amylose-lipid complex/retrograded amylopectin or from the remaining native starch material. To do this, two consecutive heating scans were applied to the original 200 mg/mL native sample. A flat baseline for the second scan confirmed no native starch material was present after the initial scan was completed (Figure 4.9). Therefore, the peaks observed in retrograded high amylose maize and potato starch were due to the melting of retrograded crystallites rather than the starch granules remaining in the native state.

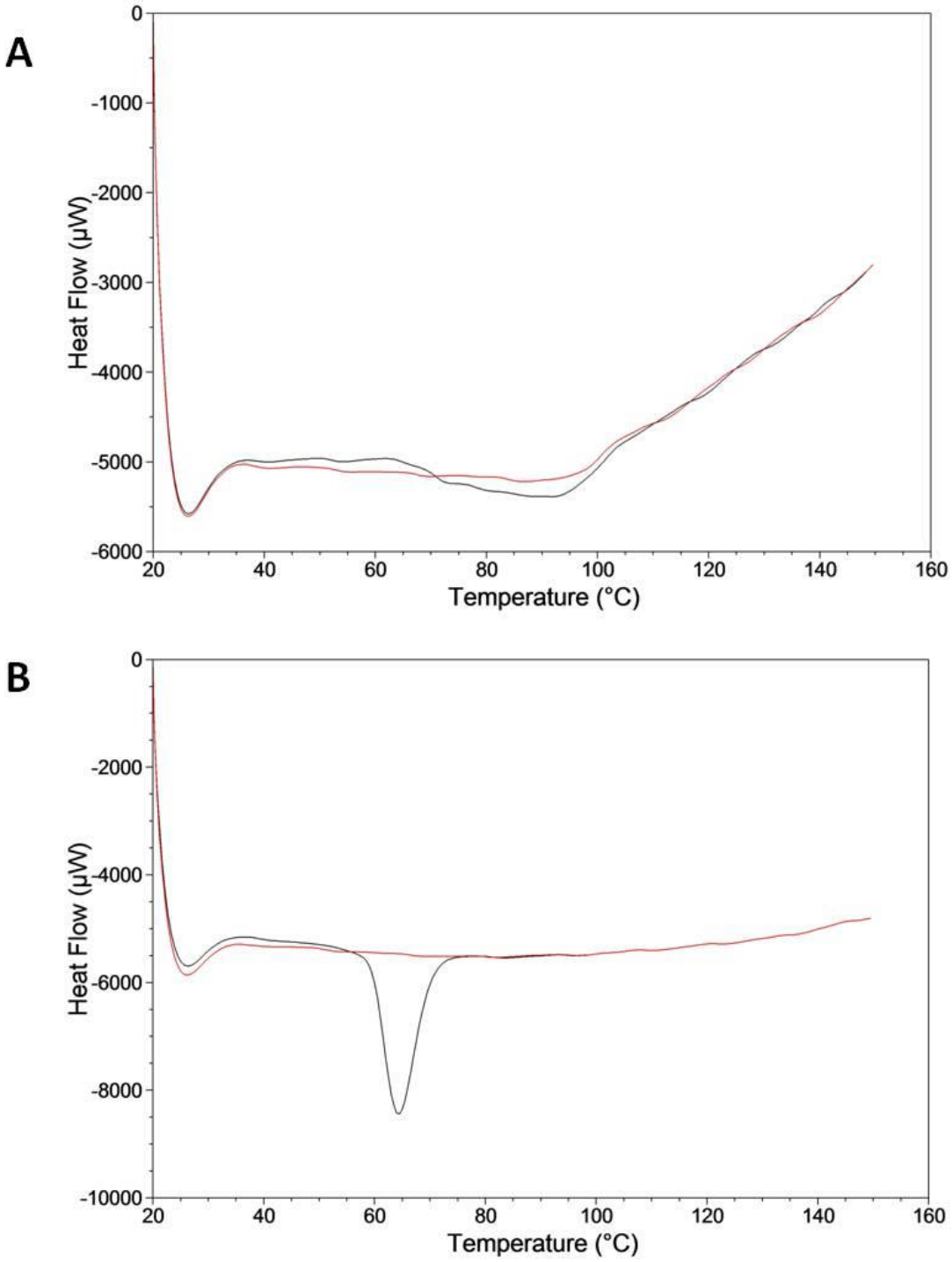

Figure 4.9. DSC thermogram of the first (native) and second (pre-gelatinised) scan for 200 mg/mL high amylose maize (A) and potato (B) starch. The first scan is shown in black and the second scan is shown in red.

In summary, peaks for the melting of crystalline starch material can only be observed when high starch concentrations are used. In addition to this, starches have to be stored at reduced temperatures for more than 48h. Such conditions increase the amount of amylose-lipid complexes and retrograded amylopectin, thereby allowing detection by DSC. However, the results presented here show a starch concentration higher than 200 mg/mL is required to detect amylose crystallites.

4.3.2.3 Critical analysis of DSC data

DSC has been proven to be an extremely valuable tool in understanding phase transitions during starch gelatinisation. The gelatinisation parameters obtained for native starches give an indication of the degree of crystallinity, and the results are in agreement with that of previous studies (Tahir *et al.*, 2010; Warren *et al.*, 2011). However, DSC does not seem to be informative for the analysis of retrograded starches at concentrations of 50 and 200 mg/mL. At a diluted starch concentration, the DSC machine is not sensitive enough to detect retrograded starch material as the quantity of crystalline material is too low. However at 200 mg/mL, the instrumental noise levels are too high to accurately analyse peaks and make reliable conclusions.

4.3.3 Powder X-ray diffraction (XRD)

4.3.3.1 Native starch

Wide angle X-ray diffraction patterns for all native starches were acquired at room temperature over a 2θ range of 3^{o} to 40^{o}. XRD is suitable for determining the type of crystalline structure based upon the distinctive X-ray scattering

pattern (Wang *et al.*, 1998). A-type starches (cereals) have a densely packed amylopectin arrangement whereas B-type starches (tubers) have a more open double helical arrangement, packed in a hexagonal array (Wang *et al.*, 1998). C-type starches contain a mixture of A and B-type crystalline orders and are commonly found in legumes. The V-type pattern, associated with the amylose-lipid complex, can also be observed with XRD (Zobel *et al.*, 1988). Examples of A, B and C-type starches are shown in Figure 4.10.

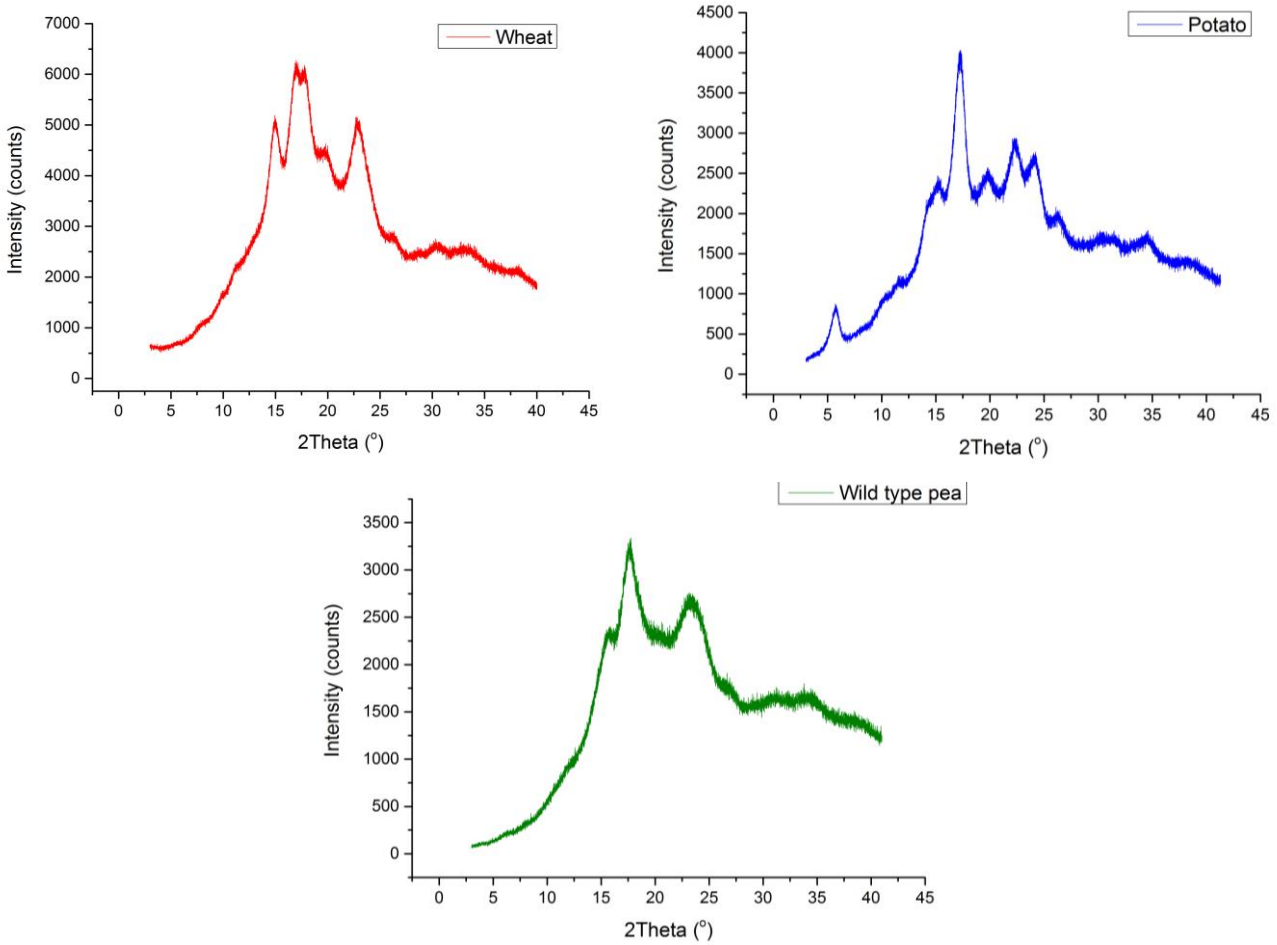

Figure 4.10. X-ray powder diffraction patterns recorded for native wheat, potato and wild type pea starch. Wheat starch shows an A-type pattern, potato starch shows a B-type pattern and wild type pea starch exhibits a C-type pattern.

The XRD patterns for A and B-type starch polymorphs show three or more distinct crystalline peaks while C-type starches show two crystalline peaks. The 2θ range at which these peaks can be observed varies depending upon the specific starch type.

A-type starches show strong XRD reflections between 15^{o}-22^{o} 2θ, B-types starches have peaks between 5-24^{o} 2θ and peaks for C-type starches are between 17-23^{o} 2θ. A-type starches have 2 sharp single peaks at 15^{o} and 22^{o} 2θ along with a double peak between 17-18^{o} 2θ. B-type starches show a double peak between 22-24^{o} 2θ, and 2 principle single peaks at 5^{o} and 17^{o} 2θ. The peak intensity is much higher for B-type starches compared with the A-type. This is believed to be due to the higher proportion of B-type crystallites with longer amylopectin chains compared with the shorter chains in the A-type (Hizukuri, 1985; Vandeputte *et al.*, 2003; Singh *et al.*, 2008). C-types starches have two distinctive peaks at 17^{o} and 23^{o} 2θ, with the latter peak being very broad compared to those observed in A and B-type polymorphs. A noticeable difference in C-type starches is the lack of a double peak. Table 4.7 summaries the differences in peak positions for A, B and C-type starches. Only large intensity peaks are represented in the table as these mainly contribute to the crystallinity content.

Table 4.7. Single and double peak positions from XRD diffraction patterns of A, B and C-type starch polymorphs.

Starch type	Example	Single peak (2θ)	Double peak (2θ)
A	Cereals	15^o and 22^o	17^o
B	Tubers	5^o and 17^o	22^o-24^o
C	Legumes	17^o and 23^o	none

Figure 4.11 shows the different X-ray patterns for starches with varying amylose contents. Maize and waxy maize starches show an A-type pattern, noted by the peak positions, whereas high amylose maize starch shows a B-type pattern which is identical to that of native potato starch (Sievert *et al.*, 1991; Gidley *et al.*, 1995; Matveeva *et al.*, 2001). The peak at 15^o 2θ for high amylose maize becomes progressively weaker, relative to maize and waxy maize, while the strongest diffraction peak observed at 17^o 2θ is a result of the double peaks in maize and waxy maize merging together. In addition, the low intensity double peak at 22-24^o 2θ is a result of the strong single peak in maize and waxy maize splitting into two separate peaks (Cheetham and Tao, 1998).

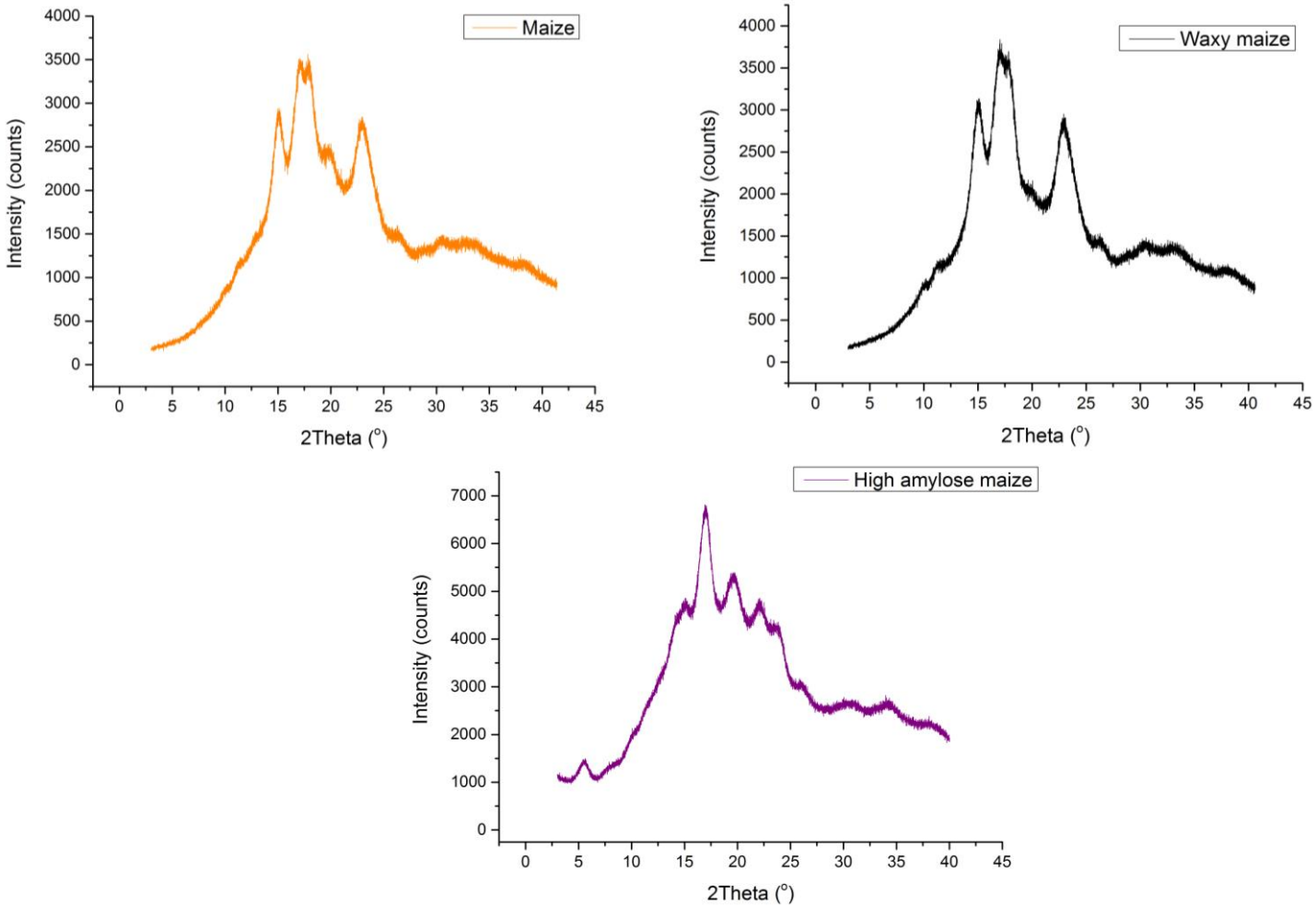

Figure 4.11. XRD pattern for native maize (orange), waxy maize (black) and high amylose maize starch (purple). Maize and waxy maize starches show A-type patterns and high amylose maize starch shows a B-type pattern.

The X-ray pattern for high amylose maize starch also shows the common V-type peak, characteristic of the amylose-lipid complex, at ~20^{o} 2θ. The V structures in native cereal starches are not detected by XRD as they are relatively amorphous, only producing a few weak lines that show crystallinity (Type I) (Buléon *et al.*, 1998; Pérez and Bertoft, 2010; Wang and Copeland, 2013). However, V-type crystalline structures in high amylose starches are detected by XRD and therefore show the characteristic V-type diffraction pattern (Type II) (Sievert *et al.*, 1991; Cheetham and Tao, 1998; Matveeva *et al.*, 2001; Lopez-Rubio *et al.*, 2008; Htoon *et al.*, 2009).

The crystallinity was calculated using OriginPro 9.1© (Table 4.8). The area under the crystalline peaks was divided by the total area under the diffractogram (sum of the area between the experimental data and the baseline) and expressed as a percentage (Gidley *et al.*, 1995; Miao *et al.*, 2009; Shrestha *et al.*, 2012; Xia *et al.*, 2012). Specific details on the calculations are presented in Chapter 2.

Table 4.8. Native starch crystallinity values averaged from three data sets (± SEM).

Starch	Crystallinity (%)
Wheat	22.3 ± 1.7
Potato	32.3 ± 0.9
Wild type pea	23.7 ± 2.1
Durum wheat	22.2 ± 0.8
Maize	24.3 ± 2.1
Waxy maize	26.0 ± 0.4
High amylose maize	21.0 ± 1.6 *(2.3 ± 0.6)
Rice	24.9 ± 0.3

**Crystallinity for the V-type structure*

Native starches have a crystallinity content of 21-32%, with the subsequent amount assigned to amorphous starch material. Some discrepancies may evolve in the calculated values due to the methodology used to determine a suitable baseline, making it difficult to obtain absolute crystallinity values. Similar starch crystallinity values have been reported by many other researchers, however, and are therefore comparable to our calculated figures for starches of similar botanical origins (Cairns *et al.*, 1997; Lopez-Rubio *et al.*, 2008). A few groups have published crystallinity values between 20-50% and suggest origin and starch hydration have major influences on crystallinity (Gidley and Bociek, 1985; Buléon *et al.*, 1998; Lopez-Rubio *et al.*, 2008). Sievert and workers have previously shown that starch samples have to be hydrated to produce sharp, detectable diffraction peaks (Bear and French,

1941; Sievert *et al.*, 1991). Therefore, in our XRD studies, starches were in the hydrated form with a moisture content ranging from 11 to 16% (Chapter 3, Section 3.3.1).

The relationship between the gelatinisation enthalpy and the degree of crystallisation for different starch samples was studied. Both parameters correlated linearly with each other (R^2=0.884) as shown in Figure 4.12. The positive relationship suggests the gelatinisation enthalpy is influenced by starch crystallinity (Fujita *et al.*, 1998). Potato starch shows the highest gelatinisation enthalpy and degree of crystallinity while high amylose maize starch has the lowest of all the tested starches. The gelatinisation enthalpy was preferred over the FTIR peak ratio, as the former represents the molecular order in the bulk of the starch sample rather than being restricted to the surface. However, a recent study by Sun et al. showed the relative crystallinity and order content determined by XRD and FTIR, respectively were in agreement with each other (Sun *et al.*, 2014).

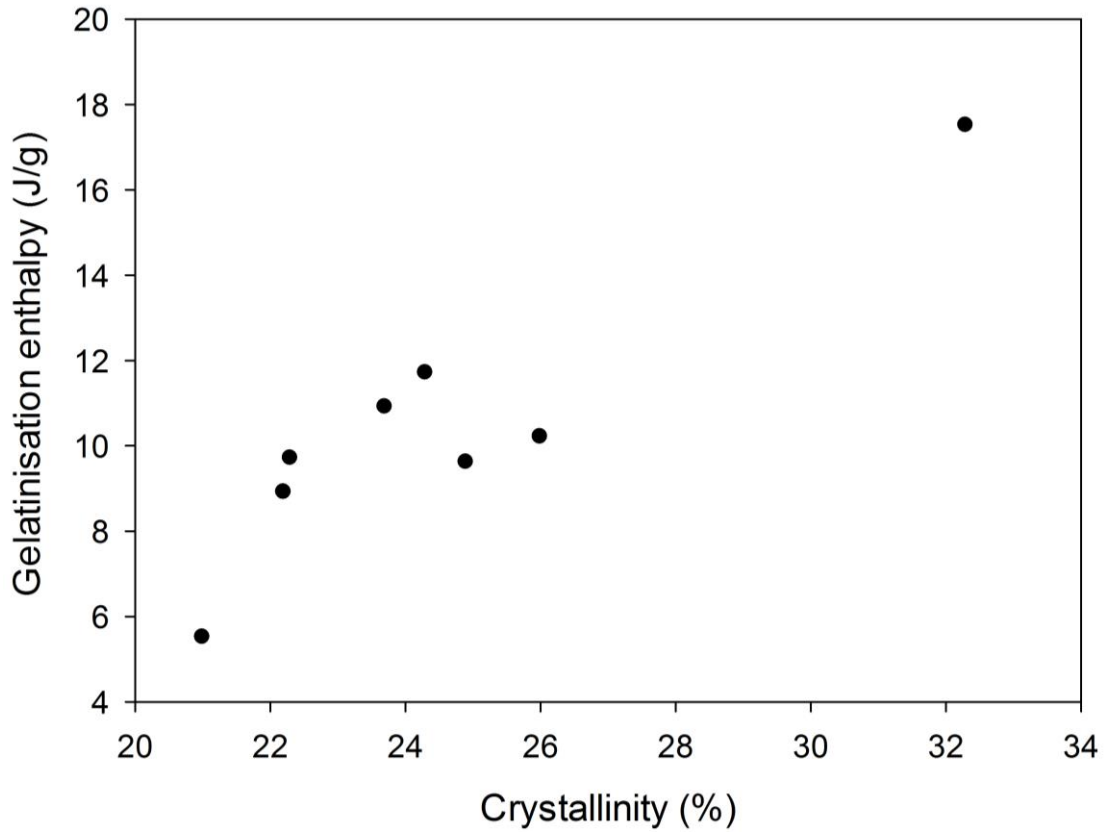

Figure 4.12. The relationship between the gelatinisation enthalpy and starch crystallinity for different native starches (correlation coefficient (R^2) of 0.844). Refer to Table 4.5 and 4.8 for sources of starches.

4.3.3.2 Gelatinised and retrograded starch

Figure 4.13 shows the XRD pattern for gelatinised wheat starch. The pattern for native wheat starch was also plotted to show the amorphous nature of the gelatinised form. As the heating process results in predominately single amorphous chains, no peaks were observed reflecting the complete loss of native crystallinity via gelatinisation.

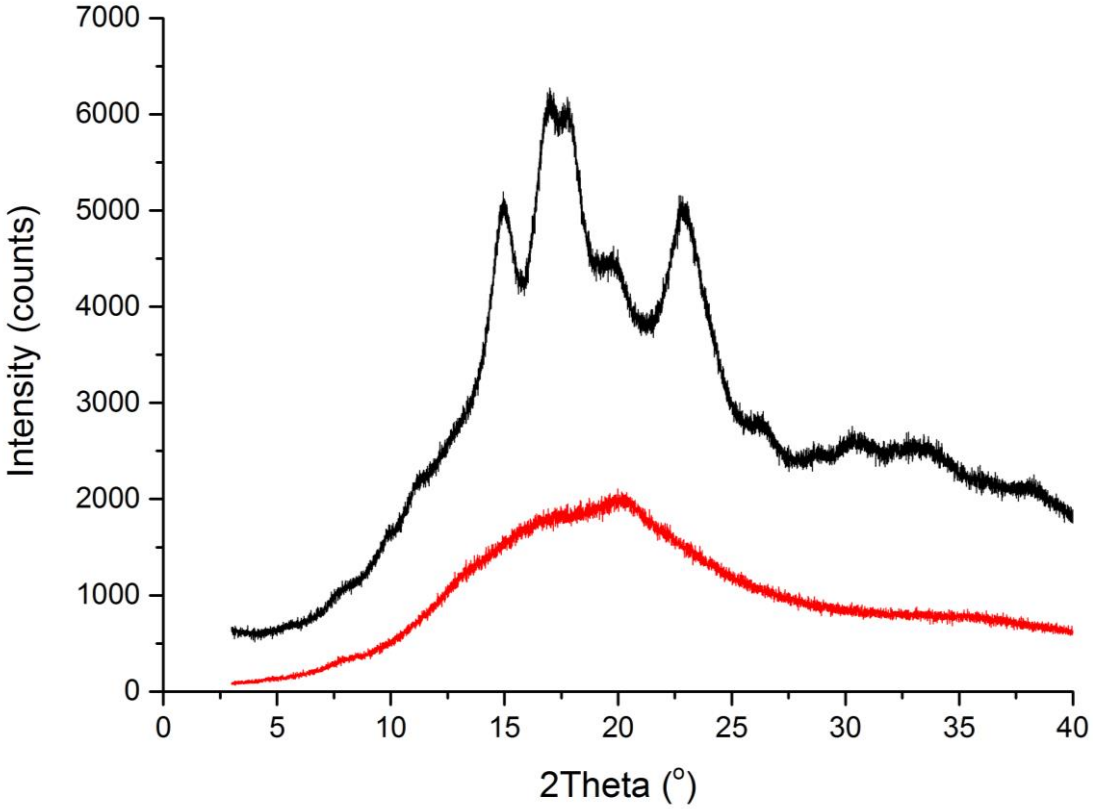

Figure 4.13. X-ray diffractograms of native (black) and gelatinised (red) wheat starch.

Many researchers have freeze dried starches to study the structure using XRD (Eerlingen *et al.*, 1994; Cairns *et al.*, 1997; Han *et al.*, 2006; Htoon *et al.*, 2009; Miao *et al.*, 2009). Therefore, in our study a 48h retrograded high amylose maize starch sample was freeze dried before an XRD scan was performed (Figure 4.14). Two prominent crystalline peaks were observed at 15° and 20° 2θ, with the latter attributable to the amylose-lipid complex. The total crystallinity was calculated to be 14.6% ± 1.2 with the V-type crystallinity being 2.9% ± 0.2. The peak reflections are due to the transformation of amylose chains into ordered/crystalline structures resulting in the characteristic B-type XRD pattern (Gidley *et al.*, 1995). However the profile shows a very poor B-type starch

pattern with broad and low intensity reflection peaks. To produce sharp XRD peaks with a well resolved pattern a certain amount of water is required to maintain structural ordering (Sievert *et al.*, 1991). Therefore, the broad peaks shown in Figure 4.15 could well be due to the low water content from freeze drying. As XRD directly measures overall starch crystallinity, it lacks the unique feature of differentiating between retrograded amylose and amylopectin crystallites. For this, thermal analysis using DSC is commonly used.

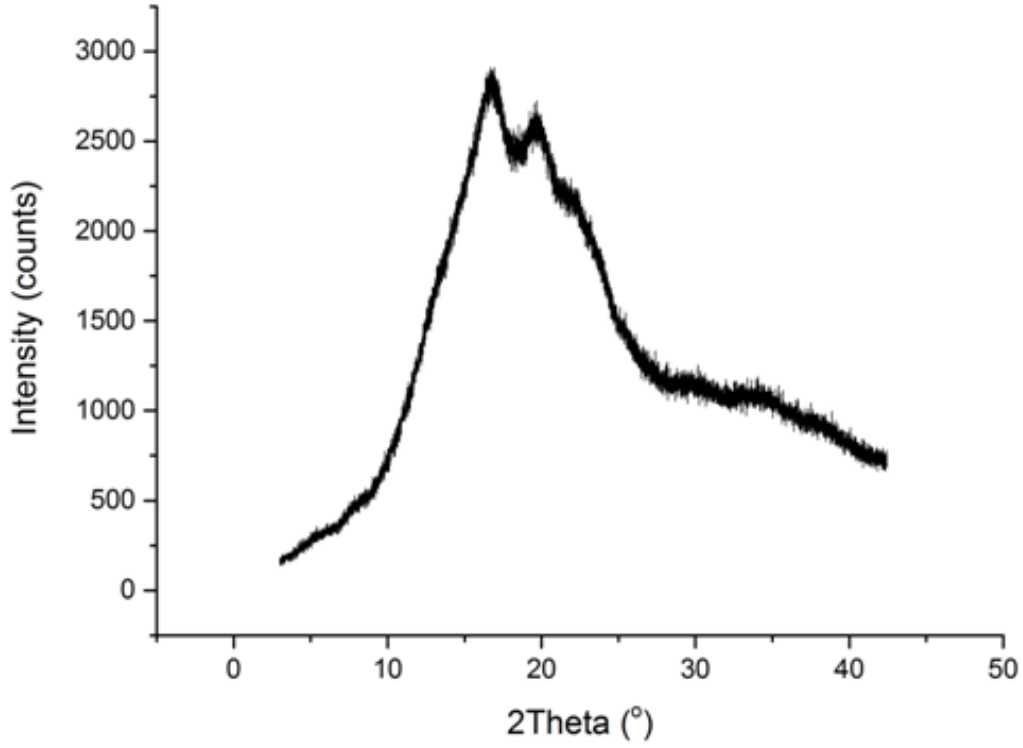

Figure 4.14. XRD pattern for 48h freeze dried retrograded high amylose maize starch.

4.3 Conclusion

The physical properties of all starches were investigated using different analytical techniques. Native, gelatinised and retrograded starches were characterised using spectral Fourier transform infrared spectroscopy (FTIR), thermal differential scanning calorimetry (DSC) and X-ray diffraction (XRD).

FTIR analysis was conducted on starches to determine the molecular order at the surface of the granules. The degree of ordered structure varied for different native starches with potato having the highest peak ratio (more order) and rice starch having the lowest ratio (least order). For gelatinised starch the ratio was extremely low as heat input results in a disordered structural organisation. Upon retrogradation however, the ratio increased as starch material forms an ordered structure. Some of this retrograded starch originates from the leaching of amylose during gelatinisation and was detected using FTIR. Therefore, FTIR is a valid method for not only the rapid determination of ordered starch material at the native granule surface, but also for monitoring retrograded amylose that has leached from the granule during hydrothermal processing.

Thermal DSC analysis provides information on the transition temperatures and gelatinisation enthalpies, with the latter used to quantify the ordered starch content. For native starches the gelatinisation temperature varied between 59-87.5^{o}C while the $\Delta_{gel}H$ ranged from 5.5 to 17.5 J/g. Gelatinised starches produced no peaks along the thermogram, as the structure lacks crystalline material. DSC analysis for retrograded starches showed a peak corresponding

to the amylose-lipid complex and for retrograded amylopectin but no peak for retrograded amylose.

In addition to FTIR and DSC analysis, XRD was also used to directly measure starch crystallinity. Native starch crystallinity values ranged from 21.0 to 32.2% while no peaks were detected for gelatinised starch indicating a completely amorphous structure. In contrast, retrograded starch yields a B-type X-ray diffraction pattern with crystalline peaks indicating an amorphous to crystalline structural transformation.

In summary, the aim of characterising native and gelatinised starch using FTIR, DSC and XRD was achieved. However, it proved very difficult to study the structural properties of retrograded starch, especially using DSC. Therefore, more work is clearly required to draw accurate conclusions regarding retrograded crystallites, especially in relation to its susceptibility to amylolysis.

Chapter 5 Log of Slope (LOS) plot analysis

5.1 Introduction

Previously, it was generally accepted that the starches in different starch-containing foods were digested at the same rate and produced similar rises in postprandial blood glucose and insulin concentrations (Bornet *et al.*, 1997). However many studies have shown marked variations in the susceptibility of the different foods, containing identical amounts of starch, to amylolysis during digestion. These variations in amylolysis are known to elicit marked fluctuations in postprandial glycaemia and insulinaemia (Crapo *et al.*, 1977; Crapo *et al.*, 1981; Seal *et al.*, 2007). Such differences are considered to be largely attributed to changes in the rate and extent of luminal digestion of starches from different botanical sources. The chemical and physical form of starch granules, encapsulation of starch by plant cell walls (dietary fibre), the presence of amylase inhibitors (e.g. phenolics, soluble forms of dietary fibre) and structural transformations during food processing are significant factors that influence the rate of digestion of starch in a food matrix. Examples of processing techniques include gelatinisation and retrogradation, with the former increasing the susceptibility to amylolysis due to the increase in disordered α-glucan chains in starch granules. *In vitro* procedures are commonly used to study amylolysis and these involve digesting starchy-based foods with α-amylase to produce digestibility curves. Such studies allow for a better understanding of the molecular basis for differences in the rate of starch digestion of different starchy foods.

Chapter 5: Log of Slope Plot

Several *in vitro* studies have previously been conducted to monitor the rate and extent of starch digestion covering both long and short term digestion phases. Relatively lengthy digestion periods (several hours) have proven to be extremely useful to mimic the *in vivo* intestinal digestion process; however shorter digestion periods (12-16 min) provide more valuable initial rate data. The enzyme kinetic model for studying the initial starch digestion phase is described in Chapter 6; therefore this chapter will only cover prolonged periods of starch digestion (i.e. up to 2 hours).

The most popular and widely known *in vitro* method to study these prolonged periods of starch digestion is the one described by Englyst and co-workers. Their classification system of starch digestion was based upon *in vitro* incubations with α-amylase over 120 minutes and from the digestibility curves starch digestion was categorised into three separate fractions. These fractions are described respectively as rapidly digestible starch (RDS), slowly digestible starch (SDS) and resistant starch (RS) (Englyst *et al.*, 1992; Englyst and Hudson, 1996). RDS is the fraction of starch digested in the first 20 minutes of incubation, with the SDS fraction digested between 20 and 120 minutes (obtained from visual inspection of starch hydrolysis curves). Undigested starch remaining from *in vitro* amylolysis is classified as resistant starch (RS), which in studies performed *in vivo* is reported to escape digestion in the small intestine (Englyst and Cummings, 1987).

Workers have shown that amylolysis of cooked/processed starch materials is described by a pseudo first-order kinetic process characterised by a single

digestibility constant (Goñi *et al.*, 1997; Dhital *et al.*, 2010). This suggests that the Englyst classification system is seriously flawed as the slowing of the rate of the reaction is a natural consequence of a reduced substrate concentration. Therefore the Englyst classification system reveals no clear molecular evidence of RSD and SDS fractions. Fitting a first-order kinetic model to the digestibility curves allow for an estimate of k, the pseudo first-order rate constant, and C_∞, the total amount of starch digested during the incubation period. Butterworth et al. developed an improved first order kinetic analysis method of starch hydrolysis curves using a 'logarithm of slope' (LOS) plot (Butterworth *et al.*, 2012). By measuring the slope of the curve at each individual data point on the digestibility curve and plotting the natural logarithms against the mean time allows estimation of reliable k and C_∞ values. The rate constant, k, is represented by the slope of the rectilinear plot and the C_∞ value can be calculated using the y axis intercept. In addition, the LOS plot approach allows for accurate determination of RDS and SDS starch fractions, should they be present, from discontinuities in the linear plot. Subsequently by using the C_∞ values, the RS content can also be estimated.

Butterworth et al. have recently calculated k and C_∞ values using the LOS plot approach, for the digestion of native and gelatinised wheat and wild type pea starches by α-amylase (Butterworth *et al.*, 2012). A similar study conducted by Matínez and workers involved digesting rice flour prepared under different extrusion conditions (Martínez *et al.*, 2014). For both studies, the k and C_∞ results calculated using the LOS plot approach agreed with the first order kinetic model by Goñi and colleagues (Goñi *et al.*, 1997), suggesting that the kinetic

parameters can be fitted to a logarithmic function. The LOS plots also revealed a discontinuity in the digestion of native starches indicating that digestion of native granular starch does not follow a single first order reaction. Instead, the digestion process is best described by two separate first order reactions that differ in their digestibility rate constant; the initial rapid rate shortly followed by a slower rate. However the LOS plot for the digestion of gelatinised starches revealed a single digestibility constant and therefore reveals the misconceptions in the Englyst classification theory of starches being digested in different phases.

Previous LOS plot studies have been limited to a few starches and have only included native and gelatinised starch forms. Therefore, given the widely reported interests in retrograded starch, the application of first order kinetics to native, gelatinised and retrograded starch digestibility plots was applied to study the effects on k and C_∞ values.

5.2 Methods

The sources of the starch samples (wheat, potato, wild type pea, durum wheat, rice, maize, waxy maize and high amylose maize) and their physicochemical characteristics are described in detail in Chapter 2 (Section 2.2). Native, gelatinised and retrograded starch suspensions (5 mg/mL) were also prepared in PBS as described in Section 2.4 of Chapter 2. The enzyme assay was carried out at 37^{o}C with samples placed in a rotator to allow constant end over end mixing. A control aliquot was taken before the addition of α-amylase (for source and type see Chapter 2, Section 2.1) to check for the presence of

endogenous sugars. Native starch samples were then digested with 4.5 nM α-amylase. Aliquots were collected at timed intervals for up to 120 min and transferred to ice cold 0.3 M Na_2CO_3 stop solution in Eppendorf tubes to stop the reaction. Eppendorf tubes were centrifuged at 13,000 g for 5 min and 400 µL of the supernatant was collected and frozen at -20^{o}C. An almost identical digestion method was performed with gelatinised and 24h retrograded starch, but with the addition of 2.25 nM α-amylase. A doubled enzyme concentration was used for the digestion of native starches to obtain detectable reducing sugar concentrations.

The reducing sugars present were measured by the Prussian blue assay which is described in more detail in Chapter 2 (Section 2.4.3). Maltose standards were also assayed along with the samples before the absorbance was read at 695nm. Using the standard curve, maltose concentrations were calculated and entered into Sigmaplot to produce a digestibility curve of maltose concentration against time. A LOS plot was then constructed by taking the slope of each individual data point and plotting the natural logarithms against the relevant mean time, which then allows k and C_∞ to be accurately estimated. Further details of the LOS plot analysis and the calculations of the kinetic parameters are provided in Chapter 2, Section 2.4.4.

5.3 Results and Discussion

Digestibility plots for native and processed starches were obtained by digesting starch samples with 4.5 nM and 2.25 nM α-amylase, respectively.

Fitting the digestibility curves for all starch digestions to the first order LOS plot equation, ln (dC/dt) = ln($C_\infty k$) – kt, allows accurate estimates for k and C_∞ values to be determined (Goñi *et al.*, 1997; Butterworth *et al.*, 2012). The LOS plot equation is differentiated from the original first-order rate equation and then expressed in a logarithmic form (refer to Scheme 1 in Chapter 1, Section 1.4.3). Table 5.8, at the end of the Chapter, summarises all the k and C_∞ values obtained from the LOS plots of native and processed starches.

5.3.1 Digestion profiles

5.3.1.1 Digestibility curves

The digestibility plots for different starches digested by PPA over 2h are shown in Figure 5.1 (non-mutant starches) and Figure 5.2 (mutant maize starches). Starches were digested in their native, gelatinised and 24h retrograded forms. However, due to the reduced rate of amylolysis of native starch, the PPA concentration varied between native and processed starch forms. For this reason native starches were digested with 4.5 nM PPA, as opposed to 2.25 nM for gelatinised and 24h retrograded starches.

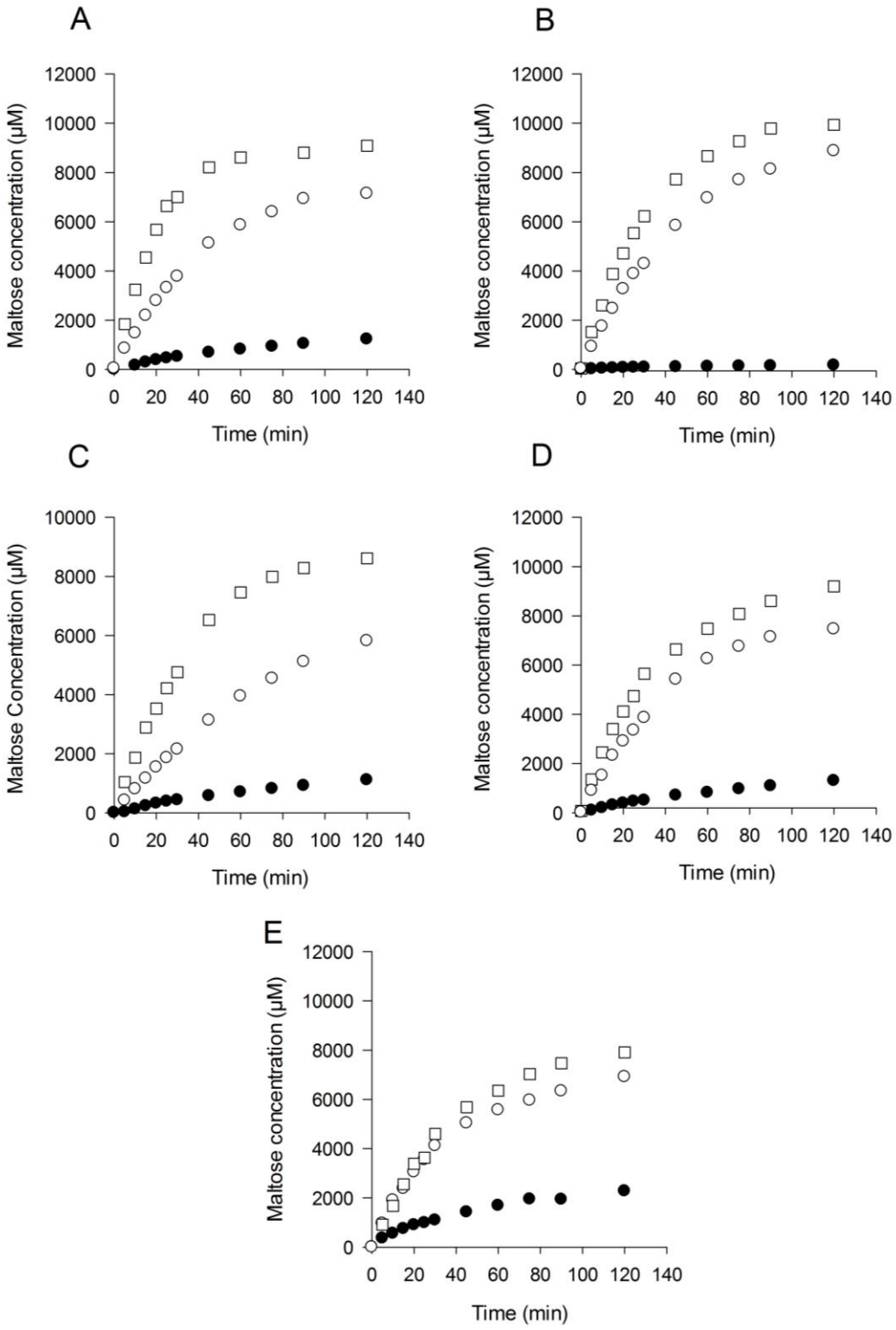

Figure 5.1. Digestibility curves of native (●), gelatinised (□) and 24h retrograded (○) starches. Wheat (A), potato (B), durum wheat (C), wild type pea (D) and rice (E) starch. Values are means from three to four data sets.

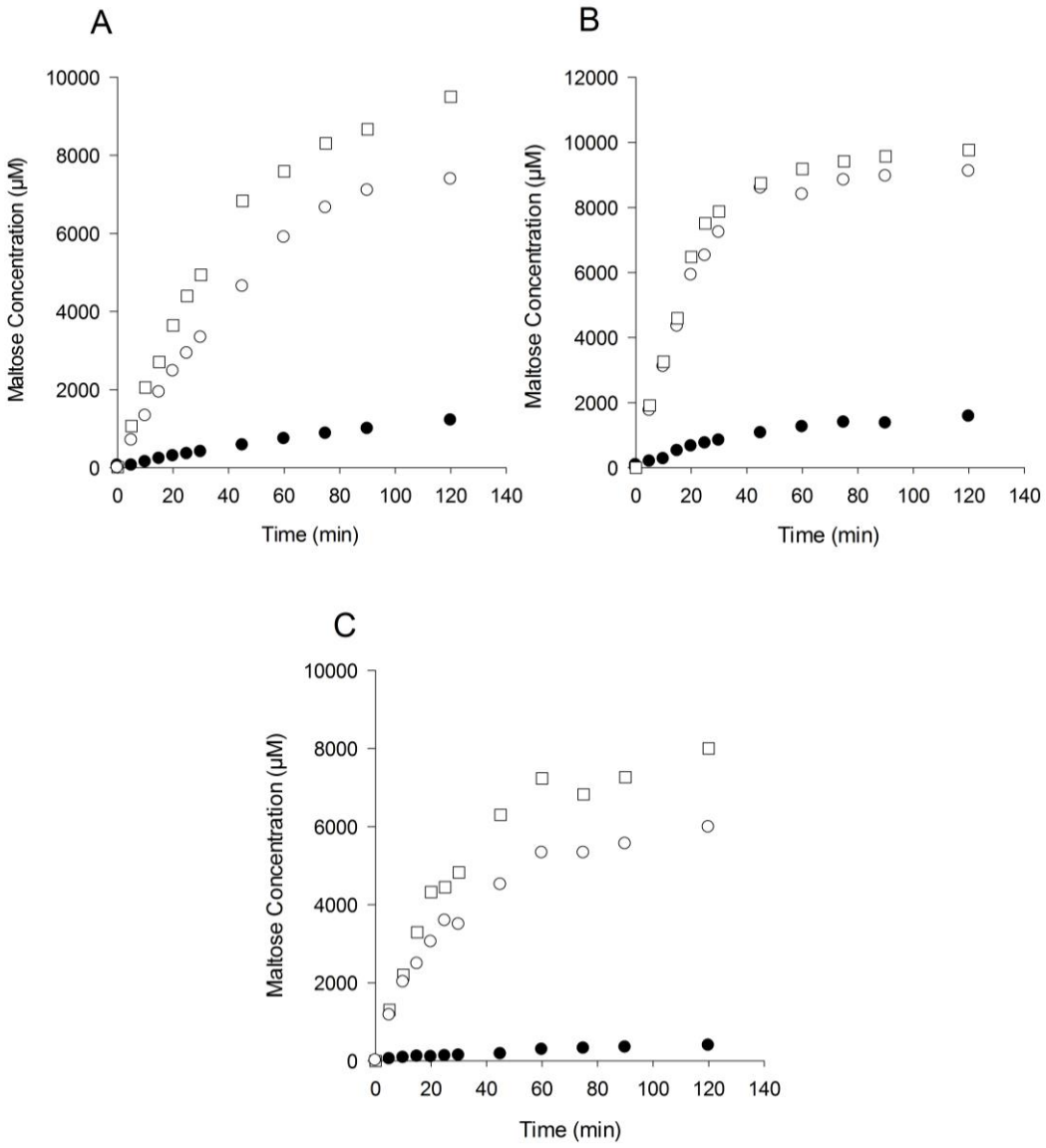

Figure 5.2. Digestibility curves of native (●), gelatinised (□) and 24h retrograded (○) starches. *Maize (A), waxy maize (B) and high amylose maize starch (C). Values are means from three to four data sets.*

Native starches prove to be much harder to digest due to the degree of crystallinity being much greater, resulting in an ordered starch structure with α-glucan chains not being readily exposed. This tight packing results in few glucan residues forming hydrogen bonds with specific amino acid side chains within the α-amylase active site (Butterworth *et al.*, 2011). As a result, the

number of occupied binding sites for α-amylase is reduced. Therefore the plots show very little digestion. Native potato starch seems to be almost entirely resistant to digestion by α-amylase as represented by the low maltose concentrations. This supports previous statements made by many groups suggesting potato starch is almost resistant to hydrolysis by pancreatic α-amylase (Englyst and Cummings, 1987; Gallant *et al.*, 1997; Dhital *et al.*, 2010). Using published results from different research groups, McCleary and Monaghan have calculated the average *in vitro* resistant starch content from uncooked potato starch to be ~80%, which correlates well with the measured *in vivo* resistant starch content of 79% (McCleary and Monaghan, 2002).

Starch gelatinisation disrupts the granule integrity and degree of crystallinity with α-glucan chains being exposed to the enzyme. Therefore the number of α-glucan chains which favourably interact with α-amylase is no longer limited. This consequently increases the susceptibility for attack by α-amylase producing more starch hydrolysis products (Butterworth *et al.*, 2012). During gelatinisation, potato starch granules have also been known to swell to a greater extent than other starch sources. This has been attributed to the phosphate groups associated with amylopectin chains facilitating the swelling of potato starch, and thereby producing a favourable substrate for α-amylase (Slaughter *et al.*, 2001).

Gelatinised starch stored for 24h at room temperature gradually begins to form a more ordered and to some extent crystalline structure, which reduces the α-amylase binding potential (Abd Karim *et al.*, 2000). The new ordered structure

is referred to as retrograded starch and consists of mainly ordered amylose chains (Eerlingen *et al.*, 1993; Eerlingen and Delcour, 1995). Therefore the relative proportion of gelatinised starch which is digestible is transformed to indigestible retrograded starch.

5.3.1.2 LOS plot for native starch

Figures 5.3 and 5.4 show the LOS plots for the digestion of different native starches. The LOS plots revealed a discontinuity between 20-30 min suggesting native starches are digested in two separate stages. These two stages have been identified as ‘rapid’ and ‘slow’, with *k* values for the former being higher than the latter.

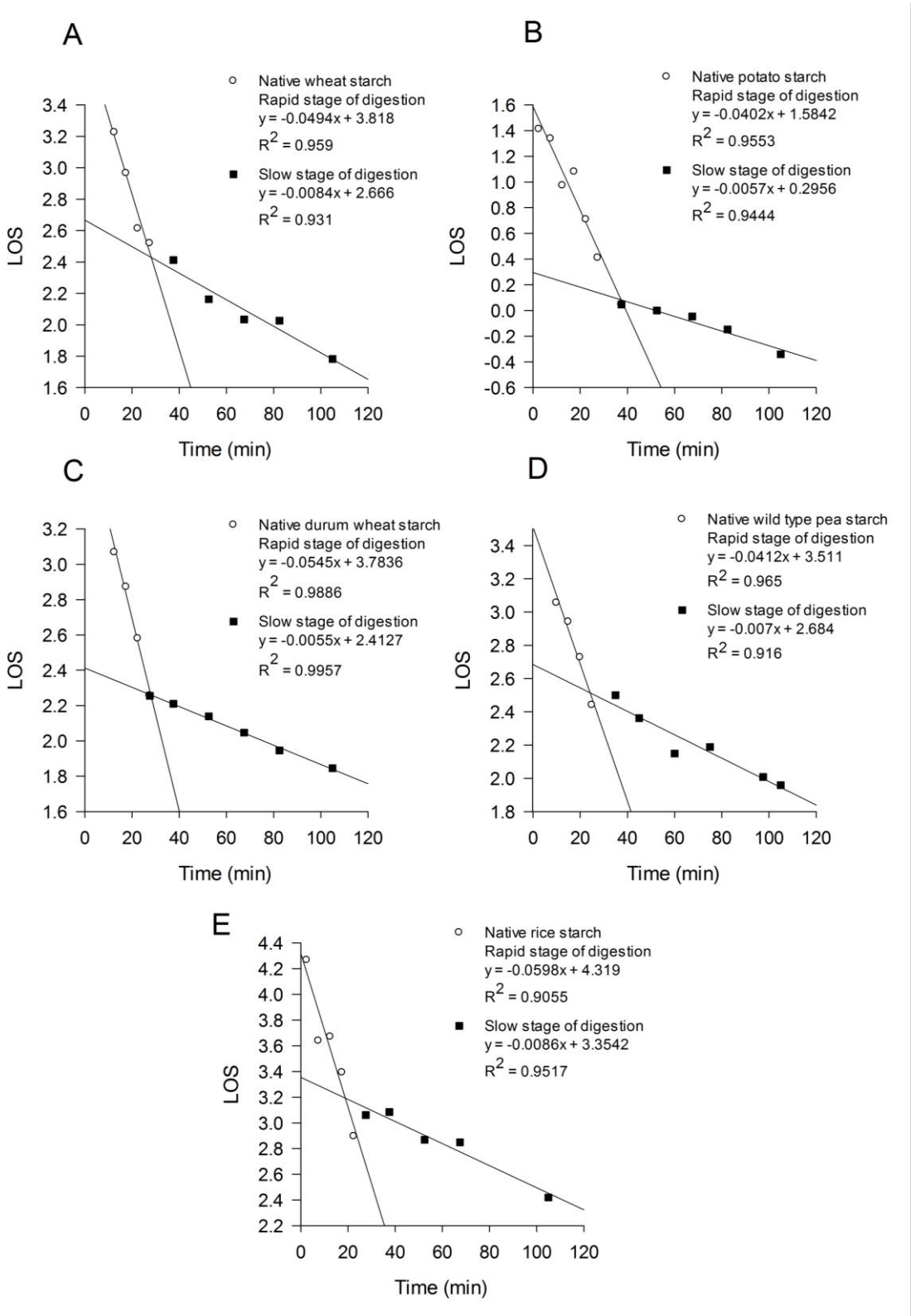

Figure 5.3. LOS plots of native wheat (A), potato (B), durum wheat (C), wild type pea (D) and rice (E) starch digestion by 4.5 nM PPA at 37°C. All plots were obtained from three to four replicate digestion assays.

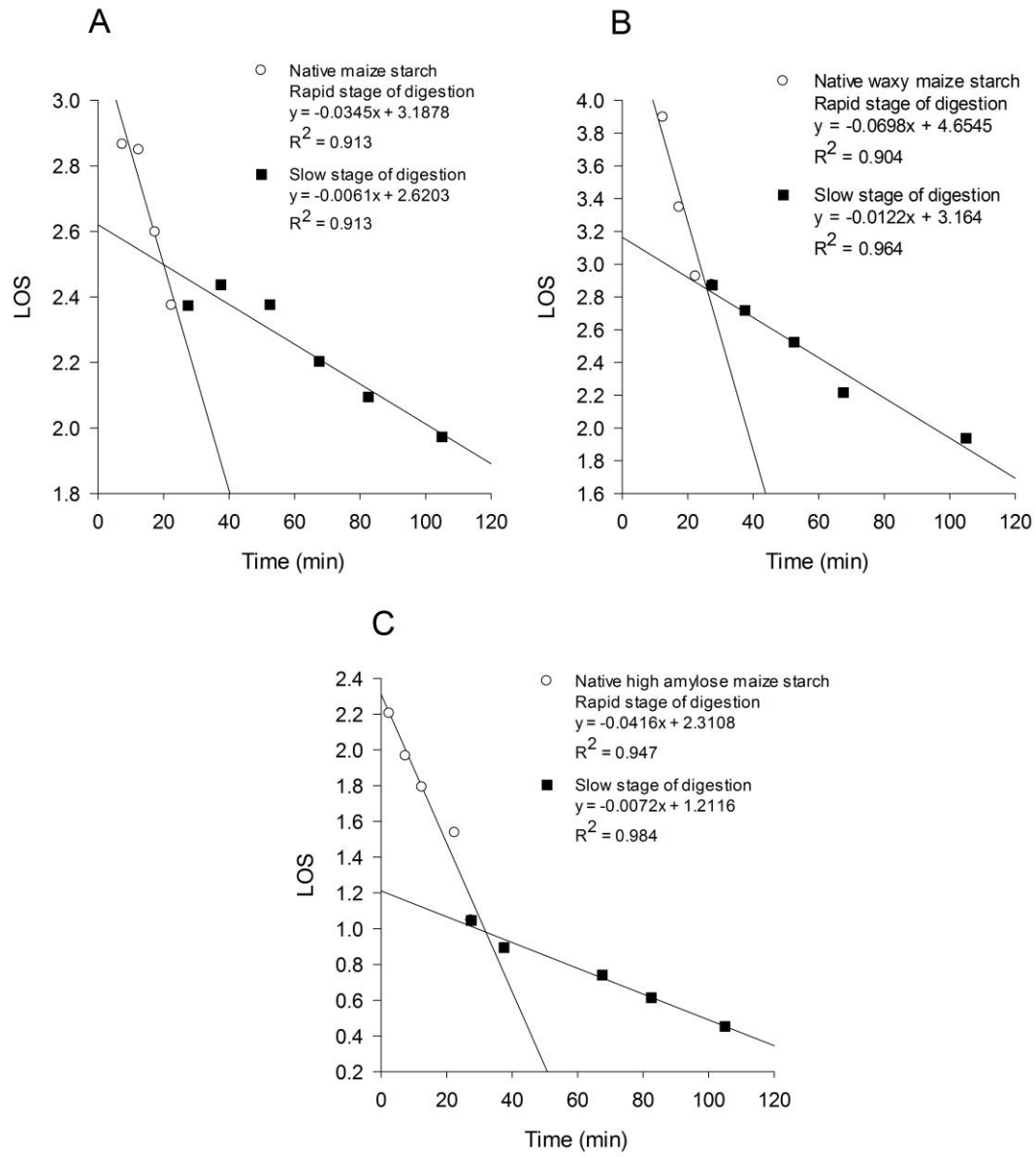

Figure 5.4. LOS plots of native maize (A), waxy maize (B) and high amylose maize (C) starch digestion by 4.5 nM PPA at 37°C.

Table 5.1. Rate constant (k) and percentage of total starch digested after 2h incubation (C_∞) calculated from the LOS plots for native starches.

Native Starch	Rapid		Slow	
	k (min^{-1})	C_∞ (%)	k (min^{-1})	C_∞ (%)
Wheat	0.049	7.0	0.008	13.1
Potato	0.040	1.0	0.006	1.6
Durum wheat	0.055	6.5	0.006	16.3
Wild type pea	0.041	6.3	0.007	15.6
Rice	0.060	10.1	0.009	26.8
Maize	0.035	5.4	0.006	17.4
Waxy maize	0.070	11.7	0.012	15.1
High amylose maize	0.042	1.9	0.007	3.6

Using the intercept, $\ln(C_\infty k)$, and the digestibility rate constant, the total digestible starch at the end of the reaction, C_∞, was calculated (Table 5.1). The rapid phase is characterised with a higher k value, due to the glucan chains located on the surface of the granule being exposed to the bulk solution and therefore readily available for attack by α-amylase. The rapid phase lasts for ~30 min for all starches except potato starch. The LOS plot of native potato revealed a rapid phase of relatively long duration in that it lasted for up to 40 min. This may suggest substrate availability at the surface of the granule is limited resulting in a reduced rate of reaction (rate = k[S]). Therefore the digestion of α-glucan chains represented by the 'rapid' phase is inevitably extended because of a low rate of catalysis at a low substrate concentration.

Also as potato starch granules have a large particle size, the surface area is relatively small making the binding between amylase and potato starch less favourable (Warren *et al.*, 2011). Therefore, as the majority of the material is hydrolysed within 40 min, the reaction characterised by the slow phase represents hydrolysis of less susceptible starch and is reflected in the low *k* and C_∞ values.

The digestion of native starch during the slow phase is reflected by a slower rate constant as the α-glucan chains are buried within the starch granule. Therefore as the substrate availability is limited, the rate of the reaction and consequently the rate constant also decrease. Starches which lack a porous surface also contribute to the reduced rate constant as there is a slower diffusion rate of enzyme into the granule (Dhital *et al.*, 2010; Dhital *et al.*, 2014). However this explanation may not be plausible for porous starch granules (cereals) and therefore limited substrate availability may be the best explanation (Helbert *et al.*, 1996).

Figure 5.5 shows the total C_∞ values at the end of the 2h reaction for the digestion of all native starches. The C_∞ figures vary quite considerably with potato starch having the lowest C_∞ and rice starch having the highest (2.6% and 36.9%, respectively). The lowest C_∞ value was attributed to native potato starch suggesting very little starch is digested due to its highly crystalline structure. As mentioned previously, many workers have shown potato starch granules lack pores, channels and cavities, which would normally allow effective penetration towards the interior of the granule (Huber and BeMiller, 2000; Dhital *et al.*,

2010; Dhital *et al.*, 2014). Therefore a high degree of crystallinity, low surface area to volume ratio and a lack of pores/channels contribute to the resistant nature of potato starch.

The results show native rice starch to be the most digestible of all starches tested. *In vitro* studies by Slaughter and workers have also shown an extremely high maximal rate (V_{max}) value for the digestion of native rice starch (Slaughter *et al.*, 2001). This is believed to be due to the higher surface area to volume ratio, relative to other starches, resulting in a higher starch concentration available for amylolysis. Other physicochemical properties such as amylose and protein content may also exert an influence on the rate and extent of rice starch digestion (Panlasigui *et al.*, 1991; Miller *et al.*, 1992; Benmoussa *et al.*, 2007).

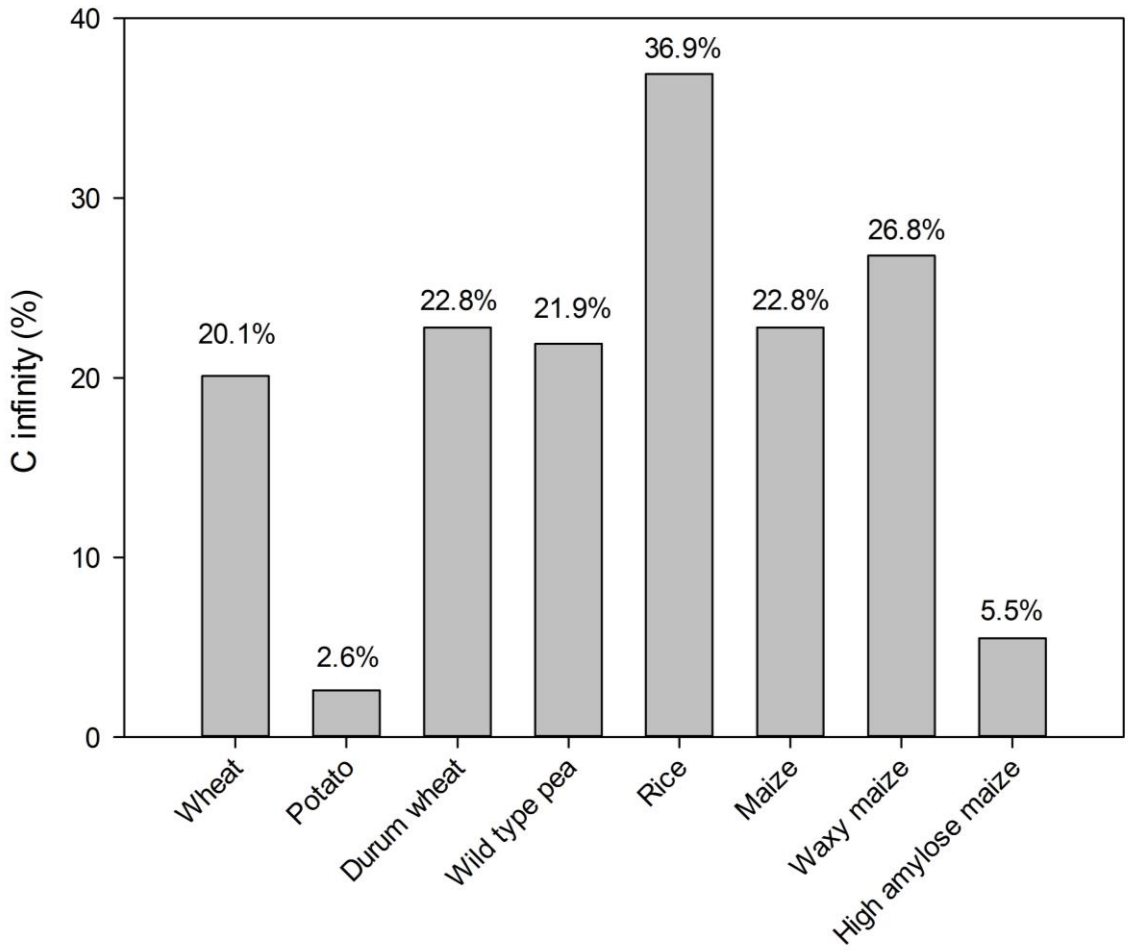

Figure 5.5. Total calculated C_∞ values for the digestion of native starches by PPA.

Estimated *k* and C_∞ values from the LOS plots were substituted back into the original first order kinetic equation ($C_t=C_\infty(1 - e^{-kt})$). This allows a computation of the digestibility curves to be plotted with the original experimental data to test the reliability of the estimated *k* and C_∞ values from the LOS plots. Figure 5.6 shows an example with native maize starch. Overall the computed digestibility curves correlated well with the experimental data.

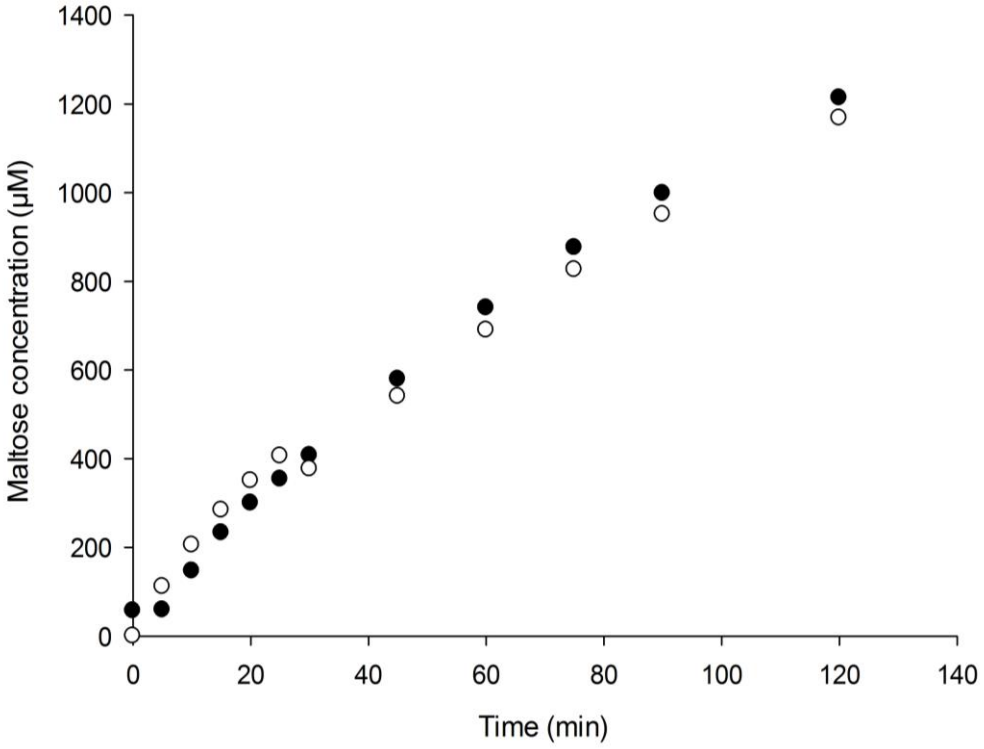

Figure 5.6. Computed digestibility curve (○), obtained by substituting k and C∞ into the first order kinetic equation, shown alongside the experimental data (●) for the digestion of native maize starch by PPA.

5.3.1.3 LOS plot for gelatinised starch

LOS plots for the digestibility of gelatinised starches shows no discontinuity (Figures 5.7 and 5.8). The absence of a break in the plot suggests nearly all the starch is rapidly digested starch and therefore a single digestibility rate constant is established. The fraction of slowly digested starch is thought to be minimal and have no significant effect on the digestibility behaviour (Butterworth *et al.*, 2012). Therefore gelatinisation significantly reduces the amount of slowly digestible starch (Sagum and Arcot, 2000; Miao *et al.*, 2009). Figure 5.7 shows the LOS plots for different starches gelatinised at 90^{o}C for 20 min followed by

digestion with 2.25 nM PPA. Figure 5.8 shows identical LOS plots but for genetically modified maize starches.

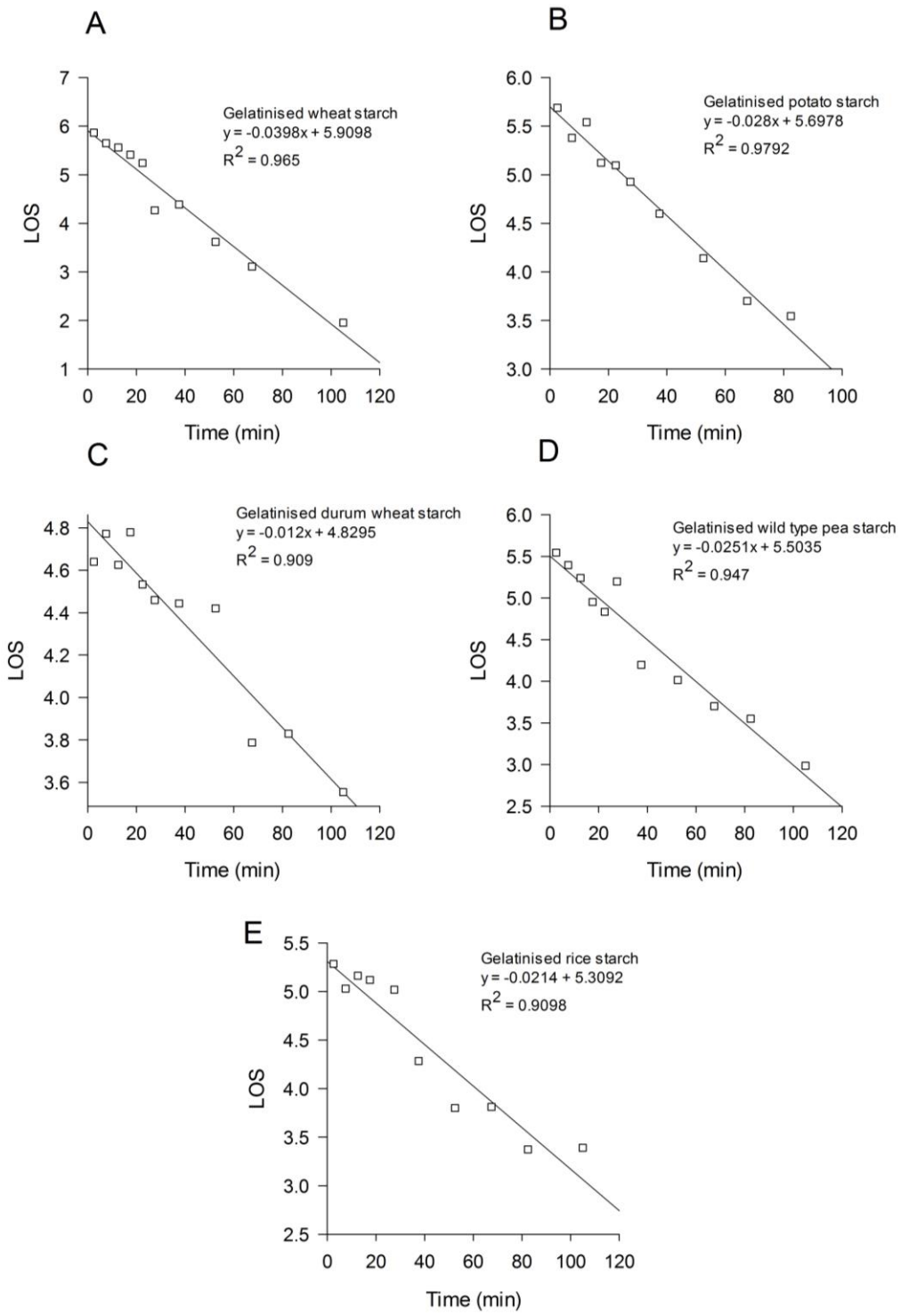

Figure 5.7. LOS plots of gelatinised wheat (A), potato (B), durum wheat (C), wild type pea (D) and rice (E) starch digestion by 2.25 nM PPA at 37°C. A least square regression line was fitted to each plot to obtain the R^2.

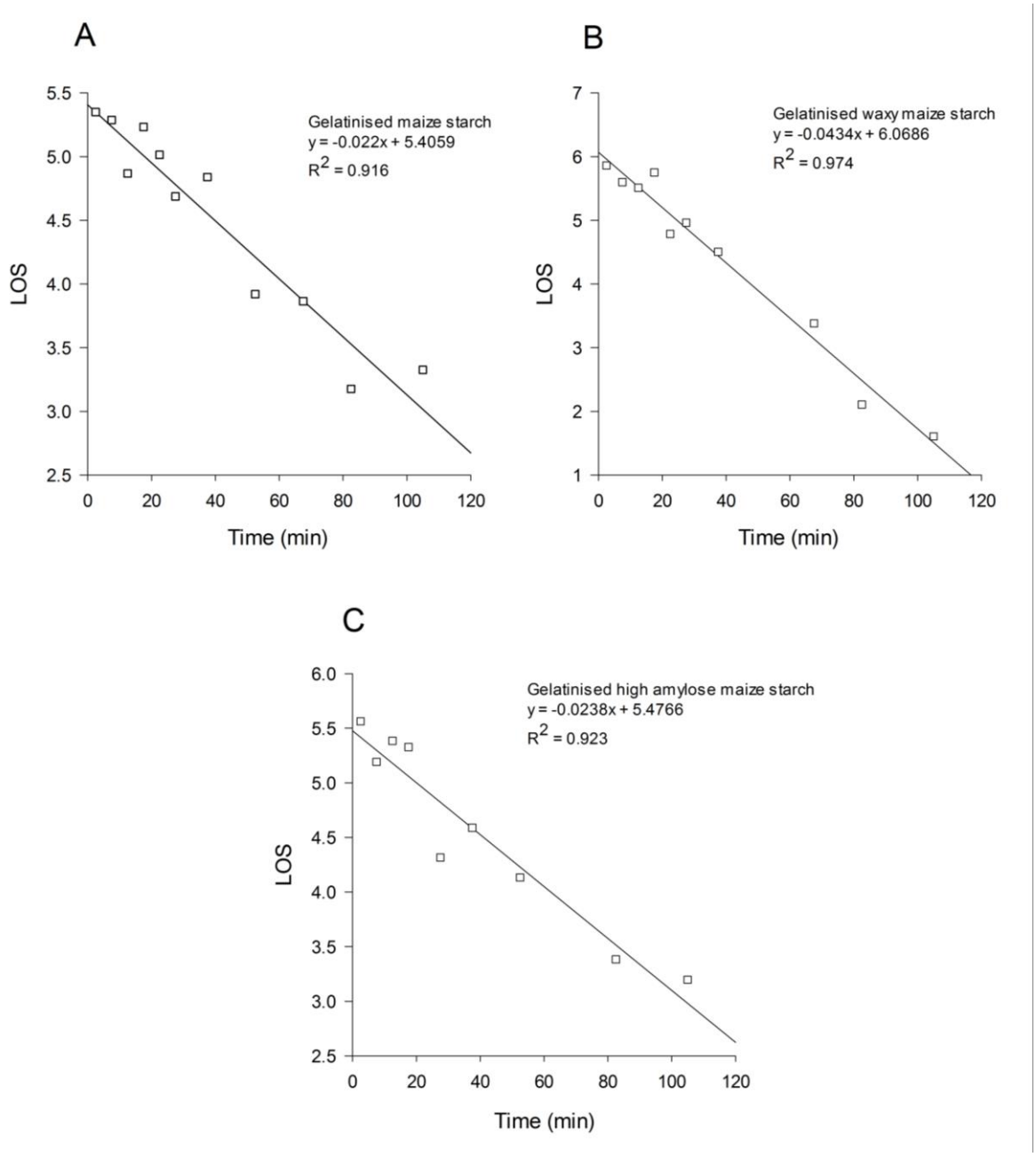

Figure 5.8. LOS plots of gelatinised maize (A), waxy maize (B) and high amylose maize (C) starch digestion.

The calculated rate constants, shown in Table 5.2, ranged from 0.01-0.04 min^{-1}. Surprisingly, gelatinised durum wheat starch revealed a lower *k* value than other tested starches. Therefore, allowing for the doubled enzyme concentration used in the digestion of native starch, the *k* value for the rapid phase in durum

wheat appears to be higher than that of the gelatinised form (0.028 min^{-1} and 0.012 min^{-1}, respectively). This becomes very difficult to explain, as glucan chains are exposed on the surface for both forms; hence the *k* values should be similar. The best possible explanation is the physicochemical properties of durum wheat starch most likely affect the enzyme activity (Medcalf and Gilles, 1965; Cunin *et al.*, 1995).

Table 5.2. Rate constant (k) and percentage of total starch digested after 2h incubation (C_∞) calculated from the LOS plots of gelatinised starches.

Gelatinised Starch		
	k (min^{-1})	C_∞ (%)
Wheat	0.040	70.8
Potato	0.028	86.8
Durum wheat	0.012	83.3
Wild type pea	0.025	77.0
Rice	0.021	76.0
Maize	0.022	75.4
Waxy maize	0.043	77.4
High amylose maize	0.024	78.1

Following gelatinisation the C_∞ values increased enormously relative to native starch, with the increase ranging from 2.8 fold for rice to 54.3 fold for potato starch. When starch granules are heat treated in excess water, the intermolecular and intramolecular hydrogen bonds which hold the helical structures together are disrupted. This causes the starch granule to transform

from a crystalline structure to a continuous amorphous structure. In addition to this, the starch granules undergo extensive swelling from heat treatment in excess water. This is noticeable mainly in potato starch due to the phosphate associated amylopectin, which promotes greater swelling compared with other gelatinised starches (Swinkels, 1985). Therefore the increased C_∞ values for gelatinised starches are due to the total loss of molecular order upon heating. This transition enables α-amylase to bind with more efficiency to the available α-glucan chains thereby increasing susceptibility to amylolysis.

5.3.1.4 LOS plot for retrograded starch

Gelatinised starch left to cool at room temperature for 24h induced retrogradation. The LOS plots for 24h retrograded starches allow k and C_∞ to be calculated (Figures 5.9 and 5.10). A single digestibility constant suggests all of the starches are still rapidly digested; however the quantity of retrograded starch material (RS III) increases due to the 24h storage process. The retrograded material is primarily retrograded amylose because the relatively short and mostly linear amylose chains re-associate much faster than the branched amylopectin chains (Khanna and Tester, 2006; Sajilata *et al.*, 2006). Many researchers have also shown that amylose leaches out of the granule during heat treatment in excess water (Obanni and Bemiller, 1996; Debet and Gidley, 2007; Zhang *et al.*, 2014). We also showed light micrographs of leached amylose chains post gelatinisation in Chapter 3, and determined the degree of ordered material using FTIR-ATR in Chapter 4. Therefore retrograded amylose chains are more likely to be located in the leached supernatant with a small amount remaining in the starch granule.

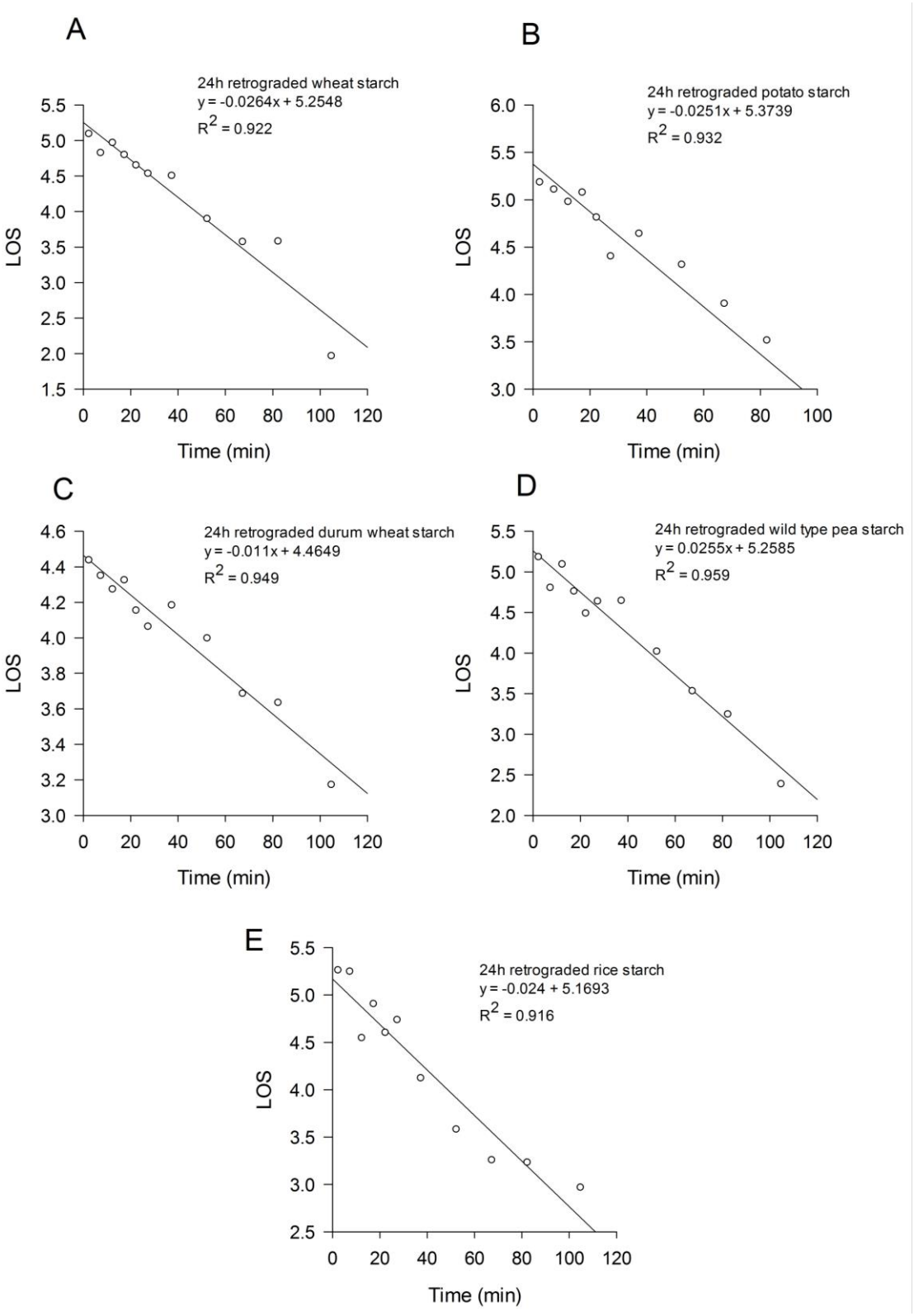

Figure 5.9. LOS plots of 24h retrograded wheat (A), potato (B), durum wheat (C), wild type pea (D) and rice (E) starch digestion by 2.25 nM PPA at 37°C.

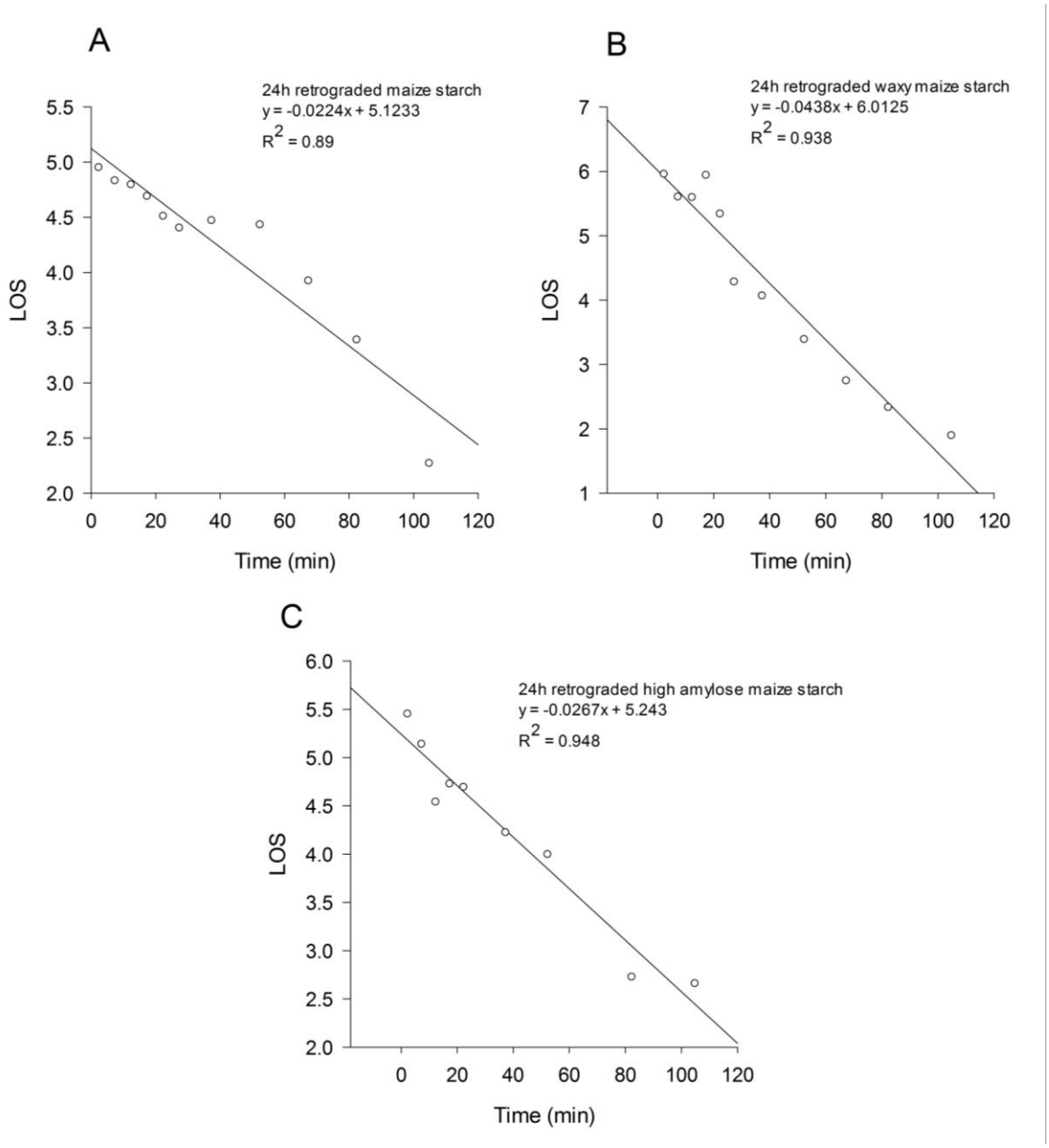

Figure 5.10. LOS plots of 24h retrograded maize (A), waxy maize (B) and high amylose maize (C) starch digestion.

Table 5.3 shows the calculated *k* and C_∞ values for 24h retrograded starches (values for gelatinised starches are also shown for easier comparisons). The C_∞ figures reduced upon storage for 24h, relative to the gelatinised form, with changes ranging from 29% for high amylose maize and 5% for waxy maize, Such changes to C_∞ values are caused by the increase in the quantity of

recrystallised starch material, particularly amylose (Frei *et al.*, 2003). This explains why the most noticeable decrease in C_∞ was observed with high amylose maize as opposed to high amylopectin waxy maize.

Table 5.3. Rate constant (k) and percentage of total starch digested after 2h incubation (C_∞) calculated from the LOS plots of 24h retrograded and gelatinised starches.

	24h retrograded		Gelatinised	
	k (min^{-1})	C_∞ (%)	k (min^{-1})	C_∞ (%)
Wheat	0.030	55.8	0.040	70.8
Potato	0.025	70.0	0.028	86.8
Durum wheat	0.011	62.5	0.012	83.3
Wild type pea	0.026	62.5	0.025	77.0
Rice	0.024	59.0	0.021	76.0
Maize	0.022	57.8	0.022	75.4
Waxy maize	0.044	73.0	0.043	77.4
High amylose maize	0.027	55.1	0.024	78.1

The recrystallisation step results in hydrogen bonds reforming between glucan chains making the α(1-4) glycosidic linkages inaccessible to α-amylase attack. The non-digestible starch fractions therefore reduce the enzyme susceptibility for retrograded starch material**.** It is important to note however that the majority of the starch material is still present in the gelatinised form. The *k* values are both very similar between gelatinised and 24h retrograded starches suggesting that the retrograded material is not digested at a slower rate. The *k* value

therefore only reflects the digestion of starch material that has not retrograded. No change in *k* values coupled with a decreasing C_∞, relative to the gelatinised starch preparations, suggests retrograded starch is inert to α-amylase digestion.

Our results support those reported for similar studies on retrograded rice starch by (Chung *et al.*, 2006) and (Zhang *et al.*, 2011). Retrograded rice starch showed increases in the quantity of RS accompanied by reduced amounts of RDS. However the remaining digestible starch material, which consists of primarily amorphous material and imperfect crystallites, is still hydrolysed by α-amylase resulting in a similar *k* value to gelatinised starch. Our results were also similar to those of other workers who fitted their data to the first order kinetic equation (Frei *et al.*, 2003; Hu *et al.*, 2004). The results from both groups indicated similar *k* values between gelatinised and retrograded rice starch. However upon retrogradation of cooked rice the C_∞ reduced relative to the gelatinised value.

In addition to the studies mentioned above, waxy and high amylose maize starches were stored under a constant temperature of 4^{o}C for 24h. Many studies have postulated that starch storage at reduced temperatures accelerates the retrogradation process and reduces the extent of hydrolysis (Frei *et al.*, 2003; Zhou *et al.*, 2010; Zhang *et al.*, 2011). Therefore in the current project the effects of starch storage at low temperatures on *k* and C_∞ were determined. Figure 5.11 shows the LOS plots of retrograded waxy and high amylose maize starch stored for 24h at 4^{o}C. These results were similar to the LOS plots produced for starch stored at room temperature, so that a single *k*

value was observed. The table in Figure 5.11 also shows a comparison of the calculated *k* and C_∞ values for gelatinised and retrograded starches (stored at 4^{o}C and room temperature, 22^{o}C). The *k* values between gelatinised and retrograded preparations remain unchanged as *k* is an intrinsic property of the enzyme (Butterworth *et al.*, 2012). In contrast to our results, Park and workers showed a decrease in *k* for waxy maize gels stored at 4^{o}C (Park *et al.*, 2009). However their results are incomplete as no digestion profile was shown in the published report and it is likely that the authors refer to a decrease in the overall rate of the reaction rather than the rate constant.

No significant change was observed in C_∞ for waxy maize starch indicating minimal amylopectin retrogradation occurred in the short storage period. However the most striking change was observed in high amylose maize starch with C_∞ decreasing by 37% relative to the gelatinised sample (78.1% vs. 41.2%). When compared with starch stored at room temperature, the C_∞ reduced from 55.1% to 41.2%, a 14% change. Such results clearly indicate that the rate of amylose retrogradation is accelerated at low temperatures, and also increases the quantity of enzyme resistant starch material.

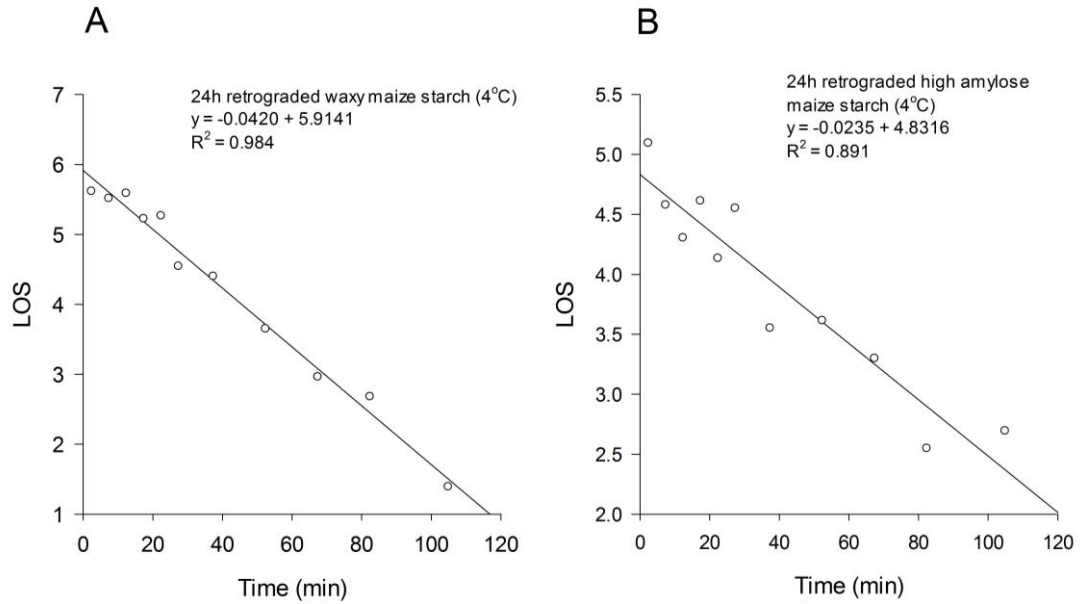

	Gelatinised starch (90°C)		24h retrograded starch (22°C)		24h retrograded starch (4°C)	
	k (min^{-1})	C_∞ (%)	*k* (min^{-1})	C_∞ (%)	*k* (min^{-1})	C_∞ (%)
Waxy maize	0.043	77.4	0.044	73.0	0.042	70.2
High amylose maize	0.024	78.1	0.027	55.1	0.024	41.2

Figure 5.11. LOS plots of 24h retrograded waxy maize (A) and high amylose maize (B) starch stored at 4°C.The table shows the calculated k and C_∞ values for gelatinised and retrograded starch stored at 22°C (room temperature) and 4°C.

5.3.2 Comparison of *k* and C_∞ values

All native starches showed a higher rate constant during the 20-30 min rapid phase compared with the corresponding slow phase (Figure 5.12A). This was attributed to the amorphous glucan chains at the periphery of the granule, compared with the chains located within the granule, which limits binding of PPA. Upon gelatinisation, *k* values increased, relative to the slow phase and remained unchanged for retrograded preparations (Figure 5.12B). It is important to note that the *k* value for gelatinised starch is similar to that of the rapid phase in native starch (taking into account the doubled α-amylase concentration). This is expected as during the rapid phase the kinetic constant represents the rate of digestion of glucan chains at the surface of the granule. Surprisingly, the *k* value for wheat and durum wheat starch during the rapid phase is different from that of the gelatinised form. The difference is probably due to the differences in granule composition between these distinct botanical sources.

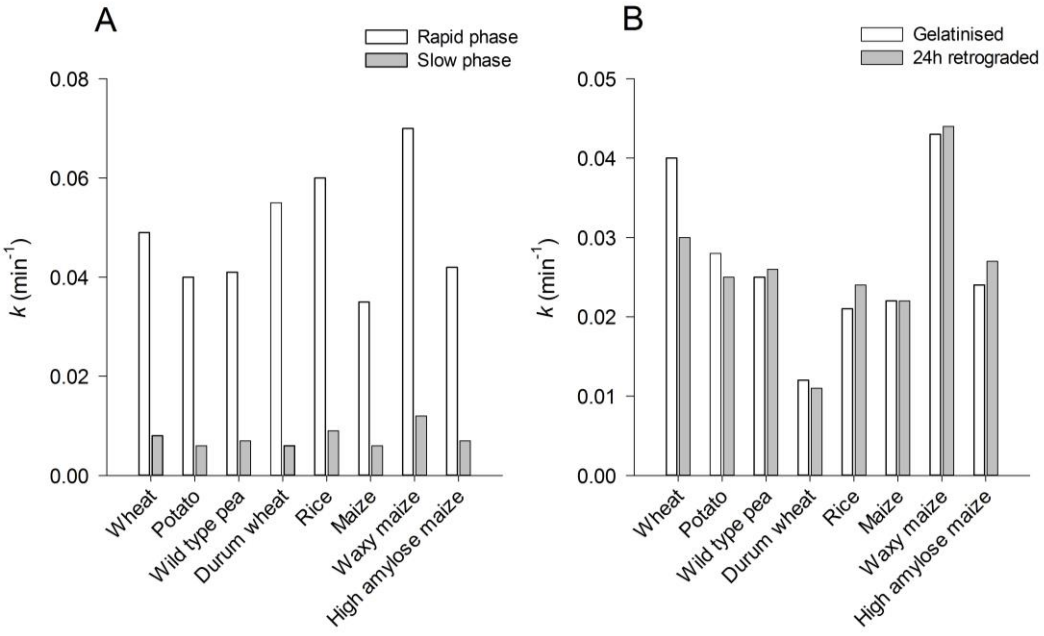

Figure 5.12. Rate constants for the digestion of native starches during the rapid and slow phase (A) and gelatinised and 24h retrograded starches (B).

Figure 5.13 shows the total C_∞ values for native, gelatinised and 24h retrograded starches. Native starches have much lower C_∞ values, as starch digestion is limited by the tight packing of glucan chains. Hydrothermal treatment results in starch gelatinisation which provides the energy required to break the weak hydrogen bonds between glucan chains. The number of polymer chains that become exposed on the surface of the granule is improved by the order-disorder transition induced by the heat treatment process. This results in greater substrate availability supported by an increase in C_∞. Starch storage for 24h induces the retrogradation effect causing the degree of crystallinity to increase and limit the action of α-amylase. This causes the opposite effect of starch gelatinisation and leads to a decrease in C_∞.

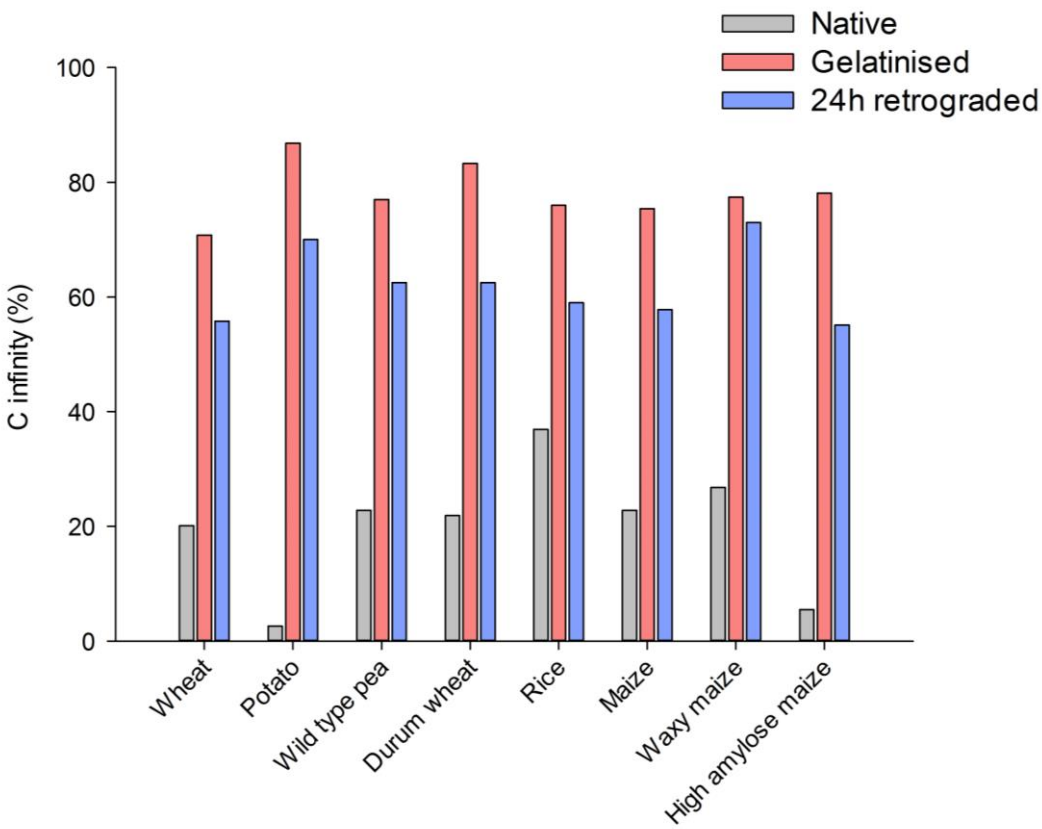

Figure 5.13. Total C_∞ values for the complete digestion of native, gelatinised and 24h retrograded starches.

Table 5.4 summarises the k and C_∞ data for all starch digestions in their native, gelatinised and 24h retrograded forms. This table allows for an easier comparison of k and C_∞ values between native and processed starch forms.

Table 5.4. Rate constant (k) and percentage of total starch digested after 2h incubation (C_∞) calculated from the LOS plots of native, gelatinised and 24h retrograded starches. The C_∞ percentages are relative to the dry weight of starch included in reaction mixtures. The values in the brackets with an asterisk represent k and C_∞ for retrograded starch stored at 4°C for 24h.

Starch	Native				Gelatinised		24h Retrograded	
	Rapid		Slow					
	k (min^{-1})	C_∞ (%)	k (min^{-1})	C_∞ (%)	k (min^{-1})	C_∞ (%)	k (min^{-1})	C_∞ (%)
Wheat	0.049	7.0	0.008	13.1	0.040	70.8	0.030	55.8
Potato	0.040	1.0	0.006	1.6	0.028	86.8	0.025	70.0
Durum wheat	0.055	6.5	0.006	16.3	0.012	83.3	0.011	62.5
Wild type pea	0.041	6.3	0.007	15.6	0.025	77.0	0.026	62.5
Rice	0.060	10.1	0.009	26.8	0.021	76.0	0.024	59.0
Maize	0.035	5.4	0.006	17.4	0.022	75.4	0.022	57.8
Waxy maize	0.070	11.7	0.012	15.1	0.043	77.4	0.044 (0.042)*	73.0 (70.2)*
High amylose maize	0.042	1.9	0.007	3.6	0.024	78.1	0.027 (0.024)*	55.1 (41.2)*

The C_∞ values were also correlated with the degree of molecular order represented by the FTIR peak ratio (refer to Chapter 4, Section 4.3.1 for peak ratio values). Figure 5.14 shows the total C_∞ for different starches decreases as the amount of ordered starch material increases. Gelatinised starch has the highest C_∞ while native starch has the lowest C_∞. Therefore the total amount of digestible starch is dependent upon the amount of molecular order/disorder within the starch granule. However due to the large separation in experimental data points between the 0.4-0.8 FITR peak ratios, no precise relationship, with a reliable R squared value, can be determined.

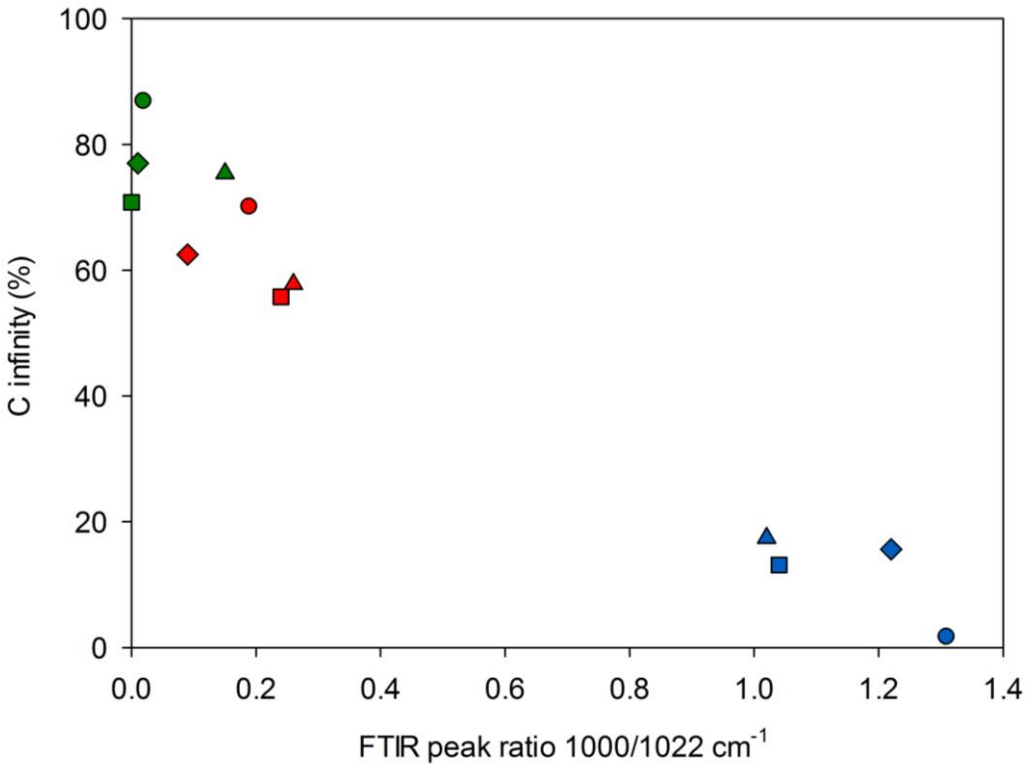

Figure 5.14. Total C_∞ values for wheat (square), potato (circle), wild type pea (diamond) and maize (triangle) starch plotted against the FTIR peak ratio 1000/1022 cm^{-1}. Native starches are presented in blue, gelatinised starches are in green and 24h retrograded starches are in red.

5.3.3 Critical analysis of the Englyst approach

The popular *in vitro* classification model of starch digestion by Englyst has suggested starches are digested in three fractions; RDS (20 min) and SDS (20-120 min) with the remaining undigested fraction termed resistant starch. However these different fractions were classified by only visual inspection of the basic digestibility curves. Previous work has suggested, using logarithmic digestibility curves, that gelatinised starches have a constant digestibility rate and follow pseudo-first order kinetics. This was further confirmed by the more recent LOS plot approach. Data presented in this Chapter, using the LOS method, indicates that the kinetics for the digestion of gelatinised and retrograded starches can be best described by a single digestibility rate constant.

5.4 Conclusion

The low C_∞ values for native starches reflect the reduced rate of digestion by α-amylase. The LOS plots for all native starches show digestion occurs in two separates stages denoted as the rapidly digested and slowly digested stage, with the latter having a lower *k* value. An increase in C_∞ was observed upon starch gelatinisation due to granular swelling and complete loss of structural organisation. However C_∞ was found to decrease when starches were stored for 24h at room temperature to induce the retrogradation effect, which seems to be mainly attributed to amylose retrogradation. The effect of retrogradation on C_∞ is even more apparent in starches stored at 4^{o}C. The digestibility constant between gelatinised and retrograded starch remained the same indicating that

the retrograded starch material is almost certainly inert to α-amylase digestion. Gelatinised and 24h retrograded LOS plots also revealed a single digestibility constant unlike native starches, which are distinguished by rapid and slow phases. Starches of the same form (native, gelatinised and retrograded) also display different k and C_∞ values, which can be attributed to the botanical starch source in question.

Chapter 6 Catalytic action of α-amylase on retrograded starch

6.1 Introduction

It has been reported by many research groups that foods with identical amounts of available starch produce different postprandial blood glucose and insulin responses. Marked increases in blood glucose and insulin concentrations following a starch-rich meal are mainly attributed to differences in the rate and extent of starch digestion by α-amylase (Jenkins *et al.*, 1987; Foster-Powell *et al.*, 2002). The rate of digestion is influenced by a multiplicity of factors including the physical structure of starch granules itself. It has been widely known that native crystalline starches are almost totally resistant to digestion while starches that have been hydrothermally treated (gelatinisation) are more susceptibility to digestion (Lee *et al.*, 1985; Buléon *et al.*, 1998; Tester *et al.*, 2006; Dona *et al.*, 2010). In addition, starches which have been heated and stored are digested at a much slower rate compared with gelatinised starches due to the process of retrogradation (Haralampu, 2000; Sajilata *et al.*, 2006). However, the commonly used GI concept, which classifies foods based on the postprandial blood glucose response, provides no valuable detailed information about the molecular mechanisms of starch digestion.

Using different characterisation techniques (discussed in Chapter 4), past studies have demonstrated the effects of gelatinisation and retrogradation on starch structure (Cooke and Gidley, 1992; Eerlingen *et al.*, 1994; Bogracheva *et al.*, 2006). To supplement the structural data, researchers have also produced

digestibility curves to better understand the complex starch digestion process (Holm *et al.*, 1988; Englyst *et al.*, 1996; Fredriksson *et al.*, 2000; Frei *et al.*, 2003; Chung *et al.*, 2008; Zhang *et al.*, 2013). The aims of these studies have been to understand why such differences in the rate and extent of starch digestion occur. However these experiments have always been performed over a prolonged duration, and therefore lack an enzymological approach as no data on catalytic function and substrate availability can be extracted. As a result, very limited information describing the accessibility of α-amylase to the starch substrate can be obtained.

A small number of studies have used the Michaelis-Menten kinetic model to quantitatively describe the action of α-amylase on starch (Slaughter *et al.*, 2001; Roder *et al.*, 2009; Tahir *et al.*, 2010; Tahir *et al.*, 2011). Enzyme kinetic parameters can be extracted from the model to analyse the initial starch digestion process. Parameters estimated include K_m (Michaelis constant), V_{max} (maximum velocity), k_{cat} (catalytic rate constant and equal to V_{max}/enzyme concentration) and k_{cat}/K_m (catalytic efficiency) (Cornish-Bowden, 1974). The first two parameters (K_m and V_{max}) are obtained directly from the Michaelis-Menten curve, and then used to calculate the last two parameters (k_{cat} and k_{cat}/K_m) provided that the enzyme concentration is known. However these studies have been limited to include only the initial digestion rate of native and gelatinised starches. Since numerous starch-based products contain retrograded starch (crisps, biscuits, cereals) (Sajilata *et al.*, 2006), it is vital to obtain information about the effect of retrograded starch on digestion kinetics to supplement the data already obtained for the native and gelatinised forms.

In this chapter, initial digestion rate profiles were obtained for native, gelatinised and retrograded starches (stored for up to 96h) from different botanical origins. The profiles were then used to calculate Michaelis-Menten kinetic parameters to provide an improved mechanistic understanding of the digestion process for retrograded starches stored for different time periods. As the complex starch structure strongly influences the rate of product release (oligosaccharides), the enzyme kinetic parameters were then related to the physicochemical starch properties described in Chapter 4.

6.2 Methods

The enzyme assay was performed as described in detail in Section 2.5 of Chapter 2. Briefly, 10 mg/mL starch suspensions containing native, gelatinised or retrograded starches were prepared in PBS. To prepare suspensions containing gelatinised starches, all the starch samples were hydrothermally treated at 90^{o}C, except the sample of high amylose maize starch, which was autoclaved at 121^{o}C. For preparation of the starch suspensions with retrograded starch, samples were hydrothermally treated and stored for up to 96h. Retrograded starch samples were separated into individual batches with storage periods of 24, 48, 72 and 96h at room temperature. Wheat, potato and high amylose maize starch however had an additional 6h and 18h storage period. To determine the effect of low temperatures on the rate of retrogradation, wheat and potato starch were stored for 7 days at 4^{o}C before *in vitro* digestion with α-amylase. Wheat and potato starch were also stored for 48h and 96h in PBS containing 0.02% sodium azide to ensure changes in digestion kinetics were not due to bacterial growth.

Native, gelatinised and retrograded starch samples were then diluted with PBS to give a range of starch concentrations from 0.5-10 mg/mL. Starch samples were digested with 1.2 nM PPA at 37^{o}C and 300 µL was collected every 4 min up to 12 min and transferred into Eppendorf tubes containing 300 µL of ice-cold stop solution. All samples were centrifuged before the supernatant was collected and frozen at -20^{o}C.

The standard Prussian blue assay (described in Section 2.4.3 in Chapter 2) was then used to determine the reducing sugars produced from starch digestion. Using a maltose standard curve, the maltose concentration from starch digestion was calculated and plotted against time to allow the initial rate to be determined. The kinetic parameters K_m, V_{max}, k_{cat} and k_{cat}/K_m were then determined by fitting data to the Michaelis-Menten equation using Sigmaplot, as discussed in Section 2.5.4 in Chapter 2.

6.3 Results

6.3.1 Starch digestibility curves

Figure 6.1A shows the maltose concentration determined, up to 12 min, for the digestion of gelatinised wheat starch at different concentrations by PPA. The gradient from this plot allows for the determination of the initial reaction velocity (v) at different starch concentrations. All values are then fitted to a Michaelis-Menten curve for enzyme kinetic parameters to be extracted (Figure 6.1B). For convenience, the figure only shows the digestion profile of wheat starch as many other starches were also tested for individual digestion profiles.

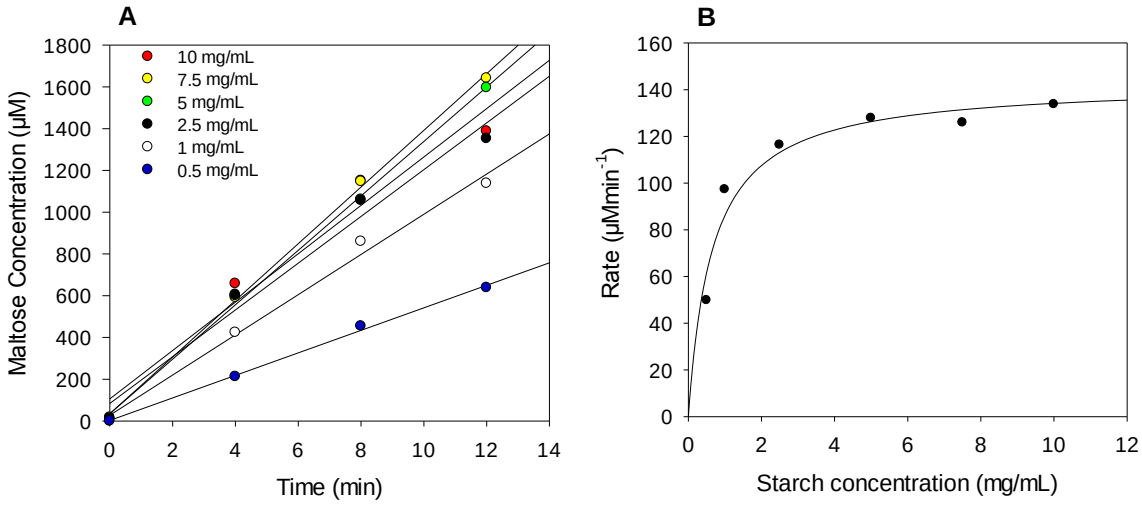

Figure 6.1. Maltose production from the digestion of gelatinised wheat starch by PPA (A) and the Michaelis-Menten plot for gelatinised wheat starch at different substrate concentrations (B).

In order to determine the effects of gelatinisation and retrogradation on starch digestibility, Figure 6.2 also shows the Michaelis-Menten plots for native, gelatinised and 24h retrograded wheat starch. A clear difference can be identified in the rate of digestion between native and processed wheat starch. Using the Michaelis-Menten plots, the V_{max} and K_m can be determined, which can then be used to calculate k_{cat} and k_{cat}/K_m.

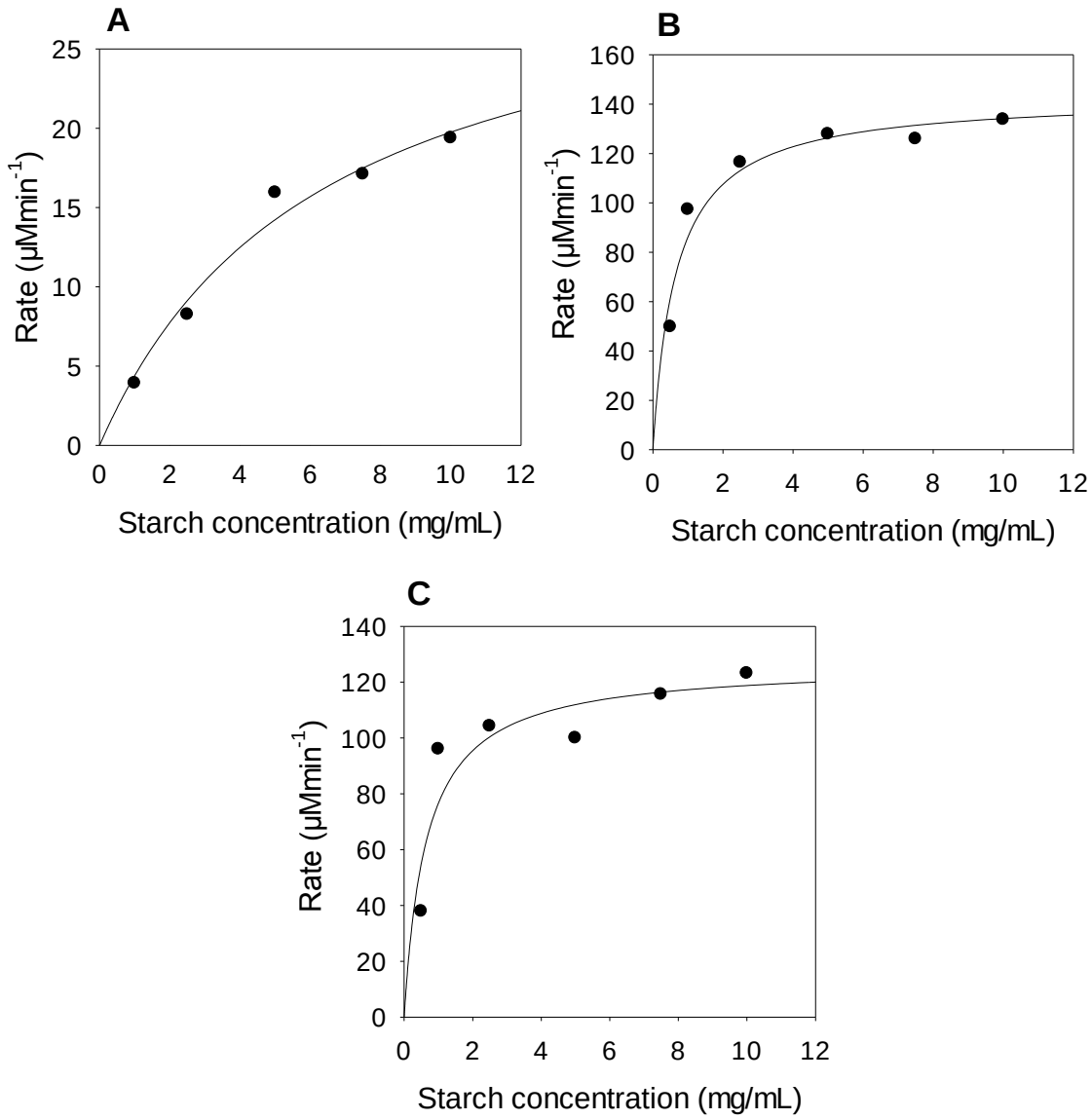

Figure 6.2. Michaelis-Menten plot for native (A) gelatinised (B) and 24h retrograded (C) wheat starch at substrate concentrations between 0.5-10 mg/mL.

6.3.2 Native starch digestion

Figure 6.3 displays the calculated V_{max}, K_m, k_{cat} and k_{cat}/K_m figures for the digestion of native starch with α-amylase. Wheat starch has the largest V_{max} value with wild type pea, maize and high amylose maize having the smallest

V_{max} values. All starches have different K_m values except maize and high amylose maize. Potato and waxy maize have the largest K_m values, while the smallest K_m value was found for maize and high amylose maize starch.

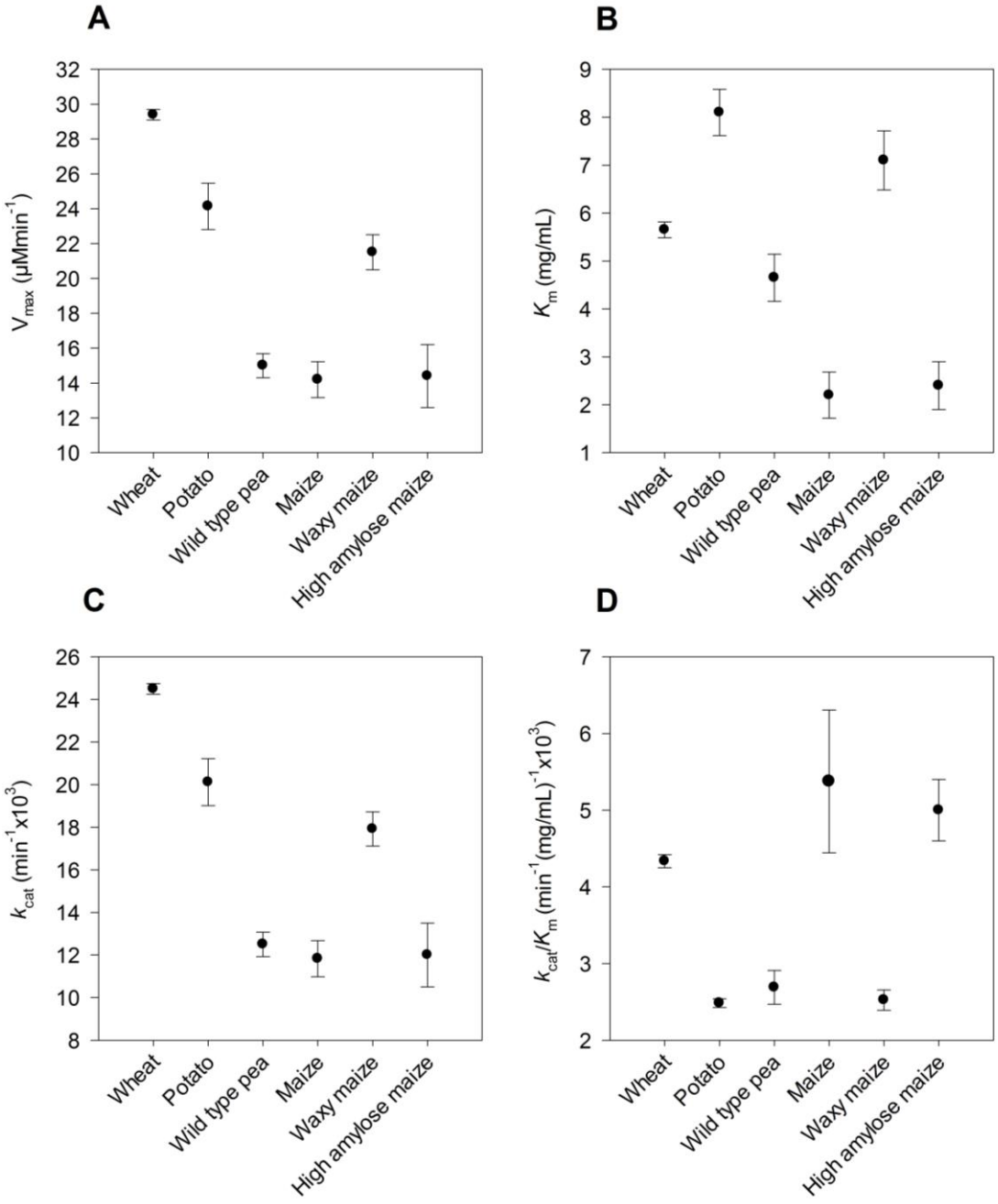

Figure 6.3. Calculated V_{max} (A), K_m (B), k_{cat} (C) and k_{cat}/K_m (D) figures from the digestion of native starch by α-amylase. All experimental values are expressed as mean values ± SEM from three-four replicates.

The k_{cat} values for native starches were calculated by using Equation 7. As the enzyme concentration is kept constant and k_{cat} is only dependent on V_{max}, the trends observed between k_{cat} and V_{max} are identical (Figure 6.3C). Wheat starch was seen to have the highest k_{cat}, while the lowest values are associated with wild type pea, maize and high amylose maize starch. In addition, wild type pea, maize and high amylose maize starch possess similar k_{cat} values.

Equation 7

$$k_{\mathrm{cat}} = \frac{\mathrm{V_{max}}}{[\alpha - \mathrm{amylase}]}$$

Equation 7. The first-order catalytic rate constant

The catalytic efficiency (k_{cat}/K_m) values for the digestion of native starch by 1.2 nM α-amylase are shown in Figure 6.3D. The k_{cat}/K_m values were calculated using V_{max} and K_m, which were originally obtained by fitting the experimental starch data to the Michaelis-Menten equation (Dona *et al.*, 2011). Therefore k_{cat}/K_m ratio provides a strong index for the overall catalytic efficiency since it includes a combination of the rate constant determining product release and the binding of α-amylase to the starch material. Maize and high amylose maize starch show the largest k_{cat}/K_m while potato, wild type pea and waxy maize have the lowest k_{cat}/K_m.

6.3.3 Digestion of processed starch (gelatinised and retrograded)

6.3.3.1 k_{cat} values for processed starch

As mentioned previously, k_{cat} is derived from V_{max} and therefore the same trends observed in V_{max} were observed for k_{cat}. The calculated k_{cat} figures for processed starch digestion are displayed in Figure 6.4 (all V_{max} values are shown in a table format in Appendix C of the Appendices section). All digested starches have different k_{cat} values upon gelatinisation (0h), with potato having the highest value and maize having the lowest. Upon storage, clear changes in k_{cat} values for all starches were observed with the exception of wild type pea and waxy maize starch, which show little or no significant change. Note additional 6h and 18h storage periods were only applied to wheat, potato and high amylose maize starch as these starches showed the biggest k_{cat} changes between 0-24h. The k_{cat} for wheat starch shows a decrease at two distinct storage times, the first decrease is between 0-6h and the second is between 48-72h storage, after which no further change is noted. Potato and high amylose maize starch both show a large decrease in k_{cat} after 18h storage, with an almost 30% and 22% reduction, respectively. Unlike wheat starch however, the k_{cat} values do not changer further. Maize starch shows very little change in k_{cat} between 0-72h storage, with the k_{cat} only beginning to decrease after 72h.

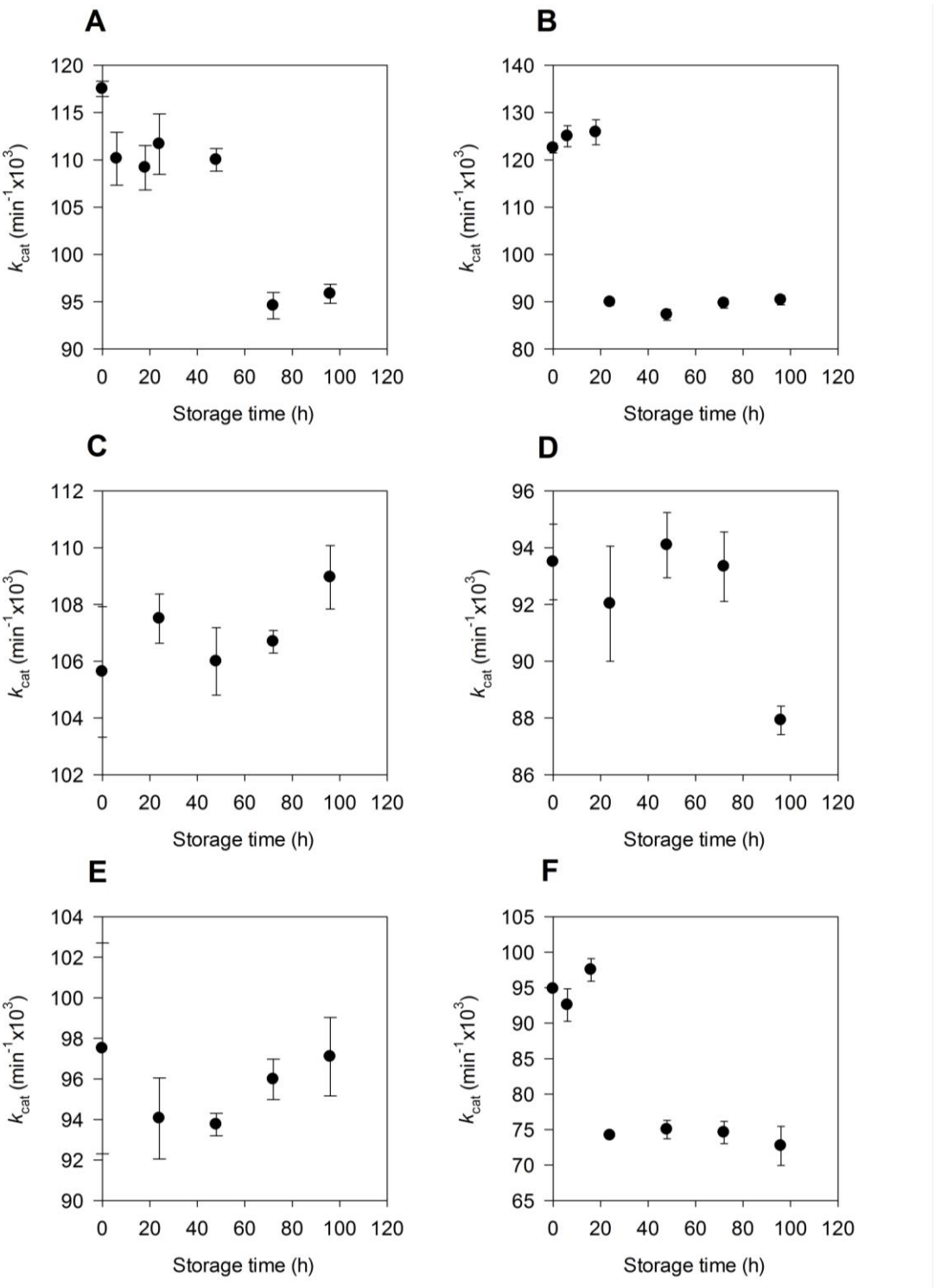

Figure 6.4. k_{cat} values for the digestion of gelatinised and retrograded starches by PPA. Wheat (A), potato (B), wild type pea (C), maize (D), waxy maize (E) and high amylose maize (F) starch. All experimental values are expressed as mean values ± SEM from three-four replicates.

6.3.3.2 K_m and k_{cat}/K_m values for processed starch

The K_m values for gelatinised and retrograded starches are shown in Table 6.1. No significant difference is observed in the K_m values when starches are stored for up to 96h, and therefore the values are shown in a table format for ease of interpretation as opposed to a graphical representation. Wheat and high amylose maize starch have larger K_m values relative to other starches used in this study, which have much smaller values. Previous work by our group also showed wheat and high amylose pea starch have relatively high K_m values (Slaughter *et al.*, 2001; Tahir *et al.*, 2011). This becomes very difficult to explain and the previous authors cited have been unable to find any reasonable suggestions for this.

Table 6.1. Calculated K_m figures from the digestion of gelatinised and retrograded starch stored between 0-96h at room temperature. K_m values are expressed as mean values ± SEM from three-four determinations.

Starch	K_m (mg/mL) Gelatinised	K_m (mg/mL) Retrograded					
		6h	18h	24h	48h	72h	96h
Wheat	0.67 ± 0.01	0.67 ± 0.01	0.69 ± 0.03	0.69 ± 0.02	0.70 ± 0.01	0.64 ± 0.01	0.67 ± 0.02
Potato	0.45 ± 0.00	0.48 ± 0.02	0.49 ± 0.01	0.42 ± 0.01	0.45 ± 0.00	0.45 ± 0.01	0.46 ± 0.01
Wild type pea	0.42 ± 0.01	n.d*	n.d*	0.45 ± 0.02	0.44 ± 0.01	0.46 ± 0.01	0.51 ± 0.02
Maize	0.47 ± 0.01	n.d*	n.d*	0.48 ± 0.01	0.52 ± 0.01	0.51 ± 0.02	0.49 ± 0.01
Waxy maize	0.47 ± 0.01	n.d*	n.d*	0.45 ± 0.01	0.45 ± 0.01	0.47 ± 0.02	0.46 ± 0.01
High amylose maize	0.81 ± 0.01	0.81 ± 0.03	0.89 ± 0.02	0.78 ± 0.01	0.82 ± 0.01	0.82 ± 0.02	0.79 ± 0.01

*n.d. = not determined

The figures for the catalytic efficiency (k_{cat}/K_m) are the most informative as it reflects the catalytic rate constant and starch availability to α-amylase. The overall catalytic efficiency for the amylolysis of gelatinised and retrograded starch is shown in Figure 6.5. Compared with native starch, the k_{cat}/K_m ratio for gelatinised starches increases substantially with the biggest increase noticed in potato. However over a 96h storage period all starches, with the exception of waxy maize, show a decrease in k_{cat}/K_m. Potato and high amylose maize starch evidently show the most dramatic change between 0-48h, with a 29% and 22% decrease in catalytic efficiency, respectively. The k_{cat}/K_m ratio for maize starch was also reduced by 9% within 48h, but this change is not as profound as that noticed in potato and high amylose maize. Thereafter the catalytic efficiency for all three starches (potato, HA and maize) does not change significantly. Wheat and wild type pea starch however show a steady fall in k_{cat}/K_m during the 96h storage period, with a decrease of 18% and 15%, respectively. It is important to note, when taking into consideration the scale of the y axis, all k_{cat}/K_m values for the replicates show very little variability as indicated by the small SEM.

A preliminary experiment was also performed with retrograded wheat starch being digested by PPA in the presence of sodium azide. The results showed no change in K_m and k_{cat}/K_m, compared with the azide-free samples, indicating bacterial contamination did not contribute to the changes observed in the kinetic parameters upon starch storage. The results can be found in Appendix D.

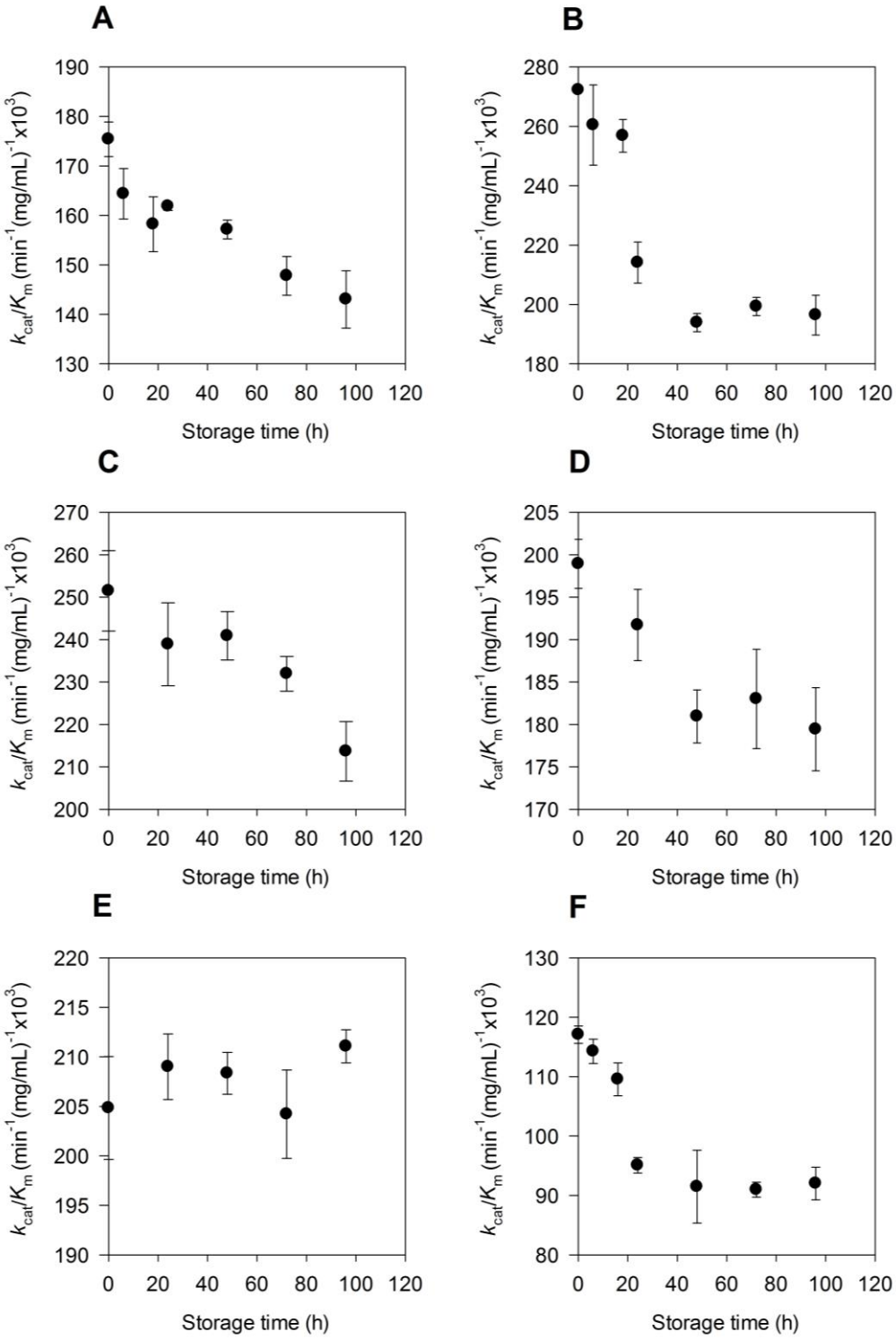

Figure 6.5. Calculated k_{cat}/K_m values for the digestion of gelatinised and retrograded starches by PPA. Wheat (A), potato (B), wild type pea (C), maize (D), waxy maize (E) and high amylose maize (F) starch. All values are expressed as mean values ± SEM from three-four replicates.

6.3.3.3 Effects of retrogradation at low temperatures

The effect of starch storage at low temperatures was studied for wheat and potato starches. When stored at room temperature, wheat and potato starch showed a marked change in enzyme kinetic parameters, particularly k_{cat}/K_m, and therefore these starches were investigated. Table 6.2 shows the K_m values obtained for retrograded starch stored for 7 days at 4°C (gelatinised wheat and potato starch is shown for comparison). The results show that no significant changes occur in K_m values for wheat and potato starch when stored at 4°C for 7 days.

Table 6.2. Apparent starch binding affinity, represented by K_m, for gelatinised and retrograded wheat and potato starch stored for 7 days at 4°C. K_m values are averaged from three determinations with SEM being 0.02 for both retrograded wheat and potato starch.

Starch	K_m (mg/mL) Gelatinised	K_m (mg/mL) Retrograded (4°C)
Wheat	0.67 ± 0.01	0.65 ± 0.02
Potato	0.45 ± 0.00	0.43 ± 0.02

Figure 6.6 shows the calculated k_{cat}/K_m values for wheat and potato starch stored for 7 days at 4°C. The k_{cat}/K_m values for gelatinised and retrograded starches stored at room temperature are also shown for comparison. The k_{cat}/K_m ratio reduces further upon storage at 4°C, with a bigger change being noticed for wheat starch than for potato starch. The k_{cat}/K_m values for both

wheat and potato starch fell by approximately 36%, relative to the gelatinised form.

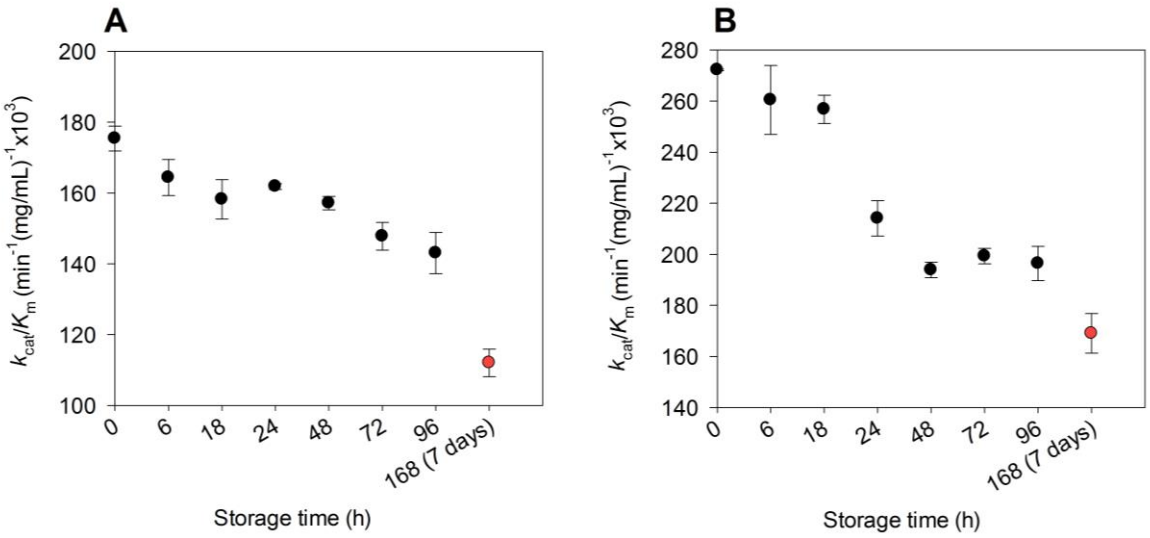

Figure 6.6. Catalytic efficiency values for retrograded wheat (A) and potato (B) starch stored for 7 days at 4°C (red). k_{cat}/K_m values are also shown for starches stored between 0-96h at room temperature (black). All values are expressed as mean values ± SEM from three replicates.

6.3.4 Comparison of enzyme kinetic parameters between native and processed starch

All kinetic parameters (K_m, V_{max}, k_{cat} and k_{cat}/K_m) were affected by starch gelatinisation and/or retrogradation. As shown in Figure 6.7, the K_m values decreased upon gelatinisation and remained constant, with no significant change, when stored at room temperature. Upon hydrothermal treatment, the k_{cat}/K_m ratio increased dramatically compared with native values. The ratio clearly shows gelatinised potato has a much higher reactivity than the other starches. Notably, the k_{cat}/K_m ratios for all retrograded starches stored for 96h

were reduced with the exception of waxy maize starch. Retrograded potato and high amylose maize show the largest change in k_{cat}/K_m with approximately 30% and 20% reductions in catalytic activity, respectively.

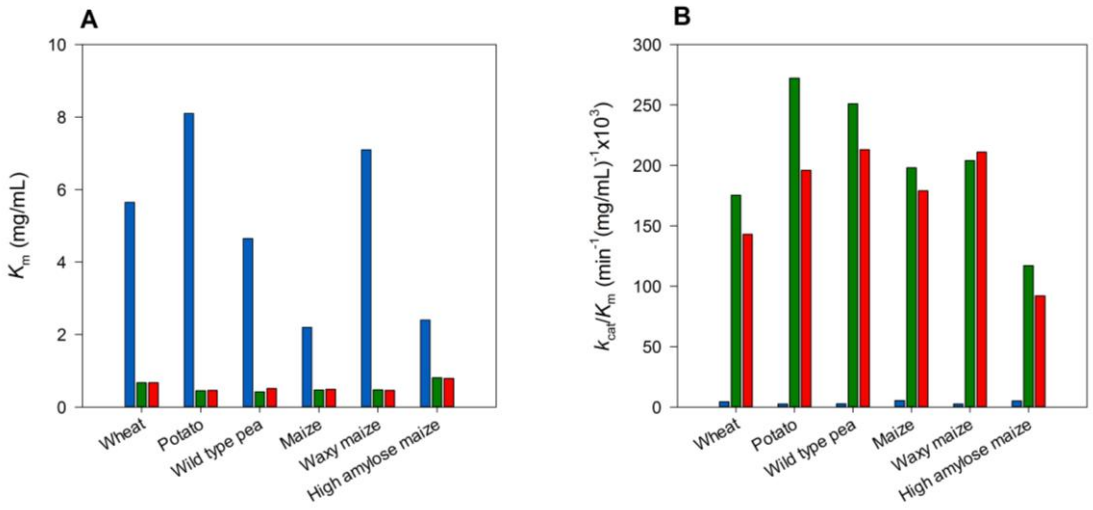

Figure 6.7. (A) K_m and (B) k_{cat}/K_m mean values for native (blue), gelatinised (green) and 96h retrograded starches (red).

6.4 Discussion

6.4.1 Amylolysis of native starches

Native starch was found to be extremely difficult to digest as shown by the enzyme kinetic parameters in the results section. The first step in the amylolysis reaction involves α-amylase binding to the starch material. The K_m, defined as the substrate concentration at half of the maximum velocity, for native starch provides some indication of the binding efficiency of α-amylase to the α-glucan chains (Warren *et al.*, 2013). A low K_m value indicates that the enzyme has a high affinity for the substrate whereas a high K_m indicates a low substrate affinity.

K_m values are much higher for native starches with potato and waxy maize samples having the highest figures. This suggests α-amylase has a lower affinity for glucan chains of potato and waxy maize relative to all other tested starches. Very little native starch is actually digested as indicated by the low V_{max} and k_{cat} figures. The catalytic constant, k_{cat}, is the second step in the amylolysis reaction, converting the enzyme substrate complex to enzyme and product. Since k_{cat} is derived from V_{max}, identical trends were observed. The k_{cat}/K_m for native starches was very low with potato having the lowest value. This is expected as the K_m value is the highest for potato reflecting the unfavourable binding step.

Native starches have a high degree of crystallinity, resulting in an ordered structure with a compact arrangement of α-glucan chains which are not readily exposed. The α-glucan chains in amylopectin have a double helical structure stabilised by the presence of water molecules forming hydrogen bonds (Imberty *et al.*, 1988). The tight packing of helical chains along with the stability provided by the formation of hydrogen bonds, results in a highly crystalline structure. As a result, the number of potential binding sites for α-amylase is expected to be limited which explains the high K_m and low k_{cat}/K_m values.

Of all native starches used in this study, potato starch proves to be extremely difficult to digest due to its B-type nature. B-type crystalline starches have a more open helical arrangement compared to A-type starches, which have a very tight helix packing. Thus this allows B-type starches to have a greater water binding potential, which may provide more stable crystallites that resist

enzymatic hydrolysis (Wang *et al.*, 1998; Tester *et al.*, 2004). In addition, potato starch has been shown to have much larger amylopectin blocklets (200-500 nm) compared with other starches, which may influence the slow rate of hydrolysis (Gallant *et al.*, 1997). Surface pores and channels in maize starch may also increase the surface area and facilitate amylase diffusion into the starch granule, but these structural features are absent in potato starch. As a result, the number of binding and diffusion sites for amylase acting on potato starch, are relatively scarce giving native potato a high level of resistance to starch digestion (Oates, 1997; Fannon *et al.*, 2004). Potato starch granules are also much larger with a size ranging from 15-75 µm and thus the surface area to unit volume ratio is relatively low. These various structural features can account for native potato starch having resistance to enzyme attack (Dhital *et al.*, 2010; Pérez and Bertoft, 2010).

6.4.2 Amylolysis of gelatinised starches

Once starch samples were hydrothermally treated at 90^{o}C, major changes were observed in all enzyme kinetic parameters. Upon gelatinisation, the original ordered crystalline structure observed for native starches becomes disordered. The heat input breaks the hydrogen bonds between polymer chains, resulting in water molecules entering the granule causing swelling and complete loss of ordered structure. Therefore the increased structural disorder exposes more glucan chains that are now more susceptible to amylolysis. This ultimately results in a greater potential for α-amylase to bind and hydrolyse the chains. As the substrate availability increases, α-amylase has a higher affinity for the exposed polymer chains, which explains the dramatic fall in K_m upon

gelatinisation. Surprisingly, K_m figures for wheat and high amylose maize starch are higher than the other gelatinised starches. These results are very similar to those reported in previous studies by our group (Slaughter *et al.*, 2001; Tahir *et al.*, 2011); however, there is no obvious explanation as to why this occurs. Higher K_m values indicate α-amylase has a lower affinity for gelatinised wheat and high amylose maize compared with the other gelatinised starches. Nevertheless, the large decrease in K_m indicates that binding affinity is greater for starches in the gelatinised form relative to the native.

As a result of these structural changes, the V_{max}, k_{cat} and k_{cat}/K_m increase upon hydrothermal treatment. The data show varying k_{cat}/K_m values for different gelatinised starches with potato having the highest and high amylose maize having the lowest figures. The overall catalytic efficiency increases upon gelatinisation for every starch but is most noticeable for potato, increasing by almost 110-fold. This is most likely due to the swelling potential of potato starch, which is known to swell hugely, relative to other starches, due to the presence of phosphate ions giving the granule a negative charge with high affinity for water (Slaughter *et al.*, 2001).

6.4.3 Amylolysis of retrograded starches

K_m values for retrograded starch show no significant change over a 96h storage period. Storage at room temperature results in an increase in the quantity of retrograded material and consequently a decrease in gelatinised material. The constant K_m suggests the fraction of starch granules accessible to α-amylase do not change and amylase binding still occurs. Therefore, K_m represents the

binding to both gelatinised and retrograded starch because if amylase had a low affinity for retrograded starch and thereby only binding to gelatinised starch, the K_m values would be higher than those of gelatinised starch (0 time point). However this is evidently not the case.

To interpret the K_m data accurately the k_{cat}/K_m figures also have to be studied. The ratio reduces upon retrogradation as the concentration of retrograded starch material increases during the storage period. However, as previously mentioned, the K_m values remain constant indicating α-amylase still binds to the new retrograded material. Therefore as k_{cat}/K_m decreases, the retrograded starch material is most likely to be resistant to hydrolysis and acts as a non-competitive inhibitor, reducing the enzyme activity.

The results here have been supported by previous characterisation work from other groups using DSC and XRD, which has suggested disordered starch granules begin to recrystallise upon cooling (Sievert *et al.*, 1991; Ward *et al.*, 1994; Gidley *et al.*, 1995; Hug-Iten *et al.*, 2003). Hydrogen bonds, originally broken during starch gelatinisation, start to re-form and provide stability between polymer chains. During this phase, the α-glucan chains start to form a tightly packed B-type ordered structure which consequently reduces the susceptibility to amylolysis upon retrogradation (Englyst and Hudson, 1996; Haralampu, 2000). However it is important to note that the starch granules do not totally revert back to the original structure, which explains why the rate of digestion is still higher than the native form.

The extent to which the catalytic efficiency reduces varies for each starch. Potato and high amylose maize starch show the biggest change between 0-48h storage relative to the small change noticed in maize starch. The reduced k_{cat}/K_m within 48h storage is believed to be due to retrograded amylose as the formation of retrograded amylopectin takes much longer and therefore plays a minor role (Silverio *et al.*, 1996). As no significant change was observed after 48h storage it can be suggested that minimal amylopectin retrogradation has occurred. Wheat and wild type pea starch however showed a steady decrease in k_{cat}/K_m over 96h, suggesting amylopectin chains are more susceptible to retrogradation than in potato, high amylose maize and maize starch. This is mostly likely due to the differences in amylopectin chain length which have been previously related to the rate of amylopectin retrogradation (Hizukuri, 1985; Yuan *et al.*, 1993; Liu and Thompson, 1998).

The catalytic efficiency values were seen to decrease for all starches except waxy maize starch. Waxy maize starch contains 99% amylopectin and thus, as many previous reports have suggested, amylopectin retrogrades much later than amylose (Miles *et al.*, 1985; Eerlingen *et al.*, 1994; Wang and Copeland, 2013). This explains why the catalytic efficiency does not change over the 96h storage period. Nevertheless, differences in the rate of retrogradation highlight the importance of the botanical starch source.

It is widely known that amylose retrogradation is a relatively faster process than amylopectin. Many research groups, using XRD, FTIR and DSC, have suggested amylose retrogradation occurs within a few hours after gelatinisation

(van Soest *et al.*, 1994; Cui and Oates, 1997) with amylopectin retrogradation continuing for some weeks (Eerlingen *et al.*, 1994). However, the rate and extent of recrystallisation depends heavily on the storage conditions, polymer concentrations and amount of amylose/amylopectin present (Ward *et al.*, 1994; Silverio *et al.*, 1996). Also starch retrogradation relies on the botanical source with cereal starches retrograding to a lesser extent than tuber starches (Singh *et al.*, 2002; Ottenhof *et al.*, 2005). Therefore not all starches retrograde at the same rate and, due to varying experimental conditions used, studies will draw slightly different conclusions regarding the specific time taken for amylose and amylopectin to retrograde. Nevertheless, it is widely accepted that amylose retrogradation is completed after 1 or 2 days (Chang and Liu, 1991; Frei *et al.*, 2003). Thus, our kinetic results from the *in vitro* digestion studies provides further evidence to support the conclusion that the initial retrogradation stage is dominated by amylose rather than amylopectin.

The two starch types that showed the biggest changes were wheat and potato. Therefore both starches were stored for 7 days at 4^{o}C to determine the effect of reduced temperature on starch retrogradation. DSC data from previous studies has demonstrated an increase in the degree of crystallinity upon storage at 4^{o}C, indicating starch retrogradation is accelerated at reduced temperatures (Eerlingen *et al.*, 1994; Cui and Oates, 1997; Zhang *et al.*, 2011). Our enzymology approach supports the conclusion of others, showing a very large decrease in k_{cat}/K_m coupled with no change in K_m upon storage at 4^{o}C. The significantly reduced rate is attributed to the increased crystalline material of

amylose and amylopectin in the wheat and potato starch samples formed during storage at 4^{o}C.

Zhang and workers recently compared digestion profiles of high and low shear processed starches and showed enzyme resistant granular ghosts were only present after low shear treatments (Zhang *et al.*, 2014). In our studies, gelatinised starches were prepared under low shear force conditions and therefore already contained the enzyme resistant granular ghosts. Therefore it is plausible to assume, in the absence of further shear, the reduced α-amylase activity is mainly due to retrograded amylose chains rather than indigestible granular ghosts, as the latter were already present in the gelatinised starch mixture.

The location of retrograded amylose is also important and therefore, as discussed in Chapter 3 and 4, light microscopy and FTIR-ATR confirmed the presence of ordered retrograded amylose material in the soluble supernatant. Therefore α-amylase probably binds to retrograded amylose chains that are present in the supernatant as a direct result of leaching during gelatinisation.

Overall it can be shown that the k_{cat}/K_m ratio is influenced by the amount of ordered starch material, reflected in the FTIR peak ratio. As shown in Figure 6.8, the k_{cat}/K_m ratio decreases as the amount of ordered carbohydrate structure increases in the order of gelatinised, retrograded and native starch. Thus, a lower rate of hydrolysis was determined for the more ordered native and retrograded starches, relative to the hydrolysis of completely disordered starch

granules associated with gelatinisation. However the nature of the relationship cannot be accurately determined as there is a large discontinuity between the 0.4-0.8 FTIR peak ratios. To avoid data overcrowding only wheat, potato and wild type pea starch have been used in the plot.

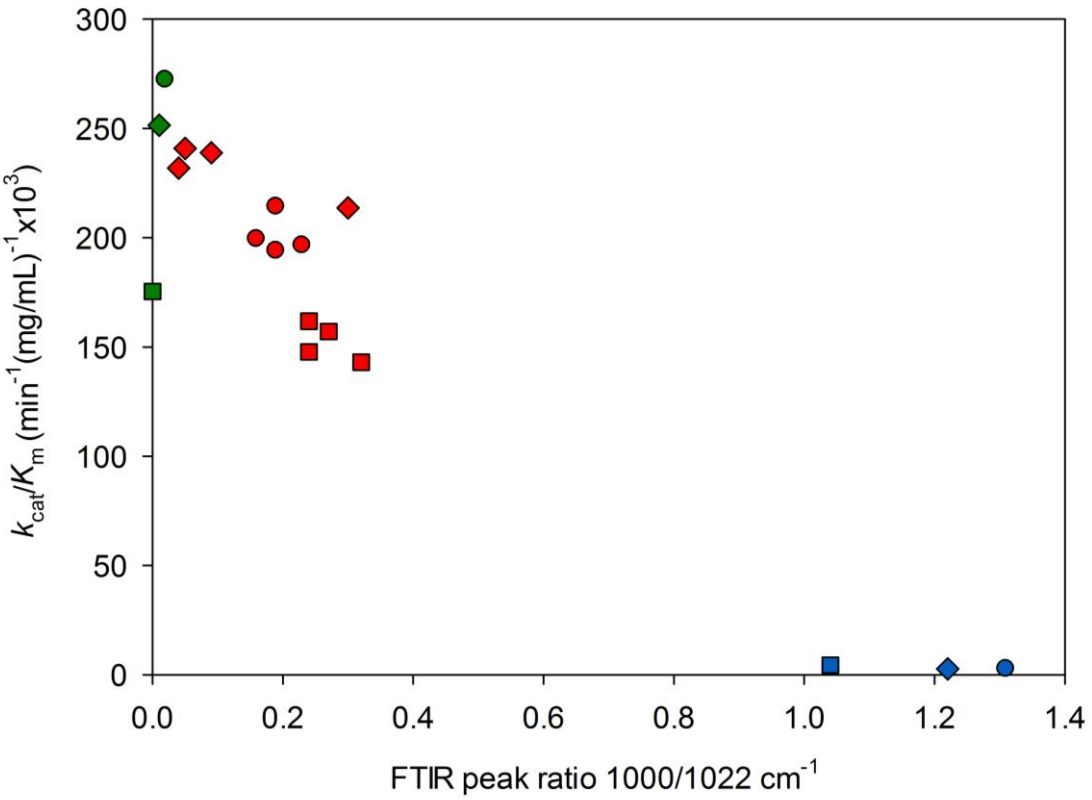

Figure 6.8. Calculated k_{cat}/K_m ratios for wheat (square), potato (circle) and wild type pea (diamond) starch plotted against the ratio of FTIR peaks at 1000 cm^{-1} and 1022 cm^{-1}. Starches were in there native (blue), gelatinised (green) and retrograded (red) forms.

6.5 Conclusion

In this chapter we determined the enzyme kinetic parameters (K_m, V_{max}, k_{cat} and k_{cat}/K_m) to improve our knowledge and understanding of the initial *in vitro* digestion of native and processed (gelatinised and retrograded) substrate starches by PPA.

Amylolysis of native starches revealed high K_m values accompanied by very low V_{max}, k_{cat} and k_{cat}/K_m figures. The results suggest α-amylase has a low affinity for the crystalline starch substrate resulting in a reduced susceptibility to enzymic hydrolysis. Upon starch gelatinisation in excess water, the k_{cat}/K_m ratio significantly increased while the K_m value decreased, indicating a greater enzyme-substrate affinity with an increased susceptibility to amylolysis. Starch stored up to 96h resulted in no change in K_m indicating that α-amylase seems able to bind to both gelatinised and retrograded starch. However the k_{cat}/K_m decreased suggesting α-amylase binds to both substrates but no digestion of retrograded starch actually occurs. The kinetic results therefore imply that retrograded starch material may possibly act as a non-competitive inhibitor to α-amylase. In conclusion, the rate and extent of *in vitro* starch digestion is strongly dependent upon the processing methods applied to starches.

Chapter 7 Retrograded high amylose maize starch

7.1 Introduction

Starch digestion is of great importance to our understanding of the impact of diet on human metabolism and long-term health. For example, it is well known that the rate and extent of starch digestion influences postprandial glycaemia and insulinaemia. Also, starch material that escapes digestion by amylolytic enzymes in the upper gastrointestinal tract is termed 'resistant starch' (RS) and this fraction is subsequently degraded by microbial fermentation in the large intestine to produce short fatty acids (Haralampu, 2000; Sajilata *et al.*, 2006). Resistant starch has been classified into four groups, summarised below (Haralampu, 2000; Htoon *et al.*, 2009):

- RS1 – starch entrapped within intact cells and therefore becomes physically inaccessible to digestive enzymes
- RS2 – native (uncooked) starch
- RS3 – retrograded (cooked and cooled) starch
- RS4 – chemically modified starch

Upon heating in excess water starch granules lose their semi-crystalline structure and the α-glucan chains become completely disordered, a process referred to as gelatinisation. Once cooled and stored, the glucan chains reacquire a condensed ordered helical structure that has enzyme-resistant properties, as they can no longer be digested. This is termed retrograded starch (RS3). Retrograded starch is commonly observed in breakfast cereals and stale bread, the latter attributed to the retrogradation of the amylopectin fraction, and

it has been made use of recently as a food ingredient due to potential nutritional benefits (e.g. as a prebiotic substrate) (Topping *et al.*, 2003).

The amount of retrograded starch material can vary considerably depending upon the botanical starch source, the processing conditions applied and the starch concentration used. Different food processing conditions can greatly affect the rate of retrogradation and it has been known for some time that storage of high amylose starches at reduced temperatures accelerates the recrystallisation process (Holl *et al.*, 1959; Sajilata *et al.*, 2006). A few research groups have also reported that starches that have undergone temperature-cycled retrogradation can also contain increased amounts of retrograded starch (RS3) (Sievert and Pomeranz, 1989; Margaretaleeman *et al.*, 2006; Zhang *et al.*, 2011).

Many groups have characterised retrograded starch physically, mainly using DSC, however these studies were conducted on samples that also contain non-retrograded material. Only a few groups have actually isolated and characterised pure retrograded starch using DSC, NMR and XRD to study the structural organisation (Sievert and Pomeranz, 1989; Eerlingen *et al.*, 1993; Gidley *et al.*, 1995). Workers have also conducted prolonged *in vitro* digestion studies on retrograded starch and concluded that the crystalline morphology is resistant to α-amylase digestion (Cui and Oates, 1997; Fredriksson *et al.*, 2000; Frei *et al.*, 2003). The results from Chapter 5 and 6 suggest retrograded starch is inert to amylase digestion and may act as a non-competitive inhibitor. Therefore the aim of study described in this chapter was to harvest,

characterise and perform enzyme inhibition studies on purified retrograded starch from high amylose maize (purified RHAM) to accurately determine the mode of inhibition.

7.2 Methods

7.2.1 Production of retrograded high amylose maize (RHAM)

The production of purified RHAM is described in more detail in Chapter 2 (Section 2.6 in Chapter 2). Briefly, a 10 mg/mL concentration of native high amylose maize starch (HAM) was prepared in water and autoclaved for 20 min at 121^{o}C. After autoclaving, the samples were stored at 4^{o}C for 24h after which the samples were then stored at 37^{o}C for another 24h. This heating-cooling cycle (i.e. 4/37^{o}C) was repeated three times to promote the retrogradation of starch material under temperature-cycled conditions (Sievert and Pomeranz, 1989). The non-retrograded starch material was digested for 18h using PPA and AMG leaving only pure retrograded high amylose maize starch. The reaction was terminated by adding ethanol and samples were centrifuged to allow starch to sediment to the bottom of the tube. The supernatant was then discarded and the paste material was freeze dried to a powder form (Scheme 3). The RS content in purified RHAM was determined using the Megazyme resistant starch assay kit (refer to Appendix B for kit contents and reagent preparations and Section 2.6.2 from Chapter 2 for the protocol used to measure the RS content).

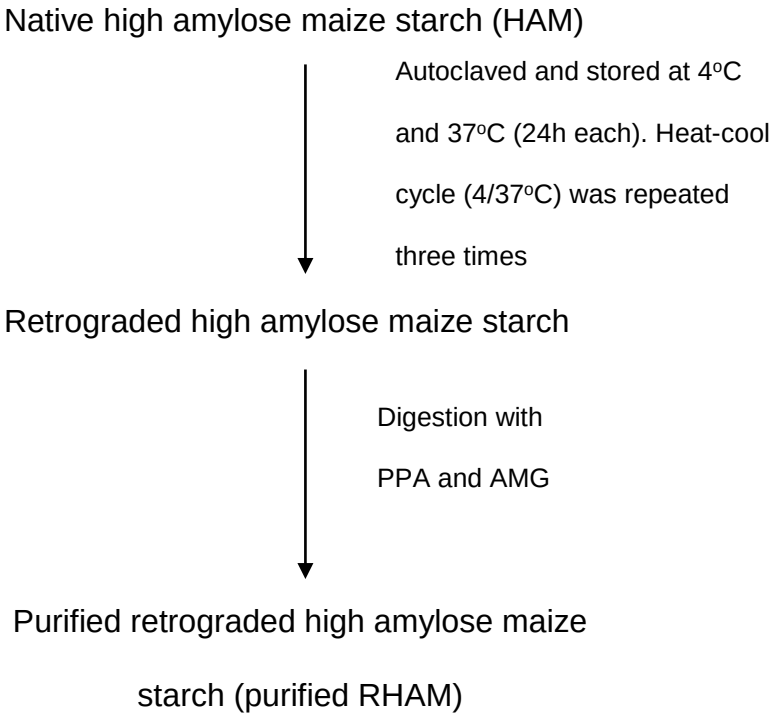

Scheme 3. Production of purified retrograded high amylose maize starch (purified RHAM).

7.2.2 Characterisation of purified RHAM

The amylose and protein content was determined using the iodine binding method and the BCA assay kit, respectively. The iodine binding method involves dissolving starch in DMSO with iodine overnight before recording the absorbance at 600 nm. The protein content was determined by first boiling purified RHAM in SDS then using the BCA assay kit to quantify the amount of protein present. The moisture content was determined by drying weighed amounts of starch in pre-dried aluminium pans overnight at 103°C and recording the difference in weight before and after drying. Further details of the characterisation methods are given in Chapter 2, Section 2.2.

Characterisation of purified RHAM was performed using XRD, DSC, FTIR-ATR and SEM. To obtain an XRD pattern, the sample was scanned over an angular range of 3-40^{o} 2θ and analysed using OriginPro 9.1©. DSC was performed on a 50 mg/mL sample over a temperature range of 20-150^{o}C with thermograms being analysed using NanoAnalyze and TA Analysis. To obtain an FTIR spectrum, a 10 mg/mL sample was prepared in dH_2O before being scanned from a wavelength range of 4000 cm^{-1} to 550 cm^{-1} at room temperature. SEM images were also produced with the technical support of Dr David McCarthy at University College London.

Initial *in vitro* digestion studies were conducted to determine the enzyme kinetic parameters (K_m, V_{max}, k_{cat} and k_{cat}/K_m) of purified RHAM. Concentrations ranging from 1-10 mg/mL were prepared in PBS and digested with 1.2 nM PPA at 37^{o}C. Aliquots of 300 µL were collected every 4 min up to 12 min and pipetted into 300 µL of ice-cold stop solution. Samples were then centrifuged at 13,000 g and 400 µL of the supernatant was collected. All samples were frozen at -20^{o}C for storage prior to the Prussian blue assay. Attempts were made to measure the initial rate of amylolysis, but no reaction rate was detected.

Inhibition studies were also performed to determine the mode of inhibition of purified RHAM on α-amylase. Varying concentrations of inhibitor and substrate (gelatinised wheat starch) were prepared in PBS, as described below.

- Inhibitor concentration – 0.25, 0.5, 0.75 and 1 mg/mL
- Substrate concentration – 0.5, 1, 1.5 and 2 mg/mL

Details of the methods used in the inhibition studies are presented in fuller form in Section 2.6.5 of Chapter 2.

7.3 Results and Discussion

7.3.1 Physical characterisation

7.3.1.1 Resistant starch, moisture, amylose/amylopectin and protein content

The resistant starch, moisture, amylose/amylopectin and protein content for purified RHAM are all displayed in Table 7.1. Note that the low moisture content was not unexpected given that samples were subjected to freeze drying.

Table 7.1. Resistant starch, moisture, amylose and protein content of purified RHAM. Data represents mean from three replicates ± SEM.

Resistant starch (%)	94.20 ± 1.11
Moisture (%)	3.49 ± 0.27
Amylose (%)	97.8 ± 1.95
Protein (%)	0.65 ± 0.03

7.3.1.2 X-ray diffraction (XRD)

X-ray diffraction allows the type of starch polymorph (A, B or C-type) to be identified from the peak positions and the proportion of crystallinity to be estimated. Figure 7.1 shows the XRD pattern obtained for purified RHAM. The diffraction pattern shows that the majority of the material remains in the amorphous state as only two crystalline peaks are observed.

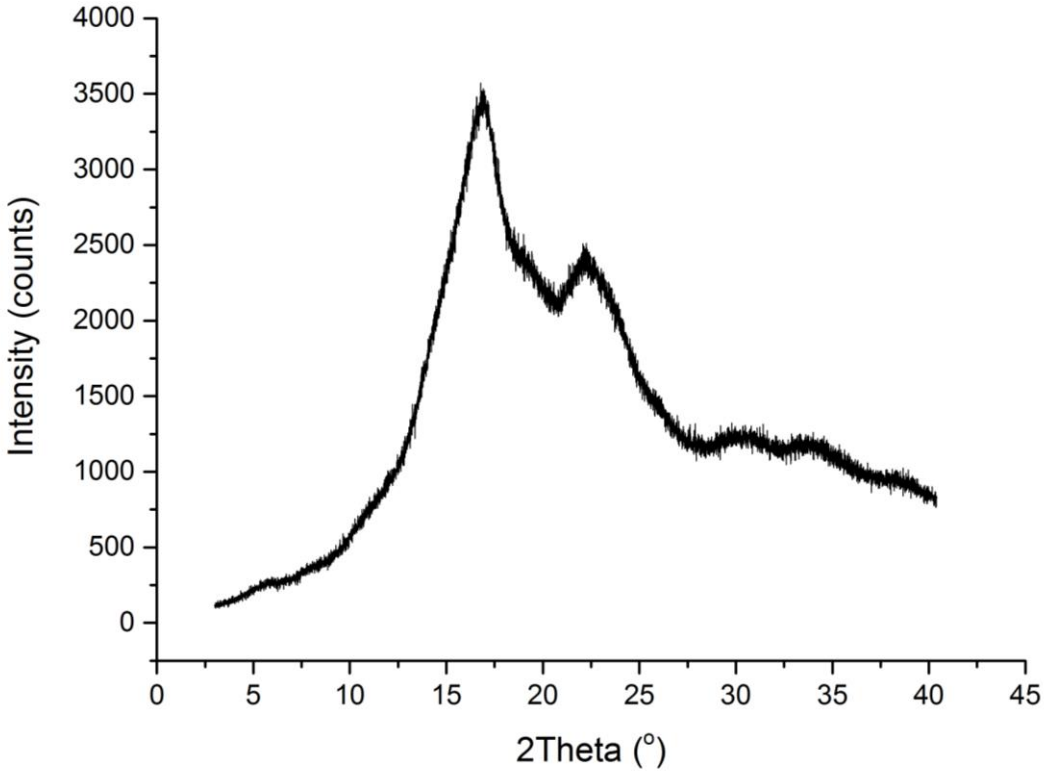

Figure 7.1. X-ray powder diffraction pattern for purified RHAM. Native high amylose maize starch was gelatinised at 121°C before being stored at cycles of 4°C and 37°C (24h each) three times. The non-retrograded starch material was digested with PPA and AMG and the remaining starch material was freeze dried to produce purified RHAM.

The XRD pattern obtained for purified RHAM was compared with that of the native form to allow for accurate peak comparisons (Figure 7.2).

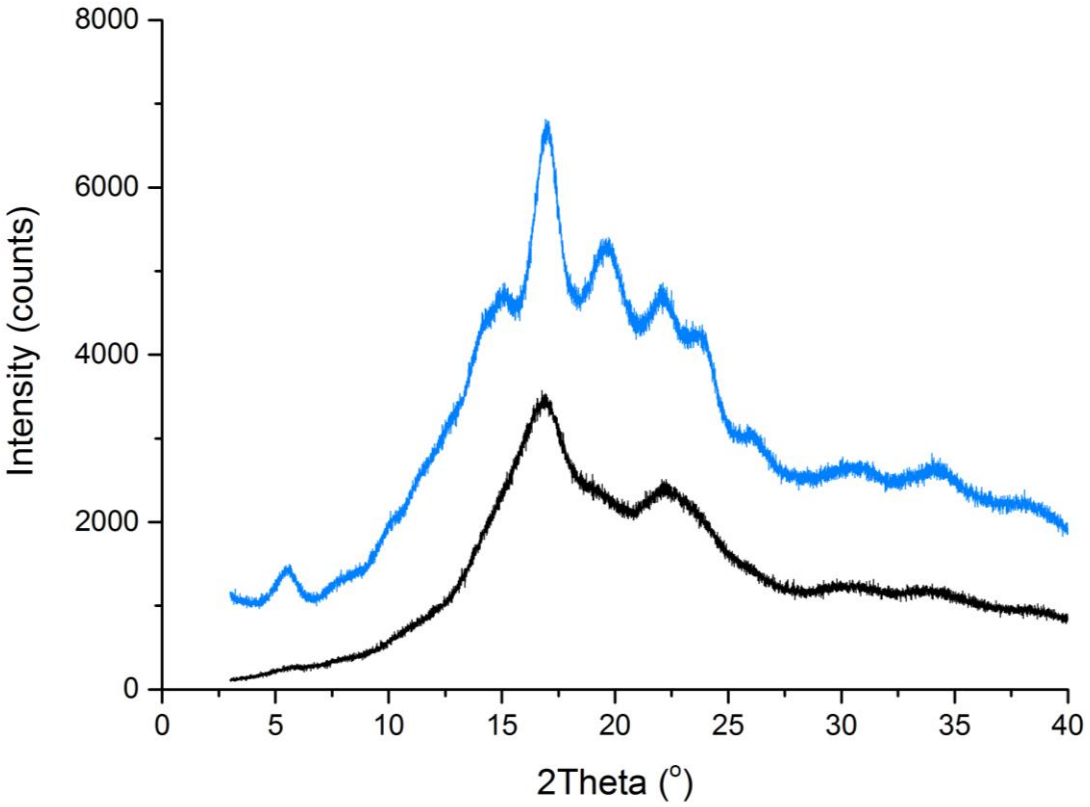

Peaks (2*θ*)	Native HAM	Purified RHAM
5° and 14°	Yes	No
16°	Yes	Yes
18°	Yes	No
Single peak between 22°	No	Yes
Double peak between 22°-25°	Yes	No

Figure 7.2. X-ray diffraction patterns of native HAM (blue) and purified RHAM (black), with the table below highlighting the differences between both starch forms.

A few peaks observed in the XRD pattern for native HAM are no longer present in purified RHAM. Figure 7.2 highlights the major changes in the XRD patterns between the native and purified RHAM form. Peaks originally observed at 5° 2*θ*

and 14° 2θ in native HAM disappear when the material is retrograded. Both native HAM and purified RHAM show a peak at 16° 2θ, but the intensity of the peak varies. Native HAM has a more defined peak compared with a broad peak observed in purified RHAM. The double peak noticed between 22°-25° 2θ for native HAM combines to form one broad peak in purified RHAM. The V-type polymorph, observed at 18° 2θ in native HAM, disappears upon retrogradation suggesting the complex melts during the autoclaving process and does not reform into a crystalline structure again.

The appearance of two broad peaks centred at 16° 2θ and 22° 2θ agrees with the XRD pattern for retrograded starch reported by other workers (Sievert *et al.*, 1991; Eerlingen *et al.*, 1993; Gidley *et al.*, 1995; Shamai *et al.*, 2003). Therefore, the XRD pattern for purified RHAM was indicative of a B-type packing geometry. However it is evident from Figure 7.2 that the B-type XRD pattern for the retrograded sample is relatively poor with weak intensity peaks. This is because the freeze drying process used to produce purified RHAM results in a low moisture content. Sievert et al. have shown a moisture content in excess of 4-5% is required to maintain structural ordering for sharp XRD diffraction peaks (Sievert *et al.*, 1991). These findings were also supported by Cheetham and workers who concluded that hydration increases the degree of crystallinity in maize starch (Cheetham and Tao, 1998). Therefore the two broad peaks with a low intensity are most likely due to the low moisture content resulting in imperfect crystallites (Zobel *et al.*, 1988; Gidley *et al.*, 1995; Cairns *et al.*, 1997).

By fitting an amorphous background to the XRD pattern, the AUC between the amorphous 'halo' and each crystalline peak can be estimated (see Section 2.3.3 in Chapter 2 for more detail). Using this method, the % of crystallinity for purified RHAM was calculated to be 18.4% ± 0.68 compared to 21% for native HAM. Curve fittings were performed in triplicates to ensure accurate fittings were applied. However, it is likely that due to the poor B-type XRD pattern the crystallinity value is underestimated.

7.3.1.3 FTIR-ATR

FTIR is a surface technique which can be used to determine the short-range molecular order of starch granules (van Soest *et al.*, 1995). Purified RHAM was scanned over a wavelength of 4000 cm^{-1} to 550 cm^{-1} to produce an FTIR spectrum. Specific absorbance peaks noticed at 1000 cm^{-1} and 1022 cm^{-1} are both sensitive to changes in molecular order. The peak intensity at 1000 cm^{-1} and 1022 cm^{-1} are characteristic bands of ordered and disordered structures, respectively (Capron *et al.*, 2007). Therefore the degree of order can be expressed as an absorbance ratio of 1000/1022 cm^{-1}. Table 7.2 shows the peak ratio for purified RHAM and native HAM (obtained from Chapter 4, page 148). The data suggests that the majority of the purified RHAM is disordered with only ~17% of the material being ordered relative to the original native form. This value is in close agreement with the 18.4% crystallinity content determined by XRD.

Table 7.2. The degree of molecular order, represented by the FTIR peak ratio 1000/1022 cm^{-1}, for purified RHAM and native HAM. Data represents mean from three replicates ± SEM.

Starch	FTIR-ATR ratio 1000/1022 cm^{-1}
Purified RHAM	0.23 ± 0.02
Native HAM	1.34 ± 0.01

7.3.1.4 Differential Scanning Calorimetry (DSC)

DSC was performed on purified RHAM to determine if a retrograded amylose peak could be observed. Figure 7.3(A) shows the whole thermogram obtained from a temperature range of 20-150^{o}C. However, as the retrograded amylose peak is the point of interest, Figure 7.3(B) only shows the thermogram from 105-150^{o}C. As we are only interested in identifying retrograded amylose, we considered that any experimental noise observed along the thermogram below ~120^{o}C could be ignored.

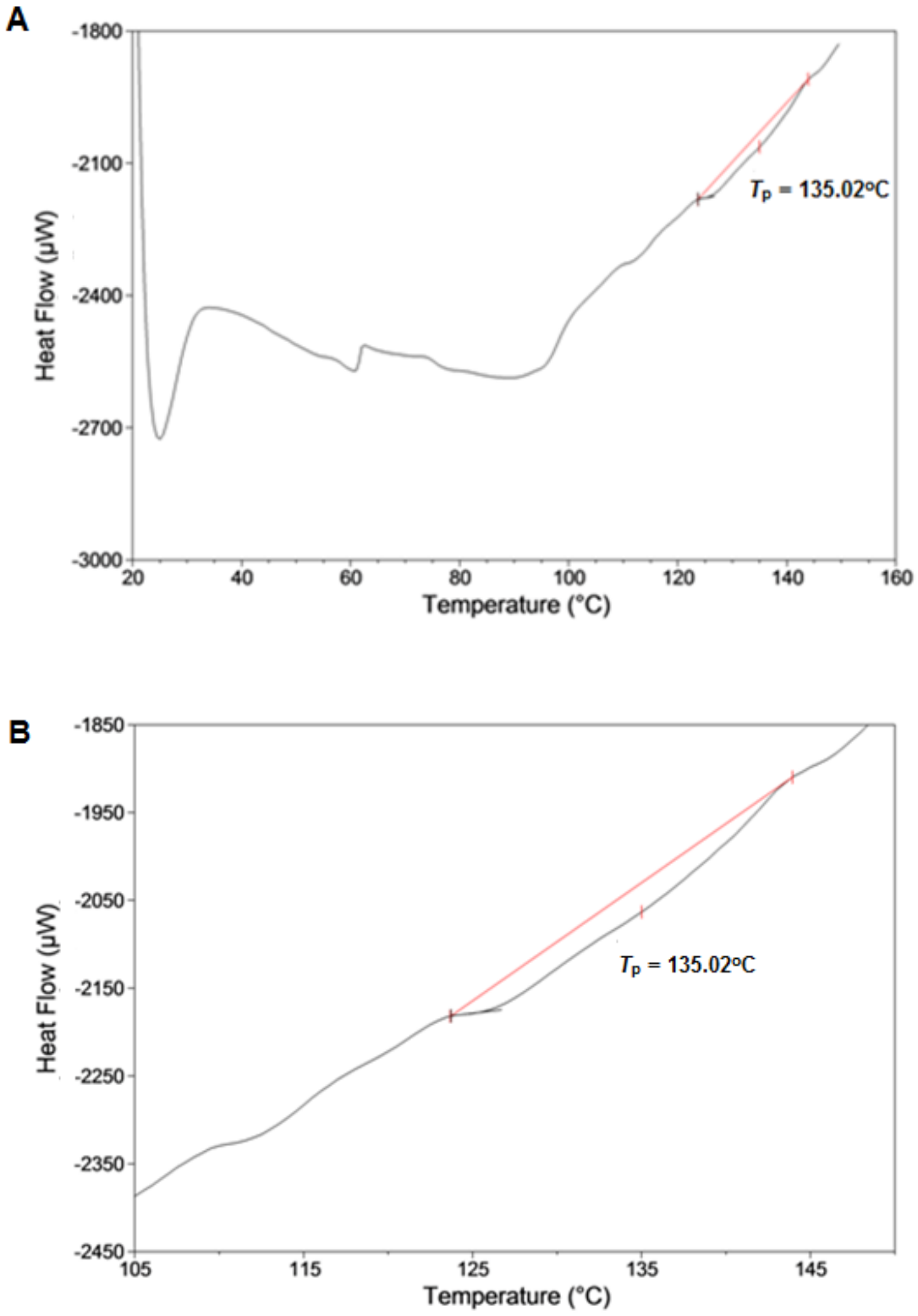

Figure 7.3. DSC thermogram of purified RHAM (A) with an enlarged view to show the melting of retrograded amylose (B).

The thermogram for purified RHAM shows a small and broad retrograded amylose peak at 135.02ºC along with an amylose-lipid complex peak at 95ºC. Table 7.3 shows the gelatinisation parameters obtained for purified RHAM. A retrogradation enthalpy of 2.75 J/g for crystalline amylose was very small compared with that calculated by previous researchers. Gidley and workers and Sievert and Pomeranz calculated a $\Delta_{ret}H$ between 25-30 and 21.2 (J/g), respectively (Sievert and Pomeranz, 1990; Gidley *et al.*, 1995). However, both authors used a starch concentration higher than that used in this study (500 and 200 mg/mL vs. 50 mg/mL) and therefore it is likely that in our studies the ordered material present was insufficient for generating reliable data from the MC DSC, i.e., we were working below the effective limit of the instrument

To obtain some indication of whether double helical material was present, Dr Frederick Warren, our collaborator at the University of Queensland, determined the amount of double helices present using ^{13}C CP/MAS NMR (Gidley and Bociek, 1985). He found that purified RHAM contained a relatively high proportion of double helices (~42.4%). This indicates NMR was able to detect more double helical content that the DSC.

Table 7.3. DSC gelatinisation parameters representing the melting of retrograded amylose in purified RHAM. Data represents mean from three replicates ± SEM.

T_o (ºC)	T_p (ºC)	T_c (ºC)	$\Delta_{ret}H$ (J/g)
125 ± 1.22	133.2 ± 3.21	141 ± 1.87	2.75 ± 0.05

7.3.1.5 Scanning electron micrographs (SEM)

SEM was used to investigate the morphology of purified RHAM (Figure 7.4). The micrographs show no intact granular structure indicating that the majority of the starch material has lost its original structural integrity. However, at a magnification of 5000x, small amounts of granular order begin to form, with small biconcave shaped like granules. A web-like pattern also connects the material together giving rise to the seemingly amorphous ‘lumps’ of starch observed at magnifications of 500x and 1000x. Furthermore, at a magnification of 10,000x, most of the structures are seen to be fairly amorphous and largely comprising of granular type aggregates.

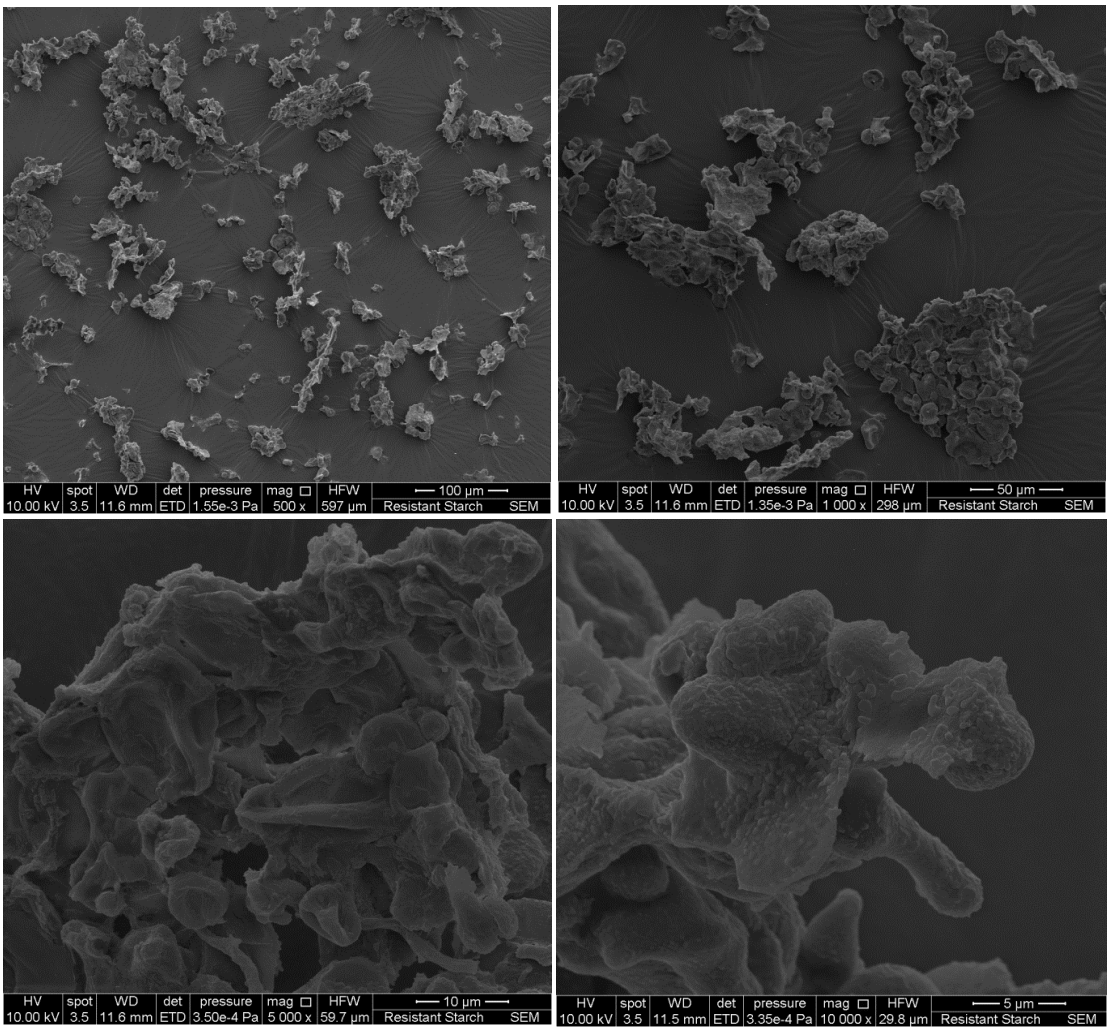

Figure 7.4. Scanning electron micrographs of purified RHAM. Top left, size bars represent 100 µm at magnification 500x. Top right, size bars represent 50 µm at magnification 1000x. Bottom left, size bars represent 10 µm at magnification 5000x. Bottom right, size bars represent 5 µm at magnification 10,000x.

Similar SEM images were obtained by Sievert and workers who showed vacuum dried resistant starch isolated from repeated cycles of heating/cooling had an amorphous and fluffy like structure (Sievert and Pomeranz, 1989). However as SEM is limited to examining starch material at a micron scale, it reveals no structural information about the molecular order and crystallinity

(Pérez and Bertoft, 2010). Therefore to provide a more complete structural analysis, SEM has to be coupled with XRD and DSC data.

7.3.2 *In vitro* digestion by α-amylase

The initial rates of amylolysis were very low so that the concentration of released maltose in the presence of PPA was virtually non-detectable by the standard Prussian blue method. Coupled with the results from the characterisation section, the mainly amorphous purified RHAM is resistant to α-amylase digestion. This supports the work published by Htoon and co-workers who showed that extracted resistant starch from high amylose maize had low levels of molecular order (Htoon *et al.*, 2009). However the group fail to give any possible explanation for the observed results. As mentioned previously purified RHAM contained approximately 42.3% ordered double helices, determined using NMR, and therefore it is likely this contributes to the resistance.

Changes in starch structure may also occur during the purification step with α-amylase and AMG and may possibly contribute to the resistance to enzymic digestion (as shown by the decreasing C_∞ and k_{cat}/K_m values for retrograded starch in Chapter 5 and 6). Overall, the results in the section show purified RHAM is clearly resistant to amylase digestion and suitable for studying the effect of purified RHAM on starch digestibility using *in vitro* inhibition studies.

7.3.3 Inhibition studies

The Linweaver-Burk plot is the most popular type of graphical representation used to study the mode of inhibition and can be obtained by re-arranging the original Michaelis-Menten equation to obtain a linear relationship to estimate V_{max} and K_m. Figure 7.5 shows the Linweaver-Burk plot for α-amylase acting on gelatinised wheat starch. The addition of purified RHAM (inhibitor) at varying concentrations significantly affects the activity of α-amylase and thereby the digestibility of gelatinised wheat starch. As four different inhibitor concentrations were used the data was plotted on individual Linweaver-Burk plots for easier interpretation.

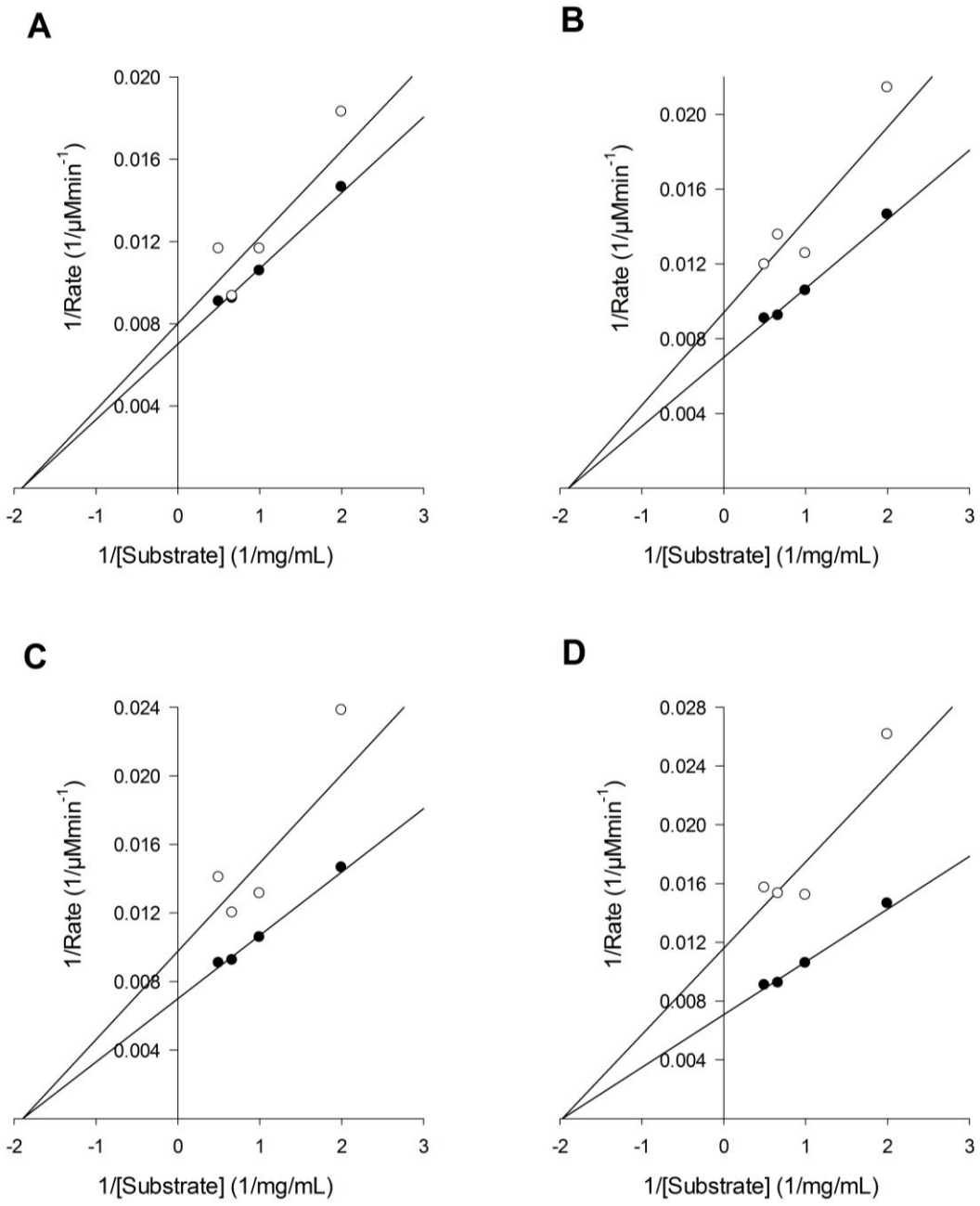

Figure 7.5. Linweaver-Burk plots obtained with purified RHAM (inhibitor) at concentrations of 0.25 (A), 0.5 (B), 0.75 (C) and 1 (D) mg/mL acting on the digestion of gelatinised wheat starch (0.5-2 mg/mL) by α-amylase. The data obtained with no inhibitor was also added in each plot, represented in black circles. The R^2 values are as follows 0.993 (no inhibitor), 0.863 (0.25 mg/mL), 0.901 (0.5 mg/mL), 0.858 (0.75 mg/mL) and 0.883 (1 mg/mL).

Table 7.4 shows the V_{max} and K_m calculated from the Linweaver-Burk plots with different concentrations of inhibitor. A non-competitive inhibitory action was noticed as the K_m showed little variation but V_{max} decreased as the inhibitor concentration was increased. The classical way of interpreting this behaviour is to assume that the inhibitor can bind to the free enzyme or/and enzyme-substrate complex while having no affect on the affinity of the enzyme for the substrate. When bound however, the inhibitor decreases the enzyme activity. Overall an almost 40% reduction in V_{max} was observed when the highest inhibitor concentration of 1 mg/mL was used.

Table 7.4. Enzyme kinetic parameters obtained from the Linweaver-Burk plots for PPA (1.2 nM) acting on gelatinised wheat starch with and without purified RHAM inhibitor. Average K_m and V_{max} values were calculated from three-four data sets ± SEM.

Inhibitor (mg/mL)	K_m (mg/mL)	V_{max} ($\mu Mmin^{-1}$)
0	0.62 ± 0.04	150.29 ± 4.50
0.25	0.56 ± 0.05	124.91 ± 2.91
0.5	0.55 ± 0.08	107.79 ± 5.53
0.75	0.54 ± 0.06	103.42 ± 7.39
1	0.49 ± 0.04	84.96 ± 0.16

Enzymologists have reported a number of disadvantages with using the Linweaver-Burk plot to describe enzyme inhibition. The Linweaver-Burk plot produces significant uncertainty in K_m and V_{max} values as majority of the data is

taken at high substrate concentrations. The slope of the graph can also be affected by the small errors present in the initial velocity (*v*) variable, which are increased in measurement when the reciprocal is taken. In addition to this, the Lineweaver-Burk plot can only identify competitive and non-competitive inhibition with any certainty and is less suitable for more complex inhibitory systems. Where the interaction between the enzyme and inhibitor is more complex, the graphical Dixon method is commonly used.

A Dixon plot allows the likely mechanism of enzyme inhibition to be determined by plotting the reciprocal of the initial reaction velocity (*v*) against the inhibitor concentration at each substrate concentration (Figure 7.6). If there is one-one binding of inhibitor and enzyme, the plot produce a straight line that allows the inhibition constant ($-K_i$), a measure of how potent the inhibitor is, to be determined. The inhibition constant is the interception point for each extrapolated straight line and can vary depending upon the type of inhibition.

From the plot it can be seen that as the inhibitor concentration for each substrate concentration increases, the reaction rate reduces. The straight lines intercept on the negative inhibitor axis as opposed to an intersection in the 4th quadrant, above the x axis. The latter pattern is seen with competitive and mixed inhibition. Therefore interception on the negative x axis indicates purified RHAM acts as a non-competitive inhibitor to α-amylase.

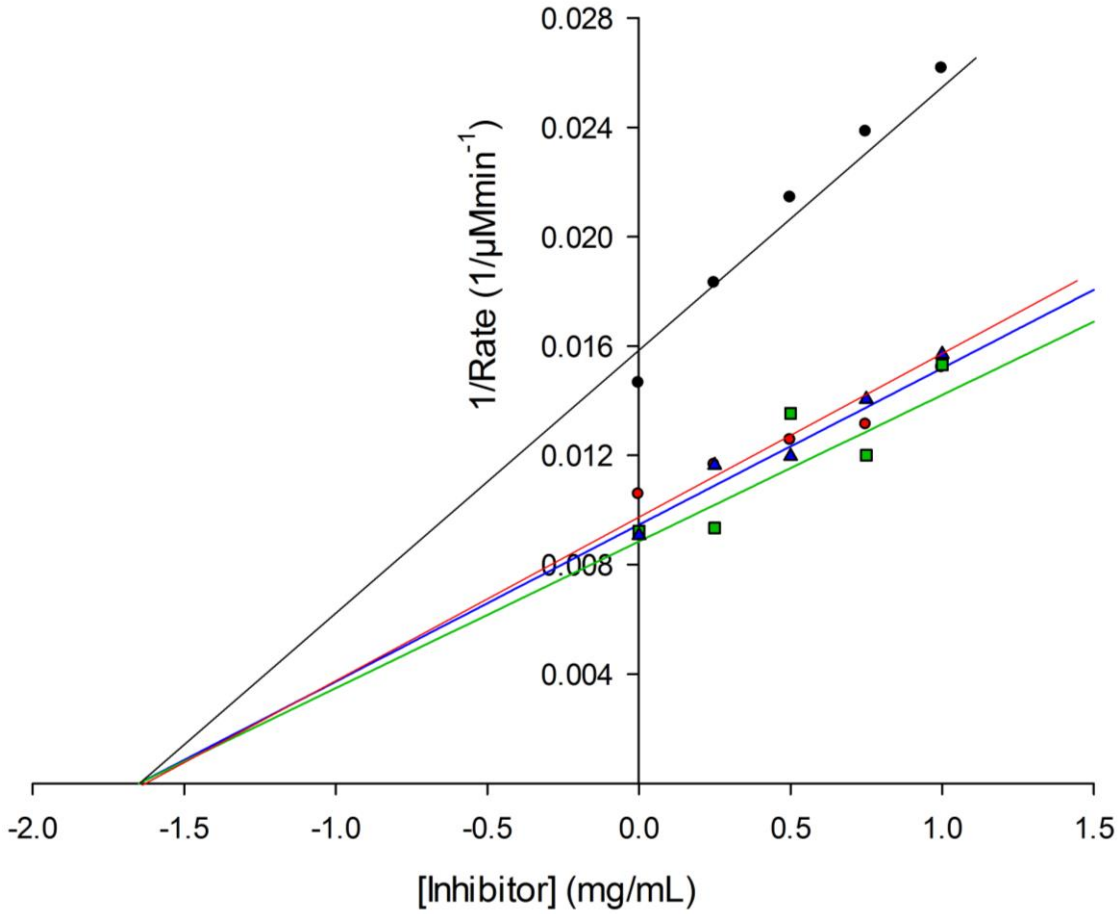

Figure 7.6. Reciprocal reaction rates (1/v) as a function of inhibitor concentration (Dixon plot). Each line represents a fixed concentration of substrate. Substrate concentrations are as follows: 0.5 (●), 1 (●), 1.5 (■) and 2 (▲) mg/mL. The R^2 values are as follows: 0.99 (0.5 mg/mL substrate), 0.96 (1 mg/mL substrate), 0.78 (1.5 mg/mL substrate), 0.97 (2 mg/mL substrate).

7.4 Conclusion

Purified RHAM was produced through repeated heating and cooling cycles followed by the digestible material being removed by α-amylase. The resistant starch content present was found to be ~94%, which is considerably higher than values reported by other workers (Sievert and Pomeranz, 1990; Eerlingen *et al.*, 1993; Htoon *et al.*, 2009). Characterisation of purified RHAM using XRD, FTIR, DSC and SEM showed that the majority of the material was in the amorphous state despite having high resistant starch contents. The amorphous material observed is different to that of gelatinised starches as the amorphous material is completely resistant to α-amylase digestion. Inhibition studies using Lineweaver-Burk plots showed no large change in K_m and a decrease in V_{max} while the Dixon plot revealed that all lines converge at the baseline commensurate with non-competitive inhibition. This confirms that purified RHAM acts as a non-competitive inhibitor to α-amylase. Therefore, although the characterisation and digestion results show purified RHAM to be primarily amorphous, albeit with ~43% of ordered double helices, it is highly resistant to digestion by α-amylase, indicating molecular order is not a prerequisite to provide enzyme resistance (Htoon *et al.*, 2009).

Chapter 8 Conclusions and future work

The mechanistic work presented in this thesis provides an improved understanding of the molecular mechanisms of starch digestion, specifically to the action of α-amylase on retrograded starch. Overall the results presented support the original hypothesis that retrogradation of starch produced a more ordered and crystalline structure, which was found to be less susceptible to amylase action and thus reduced the extent of amylolysis.

The hypothesis was tested by studying *in vitro* starch digestion starch with PPA over an initial (12 min) and prolonged (2h) course. Enzyme kinetic parameters were determined by fitting initial rates of starch hydrolysis to the Michaelis-Menten equation. Starch digestion was studied during prolonged incubations with α-amylase to produce non-linear digestibility curves. Applying the novel LOS plot approach to starch digestibility curves allows quantification of the pseudo 1st order rate constant (k) and the total digestible starch, C_∞. In addition, LOS plots also allow the identification of distinct fractions of rapidly and slowly digested starch material.

It was found that the binding and digestion of native semi-crystalline starches was highly unfavourable, as reflected in the large K_m and small k_{cat}/K_m and C_∞ values. The LOS plots for native starch digestion also revealed a rapid and slow phase resulting in distinctive rate constants for different starch fractions. The rapid phase represents hydrolysis of readily available surface starch, while the slow phase represents digestion of less available starch buried within the granule.

The digestion of gelatinised starches however resulted in a small K_m and large k_{cat}/K_m and C_∞ values, indicating the adsorption and digestion by PPA of gelatinised starch is highly favourable. The increase in starch hydrolysis is directly associated with the disorder of crystalline starch material that occurs from the gelatinisation process. The LOS plots also revealed no discontinuity, showing that the majority of the gelatinised starch material is rapidly digested.

The digestion process for retrograded starches revealed no change in K_m and k with a reduction in k_{cat}/K_m and C_∞, relative to gelatinised starch. Such kinetic changes were attributed to the decrease in quantity of digestible starch due to changes in crystallinity/order upon retrogradation. The results suggest PPA binds to retrograded starch but no digestion occurs and thus the retrograded material acts as a pure non-competitive inhibitor. The early changes in k_{cat}/K_m were attributed to amylose retrogradation while later changes were most likely due to amylopectin retrogradation (Miles *et al.*, 1985).

In order to determine the type of inhibition of retrograded starch, a starch sample that was resistant to digestion was required. Retrogradation of high amylose maize starch at cycles of 4^{o}C/37^{o}C significantly increased the resistant starch content to ~94%. FTIR-ATR showed that the majority of the material was disordered while DSC analysis revealed a broad peak at ~135^{o}C attributed to the melting of retrograded amylose crystallites. The amount of starch crystallinity was determined using powdered XRD with a value of 18.4%, although NMR studies revealed ~43% of ordered double helices. At a granular

level, SEM images showed majority of the starch material to consist of amorphous lumps associated together.

No amylolysis products were detected when PPA was added to purified RHAM indicating that the retrograded starch material was totally resistant to digestion. To determine the mode of inhibition, gelatinised wheat was digested with PPA with the addition of varying amounts of inhibitor. The initial hydrolysis rates were then fitted to a Lineweaver-Burk and Dixon plot and showed the intersection occurring on the x axis, therefore retrograded starch acts as a non-competitive inhibitor of pancreatic α-amylase.

The molecular order and crystallinity of starch granules was studied using conventional FTIR-ATR, DSC and XRD. FTIR-ATR examined the starch granule structure with a peak ratio of 1000/1022 cm^{-1} representing the amount of order to disorder. Native starch revealed a very strong peak ratio relative to the gelatinised form, suggesting the native starch structure is completely ordered relative to the disordered structure in gelatinised starch. Upon storage however, the retrograded starch material resulted in a higher peak ratio, suggesting the disordered structure begins to occupy a more ordered crystalline form.

DSC analysis was applied to determine the amount of molecular order and starch crystallinity by measuring the enthalpy change associated with starch gelatinisation (Cooke and Gidley, 1992; Bogracheva *et al.*, 2002). The different gelatinisation endotherms, resulting in different enthalpy changes, suggest

native starches have varying amounts of ordered/disordered content. DSC analysis on concentrated retrograded starch revealed the melting of the amylose-lipid complex and amylopectin crystallites.

Powdered XRD is a conventional technique used to directly estimate the amount of starch crystallinity. XRD patterns for different native starches revealed a combination of A, B and C-type starches with crystallinity values ranging from 21% to 32.3%. The XRD pattern for gelatinised wheat revealed a completely amorphous structure with no crystallinity peaks. However the scattering pattern for 48h retrograded high amylose maize starch, revealed a B-type pattern with two distinctive crystalline peaks, indicating an amorphous to crystalline structural transformation.

8.1 Future work

8.1.1 Starch structure

In addition to the analytical methods used in this project, the use of ^{13}C CP/MAS NMR would provide additional information about the complex starch structure. NMR allows for a direct measurement of the ordered double helical content and therefore provides more accurate results on starch order than the measurements obtained using FTIR-ATR and DSC. Adding a heating platform on the FTIR-ATR would allow the complete loss of molecular order to be followed during gelatinisation. The heating platform would also allow starch retrogradation to be followed immediately after gelatinisation, avoiding the 20 min cooling period normally applied to allow the sample to reach room temperature.

Studying the structure of freeze dried starches which have limited moisture produced poor XRD patterns with weak intensity peaks. This results in the AUC being underestimated and produces lower than expected crystallinity values. To provide a more accurate estimate of the crystallinity content, starch can be stored in a desiccator containing dH_2O to increase the relative humidity of the starch sample. This would produce sharper XRD peaks to provide a more accurate estimate of the starch crystallinity content.

DSC analysis of retrograded starch was extremely difficult and showed no detection of retrograded amylose material. Therefore additional experiments at higher starch concentrations may result in the detection of retrograded amylose crystallites, as the degree of retrogradation is influenced by starch concentration (Zhou *et al.*, 2010). Allowing starch samples to retrograde for different time periods allows a plot of $\Delta_{ret}H$ as a function of time to be generated. This would produce reliable data on the time taken for amylose and amylopectin crystallites to form. The yields of retrograded starch material can also be investigated by applying different processing conditions such as repeated heat/cool cycles.

It is important to note that the MC DSC and the more traditional Q2000 DSC (TA Instruments) have the same reported sensitivity (0.2 μW). However the actual specific sensitivity of the MC DSC is much higher due to the fact that it can accommodate much larger samples. Therefore as large experimental noise was detected when using MC DSC for the analysis of retrograded starches, using the less sensitive but higher resolution Q2000 DSC may be of benefit in future analysis. The lower sensitivity with a higher resolution results in less

experimental noise but still enables the separation between peaks. Therefore a useful experiment would be to compare the thermograms from both DSC devices to identify the most appropriate for the detection of retrograded starch crystallites.

The majority of the studies using DSC and XRD were also limited to one or two retrograded starch forms. Therefore studying retrograded starches from different botanical origins would provide a range of crystallinity values. Retrograded starches were also stored for no more than one week before being analysed using FTIR-ATR, DSC and XRD. Therefore, it could be useful to store starches for longer than 1 week. The extended storage time would ensure the complete retrogradation of amylopectin for prominent retrograded peak detection.

In addition to the methods commonly used to study structure, solution calorimetry and DMA are two new methods that have also been introduced. Solution calorimetry measures the energy released upon granule hydration and therefore the enthalpy change can be used to study amorphous and crystalline contents. DMA is a method that allows the structural changes that occur during starch gelatinisation to be studied. Both methods however are relatively new and still require significantly more work before they are widely accepted as suitable starch characterisation methods (Warren *et al.*, 2012).

8.1.2 Enzyme assays

Conducting *in vitro* digestion studies on retrograded starches stored for extended periods of time (more than 96h) would allow kinetic parameters to be obtained over a longer time frame. The extended storage period allows the sample to reach the complete retrogradation of both amylose and amylopectin. In addition to this, increasing the storage time will result in increased order/disorder peak ratios allowing the k_{cat}/K_m and C_∞ to be correlated with the peak ratio without any large gaps in the plot.

Many reports have suggested storing starches at reduced temperatures and applying heat/cool cycles accelerates the retrogradation process and thus producing more amylose and amylopectin crystallites (Sajilata *et al.*, 2006). In our studies, the majority of the starches were stored at room temperature and therefore determining the effects of different storage conditions on digestion kinetics could provide valuable information.

All starches tested have an amylose content ranging between 15-30%, with the exception of high amylose maize and waxy maize which have an amylose content of 79% and 1%, respectively. Therefore obtaining starches with an amylose content ranging between 30-80% allows C_∞ and k_{cat}/K_m to be plotted as a function of amylose content. This allows the effect of amylose content on starch digestion to be studied.

The inhibition studies using purified RHAM were limited to only a few inhibitor concentrations. Therefore repeating the experiment with additional inhibitor

concentrations would provide a more complete set of kinetic data for accurate inhibition analysis.

Moving away from studying retrograded starch digestion, further work is needed to study the digestion of retrograded starch in tissue samples. This approach would facilitate our understanding of how cell walls influence the access of α-amylase to starch. In addition to *in vitro* starch digestion, it would be interesting to investigate retrograded starch digestion within an *in vivo* system (animals and/or humans). This would allow the digestion kinetics, determined by *in vitro* and *in vivo* models, to be compared against each other. Such information potentially would not only provide a simple *in vitro* method to estimate GI, but also reveal the behaviour of pure starches in more complex food systems.

8.2 Final conclusion

The rate and extent of starch amylolysis is greatly affected by the storage of starch after hydrothermal processing which produces retrograded starch material. This effect was attributed to the increase in the molecular order and crystallinity of retrograded starch which limits the action of α-amylase on substrate. Retrograded starch renders α-amylase inactive by acting as a non-competitive inhibitor and therefore reduces the susceptibility to amylolysis after hydrothermal processing. The results may potentially be relevant to a better understanding of how starch in the human diet is digested and how some forms are preferable in dietary terms for the management of health and disease (e.g., Type II diabetes and obesity). Overall, the results presented in this thesis show

that different processing methods of starch directly change its structural properties and as a consequence, play a major role in starch digestion kinetics.

References

Abd Karim, A., Norziah, M. H. and Seow, C. C. (2000). "Methods for the study of starch retrogradation." Food Chemistry **71**: 9-36.

Åkerberg, A., Liljeberg, H. and Björck, I. (1998). "Effects of amylose/amylopectin ratio and baking conditions on resistant starch formation and glycaemic indices." Journal of Cereal Science **28**(1): 71-80.

Ao, Z. and Jane, J. (2007). "Characterization and modeling of the A- and B-granule starches of wheat, triticale, and barley." Carbohydrate Polymers **67**(1): 46-55.

Arvidsson-Lenner, R., Asp, N.-G., Axelsen, M., Bryngelsson, S., Haapa, E., Järvi, A., Karlström, B., Raben, A., Sohlström, A. and Thorsdottir, I. (2004). "Glycaemic index. Relevance for health, dietary recommendations and food labelling." Food & Nutrition Research **48**(2): 84-94.

Baldwin, P. (2001). "Starch granule-associated proteins and polypeptides: A review." Starch-Stärke **53**: 475-503.

Baldwin, P., Adler, J., Davies, M. and Melia, C. (1998). "High resolution imaging of starch granule surfaces by atomic force microscopy." Journal of Cereal Science **27**(3): 255-265.

Ball, S., Guan, H.-P., James, M., Myers, A., Keeling, P., Mouille, G., Buléon, A., Colonna, P. and Preiss, J. (1996). "From glycogen to amylopectin: a model for the biogenesis of the plant starch granule." Cell **86**(3): 349-352.

Bear, R. and French, D. (1941). "The significance of X-ray diffraction patterns obtained from starch granules." Journal of the American Chemical Society **63**: 2298–2305.

Beckmann, C. O. (1953). "The structure of amylopectin and glycogen." Annals of the New York Academy of Sciences **57**: 384–397.

BeMiller, J. N. and Whistler, R. L. (2009). Starch: Chemistry and Technology, Academic Press.

Benmoussa, M., Moldenhauer, K. A. and Hamaker, B. (2007). "Rice amylopectin fine structure variability affects starch digestion properties." Journal of Agricultural and Food Chemistry **55**: 1475-1479.

Benmoussa, M., Suhendra, B., Aboubacar, A. and Hamaker, B. R. (2006). "Distinctive sorghum starch granule morphologies appear to improve raw starch digestibility." Starch - Stärke **58**(2): 92-99.

Berg, J. M., Tymoczko, J. L. and Stryer, L. (2002). Biochemistry, W.H. Freeman, 2002.

Bertoft, E. (1991). "Chains of intermediate lengths in waxy-maize amylopectin." Carbohydrate Research **212**: 245–251.

Björck, I., Liljeberg, H. and Östman, E. (2000). "Low glycaemic-index foods." British Journal of Nutrition **83**(S1): 149-155.

Blazek, J. and Gilbert, E. P. (2011). "Application of small-angle X-ray and neutron scattering techniques to the characterisation of starch structure: A review." Carbohydrate Polymers **85**(2): 281-293.

Blazek, J., Salman, H., Rubio, A. L., Gilbert, E., Hanley, T. and Copeland, L. (2009). "Structural characterization of wheat starch granules differing in amylose content and functional characteristics." Carbohydrate Polymers **75**(4): 705-711.

Blennow, A., Engelsen, S. B., Nielsen, T. H., Baunsgaard, L. and Mikkelsen, R. (2002). "Starch phosphorylation: a new front line in starch research." TRENDS in Plant Science **7**(10): 445-450.

Blennow, A. and Svensson, B. (2010). "Dynamics of starch granule biogenesis – the role of redox-regulated enzymes and low-affinity carbohydrate-binding modules." Biocatalysis and Biotransformation **28**(1): 3-9.

Bogracheva, T., Meares, C. and Hedley, C. (2006). "The effect of heating on the thermodynamic characteristics of potato starch." Carbohydrate Polymers **63**(3): 323-330.

Bogracheva, T. Y., Davydova, N. I., Genin, Y. V. and Hedley, C. L. (1995). "Mutant genes at the r and rb loci affect the structure and physico-chemical properties of pea seed starches." Journal of Experimental Botany **46**: 1905-1913.

Bogracheva, T. Y., Wang, Y. L., Wang, T. L. and Hedley, C. L. (2002). "Structural studies of starches with different water contents." Biopolymers **64**(5): 268-281.

References

Boivin, M., Zinsmeister, A. R., Go, V. L. W. and DiMagno, E. P. (1987). "Effect of a purified amylase inhibitor on carbohydrate metabolism after a mixed meal in healthy humans." Mayo Clinic Proceedings **62**(4): 249-255.

Bornet, F., Fontvieille, A.-M., Rizkalla, S., Colonna, P., Blayo, A., Mercier, C. and Slama, G. (1989). "Insulin and glycemic responses in healthy humans to native starches processed in different ways: correlation with *in vitro* alpha-amylase hydrolysis." The American Journal of Clinical Nutrition **50**(2): 315-323.

Bornet, F. R. J., Billaux, M. S. and Messing, B. (1997). "Glycaemic index concept and metabolic diseases." International Journal of Biological Macromolecules **21**(1-2): 207–219.

Brand-Miller, J., Hayne, S., Petocz, P. and Colagiuri, S. (2003). "Low–glycemic index diets in the management of diabetes A meta-analysis of randomized controlled trials." Diabetes Care **26**(8): 2261-2267.

Brand, J. C., Colagiuri, S., Crossman, S., Allen, A., Roberts, D. C. and Truswell, A. S. (1991). "Low-glycemic index foods improve long-term glycemic control in NIDDM." Diabetes Care **14**(2): 95-101.

Brand, J. C., Nicholson, P. L., Thorburn, A. W. and Truswell, A. (1985). "Food processing and the glycemic index." The American Journal of Clinical Nutrition **42**(6): 1192-1196.

Bravo, L., Siddhuraju, P. and Saura-Calixto, F. (1998). "Effect of various processing methods on the in vitro starch digestibility and resistant starch content of Indian pulses." Journal of Agricultural and Food Chemistry **46**(11): 4667-4674.

Brayer, G. D., Luo, Y. and Withers, S. G. (1995). "The structure of human pancreatic α- amylase at 1.8 Å resolution and comparisons with related enzymes." Protein Science **4**(9): 1730-1742.

Brennan, C. S., Harris, N., Smith, D. and Shewry, P. R. (1996). "Structural differences in the mature endosperms of good and poor malting barley cultivars." Journal of Cereal Science **24**: 171–177.

Brouns, F., Bjorck, I., Frayn, K., Gibbs, A., Lang, V., Slama, G. and Wolever, T. (2005). "Glycaemic index methodology." Nutrition Research Reviews **18**(01): 145-171.

Brouns, F., Kettlitz, B. and Arrigoni, E. (2002). "Resistant starch and “the butyrate revolution”." Trends in Food Science & Technology **13**(8): 251-261.

Buisson, G., Duee, E., Haser, R. and Payan, F. (1987). "Three dimensional structure of porcine pancreatic alpha-amylase at 2.9 A resolution. Role of calcium in structure and activity." The EMBO Journal **6**(13): 3909-3916.

Buléon, A., Colonnaa, P., Planchota, V. and Ballb, S. (1998). "Starch granules: structure and biosynthesis." International Journal of Biological Macromolecules **23**(2): 85-112.

Butterworth, P. J. (1972). "The use of dixon plots to study enzyme inhibition." Biochimica et Biophysica Acta (BBA) - Enzymology **289**(2): 251-253.

Butterworth, P. J., Warren, F. J. and Ellis, P. R. (2011). "Human α-amylase and starch digestion: An interesting marriage." Starch - Stärke **63**(7): 395-405.

Butterworth, P. J., Warren, F. J., Grassby, T., Patel, H. and Ellis, P. R. (2012). "Analysis of starch amylolysis using plots for first-order kinetics." Carbohydrate Polymers **87**(3): 2189-2197.

Cai, C., Zhao, L., Huang, J., Chen, Y. and Wei, C. (2014). "Morphology, structure and gelatinization properties of heterogeneous starch granules from high-amylose maize." Carbohydrate Polymers **102**: 606-614.

Cairns, P., Bogracheva, T., Ring, S. G., Hedley, C. L. and Morris, V. J. (1997). "Determination of the polymorphic composition of smooth pea starch." Carbohydrate Polymers **32**(3-4): 275–282.

Capron, I., Robert, P., Colonna, P., Brogly, M. and Planchot, V. (2007). "Starch in rubbery and glassy states by FTIR spectroscopy." Carbohydrate Polymers **68**(2): 249-259.

Catley, B. and Whelan, W. (1971). "Observations on the structure of pullulan." Archives Of Biochemistry And Biophysics **143**(1): 138-142.

Chandalia, M., Garg, A., Lutjohann, D., von Bergmann, K., Grundy, S. M. and Brinkley, L. J. (2000). "Beneficial effects of high dietary fiber intake in patients with type 2 diabetes mellitus." New England Journal of Medicine **342**(19): 1392-1398.

Chang, S.-m. and Liu, L.-c. (1991). "Retrogradation of rice starches studied by differential scanning calorimetry and influence off sugars, NaCl and lipids." Journal of Food Science **56**: 564-566.

Chatakanonda, P., Chinachoti, P., Sriroth, K., Piyachomkwan, K., Chotineeranat, S., Tang, H.-R. and Hills, B. (2003). "The influence of time and conditions of harvest on the functional behaviour of cassava starch-a proton NMR relaxation study." Carbohydrate Polymers **53**(3): 233-240.

Cheetham, N. W. and Tao, L. (1998). "Variation in crystalline type with amylose content in maize starch granules: an X-ray powder diffraction study." Carbohydrate Polymers **36**: 277–284.

Chrastil, J. (1987). "Improved calorimetric determination of amylose in starches or flours." Carbohydrate Polymers **159**: 154-158.

Chung, H.-J., Liu, Q. and Hoover, R. (2009). "Impact of annealing and heat-moisture treatment on rapidly digestible, slowly digestible and resistant starch levels in native and gelatinized corn, pea and lentil starches." Carbohydrate Polymers **75**(3): 436-447.

Chung, H.-J., Shin, D.-H. and Lim, S.-T. (2008). "In vitro starch digestibility and estimated glycemic index of chemically modified corn starches." Food Research International **41**(6): 579-585.

Chung, H., Lim, H. and Lim, S. (2006). "Effect of partial gelatinization and retrogradation on the enzymatic digestion of waxy rice starch." Journal of Cereal Science **43**(3): 353-359.

Collado, L. S. and Corke, H. (1999). "Heat-moisture treatment effects on sweetpotato starches differing in amylose content." Food Chemistry **65**(3): 339-346.

Cooke, D. and Gidley, M. J. (1992). "Loss of crystalline and molecular order during starch gelatinisation: origin of the enthalpic transition." Carbohydrate Research **227**(0): 103-112.

Copeland, L., Blazek, J., Salman, H. and Tang, M. C. (2009). "Form and functionality of starch." Food Hydrocolloids **23**(6): 1527-1534.

Copeland, R. A. (2004). Enzymes: a practical introduction to structure, mechanism, and data analysis, John Wiley & Sons.

Cornish-Bowden, A. (1974). "A simple graphical method for determining the inhibition constants of mixed, uncompetitive and non-competitive inhibitors." Biochemical Journal **137**(1): 143-144.

Crapo, P., Insel, J., Sperling, M. and Kolterman, O. (1981). "Comparison of serum glucose, insulin, and glucagon responses to different types of complex

carbohydrate in noninsulin-dependent diabetic patients." American Journal of Clinical Nutrition **34**: 184-190.

Crapo, P. A., Reaven, G. and Olefsky, J. (1977). "Postprandial plasma-glucose and-insulin responses to different complex carbohydrates." Diabetes **26**(12): 1178-1183.

Cui, R. and Oates, C. (1999). "The effect of amylose–lipid complex formation on enzyme susceptibility of sago starch." Food Chemistry **65**(4): 417-425.

Cui, R. and Oates, C. G. (1997). "The effect of retrogradation on enzyme susceptibility of sago starch." Carbohydrate Polymers **32**: 65-72.

Cummings, J. and Macfarlane, G. (1991). "The control and consequences of bacterial fermentation in the human colon." Journal of Applied Bacteriology **70**(6): 443-459.

Cunin, C., Handschin, S., Walther, P. and Escher, E. (1995). "Structural changes of starch during durum wheat pasta." LWT-Food Science and Technology **28**: 323-328.

Davydova, N., Leont'ev, S. P., Genin, Y. V., Sasovc, A. Y. and Bogracheva, T. Y. (1995). "Some physico-chemical properties of smooth pea starches." Carbohydrate Polymers **27**: 109-115.

Debet, M. R. and Gidley, M. J. (2007). "Why do gelatinized starch granules not dissolve completely? Roles for amylose, protein, and lipid in granule "ghost" integrity." Journal of Agricultural and Food Chemistry **55**: 4752-4760.

Deffenbaugh, L. and Walker, C. (1989). "Comparison of starch pasting properties in the brabender viscoamylograph and the rapid visco-analyzer." Cereal Chemistry **66**(6): 493-499.

Dhital, S., Shrestha, A. K. and Gidley, M. J. (2010). "Relationship between granule size and in vitro digestibility of maize and potato starches." Carbohydrate Polymers **82**(2): 480-488.

Dhital, S., Warren, F. J., Zhang, B. and Gidley, M. J. (2014). "Amylase binding to starch granules under hydrolysing and non-hydrolysing conditions." Carbohydrate Polymers **113**: 97-107.

References

Dona, A. C., Pages, G., Gilbert, R. G. and Kuchel, P. W. (2010). "Digestion of starch: *In vivo* and *in vitro* kinetic models used to characterise oligosaccharide or glucose release." Carbohydrate Polymers **80**(3): 599-617.

Dona, A. C., Pages, G., Gilbert, R. G. and Kuchel, P. W. (2011). "Starch granule characterization by kinetic analysis of their stages during enzymic hydrolysis: 1H nuclear magnetic resonance studies." Carbohydrate Polymers **83**(4): 1775-1786.

Duggleby, R. G. (2001). "Quantitative analysis of the time courses of enzyme-catalyzed reactions." Methods **24**(2): 168-174.

Edwards, C. H., Warren, F., Milligan, P. J., Butterworth, P. and Ellis, P. (2014). "A novel method for classifying starch digestion by modelling the amylolysis of plant foods using first-order enzyme kinetic principles." Food & Function **5**: 2751-2758.

Eerlingen, R., Deceuninck, M. and Delcour, J. (1993). "Enzyme-resistant starch. II. Influence of amylose chain length on resistant starch formation." Cereal Chemistry **70**: 345-350.

Eerlingen, R. C., Crombez, M. and Delcour, J. (1993). "Enzyme-resistant starch. I. Quantitative and qualitative influence of incubation time and temperature of autoclaved starch on resistant starch formation." Cereal Chemistry **70**(3): 339-344.

Eerlingen, R. C. and Delcour, J. A. (1995). "Formation, analysis, structure and properties of type III enzyme resistant starch." Journal of Cereal Science **22**: 129-138.

Eerlingen, R. C., Jacobs, H. and Delcour, J. (1994). "Enzyme-resistant starch. V. Effect of retrogradation of waxy maize starch on enzyme susceptibility." Cereal Chemistry **71**(4): 351 -355.

Eisenthal, R., Danson, M. J. and Hough, D. W. (2007). "Catalytic efficiency and k_{cat}/K_M: a useful comparator?" Trends in Biotechnology **25**(6): 247-249.

Emi, M., Horii, A., Tomita, N., Nishide, T., Ogawa, M., Mori, T. and Matsubar, K. (1988). "Overlapping two genes in human DNA: a salivary amylase gene overlaps with a gamma-actin pseudogene that carries an integrated human endogenous retroviral DNA." Gene **62**(2): 229-235.

Englyst, H. and Cummings, J. (1987). "Digestion of polysaccharides of potato in the small intestine of man." American Journal of Clinical Nutrition **45**: 423-431.

Englyst, H. and Hudson, G. (1996). "The classification and measurement of dietary carbohydrates " Food Chemistry **57**(1): 15-21.

References

Englyst, H., Veenstra, J. and Hugdson, G. (1996). "Measurement of rapidly available glucose (RAG) in plant foods: a potential in vitro predictor of the glycaemic response." British Journal of Nutrition **75**: 327-337.

Englyst, H. N., Kingman, S. and Cummings, J. (1992). "Classification and measurement of nutritionally important starch fractions." European Journal of Clinical Nutrition **46**: 33-50.

Englyst, K. N., Englyst, H. N., Hudson, G. J., Cole, T. J. and Cummings, J. H. (1999). "Rapidly available glucose in foods: an in vitro measurement that reflects the glycemic response." The American Journal of Clinical Nutrition **69**(3): 448-454.

Englyst, K. N., Vinoy, S., Englyst, H. N. and Lang, V. (2003). "Glycaemic index of cereal products explained by their content of rapidly and slowly available glucose." British Journal of Nutrition **89**(03): 329-339.

Fannon, J. E., Gray, J. A., Gunawan, N., Huber, K. C. and Bemiller, J. N. (2004). "Heterogeneity of starch granules and the effect of granule channelization on starch modification." Cellulose **11**: 247-254.

Fannon, J. E., Hauber, R. J. and Bemiller, J. N. (1992). "Surface pores of starch granules." Cereal Chemistry **69**: 284-288.

Foster-Powell, K., Holt, S. H. and Brand-Miller, J. C. (2002). "International table of glycemic index and glycemic load values: 2002." The American Journal of Clinical Nutrition **76**(1): 5-56.

Frayn, K. N. (2009). Metabolic regulation: a human perspective, John Wiley & Sons.

Fredriksson, H., Bjorck, I., Andersson, R., Liljeberg, H., Silverio, J., Eliasson, A. and Aman, P. (2000). "Studies on a-amylase degradation of retrograded starch gels from waxy maize and high-amylopectin potato." Carbohydrate Polymers **43**: 81–87.

Fredriksson, H., Silverio, J., Andersson, R., Eliasson, A. and Åman, P. (1998). "The influence of amylose and amylopectin characteristics on gelatinization and retrogradation properties of different starches." Carbohydrate Polymers **35**: 119-134.

Frei, M., Siddhuraju, P. and Becker, K. (2003). "Studies on the in vitro starch digestibility and the glycemic index of six different indigenous rice cultivars from the Philippines." Food Chemistry **83**(3): 395-402.

Frost, G., Leeds, A. A., Doré, C. J., Madeiros, S., Brading, S. and Dornhorst, A. (1999). "Glycaemic index as a determinant of serum HDL-cholesterol concentration." The Lancet **353**(9158): 1045-1048.

Fuentes-Zaragoza, E., Riquelme-Navarrete, M., Sánchez-Zapata, E. and Pérez-Álvarez, J. (2010). "Resistant starch as functional ingredient: A review." Food Research International **43**(4): 931-942.

Fujita, S., Yamamoto, H., Sugimoto, Y., Morita, N. and Yamamori, M. (1998). "Thermal and crystalline properties of waxy wheat (*Triticum aestivum* L.) starch." Journal of Cereal Science **27**(1): 1-5.

Gallant, D. J., Bouchet, B. and Baldwin, P. M. (1997). "Microscopy of starch: evidence of a new level of granule organization." Carbohydrate Polymers **32**(3–4): 177-191.

Gibson, T. S., Solah, V. A. and McCleary, B. V. (1997). "Estimation of amylose content of starches after precipitation of amylopectin by concanavalin A." Journal of Cereal Science **25**: 111–119.

Gidley, M. (1989). "Molecular mechanisms underlying amylose aggregation and gelation." Macromolecules **22**: 351–358.

Gidley, M. and Bociek, S. M. (1985). "Molecular organization in starches: A ^{13}C CP/MAS NMR study." Journal of the American Chemical Society **107**: 7040-7044.

Gidley, M., Cooke, D., Darke, A., Hoffmann, R., Russell, A. and Greenwell, P. (1995). "Molecular order and structure in enzyme-resistant retrograded starch." Carbohydrate Polymers **28**: 23-31.

Gidley, M. J. and Bulpin, P. V. (1989). "Aggregation of amylose in aqueous systems: the effect of chain length on phase behavior and aggregation kinetics." Macromolecules **22**(1): 341-346.

Gill, P., Moghadam, T. and Ranjbar, B. (2010). "Differential scanning calorimetry techniques: Applications in biology and nanoscience." Journal of Biomolecular Techniques **21**: 167.

Goddard, M. S., Young, G. and Marcus, R. (1984). "The effect of amylose content on insulin and glucose responses to ingested rice." The American Journal of Clinical Nutrition **39**(3): 388-392.

Goñi, I., Garcia-AIonso, A. and Saura-Calixto, F. (1997). "A starch hydrolysis procedure to estimate glycemic index." Nutrition Research **17**: 427-437.

Graves, D. J. and Wang, J. H. (1972). "15 α-Glucan phosphorylases–Chemical and physical basis of catalysis and regulation." The enzymes **7**: 435-482.

Halton, T. L., Willett, W. C., Liu, S., Manson, J. E., Albert, C. M., Rexrode, K. and Hu, F. B. (2006). "Low-carbohydrate-diet score and the risk of coronary heart disease in women." New England Journal of Medicine **355**(19): 1991-2002.

Han, X.-Z., Ao, Z., Janaswamy, S., Jane, J.-L., Chandrasekaran, R. and Hamaker, B. R. (2006). "Development of a low glycemic maize starch: Preparation and characterization." Biomacromolecules **7**(4): 1162-1168.

Han, X. Z. and Hamaker, B. R. (2002). "Location of starch granule-associated proteins revealed by confocal laser scanning microscopy." Journal of Cereal Science **35**(1): 109-116.

Hanes, C. S. (1940). "The reversible formation of starch from glucose-1-phosphate catalysed by potato phosphorylase." Proceedings of the Royal Society of London. Series B-Biological Sciences **129**(855): 174-208.

Hara, H., Haga, S., Aoyama, Y. and Kiriyama, S. (1999). "Short-chain fatty acids suppress cholesterol synthesis in rat liver and intestine." The Journal of Nutrition **129**(5): 942-948.

Haralampu, S. G. (2000). "Resistant starch—a review of the physical properties and biological impact of RS3." Carbohydrate Polymers **41**: 285–292.

Helbert, W., Schülein, M. and Henrissat, B. (1996). "Electron microscopic investigation of the diffusion of Bacillus licheniformis α-amylase into corn starch granules." International Journal of Biological Macromolecules **19**(3): 165-169.

Hizukuri, S. (1985). "Relationship between the distribution of the chain length of amylopectin and the crystalline structure of starch granules." Carbohydrate Research **141**(2): 295-306.

Hizukuri, S. (1986). "Polymodal distribution of the chain lengths of amylopectins, and its significance." Carbohydrate Research **147**(2): 342–347.

Hoebler, C., Karinthi, A., Chiron, H., Champ, M. and Barry, J. (1999). "Bioavailability of starch in bread rich in amylose: metabolic responses in healthy subjects and starch structure." European Journal of Clinical Nutrition **53**(5): 360-366.

Holl, J., Szejtli, J. and Gantner, G. (1959). "Investigation of the retrogradation of amylose." Chemical Engineering **3**(2): 95-104.

Holm, J., Björck, I., Ostrowska, S., Eliasson, A. C., Asp, N. G., Larsson, K. and Lundquist, I. (1983). "Digestibility of amylose-lipid complexes in-vitro and in-vivo." Starch-Stärke **35**(9): 294-297.

Holm, J., Lundquist, I., Björck, I., Eliasson, A. and Asp, N. (1988). "Degree of starch gelatinization, digestion rate of starch in vitro, and metabolic response in rats." The American Journal of Clinical Nutrition **47**(6): 1010-1016.

Hoove, R. and Vasanthan, T. (1993). "The effect of annealing on the physicochemical properties of wheat, oat, potato and lentil starches." Journal of Food Biochemistry **17**: 303-325.

Hoover, R. and Manuel, H. (1996). "The effect of heat–moisture treatment on the structure and physicochemical properties of normal maize, waxy maize, dull waxy maize and amylomaize V starches." Journal of Cereal Science **23**: 153–162.

Hopkins, R. and Jelinek, B. (1954). "The mechanism of the β-amylase action. 1.Multichain'action on amylose." Biochemical Journal **56**(1): 136-140.

Hsein-Chih, H. W. and Sarko, A. (1978). "The double-helical molecular structure of crystalline B-amylose." Carbohydrate Research **61**(1): 7-25.

Htoon, A., Shrestha, A., Flanagan, B., Lopezrubio, A., Bird, A., Gilbert, E. and Gidley, M. (2009). "Effects of processing high amylose maize starches under controlled conditions on structural organisation and amylase digestibility." Carbohydrate Polymers **75**(2): 236-245.

Hu, P., Zhao, H., Duan, Z., Linlin, Z. and Wu, D. (2004). "Starch digestibility and the estimated glycemic score of different types of rice differing in amylose contents." Journal of Cereal Science **40**(3): 231-237.

Huber, K. C. and BeMiller, J. N. (2000). "Channels of maize and sorghum starch granules." Carbohydrate Polymers **41**: 269–276.

Hug-Iten, S., Escher, F. and Conde-Petit, B. (2003). "Staling of bread: Role of amylose and amylopectin and influence of starch-degrading enzymes." Cereal Chemistry **80(6)**: 654–661.

Hug-Iten, S., Handschin, S., Conde-Petit, B. and Escher, F. (1999). "Changes in starch microstructure on baking and staling of wheat bread." LWT-Food Science and Technology **32**: 255-260.

Imberty, A., Chanzy, H. and Perez, S. (1988). "The double-helical nature of the crystalline part of A-starch." Journal of Molecular Biology **201**: 365-378.

Jacobs, H. and Delcour, J. A. (1998). "Hydrothermal modifications of granular starch, with retention of the granular structure: A review." Journal of Agricultural and Food Chemistry **46**: 2895–2905.

Jacobs, H., Eerlingen, R., Clauwert, W. and Delcour, J. (1995). "Influence of annealing on the pasting properties of starches from varying botanical sources." Cereal Chemistry **72**(5): 480-487.

Jacobs, H., Eerlingen, R. C., Rouseu, N., Colonna, P. and Delcour, J. A. (1998). "Acid hydrolysis of native and annealed wheat, potato and pea starches-DSC melting features and chain length distributions of lintnerised starches." Carbohydrate Research **308**: 359-371.

Jacobs, H., Mischenko, N., Koch, M. H. J., Eerlingen, R. C., Delcour, J. A. and Reynaers, H. (1998). "Evaluation of the impact of annealing on gelatinisation at intermediate water content of wheat and potato starches: A differential scanning calorimetry and small angle X-ray scattering study." Carbohydrate Research **306**: 1-10.

Jane, J.-l. and Shen, J. J. (1993). "Internal structure of the potato starch granule revealed by chemical gelatinization." Carbohydrate Research **247**: 279-290.

Jane, J. L., Kasemsuwan, T., Leas, S., Zobel, H. and Robyt, J. F. (1994). "Anthology of starch granule morphology by scanning electron microscopy." Starch- Stärke **46**(4): 121-129.

Jane, J. L., Wong, K. S. and McPherson, A. E. (1997). "Branch-structure difference in starches of A- and B-type X-ray patterns revealed by their Naegeli dextrins." Carbohydrate Research **300**(3): 219-227.

Janeček, Š. (1992). "New conserved amino acid region of alpha-amylases in the third loop of their (beta/alpha) 8-barrel domains." Biochemical Journal **288**(Pt 3): 1069-1070.

Janeček, Š., Svensson, B. and Henrissat, B. (1997). "Domain evolution in the α-amylase family." Journal of Molecular Evolution **45**(3): 322-331.

Järvi, A. E., Karlström, B. E., Granfeldt, Y. E., Björck, I. E., Asp, N. and Vessby, B. (1999). "Improved glycemic control and lipid profile and normalized fibrinolytic activity on a low-glycemic index diet in type 2 diabetic patients." Diabetes Care **22**(1): 10-18.

Jayakody, L. and Hoover, R. (2008). "Effect of annealing on the molecular structure and physicochemical properties of starches from different botanical origins – A review." Carbohydrate Polymers **74**(3): 691-703.

Jenkins, D., Wolever, T., Taylor, R. H., Barker, H., Fielden, H., Baldwin, J. M., Bowling, A. C., Newman, H. C., Jenkins, A. L. and Goff, D. V. (1981). "Glycemic index of foods: a physiological basis for carbohydrate exchange." The American Journal of Clinical Nutrition **34**(3): 362-366.

Jenkins, D. J., Jenkins, A. L., Wolever, T. M., Collier, G. R., Rao, A. V. and Thompson, L. U. (1987). "Starchy foods and fiber: reduced rate of digestion and improved carbohydrate metabolism." Scandinavian Journal of Gastroenterology **22**(S129): 132-141.

Jenkins, D. J., Kendall, C. W., McKeown-Eyssen, G., Josse, R. G., Silverberg, J., Booth, G. L., Vidgen, E., Josse, A. R., Nguyen, T. H. and Corrigan, S. (2008). "Effect of a low–glycemic index or a high–cereal fiber diet on type 2 diabetes: a randomized trial." Jama **300**(23): 2742-2753.

Jenkins, P., Comerson, R., Donald, A., Bras, W., Derbyshire, G., Mant, G. and Ryan, A. (1994). "In situ simultaneous small and wide angle X- ray scattering: A new technique to study starch gelatinization." Journal of Polymer Science Part B: Polymer Physics **32**(8): 1579-1583.

Jenkins, P. J. and Donald, A. M. (1998). "Gelatinisation of starch: a combined SAXS/WAXS/DSC and SANS study." Carbohydrate Research **308**(1–2): 133-147.

Jones, D. S. (1999). "Dynamic mechanical analysis of polymeric systems of pharmaceutical and biomedical significance." International Journal of Pharmaceutics **179**(2): 167-178.

Kalichevsky, M. T., Orford, P. D. and Ring, S. G. (1990). "The retrogradation and gelation of amylopectins from various botanical sources." Carbohydrate Research **198**(1): 49-55.

Kaur, M., Sandhu, K. S. and Lim, S.-T. (2010). "Microstructure, physicochemical properties and in vitro digestibility of starches from different Indian lentil (Lens culinaris) cultivars." Carbohydrate Polymers **79**(2): 349-355.

Kearney, J. (2010). "Food consumption trends and drivers." Philosophical Transactions of the Royal Society B: Biological Sciences **365**(1554): 2793-2807.

Keeling, P. L. and Myers, A. M. (2010). "Biochemistry and genetics of starch synthesis." Annual Review of Food Science and Technology **1**(1): 271-303.

Khanna, S. and Tester, R. (2006). "Influence of purified konjac glucomannan on the gelatinisation and retrogradation properties of maize and potato starches." Food Hydrocolloids **20**(5): 567-576.

Knutson, C., Khoo, U., Cluskey, J. and Inglett, G. (1982). "Variation in enzyme digestibility and gelatinization behavior of corn starch granule fractions." Cereal Chemistry **59**: 512-515.

Knutson, C. A. (1986). "A simplified colorimetric procedure for determination of amylose in maize starches." Cereal Chemistry **63**(2): 89-92.

Knutson, C. A. (2000). "Evaluation of variations in amylose-iodine absorbance spectra." Carbohydrate Polymers **42**: 65-72.

Koch, K. and Jane, J. L. (2000). "Morphological changes of granules of different starches by surface gelatinization with calcium chloride." Cereal Chemistry **77**(2): 115–120.

Kozlov, S., Krivandin, A., Shatalova, O. V., Noda, T., Bertoft, E., Fornal, J. and Yuryev, V. (2007). "Structure of starches extracted from near-isogenic wheat lines." Journal of Thermal Analysis and Calorimetry **87**(2): 575-584.

Kuakpetoon, D. and Wang, Y.-J. (2007). "Internal structure and physicochemical properties of corn starches as revealed by chemical surface gelatinization." Carbohydrate Research **342**(15): 2253-2263.

Kubo, A., Fujita, N., Harada, K., Matsuda, T., Satoh, H. and Nakamura, Y. (1999). "The starch-debranching enzymes isoamylase and pullulanase are both involved in amylopectin biosynthesis in rice endosperm." Plant Physiology **121**(2): 399-410.

Layer, P., Rizza, R. A., Zinsmeister, A. R., Carlson, G. L. and DiMagno, E. P. (1986). "Effect of a purified amylase inhibitor on carbohydrate tolerance in normal subjects and patients with diabetes mellitus." Mayo Clinic Proceedings **61**(6): 442-447.

Le Berre-Anton V, B.-G. C., Payan F, Rougé P. (1997). "Characterization and functional properties of the alpha-amylase inhibitor (alpha-AI) from kidney bean (Phaseolus vulgaris) seeds." Biochimica et Biophysica Acta **1343**: 31-40.

Lee, P. C., Brooks, S. P., Kim, O., Heitlinger, L. A. and Lebenthal, E. (1985). "Digestibility of native and modified starches: in vitro studies with human and rabbit pancreatic amylases and in vivo studies in rabbits." The Journal of Nutrition **115**(1): 93-103.

Leeds, A., Brand Miller, J., Foster-Powell, K. and Colagiuri, S. (2003). The new glucose revolution, Hodder and Stoughton, London.

Lehmann, U. and Robin, F. (2007). "Slowly digestible starch – its structure and health implications: a review." Trends in Food Science & Technology **18**(7): 346-355.

Leloup, V., Colonna, P. and Ring, S. (1992). "Physico—chemical aspects of resistant starch." Journal of Cereal Science **16**(3): 253-266.

Leloup, V. M., Colonna, P. and Ring, S. G. (1991). "α-Amylase adsorption on starch crystallites." Biotechnology and Bioengineering **38**(2): 127-134.

Liljeberg, H., Åkerberg, A. and Björck, I. (1996). "Resistant starch formation in bread as influenced by choice of ingredients or baking conditions." Food Chemistry **56**(4): 389-394.

Lineback, D. (1986). "Current concepts of starch structure and its impact on properties." Journal of the Japanese Society of Starch Science **33**(1): 80-88.

Liu, D., Parker, M. L., Wellner, N., Kirby, A. R., Cross, K., Morris, V. J. and Cheng, F. (2013). "Structural variability between starch granules in wild type and in ae high-amylose mutant maize kernels." Carbohydrate Polymers **97**(2): 458-468.

Liu, H., Liang, R., Antoniou, J., Liu, F., Shoemaker, C. F., Li, Y. and Zhong, F. (2014). "The effect of high moisture heat-acid treatment on the structure and digestion property of normal maize starch." Food Chemistry **159**: 222-229.

Liu, H., Xie, F., Yu, L., Chen, L. and Li, L. (2009). "Thermal processing of starch-based polymers." Progress in Polymer Science **34**(12): 1348-1368.

Liu, H., Yu, L., Dean, K., Simon, G., Petinakis, E. and Chen, L. (2009). "Starch gelatinization under pressure studied by high pressure DSC." Carbohydrate Polymers **75**(3): 395-400.

Liu, Q., Charletb, G., Yellec, S. and Arul, J. (2002). "Phase transition in potato starch–water system I. Starch gelatinization at high moisture level." Food Research International **35**: 397–407.

Liu, Q. and Thompson, D. B. (1998). "Effects of moisture content and different gelatinization heating temperatures on retrogradation of waxy-type maize starches." Carbohydrate Research **314**(3): 221-235.

Liu, S. (2002). "Intake of refined carbohydrates and whole grain foods in relation to risk of type 2 diabetes mellitus and coronary heart disease." Journal of the American College of Nutrition **21**(4): 298-306.

Liu, S., Willett, W. C., Stampfer, M. J., Hu, F. B., Franz, M., Sampson, L., Hennekens, C. H. and Manson, J. E. (2000). "A prospective study of dietary glycemic load, carbohydrate intake, and risk of coronary heart disease in US women." The American Journal of Clinical Nutrition **71**(6): 1455-1461.

Longton, J. and Legrys, G. A. (1981). "Differential scanning calorimetry studies on the crystallinity of ageing wheat starch gels." Starch - Stärke **33**(12): 410-414.

Lopez-Rubio, A., Flanagan, B. M., Gilbert, E. P. and Gidley, M. J. (2008). "A novel approach for calculating starch crystallinity and its correlation with double helix content: A combined XRD and NMR study." Biopolymers **89**(9): 761-768.

Lopez-Rubio, A. and Gilbert, E. P. (2009). "Neutron scattering: a natural tool for food science and technology research." Trends in Food Science & Technology **20**(11–12): 576-586.

Ma, U. V. L., Floros, J. D., & Ziegler, G. R. (2011). "Effect of starch fractions on spherulite formation and microstructure." Carbohydrate Polymers **83**(4): 1757-1765.

MacGregor, A. and Ballance, D. (1980). "Hydrolysis of large and small starch granules from normal and waxy barley cultivars by alpha-amylases from barley malt." Cereal Chemistry **57**(6): 397-402.

MacGregor, E., Janeček, Š. and Svensson, B. (2001). "Relationship of sequence and structure to specificity in the α-amylase family of enzymes." Biochimica et Biophysica Acta (BBA)-Protein Structure and Molecular Enzymology **1546**(1): 1-20.

Mahasukhonthachat, K., Sopade, P. A. and Gidley, M. J. (2010). "Kinetics of starch digestion in sorghum as affected by particle size." Journal of Food Engineering **96**(1): 18-28.

Mamat, H., Abu Hardan, M. O. and Hill, S. E. (2010). "Physicochemical properties of commercial semi-sweet biscuit." Food Chemistry **121**(4): 1029-1038.

Man, J., Yang, Y., Huang, J., Zhang, C., Zhang, F., Wang, Y., Gu, M., Liu, Q. and Wei, C. (2013). "Morphology and structural properties of high-amylose rice starch residues hydrolysed by amyloglucosidase." Food Chemistry **138**(4): 2089-2098.

Margaretaleeman, A., Karlsson, M., Eliasson, A. and Bjorck, I. (2006). "Resistant starch formation in temperature treated potato starches varying in amylose/amylopectin ratio." Carbohydrate Polymers **65**(3): 306-313.

Martin, C. and Smith, A. (1995). "Starch biosynthesis." The Plant Cell **7**: 971-985.

Martínez, M. M., Calviño, A., Rosell, C. M. and Gómez, M. (2014). "Effect of different extrusion treatments and particle size distribution on the physicochemical properties of rice flour." Food and Bioprocess Technology **7**: 1-9.

Matveeva, Y. I., Van Soestc, J. J. G., Niemand, C., Wassermana, L. A., Protserova, V. A., Ezernitskajab, M. and Yuryev, V. P. (2001). "The relationship between thermodynamic and structural properties of low and high amylose maize starches." Carbohydrate Polymers **44**: 151–160.

McCance, R. A. and Widdowson, E. M. (2002). McCance and Widdowson's The Composition of Foods. Cambridge, Royal Society of Chemistry.

McCleary, B. and Monaghan, D. (2002). "Measurement of resistant starch." Journal of AOAC International **85**: 665-675.

McCleary, B. V., Solah, V. and Gibson, T. S. (1994). "Quantitative measurement of total starch in cereal flours and products." Journal of Cereal Science **20**(1): 51-58.

Medcalf, D. and Gilles, K. (1965). "Wheat starches I. Comparison of physicochemical properties." Cereal Chemistry **42**: 558-568.

Miao, M., Jiang, B. and Zhang, T. (2009). "Effect of pullulanase debranching and recrystallization on structure and digestibility of waxy maize starch." Carbohydrate Polymers **76**(2): 214-221.

Miles, M. J., Morris, V. J., Orford, P. D. and Ring, S. G. (1985). "The roles of amylose and amylopectin in the gelation and retrogradation of starch." Carbohydrate Research **135**(2): 271-281.

Millan-Testa, C. E., Mendez-Montealvo, M. G., Ottenhof, M.-A., Farhat, I. A. and Bello-Peä Rez, L. A. (2005). "Determination of the molecular and structural characteristics of okenia, mango, and banana starches." Journal of Agricultural and Food Chemistry **53**: 495-501.

Miller, J., Pang, E. and Bramall, L. (1992). "Rice: a high or low glycemic index food?" The American Society for Clinical Nutrition **56**: 1034-1036.

Moretti, R. and Thorson, J. S. (2008). "A comparison of sugar indicators enables a universal high-throughput sugar-1-phosphate nucleotidyltransferase assay." Analytical Biochemistry **377**(2): 251-258.

Motulsky, H. and Christopoulos, A. (2004). Fitting models to biological data using linear and nonlinear regression: A practical guide to curve fitting, Oxford University Press.

Noosuk, P., Hill, S. E., Pradipasena, P. and Mitchell, J. R. (2003). "Structure-viscosity relationships for thai rice starches." Starch - Stärke **55**(8): 337-344.

Nugent, A. (2005). "Health properties of resistant starch." Nutrition Bulletin **30**(1): 27-54.

Oates, G. C. (1997). "Towards an understanding of starch granule structure and hydrolysis." Trends in Food Science & Technology **8**: 375–382.

Obanni, M. and Bemiller, J. N. (1996). "Ghost microstructures of starch from different botanical sources." Cereal Chemistry **73**(3): 333-337.

Obrien, S. (2008). "Susceptibility of annealed starches to hydrolysis by α-amylase and glucoamylase." Carbohydrate Polymers **72**(4): 597-607.

Oostergetel, G. T. and van Bruggen, E. F. J. (1993). "The crystalline domains in potato starch granules are arranged in a helical fashion." Carbohydrate Polymers **21**(1): 7-12.

Orford, P. D., Ring, S. G., Carroll, V., Miles, M. J. and Morris, V. J. (1987). "The effect of concentration and botanical source on the gelation and retrogradation of starch." Journal of the Science of Food and Agriculture **39**(2): 169-177.

Osorio- Díaz, P., Tovar, J., Paredes- López, O., Acosta- Gallegos, J. A. and Bello- Pérez, L. A. (2005). "Chemical composition and in vitro starch bioavailability of Phaseolus vulgaris (L) cv Mayocoba." Journal of the Science of Food and Agriculture **85**(3): 499-504.

Ottenhof, M.-A., Hill, S. E. and Farhat, I. A. (2005). "Comparative study of the retrogradation of intermediate water content waxy maize, wheat, and potato starches." Journal of Agricultural and Food Chemistry **53**: 631-638.

Owusu-Apenten, R. (2004). Introduction to Food Chemistry, CRC Press.

Panlasigui, L., Thompson, L., Juliano, B., Perez, C., Yiu, S. and Greenberg, G. (1991). "Rice varieties with similar amylose content differ in starch digestibility and glycemic response in humans." The American Society for Clinical Nutrition **54**: 871-877.

Park, E. Y., Baik, B.-K. and Lim, S.-T. (2009). "Influences of temperature-cycled storage on retrogradation and in vitro digestibility of waxy maize starch gel." Journal of Cereal Science **50**(1): 43-48.

Park, J. and Johnson, M. (1949). "A submicrodetermination of glucose." Journal of Biological Chemistry **181**: 149-151.

Perera, A., Meda, V. and Tyler, R. T. (2010). "Resistant starch: A review of analytical protocols for determining resistant starch and of factors affecting the resistant starch content of foods." Food Research International **43**(8): 1959-1974.

Pérez, S. and Bertoft, E. (2010). "The molecular structures of starch components and their contribution to the architecture of starch granules: A comprehensive review." Starch - Stärke **62**(8): 389-420.

Perry, G. H., Dominy, N. J., Claw, K. G., Lee, A. S., Fiegler, H., Redon, R., Werner, J., Villanea, F. A., Mountain, J. L., Misra, R., Carter, N. P., Lee, C. and Stone, A. C. (2007). "Diet and the evolution of human amylase gene copy number variation." Nature Genetics **39**(10): 1256-1260.

Perry, P. and Donald, A. (2000). "The role of plasticization in starch granule assembly." Biomacromolecules **1**(3): 424-432.

Planchot, V., Colonna, P. and Buleon, A. (1997). "Enzymatic hydrolysis of α-glucan crystallites." Carbohydrate Research **298**(4): 319-326.

Planchot, V., Colonna, P., Gallant, D. and Bouchet, B. (1995). "Extensive degradation of native starch granules by alpha-amylase from aspergillus fumigatus." Journal of Cereal Science **21**(2): 163-171.

Primo-Martín, C., van Nieuwenhuijzen, N. H., Hamer, R. J. and van Vliet, T. (2007). "Crystallinity changes in wheat starch during the bread-making process: Starch crystallinity in the bread crust." Journal of Cereal Science **45**(2): 219-226.

Ranaldi, F., Vanni, P. and Giachetti, E. (1999). "What students must know about the determination of enzyme kinetic parameters." Biochemical Education **27**(2): 87-91.

Rendleman Jr, J. A. (2000). "Hydrolytic action of α-amylase on high-amylose starch of low molecular mass." Biotechnology and Applied Biochemistry **31**(3): 171-178.

Ridout, M. J., Parker, M. L., Hedley, C. L., Bogracheva, T. Y. and Morris, V. J. (2003). "Atomic force microscopy of pea starch granules: granule architecture of

wild-type parent, r and rb single mutants, and the rrb double mutant." Carbohydrate Research **338**(20): 2135-2147.

Robyt, J. F. and French, D. (1970). "The action pattern of porcine pancreatic α-amylase in relationship to the substrate binding site of the enzyme." Journal of Biological Chemistry **245**(15): 3917-3927.

Roder, N., Gerard, C., Verel, A., Bogracheva, T., Hedley, C., Ellis, P. and Butterworth, P. (2009). "Factors affecting the action of α-amylase on wheat starch: Effects of water availability. An enzymic and structural study." Food Chemistry **113**(2): 471-478.

Royall, P. and Gaisford, S. (2005). "Application of solution calorimetry in pharmaceutical and biopharmaceutical research." Current Pharmaceutical Biotechnology **6**(3): 215-222.

Sagum, R. and Arcot, J. (2000). "Effect of domestic processing methods on the starch, non-starch polysaccharides and in vitro starch and protein digestibility of three varieties of rice with varying levels of amylose." Food Chemistry **70**: 107-111.

Sajilata, M. G., Singhal, R. S. and Kulkarni, P. R. (2006). "Resistant starch–A review." Comprehensive Reviews in Food Science and Food Safety **5**: 1-17.

Sandstedt, R. M., Strahan, D., Ueda, S. and Abbot, R. (1962). "The digestibility of high-amylose corn starches compared to that of other starches. The apparent effect of the ae gene on susceptibility to amylase action." Cereal Chemistry **39**: 123-131.

Sarko, A. and Wu, H. C. (1978). "The crystal structures of A- , B- and C-polymorphs of amylose and starch." Starch- Stärke **30**(3): 73-78.

Sasaki, T., Yasui, T. and Matsuki, J. (2000). "Effect of amylose content on gelatinization, retrogradation, and pasting properties of starches from waxy and nonwaxy wheat and their F1 seeds." Cereal Chemistry **77**: 58–63.

Schinner, F. and Von Mersi, W. (1990). "Xylanase, CM-cellulase and invertase activity in soil: An improved method." Soil Biol. Biochem **22**(4): 511-515.

Schinzel, R. and Nidetzky, B. (1999). "Bacterial α-glucan phosphorylases." FEMS Microbiology Letters **171**(2): 73-79.

Schirmer, M., Höchstötter, A., Jekle, M., Arendt, E. and Becker, T. (2012). "Physicochemical and morphological characterization of different starches with variable amylose/amylopectin ratio." Food Hydrocolloids **32**: 52-63.

Schwall, G. P., Safford, R., Westcott, R. J., Jeffcoat, R., Tayal, A., Shi, Y.-C., Gidley, M. J. and Jobling, S. A. (2000). "Production of very-high-amylose potato starch by inhibition of SBE A and B." Nature Biotechnology **18**: 551 - 554.

Seal, C. J., Daly, M. E., Thomas, L. C., Bal, W., Birkett, A. M., Jeffcoat, R. and Mathers, J. C. (2007). "Postprandial carbohydrate metabolism in healthy subjects and those with type 2 diabetes fed starches with slow and rapid hydrolysis rates determined *in vitro*." British Journal of Nutrition **90**(05): 853-864.

Sevenou, O., Hill, S. E., Farhat, I. A. and Mitchell, J. R. (2002). "Organisation of the external region of the starch granule as determined by infrared spectroscopy." International Journal of Biological Macromolecules **31**: 79-85.

Shamai, K., Bianco-Peled, H. and Shimoni, E. (2003). "Polymorphism of resistant starch type III." Carbohydrate Polymers **54**(3): 363-369.

Shi, Y.-C., Capitani, T., Trzasko, P. and Jeffcoat, R. (1998). "Molecular structure of a low-amylopectin starch and other high-amylose maize starches." Journal of Cereal Science **27**(3): 289-299.

Shrestha, A. K., Blazek, J., Flanagan, B. M., Dhital, S., Larroque, O., Morell, M. K., Gilbert, E. P. and Gidley, M. J. (2012). "Molecular, mesoscopic and microscopic structure evolution during amylase digestion of maize starch granules." Carbohydrate Polymers **90**(1): 23-33.

Sievert, D., Czuchajowska, Z. and Pomeranz, Y. (1991). "Enzyme-resistant starch. III. X-ray diffraction of autoclaved amylomaize VII starch and enzyme-resistant starch residues." Cereal Chemistry **68**: 86-91.

Sievert, D. and Pomeranz, Y. (1989). "Enzyme-resistant starch. I. Characterization and evaluation by enzymatic, thermoanalytical, and microscopic methods." Cereal Chemistry **66**: 342-347.

Sievert, D. and Pomeranz, Y. (1990). "Enzyme-resistant starch. II. Differential scanning calorimetry studies on heat-treated starches and enzyme-resistant starch residues." Cereal Chemistry **67**: 217-221.

Silverio, J., Svensson, E., Eliasson, A.-C. and Olofsson, G. (1996). "Isothermal microcalorimetric studies on starch retrogradation." Journal of Thermal Analysis and Calorimetry **47**: 1179-1200.

Singh, J., Singh, N. and Saxena, S. K. (2002). "Effect of fatty acids on the rheological properties of corn and potato starch." Journal of Food Engineering **52**: 9–16.

Singh, N., Isono, N., Srichuwong, S., Noda, T. and Nishinari, K. (2008). "Structural, thermal and viscoelastic properties of potato starches." Food Hydrocolloids **22**(6): 979-988.

Slack, P., Baxter, E. and Wainwright, T. (1979). "Inhibition by hordein of starch degradation." Journal of The Institute of Brewing **85**: 112-114.

Slaughter, S. L., Ellis, P. R. and Butterworth, P. J. (2001). "An investigation of the action of porcine pancreatic α-amylase on native and gelatinised starches." Biochimica et Biophysica Acta **1525**: 29-36.

Slaughter, S. L., Ellis, P. R., Jackson, E. C. and Butterworth, P. J. (2002). "The effect of guar galactomannan and water availability during hydrothermal processing on the hydrolysis of starch catalysed by pancreatic a-amylase." Biochimica et Biophysica Acta **1571**: 55–63.

Sluijs, I., van der Schouw, Y. T., Spijkerman, A. M., Hu, F. B., Grobbee, D. E. and Beulens, J. W. (2010). "Carbohydrate quantity and quality and risk of type 2 diabetes in the European Prospective Investigation into Cancer and Nutrition–Netherlands (EPIC-NL) study." The American Journal of Clinical Nutrition **92**(4): 905-911.

Smith, A. M., Zeeman, S. C. and Smith, S. M. (2005). "Starch degradation." Annu. Rev. Plant Biol. **56**: 73-98.

Snow, P. and O'Dea, K. (1981). "Factors affecting the rate of hydrolysis of starch in food." The American Journal of Clinical Nutrition **34**(12): 2721-2727.

Snyder, M. and Lichstein, H. (1940). "Sodium azide as an inhibiting substance for gram-negative bacteria." The Journal of Infectious Diseases **67**: 113-115.

Souilah, R., Djabali, D., Belhadi, B., Mokrane, H., Boudries, N. and Nadjemi, B. (2014). "*In vitro* starch digestion in sorghum flour from Algerian cultivars." Food Science & Nutrition **2**(3): 251-259.

Sun, Y., Wu, Z., Hu, B., Wang, W., Ye, H., Sun, Y., Wang, X. and Zeng, X. (2014). "A new method for determining the relative crystallinity of chickpea starch by Fourier-transform infrared spectroscopy." Carbohydrate Polymers **108**: 153-158.

Suryanarayana, C. and Norton, M. G. (1998). X-ray diffraction: a practical approach, Springer.

Svensson, B. (1994). "Protein engineering in the α-amylase family: catalytic mechanism, substrate specificity, and stability." Plant Molecular Biology **25**(2): 141-157.

Svihus, B., Uhlen, A. and Harstad, O. (2005). "Effect of starch granule structure, associated components and processing on nutritive value of cereal starch: A review." Animal Feed Science and Technology **122**(3-4): 303-320.

Swinkels, J. J. M. (1985). "Composition and properties of commercial native starches." Starch - Stärke **37**(1): 1-5.

Tahir, R., Ellis, P. R., Bogracheva, T. Y., Meares-Taylor, C. and Butterworth, P. J. (2011). "A study of the structure and properties of native and hydrothermally processed wild-type, lam and r variant pea starches that affect amylolysis of these starches." Biomacromolecules **12**: 123-133.

Tahir, R., Ellis, P. R. and Butterworth, P. J. (2010). "The relation of physical properties of native starch granules to the kinetics of amylolysis catalysed by porcine pancreatic α-amylase." Carbohydrate Polymers **81**(1): 57-62.

Tan, I., Flanagan, B. M., Halley, P. J., Whittaker, A. K. and Gidley, M. J. (2007). "A method for estimating the nature and relative proportions of amorphous, single, and double-helical components in starch granules by 13C CP/MAS NMR." Biomacromolecules **8**(3): 885-891.

Tester, R. F., Karkalas, J. and Qi, X. (2004). "Starch—composition, fine structure and architecture." Journal of Cereal Science **39**(2): 151-165.

Tester, R. F., Qi, X. and Karkalas, J. (2006). "Hydrolysis of native starches with amylases." Animal Feed Science and Technology **130**(1-2): 39-54.

Tong, L., Hou, G., Chen, Y., Zhou, F., Shen, K. and Yang, A. (2012). "Experimental investigation on longitudinal residual stresses for cold-formed thick-walled square hollow sections." Journal of Constructional Steel Research **73**: 105-116.

Topping, D. L. and Clifton, P. M. (2001). "Short-chain fatty acids and human colonic function: roles of resistant starch and nonstarch polysaccharides." Physiological Reviews **81**(3): 1031-1064.

Topping, D. L., Fukushima, M. and Bird, A. R. (2003). "Resistant starch as a prebiotic and synbiotic: state of the art." Proceedings of the Nutrition Society **62**(01): 171-176.

Tovar, J., Bjoerck, I. M. and Asp, N. G. (1990). "Analytical and nutritional implications of limited enzymic availability of starch in cooked red kidney beans." Journal of Agricultural and Food Chemistry **38**(2): 488-493.

Tovar, J., Granfeldt, Y. and Bjoerck, I. M. (1992). "Effect of processing on blood glucose and insulin responses to starch in legumes." Journal of Agricultural and Food Chemistry **40**(10): 1846-1851.

Van Der Maarel, M. J., Van Der Veen, B., Uitdehaag, J., Leemhuis, H. and Dijkhuizen, L. (2002). "Properties and applications of starch-converting enzymes of the α-amylase family." Journal of Biotechnology **94**(2): 137-155.

van Soest, J. J. G., De Wit, D., Tournois, H. and VliegentharT, J. F. G. (1994). "Retrogradation of potato starch as studied by fourier transform infrared spectroscopy." Starch - Stärke **46**(12): 453-457.

van Soest, J. J. G., Tournois, H., de Wit, D. and Vliegenthart, J. F. G. (1995). "Short-range structure in (partially) crystalline potato starch determined with attenuated total reflectance Fourier-transform IR spectroscopy." Carbohydrate Research **279**: 201-214.

Vandeputte, G. E., Vermeylen, R., Geeroms, J. and Delcour, J. A. (2003). "Rice starches. III. Structural aspects provide insight in amylopectin retrogradation properties and gel texture." Journal of Cereal Science **38**(1): 61-68.

Vansteelandt, J. and Delcour, J. A. (1999). "Characterisation of starch from durum wheat (Triticum durum)." Starch - Stärke **51**: 73–80.

Varriano-Marston, E., Ke, V., Huang, G. and Ponte, J. (1980). "Comparison of methods to determine starch gelatinization in bakery foods." Cereal Chemistry **57**(4): 242-248.

Vasanthan, T. and Bhatty, R. (1996). "Physicochemical properties of small-and large-granule starches of waxy, regular, and high-amylose barleys." Cereal Chemistry **73**: 199-207.

Vilaplana, F., Hasjim, J. and Gilbert, R. G. (2012). "Amylose content in starches: Toward optimal definition and validating experimental methods." Carbohydrate Polymers **88**(1): 103-111.

Wang, S. and Copeland, L. (2013). "Molecular disassembly of starch granules during gelatinization and its effect on starch digestibility: a review." Food & Function **4**(11): 1564.

Wang, T. L., Bogracheva, T. Y. and Hedley, C. L. (1998). "Starch: as simple as A, B, C?" Journal of Experimental Botany **49**: 481–502.

Ward, K. E. J., Hoseney, R. and Seib, P. (1994). "Retrogradation of amylopectin from maize and wheat starches." Cereal Chemistry **71**: 150-155.

Warren, F. J., Butterworth, P. J. and Ellis, P. R. (2013). "The surface structure of a complex substrate revealed by enzyme kinetics and Freundlich constants for α-amylase interaction with the surface of starch." Biochimica et Biophysica Acta (BBA) - General Subjects **1830**(4): 3095-3101.

Warren, F. J., Royall, P. G., Butterworth, P. J. and Ellis, P. R. (2012). "Immersion mode material pocket dynamic mechanical analysis (IMP-DMA): A novel tool to study gelatinisation of purified starches and starch-containing plant materials." Carbohydrate Polymers **90**(1): 628-636.

Warren, F. J., Royall, P. G., Gaisford, S., Butterworth, P. J. and Ellis, P. R. (2011). "Binding interactions of α-amylase with starch granules: The influence of supramolecular structure and surface area." Carbohydrate Polymers **86**(2): 1038-1047.

Wolever, T. (2000). "Dietary carbohydrates and insulin action in humans." British Journal of Nutrition **83**(S1): 97-102.

Wolever, T. and Miller, J. B. (1995). "Sugars and blood glucose control." The American Journal of Clinical Nutrition **62**(1): 212-221.

Wolever, T. M., Jenkins, D. J., Jenkins, A. L. and Josse, R. G. (1991). "The glycemic index: methodology and clinical implications." The American Journal of Clinical Nutrition **54**(5): 846-854.

Wong, J. M., de Souza, R., Kendall, C. W., Emam, A. and Jenkins, D. J. (2006). "Colonic health: fermentation and short chain fatty acids." Journal of Clinical Gastroenterology **40**(3): 235-243.

Würsch, P., Del Vedovo, S. and Koellreutter, B. (1986). "Cell structure and starch nature as key determinants of the digestion rate of starch in legume." The American Journal of Clinical Nutrition **43**(1): 25-29.

Xia, Y., Gao, W., Jiang, Q., Li, X., Huang, L. and Xiao, P. (2012). "Physicochemical, crystalline, and thermal properties of native and enzyme hydrolyzed Pueraria lobata (Willd.) Ohwi and Pueraria thomsonii Benth. starches." Starch - Stärke **64**: 864–873.

Xie, F., Yu, L., Chen, L. and Li, L. (2008). "A new study of starch gelatinization under shear stress using dynamic mechanical analysis." Carbohydrate Polymers **72**(2): 229-234.

Xie, X., Liu, Q. and Cui, S. W. (2006). "Studies on the granular structure of resistant starches (type 4) from normal, high amylose and waxy corn starch citrates." Food Research International **39**(3): 332-341.

Yao, Y. (2004). "Maize starch-branching enzyme isoforms and amylopectin structure. In the absence of starch-branching enzyme IIb, the further absence of starch-branching enzyme Ia leads to increased branching." Plant Physiology **136**(3): 3515-3523.

Yon-Kahn, J. and Hervé, G. (2009). Molecular and cellular enzymology, Springer.

You, S.-Y., Lim, S.-T., Lee, J. H. and Chung, H.-J. (2014). "Impact of molecular and crystalline structures on in vitro digestibility of waxy rice starches." Carbohydrate Polymers **112**: 729-735.

Yuan, R., Thompson, D. and Boyer, C. (1993). "Fine structure of amylopectin in relation to gelatinization and retrogradation behavior of maize starches from three wx-containing genotypes in two inbred lines." Cereal Chemistry **70**: 81-81.

Zaidul, I., Norulaini, N., Omar, A., Yamauchi, H. and Noda, T. (2007). "RVA analysis of mixtures of wheat flour and potato, sweet potato, yam, and cassava starches." Carbohydrate Polymers **69**(4): 784-791.

Zavareze, E. d. R. and Dias, A. R. G. (2011). "Impact of heat-moisture treatment and annealing in starches: A review." Carbohydrate Polymers **83**(2): 317-328.

Zeleznak, K. J. and Hoseney, R. C. (1986). "The role of water in the retrogradation of wheat starch gels and bread crumb." Cereal Chemistry **63**: 407-411.

Zhang, B., Dhital, S., Flanagan, B. M. and Gidley, M. J. (2014). "Mechanism for starch granule ghost formation deduced from structural and enzyme digestion properties." Journal of Agricultural and Food Chemistry **63**(3): 760-771.

Zhang, B., Dhital, S. and Gidley, M. J. (2013). "Synergistic and antagonistic effects of α-amylase and amyloglucosidase on starch digestion." Biomacromolecules **14**(6): 1945-1954.

Zhang, G., Ao, Z. and Hamaker, B. (2006). "Slow digestion property of native cereal starches." Biomacromolecules **7**: 3252-3258.

Zhang, L., Hu, X., Xu, X., Jin, Z. and Tian, Y. (2011). "Slowly digestible starch prepared from rice starches by temperature-cycled retrogradation." Carbohydrate Polymers **84**(3): 970-974.

Zhou, X., Baik, B.-K., Wang, R. and Lim, S.-T. (2010). "Retrogradation of waxy and normal corn starch gels by temperature cycling." Journal of Cereal Science **51**(1): 57-65.

Zobel, H. F., Young, S. N. and Rocca, L. A. (1988). "Starch gelatinization: An X-ray diffraction study." Cereal Chemistry **65**: 443-446.

Appendices

Appendix A: Megazyme Total Starch Kit (AOAC 996.11 Official Method)

Megazyme kit contents

Bottle 1: Thermostable α-amylase (3,000 U/mL on Ceralpha reagent at pH 6.5 and 40°C).

Bottle 2: Amyloglucosidase (200 U/mL on *p*-nitrophenyl b-maltoside at pH 4.5 and 40°C)

Bottle 3: GOPOD (glucose oxidase/peroxidase) reagent buffer. Potassium phosphate buffer (0.26 M, pH 7.4), *p*-hydroxybenzoic acid (0.22 M) and sodium azide (0.4% w/v).

Bottle 4: GOPOD reagent enzymes. Glucose oxidase (>12,000 U) plus peroxidase (>650 U) and 4-aminoantipyrine (80 mg).

Bottle 5: D-Glucose standard solution (1.0 mg/ml) in 0.2 % (w/v) benzoic acid.

Bottle 6: Standardised regular maize starch control.

Preparation of reagents

Sodium acetate buffer (100 mM, pH 5.0): Glacial acetic acid (2.54 mL, 1.05 g/mL) was added to 450 mL deionised water. The pH was adjusted to 5.0 by adding 1 M NaOH. Calcium chloride dihydrate (0.37 g) was dissolved into the solution. The volume was adjusted to 1 L with deionised water and stored in a volumetric flask, at 4°C (stable for > 6 months).

Solution 1: α-Amylase (600 µL of bottle 1) was diluted into 18 mL sodium acetate buffer (1 in 30 dilution).

Solution 2: Amyloglucosidase (bottle 2) as supplied.

Solution 3: GOPOD reagent buffer (bottle 3) diluted to 1L with distilled water.

Solution 4: GOPOD reagent enzymes (bottle 4) were diluted in 20 mL solution 3. This was then added to the rest of solution 3. This solution was separated

into smaller aliquots as the solution can be freeze/thawed once. Each aliquot was covered with aluminium foil to protect from light and frozen until required (stable for > 12 months). The absorbance of the solution was checked before use and was less than 0.05 when read against deionised water, as recommended by the manufacture.

Solution 5: D-Glucose standard (bottle 5).

Solution 6: Maize starch control (bottle 6).

Appendix B: Megazyme Resistant Starch Kit (AOAC 2002.02 Official Method)

Megazyme kit contents

Bottle 1: Amyloglucosidase (AMG, 3300 U/mL on soluble starch at pH 4.5 and 40°C).

Bottle 2: Pancreatic α-amylase (Pancreatin, 10g, 3 Ceralpha Units/mg).

Bottle 3: GOPOD (glucose oxidase/peroxidase) Reagent Buffer. Potassium phosphate buffer (0.26M, pH 7.4), *p*-hydroxybenzoic acid (0.22 M) and sodium azide (0.4 % w/v).

Bottle 4: GOPOD reagent enzymes. Glucose oxidase (>12,000 U) plus peroxidase (>650 U) and 4-aminoantipyrine (80 mg).

Bottle 5: D-Glucose standard (1.0 mg/mL) in 0.2% (w/v) benzoic acid.

Bottle 6: Standardised maize starch control. Resistant starch content of 52.5%.

Preparation of Reagents

Sodium maleate buffer (100 mM, pH 6.0) plus 5 mM calcium chloride dihydrate and sodium azide (0.02% w/v). Maleic acid (23.2 g) was dissolved in 1600 mL of deionised water. The pH was adjusted to 6.0 by adding 4 M (160 g/litre) NaOH. Calcium chloride dihydrate (0.74 g) and sodium azide (0.4 g) was added to the mixture and dissolved. The volume was adjusted to 2 litres with deionised water and stored at 4^{o}C (stable for 12 months).

Sodium acetate buffer (1.2M, pH 3.8): Glacial acetic acid (69.6 mL, 1.05 g/mL) was added to 800 mL deionised water. The pH was adjusted to 3.8 by adding 4 M NaOH. The volume was adjusted to 1 L with deionised water and stored at room temperature (stable for 12 months).

Sodium acetate buffer (100 mM, pH 4.5): Glacial acetic acid (5.8 mL) was added to 900 mL deionised water. The pH was adjusted to 4.5 by adding 4 M NaOH. The volume was adjusted to 1 L with deionised water and stored at 4^{o}C (stable for 2 months).

Potassium hydroxide (2 M): potassium hydroxide (112.2 g) was added to 900 mL deionised water. The volume was adjusted to 1 L with deionised water and stored at room temperature (stable for > 2 years).

Aqueous ethanol (50% v/v): Ethanol (500 mL of 99% v/v) was added to 500 mL deionised water. The solution was stored at room temperature (stable for > 2 years).

Solution 1: A 2 mL solution of concentrated AMG (bottle 1) was pipetted into 22 mL of 0.1 M sodium maleate buffer (100 mM, pH 6.0). This gives a final concentration of 300 U/mL diluted AMG. The sample was then divided into 1 mL aliquots and stored at -20^{o}C in microcentrifuge tubes. Diluted AMG is stable to repeated freeze/thaw cycles for 5 years at -20^{o}C.

Solution 2: α-Amylase (0.2 g of bottle 2) was suspended into 20 mL sodium maleate buffer (100 mM, pH 6.0). To this, 0.2 mL of diluted AMG (300 U/mL) was added and mixed well. This gives a final concentration of 10 mg/mL α-amylase with 3 U/mL AMG. The sample was centrifuged at > 1,500 g for 10 min and the supernatant was decanted. The supernatant was then used on the day of preparation.

Solution 3: GOPOD reagent buffer (bottle 3) was diluted to 1 L with deionised water.

Solution 4: A GOPOD reagent enzyme (bottle 4) was dissolved in 20 mL of solution 3. This was then added to the rest of solution 3. This solution was separated into smaller aliquots as the solution can be freeze/thawed once. Each

aliquot was covered with aluminium foil to protect from light and frozen until required (stable for > 12 months). The absorbance of the solution was checked before use and was less than 0.05 when read against deionised water, as recommended by the manufacture. This was the Glucose Determination Reagent (GOPOD reagent).

Appendix C: V_{max} figures for gelatinised and retrograded starches

Starch	Storage time (h)						
	0	6	18	24	48	72	96
Wheat	141 ± 0.9	132 ± 3.4	131 ± 2.8	134 ± 3.8	132 ± 1.5	113 ± 1.7	115 ± 1.3
Potato	147 ± 1.2	150 ± 2.6	151 ± 3.2	108 ± 0.7	105 ± 1.4	107 ± 1.1	108 ± 1.2
Wild type pea	127 ± 2.8			129 ± 1.1	127 ± 1.4	128 ± 0.5	131 ± 1.3
Maize	112 ± 1.6			110 ± 2.4	113 ± 1.4	112 ± 1.5	105 ± 0.5
Waxy maize	117 ± 6.3			113 ± 2.4	112 ± 0.7	115 ± 1.2	116 ± 2.3
High amylose maize	114 ± 0.5	111 ± 2.8	117 ± 1.9	89 ± 0.3	90 ± 1.5	90 ± 1.9	87 ± 3.3

Appendix D: Retrograded wheat starch digestion with PPA in the presence of sodium azide (NaN_3)